UNIVERSIDAD DE CHILE
FACULTAD DE CIENCIAS FÍSICAS Y MATEMÁTICAS
DEPARTAMENTO DE INGENIERÍA ELÉCTRICA

# DISTRIBUTED SECONDARY CONTROL OF HYBRID AC/DC MICROGRIDS

TESIS PARA OPTAR AL GRADO DE DOCTOR EN INGENIERÍA ELÉCTRICA
EN COTUTELA CON LA UNIVERSIDAD DE WATERLOO, CANADA

ENRIQUE ANTONIO ESPINA GONZÁLEZ

PROFESORES GUÍA:
ROBERTO CÁRDENAS DOBSON
MEHRDAD KAZERANI

PROFESORES CO-GUÍA:
DORIS SÁEZ HUEICHAPAN
JOHN SIMPSON-PORCO

MIEMBROS DE LA COMISIÓN:
MOHAMMAD SHAHIDEHPOUR
RODRIGO PALMA BEHNKE
CESAR AZURDIA MEZA
KANKAR BHATTACHARYA
MAGDY SALAMA

SANTIAGO DE CHILE
2021

RESUMEN DE LA MEMORIA PARA OPTAR
AL TÍTULO DE DOCTOR EN INGENIERÍA ELÉCTRICA
POR: ENRIQUE ANTONIO ESPINA GONZÁLEZ
FECHA: 2021
PROF. GUÍA: ROBERTO CÁRDENAS DOBSON MEHRDAD KAZERANI
PROF. CO-GUÍA: DORIS SÁEZ HUEICHAPAN JOHN SIMPSON-PORCO

# DISTRIBUTED SECONDARY CONTROL OF HYBRID AC/DC MICROGRIDS

This Ph.D. thesis focuses on studying hybrid ac/dc-microgrids, composed of an ac-microgrid and a dc-microgrid, connected by Interlinking Converters (ICs). Specifically, this work is focused on developing distributed secondary controllers that consider the hybrid microgrid as a single entity and not as three independent systems interacting with each other. The main goal of the secondary controller is augmented with one of the following objectives: (i) achieving active power consensus between ac-DGs and dc-DGs (and ICs), or (ii) minimizing the operation cost of the microgrid. The additional control task is performed with information from the nearest neighbours from both sides of the microgrid. Two analytical closed-loop models for a hybrid microgrid are obtained in this thesis. The first one considers the consensus-based distributed control strategy proposed for active power consensus. In contrast, the second one considers the strategy proposed for minimizing the operation cost of the microgrid. The closed-loop models are used to perform several analyses of the control systems proposed. Several tests are carried out to validate the performance of the proposed control strategies in two different topologies: a 24kW prototype with a single IC and a 33kW prototype with multiple ICs.

RESUMEN DE LA MEMORIA PARA OPTAR
AL TÍTULO DE DOCTOR EN INGENIERÍA ELÉCTRICA
POR: ENRIQUE ANTONIO ESPINA GONZÁLEZ
FECHA: 2021
PROF. GUÍA: ROBERTO CÁRDENAS DOBSON MEHRDAD KAZERANI
PROF. CO-GUÍA: DORIS SÁEZ HUEICHAPAN JOHN SIMPSON-PORCO

# DISTRIBUTED SECONDARY CONTROL OF HYBRID AC/DC MICROGRIDS

Esta tesis de doctorado estudia micro-redes híbridas ac/dc, las que están compuestas por una micro-red ac y una micro-red dc, las cuales se interconectan con interlinking converters (ICs). Específicamente, este trabajo desarrolla controladores secundarios distribuidos que consideran a la micro-red híbrida como una sola entidad y no como tres sistemas independientes que interactúan entre si. El objetivo principal del control secundario es amplificado con uno de los siguientes objetivos adicionales: (i) alcanzar un consenso de potencia entre las unidades ac y las unidades dc (y los ICs), o (ii) minimizar el costo total de operación de la micro-red. La acción de control adicional se realiza con información de los vecinos más cercanos a ambos lados de la micro-red. Dos modelos analíticos de lazo cerrado para una micro-red híbrida se obtienen en esta tesis. El primero considera la estrategia propuesta para obtener consenso de potencia activa, mientras que el segundo considera la estrategia propuesta para minimizar el costo total de operación de la micro-red. Los modelos de lazo cerrado son utilizados para diferentes tipos de análisis a los sistemas de control propuestos. Se realizan numerosas pruebas para validar el desempeño de los controladores propuestos en dos diferentes topologías: un prototipo de 24kW con un IC y un prototipo de 33 kW con múltiples ICs.

*To Nicole and Marcelo, the most important people in my life, in recognition of all their love, support and encouragement to achieve all of our goals.*

⋮

*Para Nicole y Marcelo, las personas más importantes en mi vida, en reconocimiento a todo su amor, apoyo y motivación para lograr todas nuestras metas.*

# Acknowledgements

First, I would like thank Nicole and Marcelo, my LOVE, my support in difficult times, my beloved family and my motivation to achieve great things. Thank you very much for your endless love, affection, dedication and patience during this time, for always being there to support me, motivate me, understand me, encourage me and push me to go further.

My parents, Enrique and Lucy, thank you very much for all the love, affection, and support you have given me to become who I am. To my siblings, Lucy and Francisco and their families, Facundo, Catalina, Carlos and Carolina, thank you very much for always trusting me and always being there when you are needed.

My sincerest gratitude goes to my advisors, Professors Roberto Cárdenas and Doris Sáez from the University of Chile, and Professors Mehrdad Kazerani and John Simpson-Porco from the University of Waterloo, for their professional guidance, valuable advice, continual support and encouragement shown throughout my Ph.D. study. My appreciation and thanks are also extended to my Ph.D. committee members: Professors Magdy Salama, Kankar Bhattacharya, Rodrigo Palma and Cesar Azurdia. Thanks are also due to my external examiner, Professor Mohammad Shahidehpour, for coming from Illinois Institute of Technology to referee this thesis.

I also wish to thank my colleagues and friends from the Power Electronics and Drives Laboratory and the Microgrid's Control Laboratory at the University of Chile. Their fruitful discussions and support inspired me during my Ph.D.

To my alma mater USACH, the institution that helped me build a solid foundation in the knowledge of this area of engineering and actively supported me during my Ph.D.

Last but not least, I would like to express my sincere gratitude to Agencia Nacional de Investigación y Desarrollo (ANID) in Chile, which supported and financed my Ph.D. and my stay in Canada through the Scholarship CONICYTPCHA/Doctorado Nacional/2017-21171858. The following projects are kindly acknowledged: Fondecyt 1170683 "Robust Distributed Predictive Control Strategies for the Coordination of Hybrid AC and DC Microgrids", Fondequip EQM130158 "Microgrid Emulator for the Design and Validation of Novel Control Strategies", Fondequip EQM160122, "Equipment for the Emulation and Evaluation of energy storage systems" and Fondecyt 1180879, "Modular Multilevel Technologies For Future Generations of High Power Machines". The support of the Instituto Sistemas Complejos de Ingeniería (ISCI) ANID PIA/BASAL AFB180003 and AC3E ANID-BASAL Project FB0008 "Advanced Centre for Electrical and Electronic Engineering" are also acknowledged.

# Contents

# List of Tables

# List of Figures

# List of Abbreviations

| | |
|---|---|
| **BESS** | Battery Energy Storage System. |
| **DAPI** | Distributed-Averaging Proportional-Integral. |
| **DES** | Distributed Energy Storage. |
| **DG** | Distributed Generator. |
| **DiGen** | Diesel Generator. |
| **DSC** | Distributed Secondary Control. |
| **ED** | Economic Dispatch. |
| **ESS** | Energy Storage System. |
| **EV** | Electrical Vehicle. |
| **GPS** | Global Power Sharing. |
| **HBC** | Half Bridge Converter. |
| **IC** | Interlinking Converter. |
| **ICC** | Incremental Cost Consensus. |
| **INV** | Inverter. |
| **KKT** | Karush-Kuhn-Tucker. |
| **LPF** | Low-Pass-Filter. |
| **LPS** | Local Power Sharing. |
| **MAS** | Multi-Agent Systems. |
| **PCC** | Point of Common Coupling. |
| **PI** | Proportional-Integral. |
| **PLL** | Phase Locked-Loop. |
| **PR** | Proportional-Resonant. |
| **PV** | Photo-Voltaic. |

| | |
|---|---|
| **SPS** | Storage Power Sharing. |
| **SoC** | State of Charge. |
| **VC-VSC** | Voltage Controlled Voltage Source Converter. |
| **VSC** | Voltage Source Converter. |
| **WT** | Wind Turbine. |

# List of Symbols

| | |
|---|---|
| $\omega_r$ | Resonant frequency, proportional-resonant controller. |
| $k_r$ | Resonant gain, proportional-resonant controller. |
| $k_p$ | Proportional gain, proportional-integral controller. |
| $k_{\mathrm{i}}$ | Integral gain, proportional-integral controller. |
| $M_{\mathrm{ac-i}}$ | The i$^{th}$ *ac*-DG's active power droop gain. |
| $\omega_{\mathrm{i}}$ | The i$^{th}$ *ac*-DG's frequency. |
| $\omega_{MIN}$ | The *ac*-DG's minimum frequency. |
| $P_{MAX}$ | The *ac*-DG's maximum active power. |
| $N_{\mathrm{ac-i}}$ | The i$^{th}$ *ac*-DG's reactive power droop gain. |
| $E_{\mathrm{i}}$ | The i$^{th}$ *ac*-DG's voltage. |
| $E_{MIN}, E_{MAX}$ | The *ac*-DG's minimum/maximum voltage. |
| $Q_{MIN}, Q_{MAX}$ | The *ac*-DG's minimum/maximum reactive power. |
| $M_{\mathrm{dc-i}}$ | The $j^{th}$ *dc*-DG's active power droop gain. |
| $V_{\mathrm{i}}$ | The i$^{th}$ *dc*-DG's voltage. |
| $V_{MIN}$ | The *dc*-DG's minimum voltage. |
| $\hat{V}_{\mathrm{dc}}$ | Normalized voltage at the *dc*-side of the *IC*. |
| $\hat{\omega}_{\mathrm{ac}}$ | Normalized frequency at the *ac*-side of the *IC*. |
| $a_{\mathrm{i}j}$ | Element of the adjacency matrix $\mathbf{A}$. |
| $\mathrm{d}_{\mathrm{i}}$ | Diagonal in-degree of the adjacency matrix $\mathbf{A}$. |
| | |
| $\mathbb{N}_{\mathrm{ac}}$ | Set of *ac*-DGs in the *ac*-microgrid. |
| $\mathbb{N}_{\mathrm{dc}}$ | Set of *dc*-DGs in the *dc*-microgrid. |
| $\mathbb{N}_{\mathrm{IC}}$ | Set of *ICs* in the hybrid *ac*/*dc*-microgrid. |

| | |
|---|---|
| $\delta\omega_{\mathrm{D}}$ | Control action of *ac*-DG's active power droop controller. |
| $\delta E_{\mathrm{D}}$ | Control action of *ac*-DG's reactive power droop controller. |
| $P_{\mathrm{ac-i}}, Q_{\mathrm{ac-i}}$ | Instantaneous real/reactive power generated by the i$^{th}$ *ac*-DG. |
| $\psi_{\mathrm{i}}$ | Control action of frequency restoration controller. |
| $\psi_{\mathrm{ac-i}}$ | Control action of power consensus with *ac*-DGs. |
| $\psi_{\mathrm{dc-i}}$ | Control action of power consensus with *dc*-DGs. |
| $\sigma_{\mathrm{i}}$ | Time constant of frequency restoration controller. |
| $\chi_{\mathrm{i}}$ | Control action of *ac*-voltage restoration controller. |
| $\varrho_{\mathrm{i}}$ | Time constant of *ac*-voltage restoration controller. |
| $\beta_{\mathrm{i}}, b_{\mathrm{i}}$ | Positive gains of *ac*-voltage restoration controller. |
| $\delta V_{\mathrm{D}}$ | Control action of *dc*-DG's active power droop controller. |
| $\psi_{\mathrm{i}}$ | Control action of *dc*-voltage restoration controller. |
| $\psi_{\mathrm{dc-i}}$ | Control action of power consensus with *dc*-DGs. |
| $\psi_{\mathrm{ac-i}}$ | Control action of power consensus with *ac*-DGs. |
| $\rho_{\mathrm{i}}$ | Time constant of *dc*-voltage restoration controller. |
| $\gamma_{\mathrm{i}}, c_{\mathrm{i}}$ | Positive gains of *dc*-voltage restoration controller. |
| $P^{*}_{\mathrm{IC}-k}$ | Active power reference for the $k^{th}$ *IC*. |
| $\tau_k$ | Time constant of *IC* controller. |
| $\mu_k, \vartheta$ | Positive gain of *IC* controller. |
| | |
| $\mathbb{N}_{\mathrm{ac}}$ | Set of *ac*-DGs in the *ac*-microgrid. |
| $\mathbb{N}_{\mathrm{dc}}$ | Set of *dc*-DGs in the *dc*-microgrid. |
| $\mathbb{N}_{\mathrm{IC}}$ | Set of *ICs* in the hybrid *ac/dc*-microgrid. |
| $P^{\mathrm{D}}_{\mathrm{ac}}, P^{\mathrm{D}}_{\mathrm{dc}}$ | Lumped loads modelled for the optimization problem. |
| $P^{\mathrm{G}}_{\mathrm{ac-i}}$ | Power generated by the i$^{th}$ *ac*-DG. |
| $P^{\mathrm{G}}_{\mathrm{dc}-j}$ | Power generated by the $j^{th}$ *dc*-DG. |
| $P^{\mathrm{ac}}_{\mathrm{IC}-k}$ | Power transferred by the $k^{th}$ *IC*. |
| $P^{\mathrm{ac}}_{\mathrm{IC}}$ | Total power transferred at the *ac*-side of the *ICs*. |
| $P^{\mathrm{dc}}_{\mathrm{IC}}$ | Total power transferred at the *dc*-side of the *ICs*. |
| $P^{\mathrm{LOSS}}_{\mathrm{IC}}$ | Total power lost in the *ICs*. |
| $k^{\mathrm{LOSS}}$ | Percentage of the power lost in the *IC*. |
| $k_{\mathrm{IC}}, k^{\mathrm{LOSS}}_{\mathrm{IC}}$ | Parameters for power through the *IC*. |

| | |
|---|---|
| $\mathbf{P}^{\mathbf{G}}_{\mathbf{ac}}$ | Set of power generated by the *ac*-DGs. |
| $\mathbf{P}^{\mathbf{G}}_{\mathbf{dc}}$ | Set of power generated by the *dc*-DGs. |
| $\mathbf{P}^{\mathbf{ac}}_{\mathbf{IC}}$ | Set of power through the *ICs*. |
| $C_{\mathrm{ac-i}}$ | Cost function of the i$^{th}$ *ac*-DG. |
| $C_{\mathrm{dc}-j}$ | Cost function of the $j^{th}$ *dc*-DG. |
| $\{a,b,c\}_{\mathrm{ac-i}}$ | Parameters for the cost function of the i$^{th}$ *ac*-DG. |
| $\{a,b,c\}_{\mathrm{dc-i}}$ | Parameters for the cost function of the $j^{th}$ *dc*-DG. |
| $P^{\mathrm{G}-}_{\mathrm{ac-i}}, P^{\mathrm{G}+}_{\mathrm{ac-i}}$ | Limits for the power generated by the i$^{th}$ *ac*-DG. |
| $P^{\mathrm{G}-}_{\mathrm{dc}-j}, P^{\mathrm{G}+}_{\mathrm{dc}-j}$ | Limits for the power generated by the $j^{th}$ *ac*-DG. |
| $P^{\mathrm{ac}-}_{\mathrm{IC}}, P^{\mathrm{ac}+}_{\mathrm{IC}}$ | Limits for the power through the $k^{th}$*IC*. |
| $\lambda$ | Lagrange multiplier associated with the power balance constraint. |
| $\alpha^{+}_{\mathrm{ac-i}}, \alpha^{-}_{\mathrm{ac-i}}$ | Lagrange multiplier associated with the power limits of *ac*-DGs. |
| $\alpha^{+}_{\mathrm{dc}-j}, \alpha^{-}_{\mathrm{dc}-j}$ | Lagrange multiplier associated with the power limits of *dc*-DGs. |
| $\alpha^{+}_{\mathrm{IC}-k}, \alpha^{-}_{\mathrm{IC}-k}$ | Lagrange multiplier associated with the power limits of *ICs*. |
| $\lambda^{\mathrm{ac}}_{\mathrm{i}}$ | Lagrange multiplier for the i$^{th}$ *ac*-DG. |
| $\lambda^{\mathrm{dc}}_{j}$ | Lagrange multiplier for the $j^{th}$ *dc*-DG. |
| $\Omega^{\mathrm{ac}}_{\mathrm{i}}$ | Secondary control action for the i$^{th}$ *ac*-DG. |
| $k^{a,b,c,\mathrm{d},\mathrm{e}}_{\mathrm{ac-i}}, \mu^{a,b}_{\mathrm{ac-i}}$ | Positive gains of the *ac*-DG's controller. |
| $\Omega^{\mathrm{dc}}_{j}$ | Secondary control action for the $j^{th}$ *dc*-DG. |
| $k^{a,b,c,\mathrm{d},\mathrm{e}}_{\mathrm{dc}-j}, \mu^{a,b}_{\mathrm{dc}-j}$ | Positive gains of the *dc*-DG's controller. |
| $\tau^{a,b}_{\mathrm{IC}}, \mu^{a,b}_{\mathrm{IC}}$ | Positive gains of the *IC*'s controller. |
| $\lambda^{\mathrm{G}}$ | Lagrange multiplier associated with the power balance constraint. |
| $\lambda^{\mathrm{IC}}$ | Lagrange multiplier associated with the power transfer constraint. |
| $\lambda^{\mathrm{G}}_{\mathrm{ac-i}}$ | Lagrange multiplier for the i$^{th}$ *ac*-DG. |
| $\lambda^{\mathrm{G}}_{\mathrm{dc}-j}$ | Lagrange multiplier for the $j^{th}$ *dc*-DG. |
| $\lambda^{\mathrm{IC}}_{k}$ | Lagrange multiplier for the $k^{th}$ *IC*. |
| $\hat{P}^{\mathrm{ac}}_{\mathrm{IC}-g}$ | Total power estimated at the *ac*-side of the *ICs*. |
| $\hat{P}^{\mathrm{dc}}_{\mathrm{IC}-g}$ | Total power estimated at the *dc*-side of the *ICs*. |
| $\overline{k_{\mathrm{IC}}}$ | Average value of the variables $k_{\mathrm{IC}}$ received by the DGs. |
| $\overline{\lambda^{\mathrm{IC}}}$ | Average value of the variables $\lambda^{\mathrm{IC}}$ received by the DGs. |
| $\overline{\lambda^{\mathrm{G}}}$ | Average value of the variables $\lambda^{\mathrm{G}}$ received by the *ICs*. |
| | |
| $\tau_{\mathrm{d}}$ | Constant delay for experimental test #4. |
| $f_{pu}$ | Normalized frequency at the *ac*-side of the *IC*. |
| $V_{pu}$ | Normalized voltage at the *dc*-side of the *IC*. |

# Chapter 1

# Introduction

The continuous improvement in power electronic technologies, the strengthening of microprocessors, and the capability to implement more complex control strategies have allowed the researchers to address environmental concerns and focus on a significant effort in the research of microgrids. In the literature, a microgrid is defined as an electrical system capable of integrating different distributed generators (DGs) and loads, which can use both alternating or direct current (i.e., *ac* or *dc*). Moreover, a microgrid can also incorporate variable energy sources such as renewable energies operating with energy storage systems (ESS) [1]. Electric vehicles (EVs) correspond to a particular type of load since they can be used to manage the loading in the microgrid, and it is possible to implement demand-side management strategies by controlling their charge profiles [2]. The DGs supply electricity to the local loads, reducing the transmission stage's power loss [3]. Although it is possible to operate a microgrid with medium-voltages, its application at a low-voltage level is preferred [4,5]. Therefore, a massive inclusion of microgrids at the distribution level is highly probable in the short term. The operation of these systems needs to be studied to guarantee the electrical system's efficiency, safety, and reliability [6].

The general topology for an *ac*-microgrid is presented in Fig. 1.1a [7]. Traditionally, an *ac*-microgrid is composed of *ac*-energy sources, which can be renewable (such as photo-voltaic panels (PVs) or wind turbines (WTs) interfaced through power converters) or non-renewable (such as diesel generators (DiGens)) energy-based DGs, and *ac*-loads connected through a 3-wire (or 4-wire) *ac*-bus. On the other hand, since the *ac*-microgrid can supply (at least a part of) the power demanded by the loads, it can work autonomously without a connection to the main grid [8]. Therefore, the microgrid can operate in "islanded" or "grid-connected" mode, based on the status of the switch (see Fig. 1.1a) [9]. The focus of this thesis is on the "islanded" mode of operation.

Since *dc*-power generation and *dc*-loads have had significant growth in recent years, *dc*-microgrids and *dc*-distribution networks have caught the attention of researchers [10–14]. The general topology for a *dc*-microgrid is presented in Fig. 1.1b. As described before for the *ac*-microgrid, a *dc*-microgrid is comprised of renewable energy-based DGs (e.g., PVs and WTs), ESSs and *dc*-loads (*ac*-loads may also be connected through *ac*-to-*dc* converters) connected through a *dc*-bus. On the other hand, the *dc*-microgrid can also operate in "islanded" or

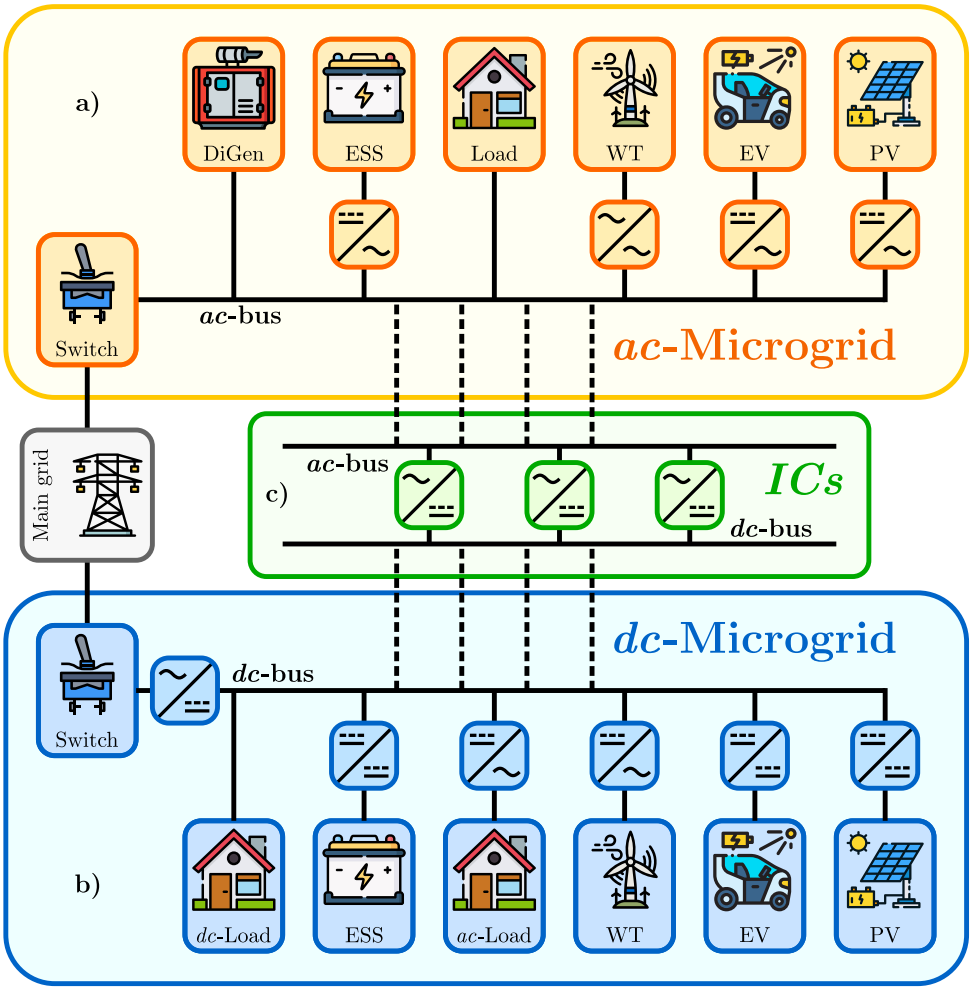


Figure 1.1: General topology for a hybrid *ac*/*dc*-microgrid. a) *ac*-microgrid. b) Interlinking converters. c) *dc*-microgrid.

"grid-connected" mode (through a *dc*-to-*ac* converter), based on the status of the switch. As mentioned before, the focus of this thesis is on the "islanded" mode operation.

Around the world, the distribution systems are mainly *ac*-distribution systems, and it is not economically (or even technically) possible to replace the existing *ac*-distribution systems with *dc*-microgrids, despite the enormous potential of the *dc*-microgrids. Therefore, it is more plausible to consider an electrical system that merges the two systems described before in the short or mid-term taking advantage of the benefits that each of them has [15]. In other words, it is possible to view the *ac*-microgrids and the *dc*-microgrids operating together, i.e., as a single entity, interfaced through one or more Interlinking Converters (*ICs*) as presented in Fig. 1.1c [16]. These systems are known as "hybrid *ac*/*dc*-microgrids", and their operation and control have become an essential topic for research [17–19]. This is the main topic for the research developed in this thesis.

The microgrid (*ac*, *dc* or hybrid *ac*/*dc*) is seen by the main grid as a single entity when operated in grid-connected mode due to having a single point of common coupling (PCC). The DGs do not have to regulate both the nominal amplitude and frequency of the voltages

in the microgrid since the main grid (stiff grid) sets those parameters. The DGs can control the exchange of active power (or reactive power in the *ac*-microgrid) between the main grid and the microgrid (i.e., the DGs act as "grid following" units) [20]. On the other hand, in an isolated microgrid (i.e., islanded mode operation), the DGs need to maintain the amplitude and frequency of the voltages within limits all the time (i.e., the DGs act as "grid forming" or "grid supporting" units). However, in the islanded mode, it is also possible to have "grid following" units.

Controlling the DGs in a hybrid *ac/dc*-microgrid (i.e., *ac*-DGs and *dc*-DGs working collaboratively) is more complex than when the microgrids are operating separately. In addition to controlling the internal variables and the interaction of the DGs within each microgrid, it is necessary to control the interaction of the DGs on both sides, that is, between *ac*-DGs and *dc*-DGs. Thus, the control of the power transfer through the *IC* is crucial for achieving the required operation of the hybrid *ac/dc*-microgrid [21]. Different objectives can be defined for the operation of the DGs. For example, one can mention active power-sharing among DGs on both sides based on power ratings of units [22,23], active power-sharing within microgrids and transferring power through the *IC* in case one microgrid is overloaded [24], to name a few. However, in all cases the hybrid *ac/dc*-microgrid is considered as 3 independent systems interacting with each other and not as a single entity.

Although the hybrid *ac/dc*-microgrid may have only one *IC*, the most general topology employs multiple *ICs*. In the former case, the most typical control strategy for the *IC* is to equalize the normalized frequency (at the *ac*-side) and voltage (at the *dc*-side) [15], However, this strategy is not as effective when the microgrid has many buses. On the other hand, in the latter case, additional controllers should be used since the voltage at the *dc*-side of the *ICs* is not necessarily equal at all the buses [22]. However, in most cases reported in the literature the secondary control is not considered.

Based on the hierarchical control approach [5], the secondary control loop can be implemented as a centralized controller, a decentralized controller or a distributed controller (see Fig. 1.2) [25, 26]. The most typical approach considers a central controller (*centralized approach*), which requires a communication link with all the agents in the microgrid, as shown in Fig. 1.2a. Therefore, this strategy is prone to single-point failures and its implementation is infeasible with a large microgrid since the computational burden is too high. The *decentralized approach* lacks a central controller and all the agents operate with local information (see Fig. 1.2b). Thus, it is hard to achieve collaborative objectives among the agents with this approach. Finally, the *distributed approach* does not require a central station for control, and agents work autonomously in a cooperative fashion to reach a global objective (see Fig. 1.2c). This approach is more robust since each agent needs to communicate only with its neighbouring agents [27].

Motivated by the aforementioned considerations, the main focus of this thesis is on developing a distributed secondary control strategy that considers the hybrid *ac/dc*-microgrid as a single entity and not as three independent systems interacting with each other. In addition to restoring the variables modified by the primary control, the proposed control strategy must be capable of assigning a secondary control objective to the DGs in the hybrid *ac/dc*-microgrid, such as sharing power between the DGs (and between the *ICs*) or minimizing

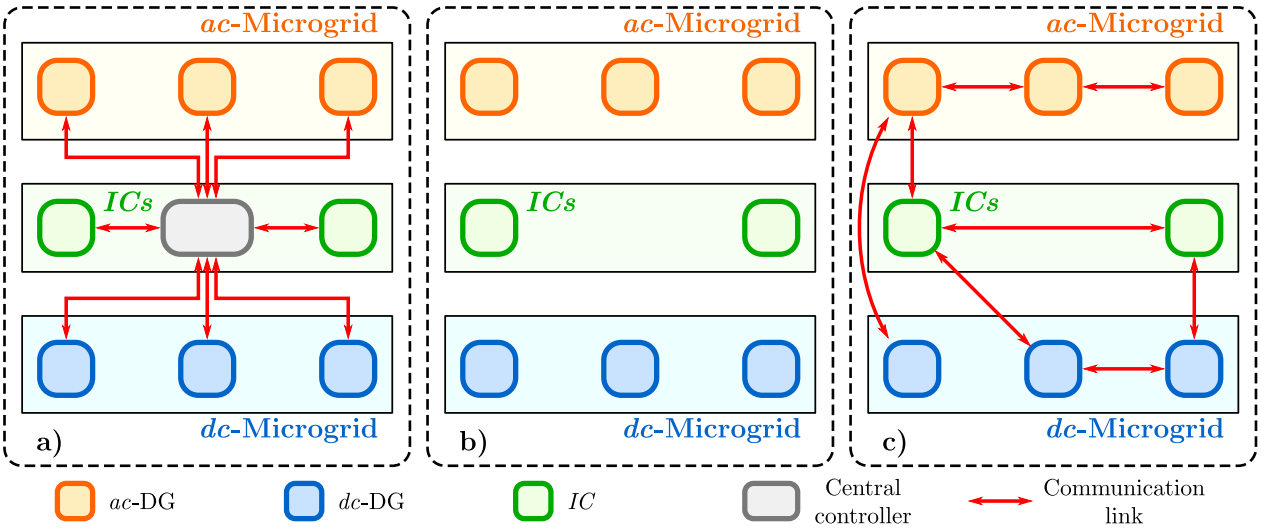


Figure 1.2: Secondary control types for microgrid control. a) Centralized. b) Decentralized. c) Distributed.

the total operating costs of the microgrid. In addition, the thesis will provide guidelines to obtain an analytical closed-loop model for the hybrid *ac*/*dc*-microgrid with the proposed control strategies, deriving the stable limits of the controllers and validating their tuning. Furthermore, several experimental and simulation tests will validate the performance of the control schemes.

The Ph.D. program of this candidate is developed under a Cotutelle Agreement (double-degree agreement) between the **University of Chile, Chile**, and the **University of Waterloo, Canada**.

## 1.1 Project Hypotheses

The main hypotheses that support this Ph.D. project are described below. Particularly, this thesis explores the implementation of distributed secondary control strategies applied to hybrid *ac*/*dc*-microgrids to regulate frequency, *ac*-voltage amplitude and *dc*-voltage magnitude, while augmenting the objective of the controller with either a power-consensus improvement or an operation cost minimization. The main feature of this strategy is to utilize a distributed communication network that considers the interlinking converters and to include them in the control scheme.

- A consensus-based distributed secondary control strategy could be designed and implemented in a hybrid *ac*/*dc*-microgrid in order to simultaneously regulate *ac*-voltage magnitude and frequency, as well as the *dc*-voltage magnitude, by including the interlinking converters in the control strategy.

- The controller could be augmented with either a power-sharing improvement or an operation cost minimization. This second control task could be performed by considering the information of the nearest neighbours from both sides of the microgrid, i.e., achieving a common consensus among *ac*-DGs and *dc*-DGs.

- The inclusion of an *IC* for the power/energy exchange between the *ac*-side and the *dc*-side of a hybrid *ac/dc*-microgrid in the distributed communication network could help the secondary control task and reduce the possibility of instability due to a failure on this device. To achieve the former, the *IC* should communicate with, at least, one DG from each sub-microgrid.

- Additionally, if the *IC* is considered in the communication network, it could be possible to automatically divide the secondary control strategy for the hybrid *ac/dc*-microgrid into two separate strategies. Separately, these strategies should be able to regulate the secondary variables within each microgrid and to perform the second objective: *(i)* independently equalize the power being generated by the *ac*-DGs and *dc*-DGs, normalized to the units' ratings, or *(ii)* re-dispatch the DGs to minimize the operation cost within each microgrid.

- If multiple *ICs* are considered in the distributed communication network, it could be possible to maintain the performance of the distributed secondary controller under contingency of one *IC*. Even though the control of the hybrid *ac/dc*-microgrid is more complex, the inclusion of multiple *ICs* helps to improve reliability and security of the electrical system.

- By considering multiple *ICs* in the distributed secondary control strategy and, hence, in the distributed communication network, it could be possible to control and to reduce the unwanted circulating currents in the *dc*-side of the *ICs*.

- The correct tuning of the distributed controllers proposed in this Thesis can be verified by the analysis of a closed-loop model of the hybrid *ac/dc*-microgrid. Moreover, the stable limits of the gains can be derived from this model.

## 1.2 Project Objectives

### General Objective

This Ph.D. research project is aimed to study and investigate the design and implementation of consensus-based distributed secondary control strategies for hybrid *ac/dc*-microgrids, treating the microgrid as one electric entity and not as three independent systems (i.e., *ac*, *dc* and *IC*).

### Specific Objectives

The research described in this thesis pursues to accomplish the following objectives:

- To design and implement a distributed secondary control strategy for achieving active power consensus among all the DGs in a hybrid *ac/dc*-microgrid, i.e., *ac*-DGs and *dc*-DGs.

- To validate (experimentally and with simulations) the effectiveness of the secondary control strategy for active power consensus.

- To design and implement a distributed secondary control strategy for minimizing (in real-time) the operation cost in a hybrid *ac/dc*-microgrid, including the losses in the *ICs* in the formulation of the optimization problem.

- To validate (with simulations) the effectiveness of the secondary control strategy for operation cost minimization.

- To obtain a small-signal closed-loop model for verifying the tuning and deriving the stable limits of the two proposed controllers. In addition, the stability of the controllers can be studied with the closed-loop model.

- To design and implement a scaled down prototype of a hybrid *ac/dc*-microgrid to validate the proposed control strategies in an experimental rig.

## 1.3 Contributions

The contributions of this work can be summarized as follows:

- Two coordinated distributed secondary control strategies for hybrid *ac/dc*-microgrids are proposed, which treat the hybrid microgrid as one electrical entity and not as three independent systems (i.e., *ac*, *dc*, and *IC*). The proposed strategies achieve seamless restoration of the variables modified by the primary control at both sides of the hybrid *ac/dc*-microgrid, while achieving either active power consensus (first strategy) or operation cost minimization (second strategy).

- The active powers transferred through the *ICs* are considered in the consensus functions and algorithms proposed in this work, which avoids circulating currents and achieves either an accurate power-sharing between the *ICs* (first strategy) or a loss minimization in the *ICs* (second strategy).

- The strategy achieves plug-and-play capability and robustness of the hybrid *ac/dc*-microgrid; power-sharing (first strategy) or cost minimization (second strategy) are achieved even if *ICs* (or DGs) are connected or disconnected.

- The viability and effectiveness of the proposed control strategies have been validated using a 24kW hybrid *ac/dc*-microgrid prototype. A simulation study is also considered for including several scenarios which cannot be validated using the lab prototype, including scenarios with multiple *ICs*.

- Two analytical models of the closed-loop systems for the hybrid *ac/dc*-microgrid with the proposed consensus-based secondary control strategies are developed, which permit small-signal stability analysis and parameter tuning for the two proposed strategies.

- The work developed during this project has resulted in the publication of 3 international conference papers [28–30] and 4 journal papers [26,31–33] submitted to top-tier indexed journals. In addition, 11 manuscripts have been published, with the candidate as a co-author [34–44]. The details of these publications and other contributions to papers related to microgrids are listed in Chapter 9.3.

## 1.4 Thesis Structure

The rest of this work is divided into nine Chapters, as follows:

**Chapter 2** extensively reviews the secondary control strategies for hybrid *ac/dc*-microgrids proposed in the literature. Particular emphasis is placed on consensus-based distributed schemes. Furthermore, optimization techniques applied to hybrid *ac/dc*-microgrids are also addressed.

**Chapter 3** proposes a secondary control strategy that simultaneously regulates *ac*-voltage magnitude and frequency, as well as the *dc*-voltage magnitude, by including the interlinking converters in the control strategy via a distributed consensus approach. This improves the power-sharing accuracy and secondary control restoration of the variables in both *ac*-and *dc*-sides of the microgrid.

**Chapter 4** introduces a new secondary control strategy that, as the one described in Chapter 3, simultaneously regulates *ac*-voltage magnitude and frequency, as well as the *dc*-voltage magnitude, while the DGs and the *ICs* (if multiple *ICs* are available) are dispatched to minimize the operation cost of the hybrid *ac/dc*-microgrid.

**Chapter 5** describes the design and construction of an experimental prototype of a hybrid *ac/dc*-microgrid composed of six *dc*-DGs, three *ac*-DGs and a single *IC*. The capabilities and characteristics of the control platform, power stage and power sources used to emulated the experimental system are detailed.

**Chapter 6** presents two analytical closed-loop models of the proposed secondary control strategies proposed in this thesis, which are used to derive the stable limits for the controller's gains and verify their tuning. Moreover, a small-signal analysis is performed with the closed-loop models obtained in this Chapter, identifying the eigenvalues of the characteristic matrix and their participation factors.

**Chapter 7** shows the experimental and simulation validation for the control strategy proposed in Chapter 3. A set of experimental tests for step-changes in the load, plug-and-play of DGs and communication issues, such as communication delays and communication failures, are included. A set of simulation tests for a microgrid with multiple *ICs* and performance comparison against other control schemes reported in the literature are included.

**Chapter 8** displays the simulation validation for the control strategy proposed in Chapter 4. A set of simulation tests for enabling the control loops and step-changes in the load at both sides are included, for hybrid *ac/dc*-microgrids considering one or more *ICs*. Finally, a comparison test for the two secondary control strategies proposed in this thesis is depicted.

**Chapter 9** summarizes the contents presented in this thesis, suggests possible directions for the future research on the topics addressed in this work, and presents a summary of the works published during this Ph.D. project, including manuscripts derived from the work in this thesis and other papers where the candidate has contributed.

# Chapter 2

# State of the Art

## 2.1 Introduction

In this Chapter, the state of the art regarding topologies and control strategies applied to microgrids is presented. The main control strategies and topologies applied to both *ac*- and *dc*-microgrids are presented. However, special attention is focused on hybrid *ac*/*dc*-microgrids considering Interlinking Converters (*ICs*) and Distributed Secondary Control (DSC) systems for hybrid *ac*/*dc*-microgrids.

The Chapter is organized as follows: a comprehensive background about hierarchical control strategies for *ac*-microgrids (Section 2.2), *dc*-microgrids (Section 2.3), and hybrid *ac*/*dc*-microgrids (Section 2.4) is presented. Section 2.5 shows the fundamentals of cooperative control of multiagent systems, which is the basis of the distributed secondary control strategies proposed in this work. Finally, Section 2.6 reviews the state of the art regarding DSC applied to *ac*-, *dc*-, and hybrid *ac*/*dc*-microgrids.

## 2.2 Control of *ac*-Microgrids

As mentioned in Chapter 1, the focus for this thesis is on the "islanded mode" operation of hybrid *ac*/*dc*-microgrids. Therefore, the DGs need to operate in coordination to supply the power demanded by the loads and ensure a good quality of the energy supplied. The most typical objective for the microgrid's control is to proportionally share the load power based on the nominal capacities of the DGs [45–48]. However, different functionalities have been proposed to coordinate the DGs, such as secondary variables restoration or power-sharing improvement [18]. Although these functionalities can be performed with a centralized control strategy, a fast communication network is required if the system's reliability has to be maintained. However, a centralized controller gets expensive and unfeasible as the number of DGs increases in the microgrid.

Droop control is the most commonly used control scheme to share the generated power among the DGs in a microgrid, which follows a decentralized approach relying solely on local measurements. Although this control strategy has a stable, reliable, and fast operation, it causes deviations of the microgrid variables (frequency and amplitude of the voltages in the *ac*-microgrids, and magnitude of the voltages in the *dc*-microgrids) from their nominal values, which is a significant drawback of this decentralized controller. Moreover, it is not possible to implement a higher level of coordination between the DGs since this control is based on local measurements only. Thus, in order to take advantage of the benefits of the decentralized and centralized (or distributed) schemes — i.e., low cost and high reliability of the former, and coordination flexibility of the latter — a hierarchical control structure should be considered.

In the hierarchical control structure, the control is separated in three main layers: the primary, the secondary and the tertiary control loops, as can be seen in Fig. 2.1 for a fully centralized approach (see Fig. 2.1a) and a distributed approach (see Fig. 2.1b). Firstly, the primary control loop corresponds to the decentralized droop control. Secondly, the secondary control loop which restores the secondary variables to their nominal values using a slow-communication-based scheme. Finally, the slower higher level tertiary control loop manages the energy exchange of the microgrid (mostly when it is operating in "grid-tied" mode); however, since the focus of this thesis is on "islanded" microgrids, this control level is not considered in this work. Additionally, an internal (or zero) control loop is needed to control the internal variables (current/voltage) of the DGs [49–51]. It is worth mentioning that the higher the control level is, the smaller the bandwidth becomes [5]. The hierarchical control loops for *ac*-microgrids are described in the following.

### 2.2.1 Primary Control of *ac*-Microgrids

The primary control loop for *ac*-microgrids is primarily responsible for setting the current and voltage at the output of the *ac*-DGs. Furthermore, it regulates the power-sharing among different *ac*-DGs in the *ac*-microgrid. The typical configuration for a power-electronic-interfaced *ac*-DG is presented in Fig. 2.2, which consists of a three-phase voltage source converter (VSC) and an LC-LCL filter connected to the *ac*-microgrid though an output impedance [52]. The primary controller comprises the inner control loop (current/voltage control loops) and the droop controller. Although a single voltage control loop is sufficient to control the output voltage in an *ac*-DG (e.g., a proportional-resonant controller is capable of controlling the

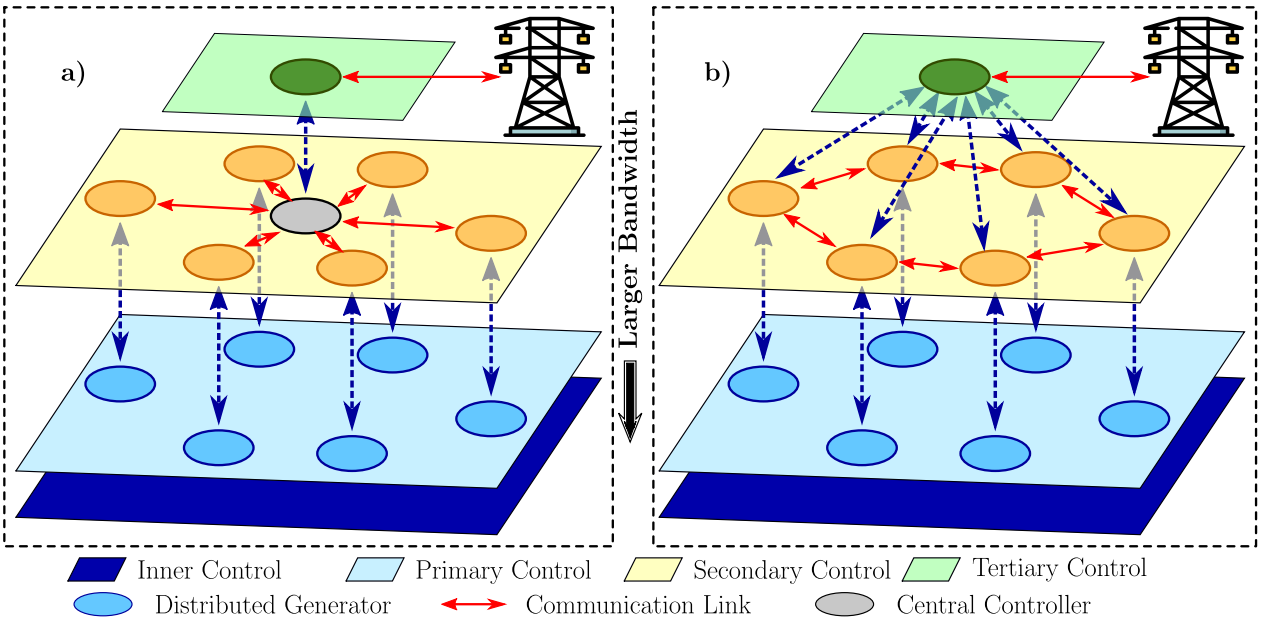


Figure 2.1: Hierarchical control structure for microgrids. a) Centralized. b) Distributed.

output voltage), it is recommended to include a nested control scheme with an inner (current) control loop and an outer (voltage) control loop. These controllers are described in the following.

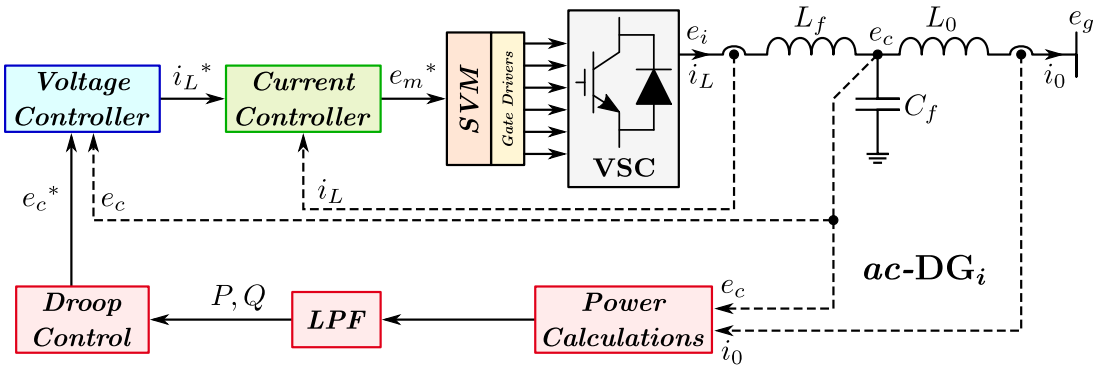


Figure 2.2: Primary control loop for the *ac*-DGs.

### Current Control

A nested controller is preferred since the (inner) current control loop is able to limit the output current for protection purposes while controlling the current injected by the VSC. The current control loop is the fastest in the system, i.e., it has the largest bandwidth. It can be implemented using different types of controllers; however, the most commonly used in the literature are the Proportional-Integral (PI) controller and the Proportional-Resonant (PR) controller. Due to the oscillatory nature of the *ac*-voltage, the currents must be converted into the *dq* synchronous reference frame for the implementation of the PI-controller. On the other hand, the PR-controller can be implemented in either the *abc* natural reference frame or the $\alpha\beta$ stationary reference frame.

Regarding the PI-controller implemented in $dq$ reference frame, it is necessary to implement an additional negative-sequence controller to operate in parallel with the positive sequence controller. Furthermore, additional controllers (one for each harmonic frequency to be compensated) must be implemented for harmonic compensation when nonlinear loads are present. On the other hand, PR-controllers in $\alpha\beta$ reference frame show some advantages over PI-controllers in $dq$ reference frame. For example, both positive and negative sequence currents can be controlled at the same time with the PR-controller. Therefore, PR-controllers are used in this work. Fig. 2.3 shows the block diagram (see green blocks) of the current PR-controller in $\alpha\beta$ frame. The general transfer function for a controller with a resonant frequency $\omega_r$ is given by (2.1).

$$PR(s) = k_p + \frac{k_r s}{s^2 + {\omega_r}^2} \tag{2.1}$$

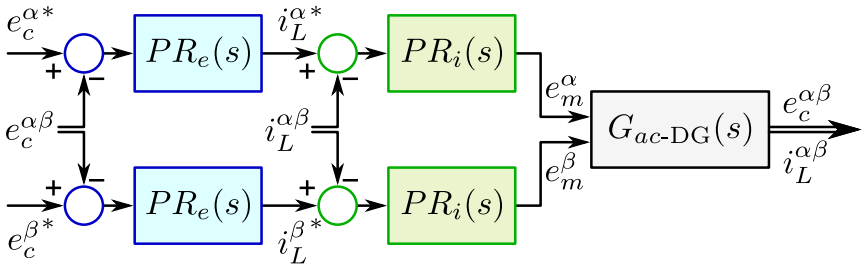


Figure 2.3: Inner control loop (voltage/current) for the $ac$-DGs.

### Voltage Control

The voltage control loop is the outer loop in the nested controller, and its bandwidth must be at least seven times smaller than that of the current control loop to avoid coupling. The voltage controller is responsible for the VSC to follow the voltage reference by setting the reference currents for the current control loop.

As described for the current control loop, voltage controllers can be implemented either in $dq$ or in $\alpha\beta$ reference frames. In this case, the PR-controller is considered. Fig. 2.3 shows the block diagram (see blue blocks) of the PR voltage controller implemented in $\alpha\beta$ reference frame, and the transfer function is shown in (2.1).

### Droop Control

The droop control is used in the primary control level to ensure the power-sharing among the generation units [5, 45, 46, 48]. This stage has the smallest bandwidth within the local controller of the $ac$-DG. The power droop controller sets the voltage reference by defining both the voltage amplitude and frequency to the inner voltage controller based on the converter output active and reactive powers.

Traditionally, and considering that the $ac$-microgrid is composed of purely inductive lines, the droop control used in the $i^{th}$ inverter to obtain an accurate active power-sharing ($P_i$) among the $ac$-DGs needs to modify the frequency of the voltages ($\omega_i$) emulating the mechanical/electrical behaviour of classical synchronous machines [53], as shown in Fig. 2.4a

for a generation unit (i.e., unidirectional active power). On the other hand, the conventional droop control of the i$^{th}$ inverter modifies the amplitude of the voltages ($E_{\mathrm{i}}$) generated to share the reactive power ($Q_{\mathrm{i}}$) among the generation units [48,54], as shown in Fig. 2.4b. The droop-slopes of the active power ($M_{\mathrm{ac}}$) and reactive power ($N_{\mathrm{ac}}$) droop-curves are given by (2.2).

$$M_{\mathrm{ac}} = \frac{\omega_{MIN} - \omega^*}{P_{MAX}}, \qquad N_{\mathrm{ac}} = \frac{E_{MIN} - E_{MAX}}{Q_{MAX} - Q_{MIN}} \tag{2.2}$$

where $\omega^*, E^*$ are the nominal frequency and voltage amplitude, respectively, $\omega_{MIN}$, $E_{MIN}$, $E_{MAX}$ are the frequency and voltage amplitude limits, and $P_{MAX}$, $Q_{MIN}$, $Q_{MAX}$ are the active and reactive power limits of the i$^{th}$ *ac*-DG. Thus, the conventional droop controllers for the i$^{th}$ *ac*-DG are described mathematically by:

$$\omega_{\mathrm{i}} = \omega^* + M_{\mathrm{ac-i}} P_{\mathrm{i}} \tag{2.3a}$$

$$|E_{\mathrm{i}}| = E^* + N_{\mathrm{ac-i}} Q_{\mathrm{i}} \tag{2.3b}$$

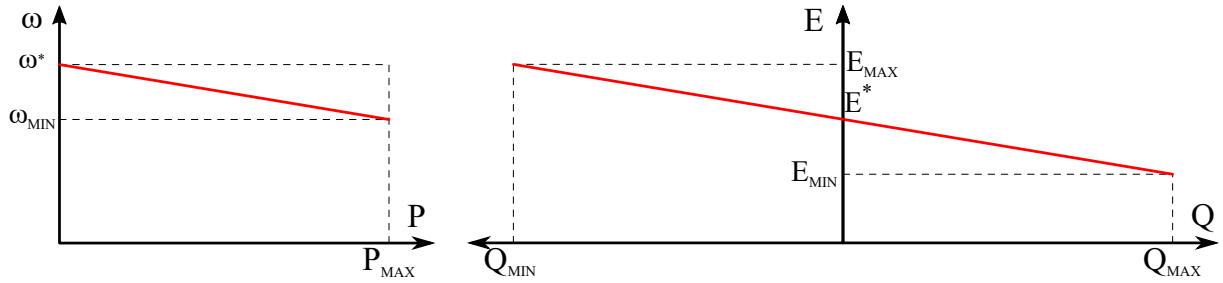


(a) Active power. (b) Reactive power.

Figure 2.4: Droop curves for control of the *ac*-microgrid.

### 2.2.2 Secondary Control of *ac*-Microgrids

As mentioned before, the primary control loop (droop controller) is an efficient decentralized scheme to achieve proportional power-sharing among the *ac*-DGs since it is fast, reliable and only relies on local measurements [55]. Nonetheless, it produces deviations in the frequency and amplitude of the *ac*-voltages and an inaccurate reactive power-sharing among *ac*-DGs due to the differences in the output voltages and line impedances. Furthermore, it is impossible to implement higher-level coordination since the control system lacks a communication network. Therefore, the main objective for the secondary control level is to resolve the drawbacks mentioned above from the primary control level.

Since secondary control level is a higher-level control, its bandwidth is smaller than that of the primary control level; thus, lowering the communication network bandwidth requirements. Centralized, decentralized and distributed secondary controllers have been addressed in the literature [56–62]. However, since the focus of this work is on distributed control strategies, this structure will be thoroughly discussed in Section 2.5, while the others are briefly discussed in the following.

### Frequency Restoration

As mentioned before, the main objective for the secondary control level is to restore the variables modified by the primary level control (droop controller). From the active power droop controller (2.3a), the frequency of the voltage of the i$^{th}$ *ac*-DG will be adjusted when the active power demand changes to share the active power among the *ac*-DGs. This deviation in the frequency may cause issues in the operation of the *ac*-microgrid [63, 64]; thus, it is necessary to regulate the frequency and ensure the system is operating at the nominal frequency. Since the frequency of the *ac*-microgrid (in steady-state) is a global variable, the frequency restoration controller may use the measurement of the frequency in the microgrid at any arbitrary node.

The most typical secondary frequency controller is presented in Fig. 2.5 [65, 66]. The frequency is restored by vertically shifting the droop curve, as shown in Fig. 2.5b. Usually, a PI controller is used to determine the amount of the displacement of the curve, as shown in Fig. 2.5a.

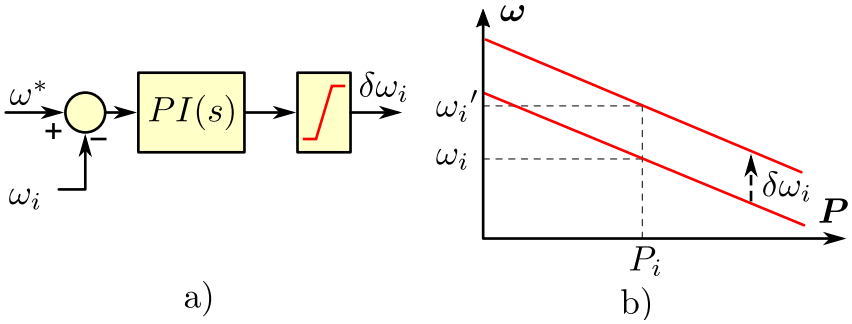


Figure 2.5: Secondary control loop for frequency restoration in the *ac*-DGs. a) Frequency restoration controller. b) Controller action.

### Voltage Amplitude Restoration

From the reactive power droop controller (2.3b), the amplitude of the voltage in the i$^{th}$ *ac*-DG will be adjusted when the reactive power demand changes to share the reactive power among the *ac*-DGs. To avoid the undesired operation of the *ac*-microgrid, it is necessary to regulate the amplitude of the voltages [2, 5].

A decentralized approach uses the local voltage of the *ac*-DG, i.e., the measured voltage at the output of the VSC. This controller is presented in Fig. 2.6 and it works shifting the droop-curve as in frequency restorer control [54, 63, 66]. However, since the local voltages are not equal at different points in the *ac*-microgrid, the voltage restoration is applied to the average voltage of the *ac*-microgrid in the centralized approach. On the other hand, the voltage restoration produces inaccurate reactive power-sharing among the *ac*-DGs, which can be controlled as follows.

In the literature, virtual impedances have been considered to improve the reactive power-sharing in *ac*-microgrids. In [63], the authors consider the implementation of a virtual impedance to share the active and reactive powers. However, it is not possible to do it accurately when the load is unbalanced or non-linear, although it is possible to share it with

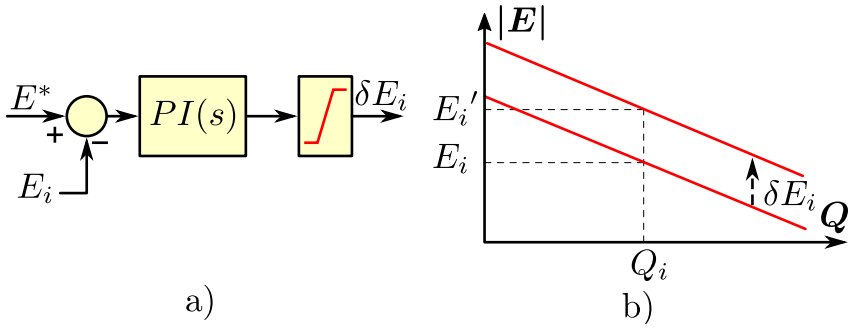


Figure 2.6: Secondary control loop for voltage restoration in the *ac*-DGs. a) Voltage restoration controller. b) Controller action.

a mismatch of the feeder impedance. The unbalanced load condition is addressed in [67] by an enhanced virtual impedance strategy, and the non-linear load condition is studied in [68]. The reactive power-sharing under unbalanced or non-linear load is achieved in [69]. However, any change in the microgrids topology (e.g., connection/disconnection of any load or feeder) may produce instability. A modification from the $Q$-$E$ droop-curve to a $Q$-$f$ droop curve was proposed in [70], which can be applied in case the lines in the *ac*-microgrid are highly resistive.

## 2.3 Control of *dc*-Microgrids

The structure for the control system of *dc*-microgrids is the same that the one described for *ac*-microgrids (see Section 2.2), i.e., the hierarchical control structure. Decentralized power-sharing is implemented in the primary control level by droop controllers, whereas the voltage regulation, power-sharing corrections, and/or optimization strategies are performed in the secondary control level. Tertiary control level is responsible for the energy exchange with external grids; however, since the focus for this thesis is on "islanded" microgrids, this control level is not considered in this work. The primary and secondary control loops for *dc*-microgrids are described in the following.

### 2.3.1 Primary Control of *dc*-Microgrids

The primary control loop for *dc*-microgrids is primarily responsible for setting the current and voltage at the output of the *dc*-DGs. Furthermore, it regulates the power-sharing among different *dc*-DGs in the *dc*-microgrid. The typical configuration for a power-electronic-interfaced *dc*-DG is presented in Fig. 2.7, which consists of a *dc*-to-*dc* converter and an LC or LCL filter connected to the *dc*-microgrid through an output impedance [52]. As for the *ac*-microgrid, the primary controller comprises the inner control loop (current/voltage control loops) and the droop controller. These controllers are described in the following.

#### Current Control

As for the *ac*-microgrid, a nested controller is preferred since the (inner) current control loop is able to limit the output current for protection purposes while controlling the current injected by the *dc*-to-*dc* converter. The current control loop is the fastest in the system, i.e.,

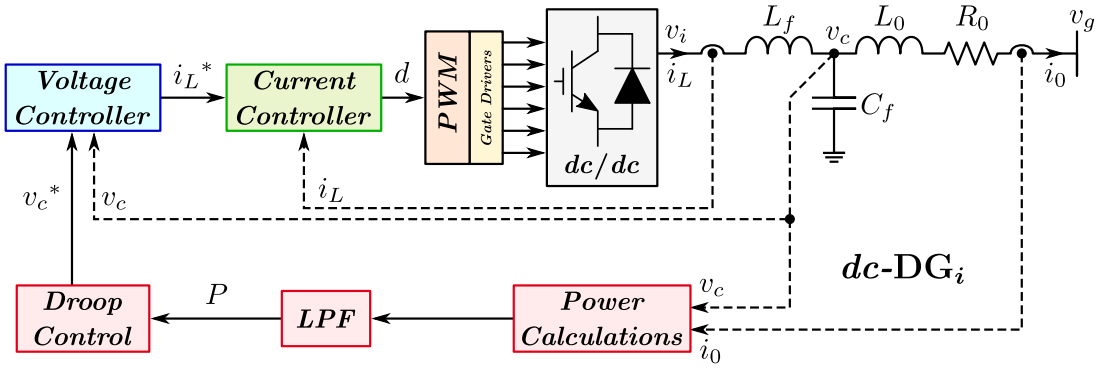


Figure 2.7: Primary control loop for a *dc*-DG.

it has the largest bandwidth. It can be implemented with several controllers; however, the most commonly used in the literature is the PI-controller. Fig. 2.8 shows the block diagram (see green block) of the current PI-controller, and its transfer function is given by (2.4). The current controller gains are set to allow stable operation with the largest possible bandwidth.

$$PI(s) = k_p + \frac{k_\mathrm{i}}{s} \tag{2.4}$$

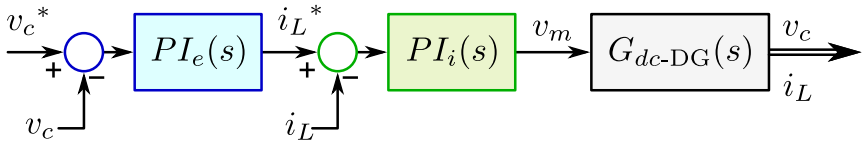


Figure 2.8: Inner control loop (voltage/current) for the *dc*-DGs.

### Voltage Control

The voltage control loop is the outer loop in the nested controller, and its bandwidth must be at least ten times smaller than that of the current control loop to avoid coupling. The voltage controller is responsible for making the *dc*-to-*dc* converter follow the voltage reference by setting the reference current for the current control loop.

As described for the current control loop, for the voltage control loop a PI-controller is implemented. Fig. 2.8 shows the block diagram (see blue block) of the PI voltage controller implemented, and the transfer function is shown in (2.4).

### Droop Control

As mentioned before, droop controllers are used in the primary control level to ease the power-sharing among the DGs. This stage has the smallest bandwidth within the local controller of the *dc*-DG. The power droop controller sets the voltage reference by defining its magnitude to the inner voltage controller based on the converter output active power.

Either current or power droop curves can be used in *dc*-microgrids to facilitate current or power-sharing between parallel *dc*-DGs, respectively. However, power droop control ($P$-$V$) is considered in this work, since the main focus is on hybrid *ac*/*dc*-microgrids which require

power-sharing or power dispatch between the two sub-microgrids. As for *ac*-microgrids, the droop controller gain is defined based on the operation limits of the *dc*-DG and the accepted voltage deviation. Fig. 2.9 shows the droop characteristics of generators in *dc*-microgrids with unidirectional power (ESS are out of the scope of this work), and the droop-slope ($M_{\mathrm{dc}}$) of the active power droop-curve is given by:

$$M_{\mathrm{dc}} = \frac{V_{MIN} - V^*}{P_{MAX}} \tag{2.5}$$

where $V^*$ is the nominal voltage magnitude, $V_{MIN}$ is the minimum voltage limit, and $P_{MAX}$ is the active power limit of the i$^{th}$ *dc*-DG. Thus, the conventional droop controller for the i$^{th}$ *dc*-DG is described mathematically by:

$$V_{\mathrm{i}} = V^* + M_{\mathrm{dc-i}} P_{\mathrm{i}} \tag{2.6}$$

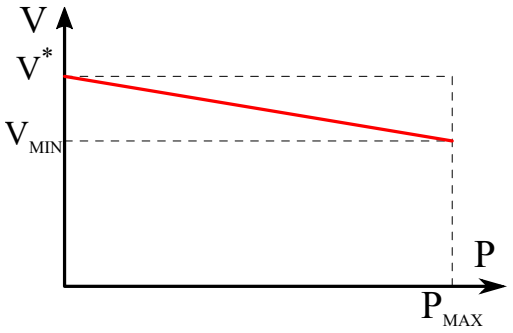


Figure 2.9: Droop curves for control of the *dc*-microgrid.

### 2.3.2 Secondary Control of *dc*-Microgrids

As mentioned before, the primary control loop (droop controller) in *dc*-microgrids produces deviations in the magnitude of the *dc*-voltages and an inaccurate power-sharing among *dc*-DGs due to the differences in the output voltages and line resistances. Furthermore, same as for the *ac*-microgrid, it is impossible to implement higher-level coordination since the control system lacks a communication network. Therefore, the main objective for the secondary control level is to resolve the drawbacks mentioned above for the primary control level.

Since secondary control level is a higher-level control, its bandwidth is smaller than that of the primary control level; thus, the bandwidth of the communication network may also be small. Centralized, decentralized and distributed secondary controllers have been studied in the literature [11, 12, 71]. However, since the focus of this work is on distributed control strategies, this structure will be thoroughly discussed in Section 2.5, while the others are briefly discussed in the following.

#### Voltage Magnitude Restoration

From the power droop controller (2.6), the voltage in the i$^{th}$ *dc*-DG will be adjusted when the power load changes to share the power among the *dc*-DGs. To avoid the undesired operation of the *dc*-microgrid, it is necessary to regulate the voltages [72, 73].

A decentralized approach uses the local voltage of the *dc*-DG, i.e., the measured voltage at the output of the VSC. This controller is presented in Fig. 2.10 and it works by vertically shifting the droop-curve [74, 75]. However, since the local voltages are not equal for different points in the *dc*-microgrid, the voltage restoration is applied to the average voltage of the *dc*-microgrid in the centralized approach. On the other hand, the voltage restoration produces inaccurate power-sharing among the *dc*-DGs, which can be controlled as follows.

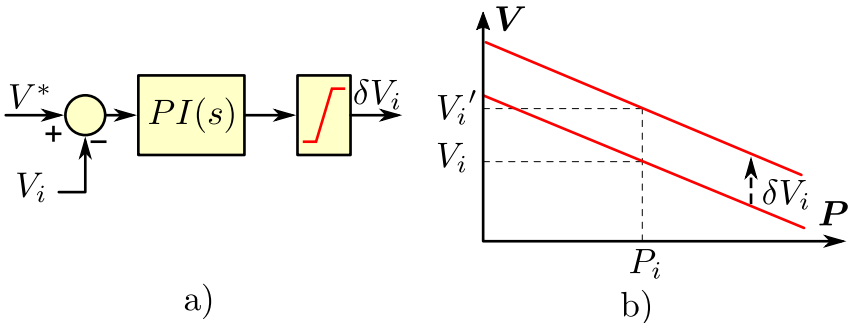


Figure 2.10: Secondary control loop for voltage restoration in the *dc*-DGs. a) Voltage restoration controller. b) Controller action.

The authors in [76] presented a low-bandwidth communication-based improved droop method for improving the power-sharing among *dc*-DGs in *dc*-microgrids with different line resistances. On the other hand, virtual resistances have been also proposed to improve the power-sharing in *dc*-microgrids [77–79].

## 2.4 Control of Hybrid *ac*/*dc*-Microgrids

As described before, a hybrid *ac*/*dc*-microgrid generally comprises an *ac*-microgrid and a *dc*-microgrid, which are interconnected through one or more bidirectional Interlinking Converters (*IC*) [15–17]. This topology facilitates the interconnection of various *ac*- and *dc*-based DGs and reduces several conversions due to the existence of independent *ac*- and *dc*-grids [18]. In the following, the basics of hybrid *ac*/*dc*-microgrid control and some relevant aspects of the *ICs* are detailed.

Hybrid *ac*/*dc*-microgrids is a research topic that has been mildly addressed in the literature. In this case, the power transferred through the *ICs* depends on the deviations of the primary variables (i.e., frequency on the *ac*-side and voltage on the *dc*-side) discussed before [6, 15, 21–24, 76]. The most commonly used power controller for the *IC* is presented in Fig. 2.11. The power controller measures the voltage at the *dc*-side ($V_{\mathrm{dc}}$) and the frequency on the *ac*-side ($\omega_{\mathrm{ac}}$), which is obtained using a phase locked-loop (PLL) from the *ac*-voltage ($E_{\mathrm{ac}}$). Later, the secondary variables are normalized using (2.7) and compared. The error is processed with a PI controller and the output of the controller is the power reference for the *IC* ($P^*_{\mathrm{IC}}$).

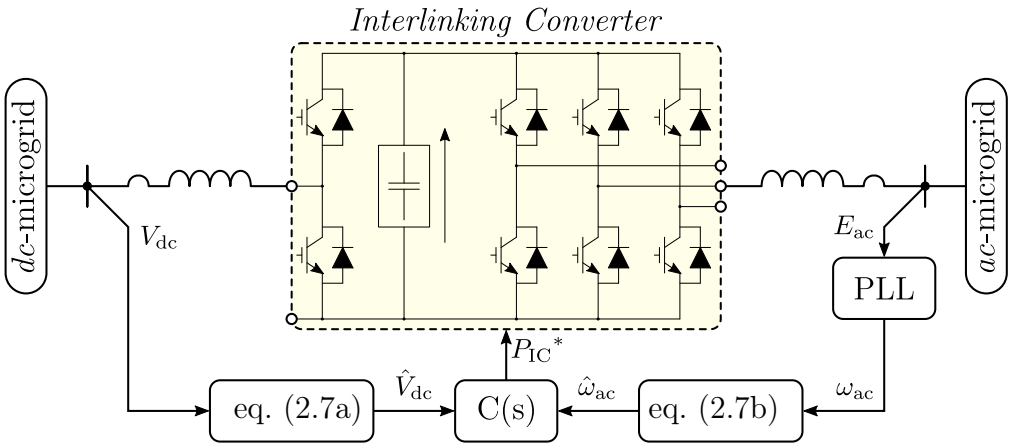


Figure 2.11: Closed-loop control system of the *IC* in hybrid *ac/dc*-microgrid.

$$\hat{V}_{\mathrm{dc}} = \frac{V_{\mathrm{dc}} - (V_{\mathrm{dc},max} + V_{\mathrm{dc},min})/2}{(V_{\mathrm{dc},max} - V_{\mathrm{dc},min})/2} \tag{2.7a}$$

$$\hat{\omega}_{\mathrm{ac}} = \frac{\omega_{\mathrm{ac}} - (\omega_{\mathrm{ac},max} + \omega_{\mathrm{ac},min})/2}{(\omega_{\mathrm{ac},max} - \omega_{\mathrm{ac},min})/2} \tag{2.7b}$$

In the literature, the main effort has been focused on the power management of the generation units at both sides (*ac* and *dc*) of the microgrid. In [16], the authors studied the operation of a hybrid *ac/dc*-microgrid with different energy sources, considering uncertainties and variability of the energy sources (e.g., wind and solar). Additionally, the voltage stability and the control of frequency and amplitude of the voltages was addressed. However, neither the secondary control loop nor the communication network was considered.

There are two main approaches proposed for active power management in hybrid *ac/dc*-microgrids. First, the power controller seeks to share the active power among all the generation units from both sides [21–23]. The work presented in [21] proposes the use of normalized droop curves on both sides of the *IC*. Thus, the active power reference for the *IC* control is generated to share the active power on both sides of the hybrid *ac/dc*-microgrid.

Second, in [24] a strategy to control the active power flowing through the *IC* from an underloaded microgrid to an overloaded microgrid is proposed. In that way, it is not possible to share the active power among generation units from different sides (i.e., the generation units only share the active power with units within the same microgrid). Thus, the *IC* can be "turned off" if both microgrids are underloaded or overloaded simultaneously. In these works, the secondary control loop is not considered, and the restoration of the voltage of the *dc*-side and/or the frequency of the *ac*-side produced by a secondary control loop would interfere with the accuracy of the power-sharing among both sides.

Depending on the size and topology of the hybrid *ac/dc*-microgrid, it may be necessary to consider the use of multiple *ICs*. However, due to the effect of line resistances in the *dc*-microgrid, the conventional *dc*-voltage based droop approaches used to manage the power

flow among *ac*- and *dc*-microgrids may produce a circulating current as well as stressing the *ICs*. To avoid that unwanted scenario, in [80] the authors propose to implement special droop characteristics to obtain the frequency and voltage reference values for the *ac*-side of *ICs*. In [81], the frequency of the *ac*-side and the voltage of the *dc*-side are considered to share the active power among the *ICs*. The introduction of a superimposed frequency in the *dc*-microgrid is considered in [82]. The secondary control loop is not considered in any of the aforementioned papers.

## 2.5 Cooperative Control of Multi-Agent Systems

In this work, techniques from distributed cooperative control of multi-agent systems (MAS) are applied to power-sharing problems in microgrids. This Section outlines the fundamental ideas used in the rest of the Thesis for developing design methods and analysis for cooperative control of MAS on graphs. Moreover, state of the art regarding distributed secondary control strategies applied to *ac*-, *dc*- and hybrid *ac/dc*-microgrids is addressed.

In MAS, each agent in a group or system can make decisions based on the information locally available from its closest neighbours, resulting in a synchronized behaviour of the overall group [83, 84]. The control protocols where each agent seeks to achieve consensus with its neighbours are considered *distributed* since they depend only on the local neighbour information as allowed by the communication graph topology. Thus, the agents in a microgrid (i.e., the DGs and *ICs*) need to communicate with their closest neighbours. The idea of a communication graph that models the information flows in a multi-agent group is now introduced.

### 2.5.1 Adjacency Matrix

The communication network interconnecting a dynamical system (e.g., the hybrid *ac/dc*-microgrid) can be modeled as a graph with directed edges corresponding to the allowed flow of information between the agents. According to [85], it is possible to describe the distributed communication network by a weighted graph $G(\mathcal{V},\mathcal{E},A)$ where $\mathcal{V}=\{1,\ldots,n\}$ is a labeling of the DGs, $\mathcal{E}\subseteq\mathcal{V}\times\mathcal{V}$ is the set of communication links, and $\mathbf{A}$ is the $n\times n$ *adjacency matrix* (or *connectivity matrix*) of the graph, with elements $a_{ij}=a_{ji}\geq 0$ (in this case the graph is said to be *undirected* since it is bidirectional). Particularly, it is considered that $(i,j)\in\mathcal{E}$ if node $i$ sends information directly to node $j$, and in this case, $a_{ij}>0$. Thus, the sparsity pattern of the adjacency matrix $\mathbf{A}$ encodes the topology of the communication layer (see example in Fig. 2.12).

As mentioned before, a graph can be represented by an adjacency matrix $\mathbf{A}=[a_{ij}]$ with weights $a_{ij}=1$ meaning that units i and $j$ can communicate with one another and $a_{ij}=0$ otherwise. It is possible to define the weighted in-degree of node $i$ ($d_i$) as the sum of $i^{th}$ row elements of $\mathbf{A}$ as shown in (2.8) [84]. Moreover, the diagonal in-degree matrix $D=\text{diag}\{d_i\}$ and the graph Laplacian matrix $L=D-A$ can be defined [86]. These concepts will be used for obtaining the closed-loop model of the proposed controllers in Chapter 6.

$$d_i=\sum_{j=1}^{n}a_{ij} \tag{2.8}$$

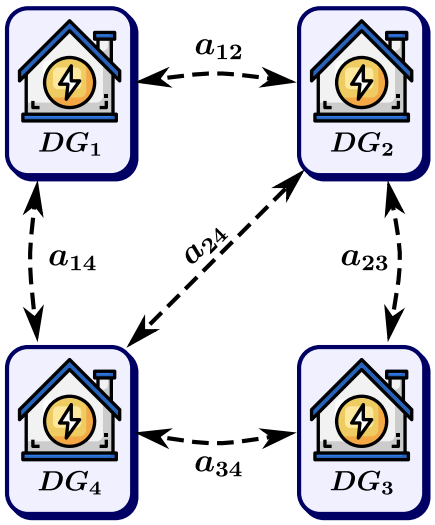


$$\mathbf{A} = \begin{pmatrix} 0 & a_{12} & 0 & a_{14} \\ a_{21} & 0 & a_{23} & a_{24} \\ 0 & a_{32} & 0 & a_{34} \\ a_{14} & a_{24} & a_{34} & 0 \end{pmatrix}$$

$$\nu = \{1, 2, 3, 4\}$$

$$\varepsilon = \{(1,2), (1,4), (2,3), (2,4), (3,4)\}$$

Figure 2.12: Example of adjacency matrix construction for four DGs.

The time response of the proposed distributed secondary control strategy is strongly related to the density of matrix **A**. The time response is slow when **A** is sparse, i.e., if most of the elements of **A** are zero, while the time response is fast if the density of **A** is high (most of the elements of **A** are equal to 1). Therefore, unlike the case of centralized or decentralized secondary control strategies, in this case the time response also depends on the size and topology of the communication network. Finally, a necessary condition for stability is that the **A** matrix must have a spanning tree, i.e., a path from any single node to any other one in the communication graph.

Now, two approaches for the consensus or synchronization problem are reviewed. First, the cooperative regulator (or leaderless consensus) problem, where all agents have the same role, is explained, which is the base for the secondary control strategies proposed for power-sharing in Chapter 3 and for cost minimization in Chapter 4. Then, the cooperative tracker (or controlled consensus) problem, where the agents synchronize to the dynamics of a leader or root node which generates a command target trajectory, which is used in the secondary controller presented in Chapter 4 for hybrid *ac/dc*-microgrids with multiple *ICs*.

### 2.5.2 Cooperative Regulator

Given dynamical systems at each node $i$ with state $x_{\mathrm{i}}(t)$, the objective for this approach is to find a distributed control protocol for each agent $i$ that drives all states to the same constant steady-state value, which is known as a consensus value. The control scheme must be distributed in that the control for agent $i$ is only allowed to depend on the state of agent $i$ and its neighbours $j \in N_{\mathrm{i}}$ in the graph topology. Thus, the local control protocols for each agent $i$ are:

$$u_{\mathrm{i}} = \dot{x}_{\mathrm{i}} = \sum_{j \in N_{\mathrm{i}}} a_{\mathrm{i}j}(x_j - x_{\mathrm{i}}) \tag{2.9}$$

where $a_{\mathrm{i}j}$ is from the adjacency matrix **A** and describes the communication network in the hybrid *ac/dc*-microgrid.

In [84], it is demonstrated that the cooperative regulator protocol (2.9) guarantees consensus and the node states come to the same steady-state values $x_{\mathrm{i}} = x_j = c, \forall \mathrm{i}, j$, namely consensus value, given by:

$$c = \sum_{\mathrm{i}=1}^{N} p_{\mathrm{i}} x_{\mathrm{i}}(0) \tag{2.10}$$

where $w_1 = [p_1, \cdots, p_N]^T$ is the normalized left eigenvector of the Laplacian L for $\lambda_1 = 0$. Finally, consensus is reached with a time constant given by (2.11), with $\lambda_2$ the second eigenvalue of L, known as the Fiedler eigenvalue.

$$\tau = \frac{1}{\mathrm{Re}\{\lambda_2\}} \tag{2.11}$$

### 2.5.3 Cooperative Tracking

For this approach, we consider the situation shown in Fig. 2.13, which depicts a leader or target node with state $x_0(t)$. The objective here is to find a distributed control protocol for each agent $i$ that drives all states to the state of the leader node. The following distributed cooperative tracker protocols are considered to solve this problem:

$$u_{\mathrm{i}} = \dot{x}_{\mathrm{i}} = \sum_{j \in N_{\mathrm{i}}} a_{\mathrm{i}j}(x_j - x_{\mathrm{i}}) + g_{\mathrm{i}}(x_0 - x_{\mathrm{i}}) \tag{2.12}$$

where the gains $g_{\mathrm{i}} \geq 0$ are known as pinning gains, $g_{\mathrm{i}} > 0$ if agent $i$ has a direct communication link with the leader node and $g_{\mathrm{i}} = 0$ otherwise.

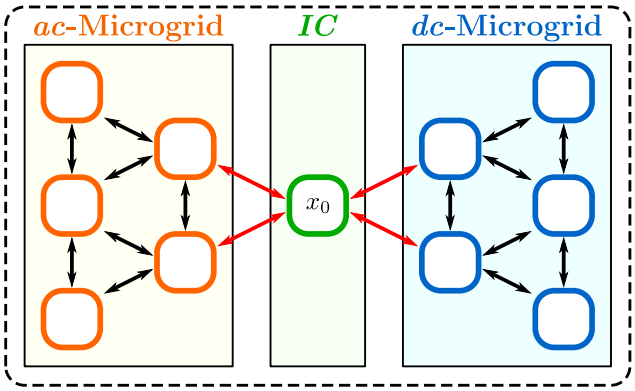


Figure 2.13: Communication graph with leader node $x_0$.

## 2.6 Distributed Secondary Control in the Literature

In the following, the main works reported in the literature regarding DSC strategies applied to *ac*-, *dc*- and hybrid *ac*/*dc*-microgrids are discussed. The distributed control systems reported in this section have been classified considering the type of microgrid studied, i.e., *ac*-strategies, *dc*-strategies and hybrid *ac*/*dc*-strategies.

### 2.6.1 DSC for *ac*-Microgrids

As discussed before, the secondary control loop for *ac*-microgrids is in charge of restoring amplitude and frequency of the voltages to their nominal values. It must be noted that the frequency is a global variable of the microgrid. On the contrary, the voltage is a local variable (i.e., different values of voltages could be obtained, in steady-state, at different points of the microgrid). Therefore, different criteria can be considered for achieving voltage regulation in the microgrid, for example, by (i) regulating the converters' output voltage close to the nominal value, (ii) regulating the average voltage of the microgrid, or (iii) regulating the voltage in some specific points of the microgrid.

Different DSC strategies for *ac*-microgrids have been proposed in the literature. The authors in [87, 88] propose to use the average values of voltage magnitude and frequency to improve the primary control droop characteristics. Other works, based on techniques from the cooperative control of MAS, have proposed secondary control schemes that ensure asymptotic convergence of the controlled variables [85, 89–92]. A secondary control system based on an input-output feedback linearization approach was proposed in [89, 91]. The proposed methodology allows a non-linear formulation to be solved by conventional asymptotic consensus protocols. The non-linear relationship is developed for the voltage loop based on [49], and the feedback linearization relies on Lie's algebra. The methods presented in [91] inspire further developments in secondary control [85, 90].

In [85], the authors proposed a simplified methodology for the application of distributed cooperative secondary control over traditional droop based converter-based microgrids. The strategy considers a distributed averaging algorithm to restore the voltage amplitude and frequency while maintaining the active and reactive power-sharing. This controller acts over primary droop control schemes by applying an integral control with a consensus protocol referred to as Distributed-Averaging Proportional-Integral (DAPI) controller. The DAPI system is the basis of the control strategies proposed in this work, and it is further explained as follows:

Firstly, the DAPI *frequency controller* is proposed for restoring the frequency in the *ac*-microgrid and to ensure an accurate active power-sharing among units:

$$\omega_{\mathrm{i}} = \omega^* - m_{\mathrm{i}} P_{\mathrm{i}} + \Omega_{\mathrm{i}} \tag{2.13}$$

$$k_{\mathrm{i}} \frac{\mathrm{d}\Omega_{\mathrm{i}}}{\mathrm{d}t} = -\left(\omega_{\mathrm{i}} - \omega^*\right) - \sum\nolimits_{j \in \mathbb{N}_{\mathrm{ac}}} a_{\mathrm{i}j} \left(\Omega_{\mathrm{i}} - \Omega_j\right) \tag{2.14}$$

where $\Omega_{\mathrm{i}}$ is the secondary control variable, $k_{\mathrm{i}}$ is a positive gain for adjusting the transient response of the controller, $\omega_{\mathrm{i}}$ is the frequency and $P_{\mathrm{i}}$ is the active power of the $\mathrm{i}^{th}$ *ac*-DG, and $a_{\mathrm{i}j} = a_{j\mathrm{i}}$ is the element of the matrix $\mathbf{A}$ described in Section 2.5.1. The standard droop controller with the additional secondary control input $\Omega_{\mathrm{i}}$ is shown in (2.13), while (2.14) ensures the frequency restoration since, in steady-state, the derivative on the left side of the equation is zero and, then, $\omega_{\mathrm{i}} = \omega^*$. Additionally, the condition $\Omega_{\mathrm{i}} = \Omega_j$ has to be fulfilled for all the *ac*-DGs $\mathrm{i}, j \in \mathbb{N}_{\mathrm{ac}}$ to guarantee that all droop curves are equally shifted. The latter condition ensures that the active power-sharing is maintained.

Secondly, the DAPI *voltage controller* is proposed to restore the voltage amplitude in the

microgrid and to improve the reactive power-sharing among units:

$$E_{\mathrm{i}} = E^* - n_{\mathrm{i}} Q_{\mathrm{i}} + \mathrm{e}_{\mathrm{i}} \tag{2.15}$$

$$\kappa_{\mathrm{i}} \frac{\mathrm{d}\mathrm{e}_{\mathrm{i}}}{\mathrm{d}t} = -\beta_{\mathrm{i}} \left(E_{\mathrm{i}} - E^*\right) - \sum\nolimits_{j \in \mathbb{N}_{\mathrm{ac}}} b_{\mathrm{i}j} \left( \frac{Q_{\mathrm{i}}}{Q_{\mathrm{i}}^*} - \frac{Q_j}{Q_j^*} \right) \tag{2.16}$$

where $\mathrm{e}_{\mathrm{i}}$ is the secondary control variable, $\beta_{\mathrm{i}}$ and $\kappa_{\mathrm{i}}$ are positive gains for adjusting the transient response of the controller, $E_{\mathrm{i}}$ is the $\mathrm{i}^{th}$ voltage and $Q_{\mathrm{i}}^*$ is the $\mathrm{i}^{th}$ reactive power rating, and $b_{\mathrm{i}j} = b_{j\mathrm{i}}$ is the element of the *adjacency matrix of a communication network* $\mathbf{B}$ described in [85]. The equation (2.15) corresponds to the standard voltage droop controller with the additional secondary control input $\mathrm{e}_{\mathrm{i}}$, while (2.16) allows to choose between controlling the local voltage $E_{\mathrm{i}}$ ($\mathbf{B} = 0$), the reactive power-sharing ($\beta_{\mathrm{i}} = 0$) or a trade-off between both controls ($\mathbf{B} \neq 0, \beta_{\mathrm{i}} \neq 0$). This trade-off between control of the voltage and reactive power-sharing is well-known and previously studied in the literature [93].

### Approaches for Power-sharing and Variables Restoration

Other approaches have been proposed for improving the power-sharing while the secondary variables are restored [94, 95]. In [94], a fully distributed control methodology for secondary control of *ac*-microgrids is proposed. The authors claim that the proposed scheme maintains the average voltage of the microgrid at the rated value while the $Q$-$V$ droop coefficients are fine-tuned to mitigate any reactive power mismatch. Furthermore, the authors state that, unlike most conventional methods, the proposed controller does not utilize any explicit frequency measurement to regulate all inverter frequencies at the nominal value while sharing the active power demand among them. The proposed scheme estimates the average normalized active power using a dynamic consensus protocol and, accordingly, regulates the microgrid's frequency and shares the active power demand proportional to inverters' rating. Plug-and-play capability, and resiliency to different communication topologies and constraints such as limited bandwidth, delay, and packet loss, are verified through experiments. In [95], dynamic weights are reassigned to reach different targets. It is claimed that the strategy discussed in [95] could enhance the stability of the system, achieving a better dynamic response. The authors in [96] propose a distributed strategy to improve only the reactive power-sharing.

Several variations and modifications to the distributed secondary control algorithms have been proposed and studied. For instance, in [97–99], techniques of predictive control are utilized to restore the frequency and voltage amplitudes to nominal values. Another type of modification in the control algorithms is developed in [100–103], where finite-time consensus control is employed to restore both frequency and voltage in the microgrid. The proposed algorithms are designed to achieve the restoration of secondary variables (frequency and voltage) in a finite time. It is also claimed that these control strategies increase the convergence speed and the robustness against noise and uncertainties. However, these topics are outside the scope of this work.

### Approaches for Economic Dispatch

The conventional centralized dispatch problem can be solved in a distributed manner. In this sense, it should be highlighted that in contrast to the centralized approach, distributed algorithm achieve the minimum cost by considering the communication between DGs. The

most typical approach for minimizing the cost of the microgrid is considering the incremental cost consensus (ICC) [104–108].

In [104], a multiagent based distributed method is proposed to minimize operation cost of the *ac*-microgrid. Each *ac*-DG acts as an agent which regulates the power individually using proposed frequency scheduling method. Optimal power command is obtained through a consensus algorithm with only light communication between neighbouring agents. The authors in [105] propose a method similar to that proposed in [104], however, the finite-time convergence properties for distributed secondary frequency and voltage controllers are demonstrated. The limits for the operation of the *ac*-DGs are not considered in the aforementioned papers.

Delay effects and communication issues are thoroughly studied in [106,107]. The impact of time delays on the stability of the distributed economic dispatch algorithm is carefully studied in [106], and the generalized Nyquist criterion is considered to derive the maximum allowable delay bounds for the strategy presented in [106]. The effectiveness of the proposed algorithm and a verification of the correctness of the theoretical results are validated through simulation tests. In [107], the authors claim that whether the communication delays exist or not, the control protocols always guarantee that the output voltage amplitude and frequency of each distributed generator track to the reference values and maintain the optimal active power-sharing and the accurate reactive power-sharing properties. The plug-and-play capability is also validated in [107].

The power limits of the *ac*-DGs are considered in the strategies proposed in [108, 109]. Here, the authors propose a distributed control strategy for frequency control, congestion management, and optimal dispatch in isolated microgrids. The control scheme avoids lines overloading in the microgrid with a distributed approach, while restoring the secondary variables and optimizing the operation of the microgrid. The authors in [108] also derive a closed-loop model of the microgrid with the proposed scheme, in order to perform an eigenvalue analysis and small-signal stability analysis. Furthermore, the closed-loop model of the system is used to derive the stable limits for the parameters of the controller.

### Approaches for Power Quality Issues

The loads in a low-voltage *ac*-microgrid are typically unbalanced and non-linear with several connections and disconnections of single-phase loads, which can produce power quality issues in the *ac*-microgrid. Thus, the DSC has been extended for improving the power quality in *ac*-microgrids by considering imbalance and harmonics issues. Two approaches have been addressed in the literature. In the first approach, the strategy aims to improve the unbalanced and distorted currents-sharing among the *ac*-DGs [110,111]. Conversely, the second approach is focused on compensating the voltages at some buses in the microgrid (buses where critical loads or more sensitive systems are connected) [112].

In [93], a distributed dynamic consensus algorithm to improve the negative sequence components current-sharing while enhancing the voltage quality at the PCC is proposed. This strategy is based on the symmetrical components theory. Therefore, to share the negative sequence component of the current among the *ac*-DGs, a negative sequence component of the voltage is included in the reference voltage to be synthesized by the $i^{th}$ *ac*-DG. This proposal

ensures an accurate imbalance sharing. The *ac*-microgrid considered in [93] corresponds to two 3-leg converters in parallel configuration feeding an unbalanced load. Experimental results are provided that validate the proposal. However, it is not discussed how to extend the proposal for a more complex microgrid configuration. Moreover, it is challenging to implement the reported methodology in a microgrid with more than two *ac*-DGs.

#### Approaches for Energy Storage Systems

Distributed secondary control strategies have been proposed for equalizing the state of charge (SoC) of battery energy storage systems (BESS) in *ac*-microgrids [113, 114]. In [113], the authors use frequency scheduling instead of adaptive droop gain to regulate the active power of the distributed energy storage (DES). Each DES unit is taken as an agent and it schedules its own frequency reference given by the real power droop controller according to the SoC values of all other DES units. Each agent uses a dynamic average consensus algorithm to obtain the average SoC value of DES. On the other hand, the scheme proposed in [114], achieves power regulation by adjusting the virtual resistances of voltage-controlled inverters with an autonomous current-sharing controller. However, BESSs are not considered in this work.

Although several alternatives for distributed secondary control in *ac*-microgrids have been analyzed, none of the previous works discussed in this section considers the existence of either the *dc*-side or the *IC* in a hybrid *ac*/*dc*-microgrid. Next, the works proposed for *dc*-microgrids are reviewed.

### 2.6.2 DSC for *dc*-Microgrids

As discussed before, the secondary control loop for *dc*-microgrids is responsible for restoring magnitude of the voltages to their nominal values. As mentioned before, since the voltage is a local variable, the same criteria discussed for *ac*-microgrids can be defined for *dc*-microgrids, i.e., by regulating (i) the converters' output voltage, (ii) the average voltage of the microgrid, or (iii) the voltage at some specific points of the microgrid. The secondary control loop in *dc*-microgrids can include an additional control objective. The most common goal for the secondary control loop is to improve the power-sharing among *dc*-DGs while restoring the average voltage to its nominal value. Different approaches are reviewed in the following.

#### Approaches for Power-sharing and Variables Restoration

As mentioned before, the main challenge in this strategy is to restore the average voltage of the *dc*-DGs without deteriorating the power/current sharing. However, it is not possible to simultaneously achieve a good voltage regulation and an accurate power-sharing between the *dc*-DGs (i.e., the problem is similar to the Q-V problem in *ac*-microgrids). An optimal control strategy is proposed in [115] to solve the problem of optimal voltage and power regulation for *dc*-DGs with a distributed communication network. Here, the authors show the good performance of the proposed strategy with variable and distributed generation. However, this strategy requires the full information of the microgrid; otherwise, the optimal control is reduced to several controls, including conventional droop control.

A distributed approach is presented in [116–118]. In these works a distributed-adaptive

droop mechanism is proposed for secondary/primary control of *dc*-microgrids. The controller on each agent exchanges data with only its neighbouring agents on a sparse communication graph spanned across the microgrid. To achieve a good voltage regulation and an accurate current/power sharing, this control strategy can be divided in two main stages or modules: (i) a voltage regulator based on an observer for estimating the average voltage in the microgrid, and (ii) a current regulator to fine-tune the droop coefficients for different load conditions. In [28], a simplified version of the controller proposed in [116] was presented. This strategy utilizes power-sharing consensus instead of using a current-sharing consensus, and the voltage regulation is based on measured voltages instead of estimated voltages, which simplifies the controller.

A DSC applied for voltage regulation and droop slope correction is discussed in [119, 120]. The controller is proposed to modify the droop slope in order to change the output impedance in each converter, to achieve load current sharing. In [121], a low voltage *dc*-microgrid with merged *ac* and *dc* characteristics has been considered to propose an alternative droop scheme for low-voltage *dc*-microgrids with both primary power-sharing and secondary voltage regulation merged. Two droop expressions are proposed in this work. The first expression is for regulating the *ac*-frequency and active power generated by the *dc*-DGs, while the second one is for relating the *dc*-voltage to the power term. It is claimed in [121] that better active power-sharing and proper average voltage regulation in the *dc*-microgrid are achieved.

### Approaches for Economic Dispatch

The ICC approach for *ac*-microgrids discussed in the previous section can be extended to *dc*-microgrids, where a consensus algorithm is considered to achieve equal incremental cost in all the generating units. The distributed economic dispatch (ED) of *dc*-microgrids, unlike the distributed ED of *ac*-microgrids, modifies the voltage droop control scheme. In this context, the ED is solved at the same time that the global average voltage is restored [122, 123].

In [122], the ED is achieved by modifying the voltage reference from the droop controllers for the *dc*-microgrid through a PI controller, which modifies the output power of the $i^{th}$ *dc*-DG to be equal to the optimal output power. The optimal power is obtained using an ICC algorithm similar to that discussed for the *ac*-microgrid. However, this work has some limitations: the power limits for *dc*-DGs are not considered. Moreover, this strategy only regulates the local output voltage of each *dc*-DG instead of the global voltage of the microgrid, not being able to guarantee the optimal operation. In [123], the global voltage regulation issue is addressed, and the distributed consensus technique is used for ED and voltage control of the microgrid. The voltage reference for the local controller is modified by adding voltage deviations to the reference voltage. Unlike [122], the works reported in [123, 124] include the operation limits for the active power generated by the *dc*-DGs.

In [125, 126], a distributed adaptive droop control algorithm is proposed for optimal dispatch and current regulation by applying a consensus algorithm. In these works, an ED problem is considered to obtain the incremental cost considering power losses, where a penalty term is added to the cost function. The transmission losses are approximated by the square of the output power of each generating unit. Although this penalty term is added for considering the transmission losses in the cost function, the power-losses are not modelled in [125]. On the other hand, the losses are assumed constant in [126].

Several works include time delay analysis in their proposed consensus algorithms to evaluate their performance in this scenario. As reported in [127], time delays affect the convergence and performance of consensus algorithms. Thus, in [106, 122, 128], the effects of a constant communication delay on the ED problem are studied using simulation work, while in [127], time-varying delays are analyzed. Finally, uncertainties have also been addressed in the literature: for instance, in [129] the authors proposed a distributed controller for economic dispatch with random wind energy power.

#### Approaches for Energy Storage Systems

DSC strategies to achieve SoC equalization among the energy storage units in *dc*-microgrids have been reported in the literature [130, 131]. Besides the typical tasks of the secondary control system (i.e., voltage restoration and power-sharing), in [130], the charge and discharge of the batteries is monitored, and the SoCs are equalized, simultaneously, by using a distributed controller which regulates the BESS droop coefficients. Alternatively, adaptive virtual impedances adjusted using distributed control algorithms can be utilized to achieve SoC equalization among the BESS located in a microgrid (see [114]). It is claimed that virtual impedance-based methods are intrinsically more stable because droop variations can affect the stability of *ac*- and *dc*-microgrids [114]. In [131], ultracapacitors are included in the BESS, which posses two time-scales, one for the batteries (slower) and the other for the ultracapacitors (faster). In [132], a feedback linearization technique is used to obtain a second-order consensus strategy of the voltage applied to equalize the SoC of a BESS. The strategy proposed in [133] balance the SoC of the BESS while optimizing the operation of the microgrid.

Although several alternatives for distributed secondary control in *dc*-microgrids have been analyzed, none of the previous works discussed in this section considers the existence of either the *ac*-side or the *IC* in a hybrid *ac/dc*-microgrid. Next, the works proposed for hybrid *ac/dc*-microgrids are reviewed.

### 2.6.3 DSC for Hybrid *ac/dc*-Microgrids

To the best of the candidate's knowledge, the study of distributed secondary control strategies for integrating the secondary control loop of both sides in the hybrid *ac/dc*-microgrid has been slightly addressed in the literature. Conversely, the secondary control loop on each side is applied independently of the other side and the operation of the *IC* depends on the secondary control variables, i.e., the power-sharing among both microgrids might be inaccurate if the secondary control variables are restored to their nominal values. Moreover, the optimal operation of hybrid *ac/dc*-microgrids as a single entity has not been addressed.

A distributed control scheme for reliable autonomous operation of a hybrid three-port *ac*/*dc*/DES microgrid is presented in [23]. First, the authors consider a fully decentralized control, which is achieved by local power sharing (LPS) in individual *ac*- or *dc*-microgrid, global power sharing (GPS) throughout *ac*- and *dc*-microgrids, and storage power sharing (SPS) among distributed storage units. Upon fully decentralized control, each power module can operate independently without communication links. This benefits riding through communication malfunction in multilayer supervision control system. Secondly, a multilevel

power exchange control for scheduling LPS, GPS, and SPS is considered to reduce unnecessary power exchange between *ac*- and *dc*-microgrids and operations of DES units with the benefit of reducing power exchange losses and prolonging storage lifetime.

In [134, 135], the authors proposed a distributed coordination control strategy for the hybrid *ac*/*dc*-microgrid. In [134], it is claimed that this control strategy regulates not only *dc* current and reactive power-sharing among DGs in *ac*- and *dc*-microgrids but also maintains power-sharing among two microgrids and restores the *ac*-frequency and *dc*-voltage to their nominal values. The proposed control strategy is based on a distributed consensus algorithm. In [135], the goal is to implement power-sharing among all DGs in the hybrid *ac*/*dc*-microgrid and among the *ICs* in a distributed manner, without the need for additional proportional-integral controllers. However, in [134, 135], the control of the *ICs* is based on the normalized droop curves of the *ac*- and *dc*-microgrids [21]. This behaviour is jeopardized when restoration is applied to the frequency and *dc*-voltage.

The integration of a global DSC strategy in DGs at both sides of the microgrid has been addressed in [28]. The authors propose a distributed control that ensures the regulation of the frequency (at the *ac*-side) and the amplitude (at both sides) of the voltages. Additionally, with the proposed strategy, all the DGs achieve an accurate power-sharing. The results obtained using simulation are presented and discussed in [28] to validate the capability of the proposed scheme to transfer power from the *dc*-side to the *ac*-side (and vice-versa), and its plug-and-play capability. However, in this work, the *IC* is not considered in the secondary control strategy.

In conclusion, there is still room for research on this topic since all proposed control strategies have drawbacks and they do not consider a secondary distributed control approach to integrate the secondary variables restoration of both sides in a hybrid *ac*/*dc*-microgrid as a single entity.

## 2.7 Summary

In this Chapter, the hierarchical control structures of *ac*-, *dc*-, and hybrid *ac*/*dc*-microgrids were presented. Deviations in secondary variables (frequency and voltage magnitude deviations in *ac*-microgrids, as well as voltage magnitude deviations in *dc*-microgrids) produced by the primary control level (decentralized droop controllers) are regulated by considering a higher level control, namely secondary control level. Moreover, *dc*-microgrids implementing $P$-$V$ droops suffer from inaccurate power-sharing due to different line resistances and terminal voltages of *dc*-DGs. Similarly, inaccurate reactive power-sharing among droop-controlled *ac*-DGs in an *ac*-microgrid is obtained.

Secondary controllers use slow communication links to restore the secondary variables, while attaining additional objectives such as improving power-sharing accuracy and power quality (in *ac*-microgrids), equalization of SoC in BESS, or optimal operation of the DGs in the microgrids. Distributed controllers are more suitable for microgrids with a high number of DGs than centralized and decentralized schemes since the reliability and security of the microgrid improves when considering these types of architecture. However, in the literature, hybrid *ac*/*dc*-microgrids are typically considered as three independent systems interacting

with each other when implementing the secondary control loop.

In hybrid *ac/dc*-microgrids, a crucial device is the *IC*, which is a power electronics device capable of interconnecting the *ac*-microgrid with the *dc*-microgrids. The *ICs* must handle bidirectional power flow in order to transfer power from one side to the other one, in order to fulfill a goal such as avoiding the overloading of a microgrid or reducing the total operation cost. When the hybrid *ac/dc*-microgrid has several *ICs* it is necessary to regulate the power through them.

# Chapter 3

# Control Strategy Proposed for Power-Sharing

## 3.1 Introduction

In this Chapter, the consensus-based distributed secondary control (DSC) strategy proposed for power-sharing among all agents in the *ac/dc*-microgrid is presented. In the DSC scheme proposed in this Chapter, each DG will achieve *real power-sharing* with all other DGs of the hybrid microgrid, i.e., *ac*-DGs and *dc*-DGs, and each *ac*-DG will approximately achieve *reactive power-sharing* with all other *ac*-DGs.

The main challenge for this Chapter is to design a control strategy applied to hybrid *ac/dc*-microgrids (*ac/dc*-DSC) that restores the secondary variables to their nominal values, and improves (or, at least, not degrade) power-sharing among DGs. Moreover, the control system has to identify when the *IC* is not available because, in that case, it is not possible to transfer power between the two sides of the hybrid *ac/dc*-microgrid (i.e., there is no electrical path for transferring power).

This Chapter is organized as follows: Section 3.2 presents a distributed secondary control strategy for power-sharing in a hybrid *ac/dc*-microgrid. The inner, primary and secondary control loops for the *ac*-DGs and *dc*-DGs are presented in Section 3.3 and Section 3.4, respectively. The controllers for the *ICs* are depicted in Section 3.5 for the case where a single *IC* is connected to the microgrid, and in Section 3.6 when multiple *ICs* are transferring power between the two sides of the microgrid. Finally, Section 3.7 summarizes the control strategy proposed for power-sharing among all the agents in the *ac/dc*-microgrid.

## 3.2 Control Strategy for Power-Sharing

In this strategy, the standard power-voltage ($P/V$) droop controller [72] is considered as the primary control system in the *dc*-microgrid, and the standard ($P/f$) and ($Q/V$) droop controllers [60] are used as the primary control systems in the *ac*-microgrid. As the frequency is a global variable in the *ac*-microgrid, accurate active power-sharing is achieved in the *ac*-

microgrid. On the other hand, the amplitude of the voltages is a local variable. Thus, it is not possible to achieve both accurate power-sharing and voltage restoration simultaneously for each DG on either side of the microgrid [85].

A hybrid *ac*/*dc*-microgrid is considered in this section, which consists of *ac*-DGs, *dc*-DGs, and *ICs*, and the sets of these devices are labelled as $\mathbb{N}_{\text{ac}} = \{1, \ldots, n\}$, $\mathbb{N}_{\text{dc}} = \{n+1, \ldots, n+m\}$, and $\mathbb{N}_{\text{IC}} = \{n+m+1, \ldots, n+m+g\}$, respectively. The general topology for the hybrid *ac*/*dc*-microgrid is shown in Fig. 3.1. A global secondary control strategy for hybrid *ac*/*dc*-microgrids should restore the secondary variables on both sides of the microgrid; moreover, should ensure power-sharing between all *ac*-DGs and *dc*-DGs. To achieve the latter objective, the power flowing through the *IC* must be adjusted. In the following, several distributed control mechanisms for achieving these goals are introduced. These control laws will use peer-to-peer communication among *dc*-DGs, *ac*-DGs, and *ICs*, as described in Section 3.1. Even though the control strategy considers communication links between the units, a generalization of a communication channel is considered in this work, i.e., the thesis does not consider specific communication links (such as wireless systems, fibre optic communication links, among others).

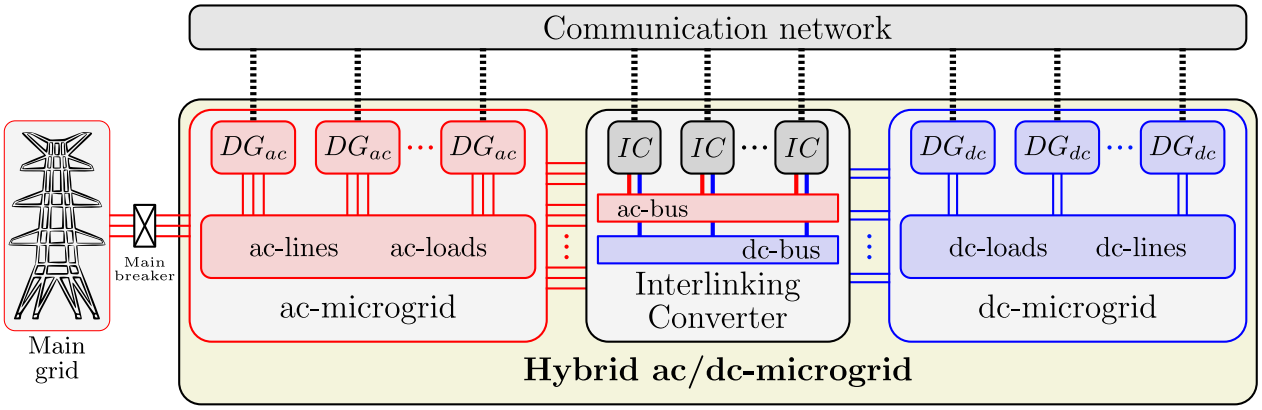


Figure 3.1: General topology of a hybrid *ac*/*dc*-microgrid. If the main breaker is closed, it is a "grid-tied" microgrid; otherwise, it is an "islanded" microgrid.

## 3.3 Control Strategy Proposed for *ac*-Microgrid

### 3.3.1 Inner and Primary Control Loops

In *ac*-microgrids, three-phase voltage source converters (VSCs) are the most commonly used power electronic devices used to interface the *ac*-DGs with the network. In this case, the voltage-controlled VSCs (VC-VSCs) are considered due to their capability to operate in droop controlled mode, i.e., to synthesize voltages with variable frequency and amplitude. The structure and control loops for a droop controlled VC-VSC are depicted in Fig. 3.2. A low-pass LC filter is considered to interface the *ac*-DGs with the *ac*-microgrid.

A nested structure is considered for the controllers in the inner control loop of the *ac*-DGs, which consists of an outer voltage controller (slower) and an inner current controller (faster). Event though any kind of controller is able to synthesize the *ac*-DG's output *ac*-voltage, a proportional-resonant (PR) controller is considered in both stages of the nested controller.

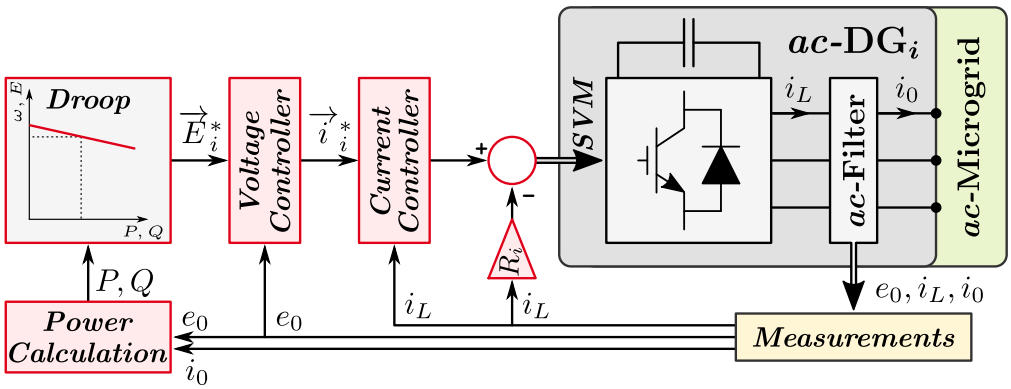


Figure 3.2: Inner and primary control loops for the *ac*-DGs.

The typical structure for a PR controller ($C_{\mathrm{PR}}(s)$) is given by:

$$C_{\mathrm{PR}}(s) = k_P + \frac{2k_{\mathrm{i}}s}{s^2 + {\omega_0}^2} \tag{3.1}$$

where $k_P$ and $k_{\mathrm{i}}$ are the proportional and integral gains of the controller, respectively, and $\omega_0$ is the resonant frequency. An important feature of the PR controller is that it is possible to program it with a variable resonant frequency; thus, it is possible to adjust the response of the controller according to the changes in the frequency due to the droop controller. As depicted in Fig. 3.2, the reference currents ($\vec{\mathrm{i}}^{\,*}_{\mathrm{i}}$) are set by the outer voltage loop, while the reference voltages (i.e., the output voltage magnitude and frequency) are set by the outer droop controllers and the secondary control loops, as will be described in the next Section. The typical structure for the droop controllers is given by:

$$\delta\omega_{\mathrm{D}} = M_{\mathrm{ac}}P_{\mathrm{ac}} \tag{3.2a}$$
$$\delta E_{\mathrm{D}} = N_{\mathrm{ac}}Q_{\mathrm{ac}} \tag{3.2b}$$

where $\delta\omega_{\mathrm{D}}$ and $\delta E_{\mathrm{D}}$ are the control actions of the droop control, $M_{\mathrm{ac}} < 0$ and $N_{\mathrm{ac}} < 0$ are the droop slopes, $P_{\mathrm{ac}}$ and $Q_{\mathrm{ac}}$ are the active and reactive power generated by the *ac*-DG, respectively.

### 3.3.2 Secondary Control Loops

The secondary control loop for *ac*-DGs aims to restore the frequency $\omega_{\mathrm{i}}$ and the amplitude $E_{\mathrm{i}}$ of the ac-voltage to their nominal values $\omega^*$ and $E^*$, while maintaining satisfactory power-sharing. In the proposed DSC for the *ac*-DGs in the *ac*-microgrid (*ac*-DSC), the communicated variables in the *ac*-microgrid are the active and reactive powers $P_{\mathrm{i}}$ and $Q_{\mathrm{i}}$ in p.u., which are given by

$$\begin{aligned} P_{\mathrm{i}} &:= P_{\mathrm{ac-i}}/S_{\mathrm{max-i}}, \qquad \mathrm{i} \in \mathbb{N}_{\mathrm{ac}}, \\ Q_{\mathrm{i}} &:= Q_{\mathrm{ac-i}}/S_{\mathrm{max-i}}, \qquad \mathrm{i} \in \mathbb{N}_{\mathrm{ac}}, \end{aligned} \tag{3.3}$$

where $P_{\mathrm{ac-i}}$ ($Q_{\mathrm{ac-i}}$) is the instantaneous real (reactive) power generated by the i$^{th}$ *ac*-DG, and $S_{\mathrm{max-i}}$ is the rated apparent power of the i$^{th}$ *ac*-DG. For the *ac*-microgrid, the secondary variables are the frequency ($\omega_{\mathrm{i}}$) and the amplitude ($E_{\mathrm{i}}$) of the voltages, while the consensus variables are the active power in p.u. ($P_{\mathrm{i}}$) and the reactive power in p.u. ($Q_{\mathrm{i}}$). Following the

traditional approach, two *ac*-DSCs are proposed: the first one for active power-sharing and frequency restoration, and the second one for reactive power-sharing and voltage restoration.

The *ac*-DSC for active power-sharing and frequency restoration is given by:

$$\omega_{\mathrm{i}} = \omega^* + M_{\mathrm{ac-i}} P_{\mathrm{ac-i}} + \psi_{\mathrm{i}} \tag{3.4a}$$

$$\sigma_{\mathrm{i}} \dot{\psi}_{\mathrm{i}} = -\left(\omega_{\mathrm{i}} - \omega^*\right) + \psi_{\mathrm{ac-i}} + \psi_{\mathrm{dc-i}} \tag{3.4b}$$

$$\psi_{\mathrm{ac-i}} = -\sum\nolimits_{j \in \mathbb{N}_{\mathrm{ac}}} a_{\mathrm{i}j} \left(P_{\mathrm{ac-i}} - P_{\mathrm{ac-}j}\right) \tag{3.4c}$$

$$\psi_{\mathrm{dc-i}} = -\sum\nolimits_{j \in \mathbb{N}_{\mathrm{dc}}} a_{\mathrm{i}j} \left(P_{\mathrm{ac-i}} - P_{\mathrm{dc-}j}\right) \tag{3.4d}$$

for $\mathrm{i} \in \mathbb{N}_{\mathrm{ac}}$, where $P_{\mathrm{ac-}j}$ is the instantaneous power in p.u. generated by the $j^{th}$ *ac*-DG $\in \mathbb{N}_{\mathrm{ac}}$, and $P_{\mathrm{dc-}j}$ is the instantaneous power in p.u. generated by the $j^{th}$ *dc*-DG $\in \mathbb{N}_{\mathrm{dc}}$.

The *ac*-DSC for reactive power-sharing and voltage restoration is given by:

$$E_{\mathrm{i}} = E^* + N_{\mathrm{ac-i}} \cdot Q_{\mathrm{ac-i}} + \chi_{\mathrm{i}} \tag{3.5a}$$

$$\varrho_{\mathrm{i}} \dot{\chi}_{\mathrm{i}} = -\beta_{\mathrm{i}} \left(E_{\mathrm{i}} - E^*\right) - b_{\mathrm{i}} \sum\nolimits_{j \in \mathbb{N}_{\mathrm{ac}}} a_{\mathrm{i}j} \left(Q_{\mathrm{i}} - Q_j\right) \tag{3.5b}$$

for $\mathrm{i} \in \mathbb{N}_{\mathrm{ac}}$. The gains $M_{\mathrm{ac-i}}, N_{\mathrm{ac-i}} < 0$ are the primary droop gains, and $\sigma_{\mathrm{i}}, \varrho_{\mathrm{i}} > 0$ are time constants. The gains $\beta_{\mathrm{i}}, b_{\mathrm{i}} > 0$ can be tuned to produce a compromise between voltage regulation accuracy and reactive power-sharing accuracy. A block diagram of the proposed distributed secondary control strategy for the *ac*-DGs is shown in Fig. 3.3.

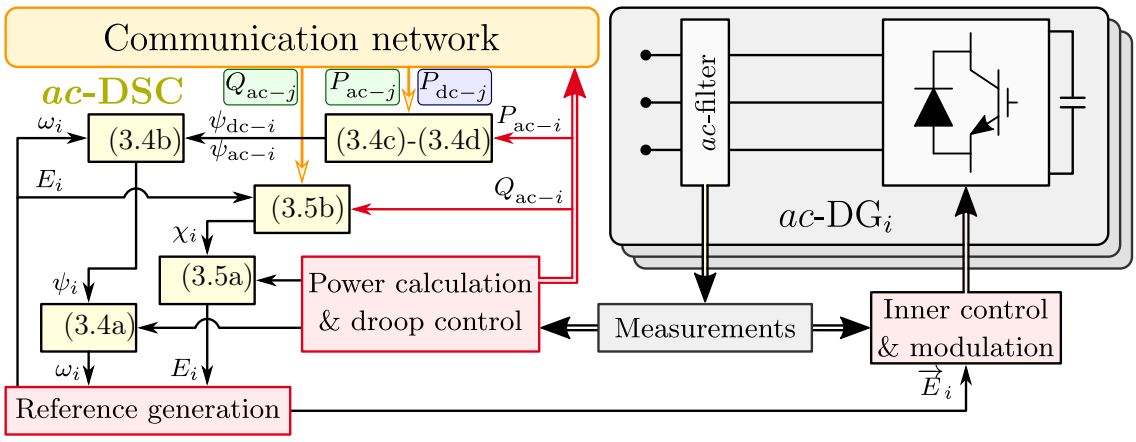


Figure 3.3: Proposed distributed secondary control for *ac*-microgrid (*ac*-DSC).

Although relatively similar control strategies have been studied before (see [99]), the key difference in this work is that the active power consensus of *ac*-DGs is extended to *dc*-DGs (and later, to *ICs*). This is reflected in the term $\psi_{\mathrm{dc-i}}$ [see (3.4d)], which illustrates the interaction between *ac*-DGs and *dc*-DGs, and in next sections.

## 3.4 Control Strategy Proposed for *dc*-Microgrid

### 3.4.1 Inner and Primary Control Loops

In *dc*-microgrids, several types of power electronic devices can be used to interface the *dc*-DGs with the network, depending on the system's requirements. Both unidirectional and bidirectional *dc*-to-*dc* converters can be used depending on the nature of the DG source. However, it must be able to operate in droop controlled mode, i.e., to synthesize voltages with variable magnitude. The structure and control loops for a droop controlled HBC is depicted in Fig. 3.4. A low-pass filter is considered to interface the *dc*-DGs with the *dc*-microgrid.

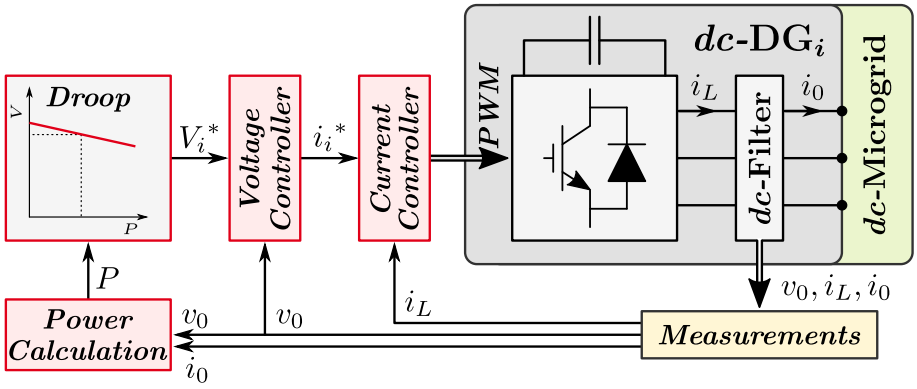


Figure 3.4: Inner and primary control loops for the *dc*-DGs.

A nested structure is considered for the controllers in the inner control loop of the *dc*-DGs, which consists of an outer voltage controller (slower) and an inner current controller (faster). Even though any kind of controller is able to synthesize the *dc*-DG's output *dc*-voltage, a proportional-integral (PI) controller is considered in this work. The typical structure for a PI controller ($C_{\mathrm{PI}}(s)$) is given by:

$$C_{\mathrm{PI}}(s) = k_P + \frac{k_{\mathrm{i}}}{s} \tag{3.6}$$

where $k_P$ and $k_{\mathrm{i}}$ are the proportional and integral gains of the controller, respectively. As depicted in Fig. 3.4, the reference current ($\mathrm{i_i}^*$) are set by the outer voltage loop, while the reference voltage (i.e., the output voltage magnitude) is set by the outer droop controllers and the secondary control loops, as will be described in the next Section. The typical structure for the droop controller is given by:

$$\delta V_{\mathrm{D}} = M_{\mathrm{dc}} P_{\mathrm{dc}} \tag{3.7}$$

where $\delta V_{\mathrm{D}}$ is the output of the droop controller, $M_{\mathrm{dc}} < 0$ is the droop slope, and $P_{\mathrm{dc}}$ is the active power generated by the *dc*-DG.

### 3.4.2 Secondary Control Loop

The secondary control loop for *dc*-DGs aims to restore the *dc*-voltages $V_{\mathrm{i}}$ to their nominal value $V^*$ while maintaining satisfactory power-sharing among DGs. In the proposed DSC for

the *dc*-DGs in the *dc*-microgrid (*dc*-DSC), the variable shared by the *dc*-DGs to the other DGs is the power $P_{\mathrm{i}}$ in p.u. generated by the i$^{th}$ *dc*-DG, given by

$$P_{\mathrm{i}} \coloneqq P_{\mathrm{dc-i}}/P_{\mathrm{max-i}}, \qquad \mathrm{i} \in \mathbb{N}_{\mathrm{dc}}, \tag{3.8}$$

where $P_{\mathrm{dc-i}}$ is the instantaneous power generated by the i$^{th}$ *dc*-DG and $P_{\mathrm{max-i}}$ is the rated power of the i$^{th}$ *dc*-DG. For the *dc*-microgrid, the secondary variable is the *dc*-voltage $V_{\mathrm{i}}$, while the consensus variable is the p.u. power $P_{\mathrm{i}}$. Then, the proposed *dc*-DSC for power-sharing and voltage restoration is

$$V_{\mathrm{i}} = V^* + M_{\mathrm{dc-i}} \cdot P_{\mathrm{dc-i}} + \varphi_{\mathrm{i}} \tag{3.9a}$$

$$\rho_{\mathrm{i}}\dot{\varphi}_{\mathrm{i}} = -\gamma_{\mathrm{i}}\left(V_{\mathrm{i}} - V^*\right) + \varphi_{\mathrm{dc-i}} + \varphi_{\mathrm{ac-i}} \tag{3.9b}$$

$$\varphi_{\mathrm{dc-i}} = -c_{\mathrm{i}} \sum\nolimits_{j\in\mathbb{N}_{\mathrm{dc}}} a_{\mathrm{i}j}\left(P_{\mathrm{dc-i}} - P_{\mathrm{dc-}j}\right) \tag{3.9c}$$

$$\varphi_{\mathrm{ac-i}} = -c_{\mathrm{i}} \sum\nolimits_{j\in\mathbb{N}_{\mathrm{ac}}} a_{\mathrm{i}j}\left(P_{\mathrm{dc-i}} - P_{\mathrm{ac-}j}\right) \tag{3.9d}$$

where $\mathrm{i} \in \mathbb{N}_{\mathrm{dc}}$, $M_{\mathrm{dc-i}} < 0$ is the primary control gain, and $\rho_{\mathrm{i}} > 0$ is a time constant. The gains $\gamma_{\mathrm{i}}$ and $c_{\mathrm{i}}$ can be tuned to produce a trade-off between voltage regulation accuracy and power-sharing accuracy. A block diagram of the proposed *dc*-DSC is shown in Fig. 3.5.

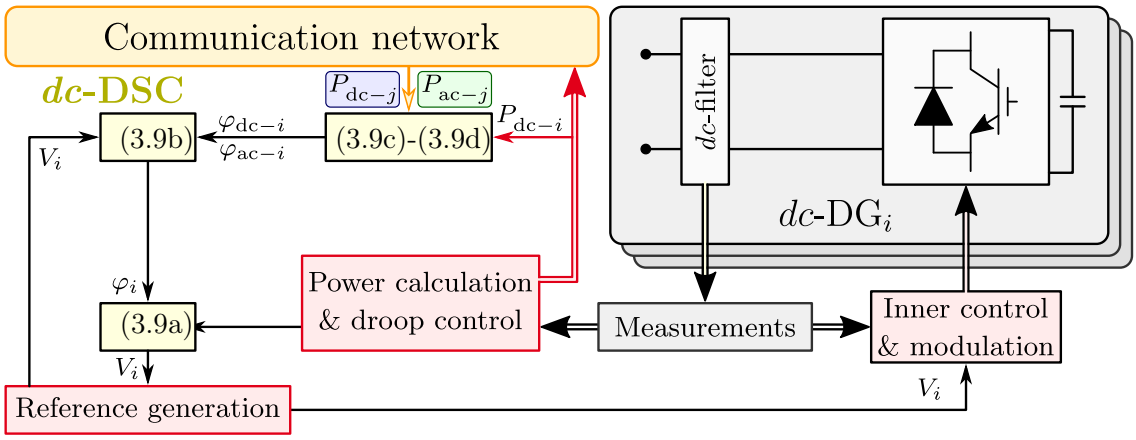


Figure 3.5: Proposed distributed secondary control for *dc*-microgrid (*dc*-DSC).

## 3.5 Control Strategy Proposed for a Single *IC*

### 3.5.1 Inner Control Loop

In hybrid *ac*/*dc*-microgrids, a power electronic device which allows *ac*/*dc* conversion and bidirectional power flow is required to interconnect the two sides of the microgrid. In this case, a two stage *ac*/*dc*/*dc* converter is considered for the *IC*, as shown in Fig. 3.6. Thus, the *IC* possesses two electrical ports; the first one is an *ac*-port which is connected to the *ac*-microgrid, while the second one is a *dc*-port connected to the *dc*-microgrid. The two ports are linked by a *dc*-link, which needs to maintain a constant *dc*-voltage ($E_{\mathrm{dc}}$). A low-pass filter is considered at each port to interface the *IC* with the DGs on the respective side.

The controllers in the inner loop of the *IC* must control independently the *ac*-and *dc*-variables. Moreover, only the converter from one side must regulate the *dc*-link voltage,

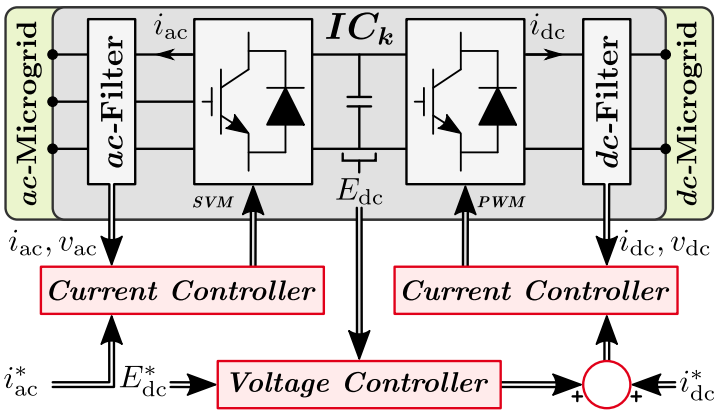


Figure 3.6: Inner control loop for the *ICs*.

while the other converter is in charge of regulating the power transfer. In this case, the converter on the *dc*-side of the *IC* is responsible for regulating the *dc*-link voltage ($E^*_{\rm dc}$). In addition, it is possible to feed-forward the current reference which allows to transfer the power set by the secondary control loop ($\mathrm{i}^*_{\rm dc}$), as described in the next Section. Due to the nature of the signals controlled at this side (the voltage and the current are *dc*-signals), a nested PI structure ($C_{\rm PI}(s)$) is considered for the controllers in the inner control loop of the *dc*-side of the *IC*. On the other hand, a PR controller ($C_{\rm PR}(s)$) is used to control the power transfer by the *IC*, according to the current reference ($\mathrm{i}^*_{\rm ac}$) obtained from the power reference ($P^*_{\rm IC}$) set by the secondary control loop, as will be described in next Section.

### 3.5.2 Secondary Control Loop

The novel consensus-based DSC strategy for the *ICs* proposed in this work (*ic*-DSC) is slightly different than those used for *ac*-DGs and *dc*-DGs. The *IC* has to regulate the power transfer between the two sides of the microgrid. This has to be realized seamlessly, and without affecting the power-sharing among the DGs. To achieve this, the *IC* sends its own status (1: ON, 0: OFF) to the DGs in order to enable the power-consensus between the two sides of the microgrid, while the *IC* receives the power in p.u. being generated by the *ac*-DGs ($P_{\rm ac}$) and by the *dc*-DGs ($P_{\rm dc}$). Therefore, the power reference $P^*_{{\rm IC}-k}$ for the single $k^{th}$ *IC* ($k = n + m + 1$) is updated as

$$\tau_k \dot{P}^*_{{\rm IC}-k} = -\sum_{{\rm i}\in\mathbb{N}_{\rm ac}} \sum_{j\in\mathbb{N}_{\rm dc}} a_{{\rm i}k} a_{jk} \left(P_{{\rm ac}-{\rm i}} - P_{{\rm dc}-j}\right) \tag{3.10}$$

where $\tau_k > 0$ is a time constant. Note that the DGs communicating with the *IC* are included in the control law (3.10). In this work, the sign convention is that $P^*_{{\rm IC}-k} > 0$ if power flows from the *dc*-microgrid to the *ac*-microgrid.

A block diagram of the proposed *ic*-DSC is shown in Fig. 3.7.

From (3.10), note that the power reference for the *IC* will be adjusted to ensure power-sharing among DGs in both sides of the hybrid *ac*/*dc*-microgrid. Additionally, if the *IC* is out of service, it is possible to split the proposed control system into two separate controllers (*ac*-DSC and *dc*-DSC), and change the global power-sharing to a sub-microgrid power-sharing.

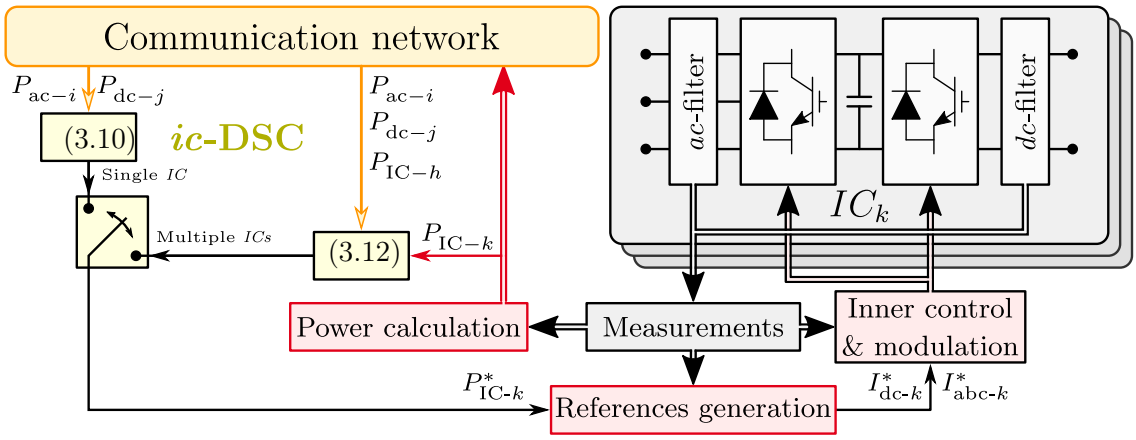


Figure 3.7: Proposed distributed secondary control for $IC$.

In this way, voltage/frequency regulation in each sub-microgrid can be achieved despite the temporary absence of the $IC$. Moreover, all the secondary control tasks are maintained within each microgrid, and the advantages of distributed controllers over the centralized ones are maintained. However, if the lone $IC$ in a hybrid $ac/dc$-microgrid fails, it will be impossible to transfer power from the $ac$-side to $dc$-side or vice-versa. Hence, the use of multiple $ICs$ in hybrid $ac/dc$-microgrids is highly recommended, as discussed in the next subsection.

Regarding the communication in (3.10), the proposed strategy works properly if at least one $ac$-DG and one $dc$-DG are communicating with the $IC$. This is illustrated using the hybrid microgrid topology shown in Fig. 3.8. Red dotted lines show the communication links between units. In this example, the hybrid $ac/dc$-microgrid is composed of 3 $ac$-DGs, 3 $dc$-DGs and 1 $IC$. The $IC$ communicates with 2 DGs on each side of the microgrid. The adjacency matrix $\mathbf{A}$ here models a connected bidirectional communication network. The elements in $\mathbf{A}$ are $a_{ij} = 1$ if a communication link exists between the i$^{th}$ and the $j^{th}$ unit, and $a_{ij} = 0$ otherwise.

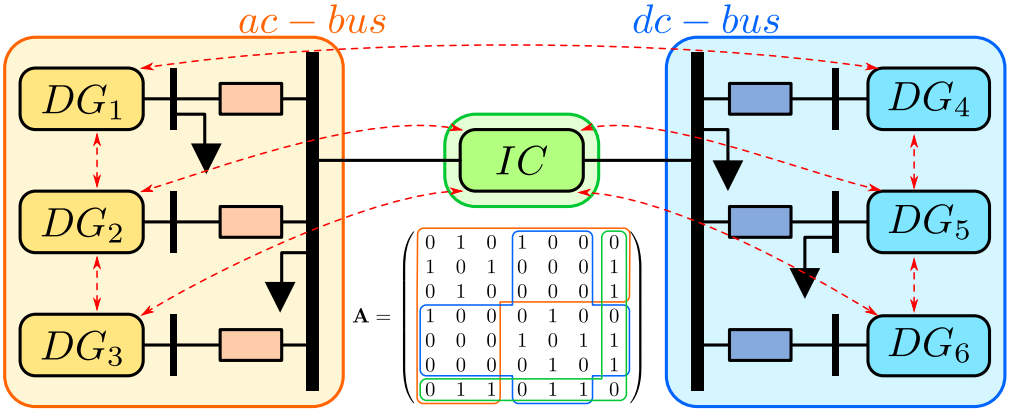


Figure 3.8: Example topology of a hybrid $ac/dc$-microgrid with the adjacency matrix.

## 3.6 Control Strategy Proposed for Multiple *ICs*

As mentioned before, by considering multiple *ICs* in the hybrid *ac/dc*-microgrid, it is possible to improve its reliability due to the existence of multiple paths for transferring power between sub-microgrids. However, the existence of multiple *ICs* increases the complexity of the microgrid control and —depending on the control strategy utilized— can generate circulating currents among the *ICs*. These circulating currents must be eliminated to avoid overloading of converters or line congestion [82].

Thus, based on the single *IC* controller proposed in (3.10), an additional term to achieve a power consensus among multiple *ICs* is introduced. The variable shared by the *ICs* is the power $P_k$ in p.u. being transferred through the $k^{th}$ *IC*.

$$P_k \coloneqq P_{\mathrm{IC}-k}/P_{\mathrm{max}-k}, \quad k \in \mathbb{N}_{\mathrm{IC}}, \tag{3.11}$$

where $P_{\mathrm{IC}-k}$ is the instantaneous power through the $k^{th}$ *IC* and $P_{\mathrm{max}-k}$ is its rated power. The *ic*-DSC proposed in this work for the $k^{th}$ *IC*, considering $g$ *ICs* in the microgrid, is given by

$$\dot{P}^{*}_{\mathrm{IC}-k} = -\mu_k \sum_{\mathrm{i}\in\mathbb{N}_{\mathrm{ac}}} \sum_{j\in\mathbb{N}_{\mathrm{dc}}} a_{\mathrm{i}k} a_{jk} \left(P_{\mathrm{ac}-\mathrm{i}} - P_{\mathrm{dc}-j}\right) - \vartheta_k \sum_{h\in\mathbb{N}_{\mathrm{IC}}} a_{hk} \left(P_{\mathrm{IC}-k} - P_{\mathrm{IC}-h}\right) \tag{3.12}$$

where $\mu_k$ and $\vartheta_k$ are positive gains for adjusting the transient response and the accuracy of power-sharing. The proposed *ic*-DSC contributes to both power-sharing among DGs on the two sides of the hybrid *ac/dc*-microgrid and power-sharing among *ICs*. Additionally, if any *IC* is out of service, the others can be used for transferring power between the two sub-microgrids, as long as their power ratings are not exceeded. The ratio of power-sharing among *ICs* can also be controlled by adjusting the second term on the right side of (3.12). Nevertheless, to control this ratio, it is necessary to have a general knowledge of the hybrid *ac/dc*-microgrid and to perform additional studies (e.g., optimal power flow) which are typically utilized at the hierarchical tertiary control level. The tertiary control level is outside the scope of this work.

## 3.7 Summary

In this Chapter, a consensus-based distributed secondary control strategy for hybrid *ac/dc*-microgrids has been proposed. This strategy considers the hybrid *ac/dc*-microgrid as a single entity, not three independent ones interacting with one another. The strategy is capable of restoring the variables modified by the primary control loop to their nominal values, while maintaining an accurate power-sharing among DGs on both sides of the microgrid. Additionally, when the hybrid *ac/dc*-microgrid has multiple *ICs*, accurate power-sharing among them is also ensured.

The proposed strategy considers a reduced communication layer, as each DG is communicating only with its neighbouring DGs. Due to the fact that *ICs* also participate in the communication layer, the secondary control strategy can be adapted to each side separately in case the *ICs* are not available. The tuning of the controllers proposed in this Chapter is addressed in Chapter 6. The validation of the proposed control strategy is reported in Chapter 7 using an experimental $24kW$ hybrid *ac/dc*-microgrid.

# Chapter 4

# Control Strategy Proposed to Minimize Operating Costs

## 4.1 Introduction

In this Chapter, a new consensus-based distributed secondary control (DSC) strategy is proposed for minimizing the operation cost among all the agents in the hybrid *ac*/*dc*-microgrid. In the DSC proposed in this Chapter, each DG achieves *incremental cost consensus* with all other DGs of the hybrid microgrid, i.e., *ac*-DGs and *dc*-DGs, while operating within limits. The main challenge for this Chapter is to design a control strategy for hybrid *ac*/*dc*-microgrids that minimizes the operational cost while restoring the secondary variables to their nominal values.

The formulation of the control strategy differs according to the number of *ICs* utilized in the microgrid. Thus, the main differences for the formulation of the control strategy considering one or more *ICs* are explained in this Chapter, which is organized as follows: the optimization problem considering a single *IC* is formulated in Section 4.2, while its proposed control strategy is presented in Section 4.3. Conversely, the formulation of the optimization problem considering multiple *ICs* and the control strategy proposed to solve this problem are presented in Section 4.4 and Section 4.5, respectively.

## 4.2 Single Interlinking Converter Formulation

First, the formulation of the optimization problem considers a single *IC* in the hybrid *ac*/*dc*-microgrid. The formulation of the optimization problem is explained in the following.

### 4.2.1 System Modelling

Fig. 4.1 shows a simplified topology for a hybrid *ac*/*dc*-microgrid, which consists of *ac*-DGs, *dc*-DGs and a single *IC*. The set of these devices are labelled as $\mathbb{N}_{\text{ac}} = \{1, \ldots, n\}$, $\mathbb{N}_{\text{dc}} = \{n+1, \ldots, n+m\}$, and $\mathbb{N}_{\text{IC}} = \{n+m+1\}$. For simplicity, a lumped load is modelled in each side of the microgrid (*ac*-Load and *dc*-Load).

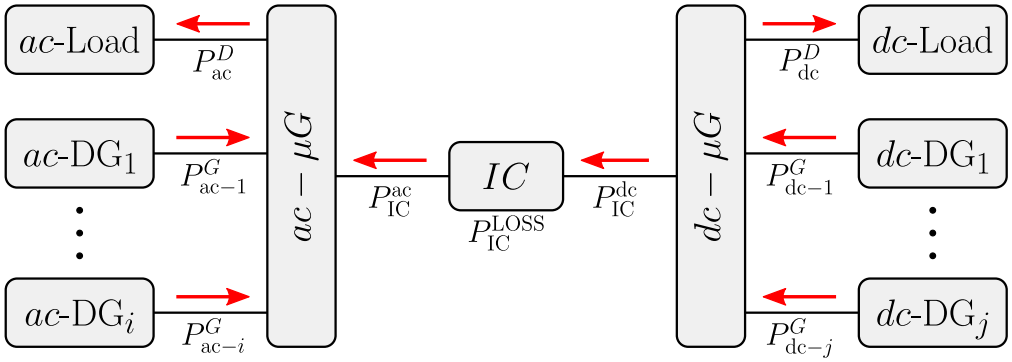


Figure 4.1: General topology for a hybrid *ac*/*dc*-microgrid with a single *IC*.

From Fig. 4.1 the following equations can be deduced:

$$P^{\text{ac}}_{\text{IC}} = P^{\text{D}}_{\text{ac}} - \sum_{\text{i}\in\mathbb{N}_{\text{ac}}} P^{\text{G}}_{\text{ac}-\text{i}} \tag{4.1a}$$

$$P^{\text{dc}}_{\text{IC}} = \sum_{j\in\mathbb{N}_{\text{dc}}} P^{\text{G}}_{\text{dc}-j} - P^{\text{D}}_{\text{dc}} \tag{4.1b}$$

$$P^{\text{LOSS}}_{\text{IC}} = P^{\text{dc}}_{\text{IC}} - P^{\text{ac}}_{\text{IC}} \tag{4.1c}$$

where $P^{\text{LOSS}}_{\text{IC}}$ is the power loss in the *IC*. Red arrows show the direction of the power flow in the microgrid: DGs supply power to the system, loads absorb power from the system, and the direction of the power flow in the *IC* has been arbitrarily defined.

Since the modelled *IC* lacks an energy storage unit, from (4.1c) follows that variables in the *IC* are not independent and two of them can be expressed as a function of the other variable in the *IC* (i.e., the power $P^{\text{ac}}_{\text{IC}}$ or $P^{\text{dc}}_{\text{IC}}$). Moreover, only power at one port of the *IC* can be controlled. Arbitrarily, in this case, the power in the *ac*-port $P^{\text{ac}}_{\text{IC}}$ is the variable controlled in the *IC* and it is the variable defined as independent in the *IC*. The power losses in the *IC* can be empirically modelled as a fraction of the power flowing through this device ($k^{\text{LOSS}}$ %) [136]. Then, the variables in the *IC* are expressed as shown in (4.2), where constants $k_{\text{IC}}$ and $k^{\text{LOSS}}_{\text{IC}}$ depend on the direction of the power through the *IC*, and are shown in Table 4.1.

$$P^{\text{dc}}_{\text{IC}}(P^{\text{ac}}_{\text{IC}}) = k_{\text{IC}} P^{\text{ac}}_{\text{IC}} \tag{4.2a}$$

$$P^{\text{LOSS}}_{\text{IC}}(P^{\text{ac}}_{\text{IC}}) = k^{\text{LOSS}}_{\text{IC}} P^{\text{ac}}_{\text{IC}} \tag{4.2b}$$

Table 4.1: Parameters for equation (4.2).

| | Power flow | $k_{\text{IC}}$ | $k_{\text{IC}}^{\text{LOSS}}$ |
|---|---|---|---|
| $P_{\text{IC}}^{\text{ac}} > 0$ | from $dc$ to $ac$ | $\frac{1}{1-k^{\text{LOSS}}}$ | $\frac{k^{\text{LOSS}}}{1-k^{\text{LOSS}}}$ |
| $P_{\text{IC}}^{\text{ac}} < 0$ | from $ac$ to $dc$ | $1 - k^{\text{LOSS}}$ | $-k^{\text{LOSS}}$ |

Now, replacing (4.2a) in (4.1b), and combining it with (4.1a), we obtain:

$$P_{\text{IC}}^{\text{ac}}(\mathbf{P_{ac}^G}, \mathbf{P_{dc}^G}) = \frac{1}{1+k_{\text{IC}}} \left( P_{\text{ac}}^{\text{D}} - \sum_{\text{i}\in\mathbb{N}_{\text{ac}}} P_{\text{ac-i}}^{\text{G}} + \sum_{j\in\mathbb{N}_{\text{dc}}} P_{\text{dc}-j}^{\text{G}} - P_{\text{dc}}^{\text{D}} \right) \tag{4.3}$$

where $\mathbf{P_{ac}^G} = \{P_{\text{ac-i}}^{\text{G}} : \text{i} \in \mathbb{N}_{\text{ac}}\}$ and $\mathbf{P_{dc}^G} = \{P_{\text{dc}-j}^{\text{G}} : j \in \mathbb{N}_{\text{dc}}\}$ are the set of power generated by the $ac$-DGs and $dc$-DGs, respectively.

In addition, a quadratic cost function for the operation cost of the $ac$-DGs ($C_{\text{ac-i}},\ \forall \text{i} \in \mathbb{N}_{\text{ac}}$) and $dc$-DGs ($C_{\text{dc}-j},\ \forall j \in \mathbb{N}_{\text{dc}}$) is considered, which is defined as follows:

$$C_{\text{ac-i}}(P_{\text{ac-i}}^{\text{G}}) = a_{\text{ac-i}} \left(P_{\text{ac-i}}^{\text{G}}\right)^2 + b_{\text{ac-i}} P_{\text{ac-i}}^{\text{G}} + c_{\text{ac-i}} \quad [\$/h], \qquad \forall \text{i} \in \mathbb{N}_{\text{ac}} \tag{4.4a}$$

$$C_{\text{dc}-j}(P_{\text{dc}-j}^{\text{G}}) = a_{\text{dc}-j} \left(P_{\text{dc}-j}^{\text{G}}\right)^2 + b_{\text{dc}-j} P_{\text{dc}-j}^{\text{G}} + c_{\text{dc}-j} \quad [\$/h], \quad \forall j \in \mathbb{N}_{\text{dc}} \tag{4.4b}$$

where $a_{\text{ac-i}} \in \mathbb{R}_{>0}$ and $b_{\text{ac-i}}, c_{\text{ac-i}} \in \mathbb{R}_{\geq 0}$ are parameters for the cost function of the $\text{i}^{th}$ $ac$-DG, and $a_{\text{dc}-j} \in \mathbb{R}_{>0}$ and $b_{\text{dc}-j}, c_{\text{dc}-j} \in \mathbb{R}_{\geq 0}$ are parameters for the cost function of the $j^{th}$ $dc$-DG.

For future use, the following partial derivatives are calculated:

$$\frac{\partial P_{\text{IC}}^{\text{ac}}}{\partial P_{\text{ac-i}}^{\text{G}}} = \frac{-1}{1+k_{\text{IC}}}, \qquad \frac{\partial P_{\text{IC}}^{\text{ac}}}{\partial P_{\text{dc}-j}^{\text{G}}} = \frac{1}{1+k_{\text{IC}}}, \qquad \frac{\partial P_{\text{IC}}^{\text{LOSS}}}{\partial P_{\text{IC}}^{\text{ac}}} = k_{\text{IC}}^{\text{LOSS}} \tag{4.5}$$

### 4.2.2 Optimization Problem Formulation

The optimization problem considered in this work determines the least-cost dispatch of controllable DG units in a hybrid $ac/dc$-microgrid while maintaining generation power within limits. Constraints impose the later condition on DG power injections. The formulation is based on a system representation without line losses as follows:

$$\underset{\mathbf{P_{ac}^G}, \mathbf{P_{dc}^G}}{\text{minimize}} \quad \sum_{\text{i}\in\mathbb{N}_{\text{ac}}} C_{\text{ac-i}}\left(P_{\text{ac-i}}^{\text{G}}\right) + \sum_{j\in\mathbb{N}_{\text{dc}}} C_{\text{dc}-j}\left(P_{\text{dc}-j}^{\text{G}}\right) \tag{4.6a}$$

$$\text{subject to} \quad P_{\text{ac}}^{\text{D}} + P_{\text{dc}}^{\text{D}} + P_{\text{IC}}^{\text{LOSS}} = \sum_{\text{i}\in\mathbb{N}_{\text{ac}}} P_{\text{ac-i}}^{\text{G}} + \sum_{j\in\mathbb{N}_{\text{dc}}} P_{\text{dc}-j}^{\text{G}}, \tag{4.6b}$$

$$P_{\text{ac-i}}^{\text{G}-} \leq P_{\text{ac-i}}^{\text{G}} \leq P_{\text{ac-i}}^{\text{G}+}, \quad \text{i} \in \mathbb{N}_{\text{ac}}, \tag{4.6c}$$

$$P_{\text{dc}-j}^{\text{G}-} \leq P_{\text{dc}-j}^{\text{G}} \leq P_{\text{dc}-j}^{\text{G}+}, \quad j \in \mathbb{N}_{\text{dc}}, \tag{4.6d}$$

$$P_{\text{IC}}^{\text{ac}-} \leq P_{\text{IC}}^{\text{ac}} \leq P_{\text{IC}}^{\text{ac}+} \tag{4.6e}$$

where (4.6b) is the power balance constraint (equality condition), and (4.6c)-(4.6e) are the power limits constraints (inequality conditions). The upper limits are defined by the superscripts G+ and ac+, while the lower limits are defined by the superscripts G- and ac-. In this problem

(a) the power generated by the DGs ($P^{\mathrm{G}}_{\mathrm{ac-i}}$ and $P^{\mathrm{G}}_{\mathrm{dc}-j}$) are **optimization variables**,

(b) the power loads ($P^{\mathrm{D}}_{\mathrm{ac}}$ and $P^{\mathrm{D}}_{\mathrm{dc}}$) are **constants** for the optimization problem, and

(c) the power transferred through the *IC* ($P^{\mathrm{ac}}_{\mathrm{IC}}$) is a **function of the optimization variables**.

Considering the optimization problem formulated in (4.6a)-(4.6e), the Lagrangian function can be written as follows:

$$
\begin{aligned}
&\mathbb{L}\left(P^{\mathrm{G}}_{\mathrm{ac-i}}, P^{\mathrm{G}}_{\mathrm{dc}-j}, \lambda, \alpha^{+}_{\mathrm{ac-i}}, \alpha^{-}_{\mathrm{ac-i}}, \alpha^{+}_{\mathrm{dc}-j}, \alpha^{-}_{\mathrm{dc}-j}, \alpha^{+}_{\mathrm{IC}}, \alpha^{-}_{\mathrm{IC}}\right) = \\
&\qquad \sum\nolimits_{\mathrm{i}\in\mathbb{N}_{\mathrm{ac}}} C_{\mathrm{ac-i}}\left(P^{\mathrm{G}}_{\mathrm{ac-i}}\right) + \sum\nolimits_{j\in\mathbb{N}_{\mathrm{dc}}} C_{\mathrm{dc}-j}\left(P^{\mathrm{G}}_{\mathrm{dc}-j}\right) \\
&\qquad + \lambda\left(P^{\mathrm{D}}_{\mathrm{ac}} + P^{\mathrm{D}}_{\mathrm{dc}} + P^{\mathrm{LOSS}}_{\mathrm{IC}} - \sum\nolimits_{\mathrm{i}\in\mathbb{N}_{\mathrm{ac}}} P^{\mathrm{G}}_{\mathrm{ac-i}} - \sum\nolimits_{j\in\mathbb{N}_{\mathrm{dc}}} P^{\mathrm{G}}_{\mathrm{dc}-j}\right) \\
&\qquad + \sum\nolimits_{\mathrm{i}\in\mathbb{N}_{\mathrm{ac}}} \left[\alpha^{+}_{\mathrm{ac-i}}\left(P^{\mathrm{G}}_{\mathrm{ac-i}} - P^{\mathrm{G+}}_{\mathrm{ac-i}}\right) + \alpha^{-}_{\mathrm{ac-i}}\left(P^{\mathrm{G-}}_{\mathrm{ac-i}} - P^{\mathrm{G}}_{\mathrm{ac-i}}\right)\right] \\
&\qquad + \sum\nolimits_{j\in\mathbb{N}_{\mathrm{dc}}} \left[\alpha^{+}_{\mathrm{dc}-j}\left(P^{\mathrm{G}}_{\mathrm{dc}-j} - P^{\mathrm{G+}}_{\mathrm{dc}-j}\right) + \alpha^{-}_{\mathrm{dc}-j}\left(P^{\mathrm{G-}}_{\mathrm{dc}-j} - P^{\mathrm{G}}_{\mathrm{dc}-j}\right)\right] \\
&\qquad + \sum\nolimits_{k\in\mathbb{N}_{\mathrm{IC}}} \left[\alpha^{+}_{\mathrm{IC}}\left(P^{\mathrm{ac}}_{\mathrm{IC}} - P^{\mathrm{ac+}}_{\mathrm{IC}}\right) + \alpha^{-}_{\mathrm{IC}}\left(P^{\mathrm{ac-}}_{\mathrm{IC}} - P^{\mathrm{ac}}_{\mathrm{IC}}\right)\right]
\end{aligned}
\tag{4.7}
$$

where the Lagrange multiplier $\lambda$ is associated with the power balance constraint (4.6b), $\{\alpha^{+}_{\mathrm{ac-i}}, \alpha^{-}_{\mathrm{ac-i}}, \alpha^{+}_{\mathrm{dc}-j}, \alpha^{-}_{\mathrm{dc}-j}\}$ with the maximum and minimum power outputs of DGs in equations (4.6c)-(4.6d), and $\{\alpha^{+}_{\mathrm{IC}}, \alpha^{-}_{\mathrm{IC}}\}$ with the power limits of the *IC* in equation (4.6e). Since the objective function of the optimization problem is strictly convex and the constraints are linear, if the problem is feasible then it has a unique globally optimal solution.

Now, considering (4.5) and (4.7), the KKT optimality conditions of the optimization

problem are as follows:

*Stationary condition* :

$$\frac{\partial \mathbb{L}}{\partial P^{\mathrm{G}}_{\mathrm{ac-i}}} = \nabla C_{\mathrm{ac-i}}\left(P^{\mathrm{G}}_{\mathrm{ac-i}}\right) + \lambda\left(\frac{-k^{\mathrm{LOSS}}_{\mathrm{IC}}}{1+k_{\mathrm{IC}}} - 1\right) + \alpha^{+}_{\mathrm{ac-i}} - \alpha^{-}_{\mathrm{ac-i}} + \alpha^{+}_{\mathrm{IC}}\left(\frac{-k^{\mathrm{LOSS}}_{\mathrm{IC}}}{1+k_{\mathrm{IC}}}\right) + \alpha^{-}_{\mathrm{IC}}\left(\frac{k^{\mathrm{LOSS}}_{\mathrm{IC}}}{1+k_{\mathrm{IC}}}\right) = 0, \quad \mathrm{i} \in \mathbb{N}_{\mathrm{ac}} \tag{4.8a}$$

$$\frac{\partial \mathbb{L}}{\partial P^{\mathrm{G}}_{\mathrm{dc}-j}} = \nabla C_{\mathrm{dc}-j}\left(P^{\mathrm{G}}_{\mathrm{dc}-j}\right) + \lambda\left(\frac{k^{\mathrm{LOSS}}_{\mathrm{IC}}}{1+k_{\mathrm{IC}}} - 1\right) + \alpha^{+}_{\mathrm{dc}-j} - \alpha^{-}_{\mathrm{dc}-j} + \alpha^{+}_{\mathrm{IC}}\left(\frac{k^{\mathrm{LOSS}}_{\mathrm{IC}}}{1+k_{\mathrm{IC}}}\right) + \alpha^{-}_{\mathrm{IC}}\left(\frac{-k^{\mathrm{LOSS}}_{\mathrm{IC}}}{1+k_{\mathrm{IC}}}\right) = 0, \quad j \in \mathbb{N}_{\mathrm{dc}} \tag{4.8b}$$

*Complementary slackness* :

$$\alpha^{+}_{\mathrm{ac-i}}\left(P^{\mathrm{G}}_{\mathrm{ac-i}} - P^{\mathrm{G}+}_{\mathrm{ac-i}}\right) = 0, \quad \mathrm{i} \in \mathbb{N}_{\mathrm{ac}} \tag{4.8c}$$

$$\alpha^{-}_{\mathrm{ac-i}}\left(P^{\mathrm{G}-}_{\mathrm{ac-i}} - P^{\mathrm{G}}_{\mathrm{ac-i}}\right) = 0, \quad \mathrm{i} \in \mathbb{N}_{\mathrm{ac}} \tag{4.8d}$$

$$\alpha^{+}_{\mathrm{dc}-j}\left(P^{\mathrm{G}}_{\mathrm{dc}-j} - P^{\mathrm{G}+}_{\mathrm{dc}-j}\right) = 0, \quad j \in \mathbb{N}_{\mathrm{dc}} \tag{4.8e}$$

$$\alpha^{-}_{\mathrm{dc}-j}\left(P^{\mathrm{G}-}_{\mathrm{dc}-j} - P^{\mathrm{G}}_{\mathrm{dc}-j}\right) = 0, \quad j \in \mathbb{N}_{\mathrm{dc}} \tag{4.8f}$$

$$\alpha^{+}_{\mathrm{IC}}\left(P^{\mathrm{ac}}_{\mathrm{IC}} - P^{\mathrm{ac}+}_{\mathrm{IC}}\right) = 0 \tag{4.8g}$$

$$\alpha^{-}_{\mathrm{IC}}\left(P^{\mathrm{ac}-}_{\mathrm{IC}} - P^{\mathrm{ac}}_{\mathrm{IC}}\right) = 0 \tag{4.8h}$$

*Primal feasibility* :

(4.6b), (4.6c), (4.6d) and (4.6e)

*Dual feasibility* :

$$\alpha^{+}_{\mathrm{ac-i}}, \alpha^{-}_{\mathrm{ac-i}} \geq 0, \quad \mathrm{i} \in \mathbb{N}_{\mathrm{ac}} \tag{4.8i}$$

$$\alpha^{+}_{\mathrm{dc}-j}, \alpha^{-}_{\mathrm{dc}-j} \geq 0, \quad j \in \mathbb{N}_{\mathrm{dc}} \tag{4.8j}$$

$$\alpha^{+}_{\mathrm{IC}}, \alpha^{-}_{\mathrm{IC}} \geq 0 \tag{4.8k}$$

Note that for each $\mathrm{i} \in \mathbb{N}_{\mathrm{ac}}$ and $j \in \mathbb{N}_{\mathrm{dc}}$, (4.8a) and (4.8b) can each be solved to obtain the Lagrange multiplier $\lambda$; as useful notation, the corresponding solutions are denoted as

$$\lambda^{\mathrm{ac}}_{\mathrm{i}} := \frac{1+k_{\mathrm{IC}}}{1+k_{\mathrm{IC}}+k^{\mathrm{LOSS}}_{\mathrm{IC}}}\left(\nabla C_{\mathrm{ac-i}}\left(P^{\mathrm{G}}_{\mathrm{ac-i}}\right) + \alpha^{+}_{\mathrm{ac-i}} - \alpha^{-}_{\mathrm{ac-i}}\right) - \frac{k^{\mathrm{LOSS}}_{\mathrm{IC}}}{1+k_{\mathrm{IC}}+k^{\mathrm{LOSS}}_{\mathrm{IC}}}\left(\alpha^{+}_{\mathrm{IC}} - \alpha^{-}_{\mathrm{IC}}\right), \quad \forall \mathrm{i} \in \mathbb{N}_{\mathrm{ac}} \tag{4.9a}$$

$$\lambda^{\mathrm{dc}}_{j} := \frac{1+k_{\mathrm{IC}}}{1+k_{\mathrm{IC}}-k^{\mathrm{LOSS}}_{\mathrm{IC}}}\left(\nabla C_{\mathrm{dc}-j}\left(P^{\mathrm{G}}_{\mathrm{dc}-j}\right) + \alpha^{+}_{\mathrm{dc}-j} - \alpha^{-}_{\mathrm{dc}-j}\right) + \frac{k^{\mathrm{LOSS}}_{\mathrm{IC}}}{1+k_{\mathrm{IC}}-k^{\mathrm{LOSS}}_{\mathrm{IC}}}\left(\alpha^{+}_{\mathrm{IC}} - \alpha^{-}_{\mathrm{IC}}\right), \quad \forall j \in \mathbb{N}_{\mathrm{dc}} \tag{4.9b}$$

where, by optimality, we must have that (4.10) holds. We can interpret $\lambda^{\mathrm{ac}}_{\mathrm{i}}$ as a Lagrange multiplier for the $\mathrm{i}^{th}$ DG on the *ac*-side, and $\lambda^{\mathrm{dc}}_{j}$ as a Lagrange multiplier for the $j^{th}$ DG on the *dc*-side.

$$\lambda = \lambda^{\mathrm{ac}}_{\mathrm{i}} = \lambda^{\mathrm{dc}}_{j}, \quad \forall \mathrm{i} \in \mathbb{N}_{\mathrm{ac}}, \ \forall j \in \mathbb{N}_{\mathrm{dc}} \tag{4.10}$$

Replacing (4.2) in (4.1c), the following expression can be obtained:

$$k_{\mathrm{IC}}^{\mathrm{LOSS}} = k_{\mathrm{IC}} - 1 \tag{4.11}$$

Now, replacing (4.11) in (4.9), we obtain a reduced expression in terms of $k_{\mathrm{IC}}$ for $\lambda_{\mathrm{i}}^{\mathrm{ac}}$ ($\forall \mathrm{i} \in \mathbb{N}_{\mathrm{ac}}$) and $\lambda_{j}^{\mathrm{dc}}$ ($\forall j \in \mathbb{N}_{\mathrm{dc}}$), as shown in (4.12). In this formulation, the DGs need to know the constant $k_{\mathrm{IC}}$ [see Table 4.1] and the variables $\{\alpha_{\mathrm{IC}}^{+}, \alpha_{\mathrm{IC}}^{-}\}$ from the *IC*; therefore, it is necessary to have a communication link between the DGs and the *IC*. In case the communication link does not exist (e.g., in a distributed configuration), the variables can be estimated using a distributed observer.

$$\lambda_{\mathrm{i}}^{\mathrm{ac}} = \frac{k_{\mathrm{IC}}+1}{2k_{\mathrm{IC}}}\left(\nabla C_{\mathrm{ac-i}}\left(P_{\mathrm{ac-i}}^{\mathrm{G}}\right) + \alpha_{\mathrm{ac-i}}^{+} - \alpha_{\mathrm{ac-i}}^{-}\right) - \frac{k_{\mathrm{IC}}-1}{2k_{\mathrm{IC}}}\left(\alpha_{\mathrm{IC}}^{+} - \alpha_{\mathrm{IC}}^{-}\right), \quad \forall \mathrm{i} \in \mathbb{N}_{\mathrm{ac}} \tag{4.12a}$$

$$\lambda_{j}^{\mathrm{dc}} = \frac{k_{\mathrm{IC}}+1}{2}\left(\nabla C_{\mathrm{dc}-j}\left(P_{\mathrm{dc}-j}^{\mathrm{G}}\right) + \alpha_{\mathrm{dc}-j}^{+} - \alpha_{\mathrm{dc}-j}^{-}\right) + \frac{k_{\mathrm{IC}}-1}{2}\left(\alpha_{\mathrm{IC}}^{+} - \alpha_{\mathrm{IC}}^{-}\right), \forall j \in \mathbb{N}_{\mathrm{dc}} \tag{4.12b}$$

Based on the optimality conditions of the optimal dispatch problem, a distributed secondary control strategy is designed with the objective of providing secondary variables regulation in the hybrid *ac*/*dc*-microgrid (i.e., frequency and voltage amplitude regulation in the *ac*-microgrid, and voltage regulation in the *dc*-microgrid), while driving the hybrid *ac*/*dc*-microgrid with a single *IC* to an optimal dispatch that complies with the KKT conditions (4.8).

## 4.3 Proposed Control Scheme for a Single *IC*

The distributed control scheme proposed in this Chapter aims to regulate the secondary variables in a hybrid *ac*/*dc*-microgrid, while maintaining optimality of dispatch. As explained in Chapter 3, the control scheme is designed for the three components of the hybrid *ac*/*dc*-microgrid, which are the *ac*-DGs, the *dc*-DGs, and the *IC*. On the other hand, the design of the control scheme is based on the convex optimization problem (4.6a), (4.6b), (4.6c) and (4.6d) presented in Section 4.2.2.

### 4.3.1 Control scheme proposed for the *ac*-DGs

The control scheme proposed for the *ac*-DGs is responsible for regulating the frequency on the *ac*-side of the microgrid, while minimizing the operation cost of all the DGs in the hybrid *ac*/*dc*-microgrid (4.13). It is important to note that the formulation of the optimization problem does not include reactive power injections, since it is assumed that the *ac*-DSC described in Section 3.3 controls reactive power injections to maintain voltages in the *ac*-side regulated. Thus, this proposal focuses on frequency and *dc*-voltage control by means of

optimally dispatching of real power of DG units.

$$\omega_{\rm i} = \omega^* + M_{\rm ac-i} P^{\rm G}_{\rm ac-i} + \Omega^{\rm ac}_{\rm i} \tag{4.13a}$$

$$\dot{\Omega}^{\rm ac}_{\rm i} = -k^a_{\rm ac-i}\left(\omega_{\rm i} - \omega^*\right) - k^b_{\rm ac-i} \sum_{j\in\mathbb{N}_{\rm ac}} a_{{\rm i}j}\left(\lambda^{\rm ac}_{\rm i} - \lambda^{\rm ac}_j\right) - k^c_{\rm ac-i} \sum_{j\in\mathbb{N}_{\rm dc}} a_{{\rm i}j}\left(\lambda^{\rm ac}_{\rm i} - \lambda^{\rm dc}_j\right) \tag{4.13b}$$

$$\dot{\alpha}^+_{\rm ac-i} = \mu^a_{\rm ac-i} \max\left\{P^{\rm G}_{\rm ac-i} - P^{\rm G+}_{\rm ac-i} + \frac{k^{\rm d}_{\rm ac-i}}{\mu^a_{\rm ac-i}}\alpha^+_{\rm ac-i}, 0\right\} - k^{\rm d}_{\rm ac-i}\alpha^+_{\rm ac-i} \tag{4.13c}$$

$$\dot{\alpha}^-_{\rm ac-i} = \mu^b_{\rm ac-i} \max\left\{P^{\rm G-}_{\rm ac-i} - P^{\rm G}_{\rm ac-i} + \frac{k^{\rm e}_{\rm ac-i}}{\mu^b_{\rm ac-i}}\alpha^-_{\rm ac-i}, 0\right\} - k^{\rm e}_{\rm ac-i}\alpha^-_{\rm ac-i} \tag{4.13d}$$

$$\lambda^{\rm ac}_{\rm i} = \frac{\hat{k}^{\rm IC}_{\rm i} + 1}{2\hat{k}^{\rm IC}_{\rm i}}\left(\nabla C_{\rm ac-i}\left(P^{\rm G}_{\rm ac-i}\right) + \alpha^+_{\rm ac-i} - \alpha^-_{\rm ac-i}\right) - \frac{\hat{k}^{\rm IC}_{\rm i} - 1}{2\hat{k}^{\rm IC}_{\rm i}}\hat{\alpha}^{\rm IC}_{\rm i} \tag{4.13e}$$

The proposed controller drives the system to an optimal dispatch point, while complying with the KKT conditions of the optimization problem. The term $\Omega^{\rm ac}_{\rm i}$ in (4.13a) is a secondary control action to drive the units to their optimal dispatch level. Specifically, the frequency droop controller in (4.13a) is perturbed by the control action $\Omega^{\rm ac}_{\rm i}$, in order to change the dispatch of the *ac*-DGs until all DGs satisfy the consensus condition (4.10), which corresponds to the (unique) dual variable associated with the demand-supply balance equation of the hybrid *ac/dc*-microgrid's optimal dispatch problem, (4.6b). Variables $k^a_{\rm ac-i}$, $k^b_{\rm ac-i}$ and $k^c_{\rm ac-i}$ are positive gains of the controller. In steady-state, the optimality condition (4.10) is enforced by (4.13b), (4.15b) and (4.16a).

The $\lambda^{\rm ac}_{\rm i}$ of each *ac*-DG that complies with the stationarity condition can be calculated from (4.13e). The terms $\hat{k}^{\rm IC}_{\rm i}$ and $\hat{\alpha}^{\rm IC}_{\rm i}$ are the estimate of the variables $k_{\rm IC}$ and $\alpha^+_{\rm IC} - \alpha^-_{\rm IC}$ from the *IC*, respectively. Since the *ac*-DGs need information from the *IC* and a communication link between all the DGs and the *IC* is not mandatory (the distributed approach is based on the existence of communication links between neighbouring agents), the cooperative tracking explained in Section 2.5 is considered among the *ac*-DGs to communicate the information from the *IC* to all the *ac*-DGs. Thus, the observers implemented are as follows:

$$\dot{\hat{k}}^{\rm IC}_{\rm i} = -\sum_{j\in\mathbb{N}_{\rm ac}} a_{{\rm i}j}\left(\hat{k}^{\rm IC}_{\rm i} - \hat{k}^{\rm IC}_j\right) - \sum_{j\in\mathbb{N}_{\rm dc}} a_{{\rm i}j}\left(\hat{k}^{\rm IC}_{\rm i} - \hat{k}^{\rm IC}_j\right) - g_{\rm i}\left(\hat{k}^{\rm IC}_{\rm i} - k_{\rm IC}\right) \tag{4.14a}$$

$$\dot{\hat{\alpha}}^{\rm IC}_{\rm i} = -\sum_{j\in\mathbb{N}_{\rm ac}} a_{{\rm i}j}\left(\hat{\alpha}^{\rm IC}_{\rm i} - \hat{\alpha}^{\rm IC}_j\right) - \sum_{j\in\mathbb{N}_{\rm dc}} a_{{\rm i}j}\left(\hat{\alpha}^{\rm IC}_{\rm i} - \hat{\alpha}^{\rm IC}_j\right) - g_{\rm i}\left(\hat{\alpha}^{\rm IC}_{\rm i} - (\alpha^+_{\rm IC} - \alpha^-_{\rm IC})\right) \tag{4.14b}$$

where $g_{\rm i} > 0$ if *ac*-DG$_{\rm i}$ has a direct communication link with the *IC* and $g_{\rm i} = 0$ otherwise.

In (4.13e), variables $\alpha^+_{\rm ac-i}$ and $\alpha^-_{\rm ac-i}$ are local control actions to keep the active power dispatch of *ac*-DGs within limits, which in equilibrium correspond to the dual variables associated with maximum and minimum active power limits, respectively. The control actions $\alpha^+_{\rm ac-i}$ and $\alpha^-_{\rm ac-i}$ are obtained from equations (4.13c) and (4.13d), respectively. In these equations, an increase in the values of the control actions is induced whenever *ac*-DG$_{\rm i}$ goes beyond its maximum or minimum active power dispatch levels, respectively. Also, control actions $\alpha^+_{\rm ac-i}$ and $\alpha^-_{\rm ac-i}$ are driven down to zero by the controller if the active power dispatch of

$ac$-DG$_\mathrm{i}$ is strictly within limits, where $k^{\mathrm{d}}_{\mathrm{ac-i}}$, $k^{\mathrm{e}}_{\mathrm{ac-i}}$, $\mu^{a}_{\mathrm{ac-i}}$ and $\mu^{b}_{\mathrm{ac-i}}$ are positive gains of the controllers.

In summary, the $ac$-DG$_\mathrm{i}$ shares the following information with its neighbours:

- It sends the value of $\lambda^{\mathrm{ac}}_{\mathrm{i}},\ \mathrm{i} \in \mathbb{N}_{\mathrm{ac}}$, to the $ac$-DGs, $dc$-DGs and to the $IC$ [see (4.12a)].
- It receives the value of $\lambda^{\mathrm{ac}}_{j},\ j \in \mathbb{N}_{\mathrm{ac}}$, from the $ac$-DGs [see (4.13b)].
- It receives the value of $\lambda^{\mathrm{dc}}_{j},\ j \in \mathbb{N}_{\mathrm{dc}}$, from the $dc$-DGs [see (4.13b)].
- It sends/receives the values of $\hat{k}^{\mathrm{IC}}_{\mathrm{i}}$ and $\hat{\alpha}^{\mathrm{IC}}_{\mathrm{i}}$ to the $ac$-DGs and $dc$-DGs [see (4.14)].
- It receives the values of $k_{\mathrm{IC}}$, $\alpha^{+}_{\mathrm{IC}}$ and $\alpha^{-}_{\mathrm{IC}}$ from the $IC$ [see (4.16b) and (4.16c)].

### 4.3.2 Control scheme proposed for the *dc*-DGs

The control scheme proposed for the $dc$-DGs is responsible for regulating the voltage of the $dc$-side of the microgrid, while minimizing the operation cost of all the DGs in the hybrid $ac/dc$-microgrid (4.15).

$$V_j = V^* + M_{\mathrm{dc-}j} P^{\mathrm{G}}_{\mathrm{dc-}j} + \Omega^{\mathrm{dc}}_{j} \tag{4.15a}$$

$$\dot{\Omega}^{\mathrm{dc}}_{j} = -k^{a}_{\mathrm{dc-}j}\left(V_j - V^*\right) - k^{b}_{\mathrm{dc-}j} \sum_{\mathrm{i}\in\mathbb{N}_{\mathrm{dc}}} a_{\mathrm{ij}} \left(\lambda^{\mathrm{dc}}_{j} - \lambda^{\mathrm{dc}}_{\mathrm{i}}\right) - k^{c}_{\mathrm{dc-}j} \sum_{\mathrm{i}\in\mathbb{N}_{\mathrm{ac}}} a_{\mathrm{ij}} \left(\lambda^{\mathrm{dc}}_{j} - \lambda^{\mathrm{ac}}_{\mathrm{i}}\right) \tag{4.15b}$$

$$\dot{\alpha}^{+}_{\mathrm{dc-}j} = \mu^{a}_{\mathrm{dc-}j} \max\left\{ P^{\mathrm{G}}_{\mathrm{dc-}j} - P^{\mathrm{G+}}_{\mathrm{dc-}j} + \frac{k^{\mathrm{d}}_{\mathrm{dc-}j}}{\mu^{a}_{\mathrm{dc-}j}} \alpha^{+}_{\mathrm{dc-}j}, 0 \right\} - k^{\mathrm{d}}_{\mathrm{dc-}j} \alpha^{+}_{\mathrm{dc-}j} \tag{4.15c}$$

$$\dot{\alpha}^{-}_{\mathrm{dc-}j} = \mu^{b}_{\mathrm{dc-}j} \max\left\{ P^{\mathrm{G-}}_{\mathrm{dc-}j} - P^{\mathrm{G}}_{\mathrm{dc-}j} + \frac{k^{\mathrm{e}}_{\mathrm{dc-}j}}{\mu^{b}_{\mathrm{dc-}j}} \alpha^{-}_{\mathrm{dc-}j}, 0 \right\} - k^{\mathrm{e}}_{\mathrm{dc-}j} \alpha^{-}_{\mathrm{dc-}j} \tag{4.15d}$$

$$\lambda^{\mathrm{dc}}_{j} = \frac{\hat{k}^{\mathrm{IC}}_{j} + 1}{2} \left( \nabla C_{\mathrm{dc-}j}\left(P^{\mathrm{G}}_{\mathrm{dc-}j}\right) + \alpha^{+}_{\mathrm{dc-}j} - \alpha^{-}_{\mathrm{dc-}j} \right) + \frac{\hat{k}^{\mathrm{IC}}_{j} - 1}{2} \hat{\alpha}^{\mathrm{IC}}_{j} \tag{4.15e}$$

The proposed controller drives the system to an optimal dispatch point, i.e., it complies with the KKT conditions of the optimization problem. The term $\Omega^{\mathrm{dc}}_{j}$ in (4.15a) is a secondary control action to drive the units to their optimal dispatch level. Specifically, the voltage droop controller in (4.15a) is perturbed by the control action $\Omega^{\mathrm{dc}}_{j}$, in order to change the dispatch of the $dc$-DGs until all DGs reach the same value of $\lambda$, which corresponds to the (unique) dual variable associated with the demand-supply balance equation of the hybrid $ac/dc$-microgrid's optimal dispatch problem, (4.6b). Variables $k^{a}_{\mathrm{dc-}j}$, $k^{b}_{\mathrm{dc-}j}$ and $k^{c}_{\mathrm{dc-}j}$ are positive gains of the controller. In steady-state, the optimality condition (4.10) is enforced by (4.13b), (4.15b) and (4.16a)

The $\lambda^{\mathrm{dc}}_{j}$ of each $dc$-DG that complies with the stationarity condition can be calculated from (4.15e). The terms $\hat{k}^{\mathrm{IC}}_{j}$ and $\hat{\alpha}^{\mathrm{IC}}_{j}$ are the estimate of the variables $k_{\mathrm{IC}}$ and $\alpha^{+}_{\mathrm{IC}} - \alpha^{-}_{\mathrm{IC}}$ from the $IC$, respectively, and were explained in (4.14).

Variables $\alpha^{+}_{\mathrm{dc}-j}$ and $\alpha^{-}_{\mathrm{dc}-j}$ are local control actions to keep the active power dispatch of *dc*-DGs within limits, which in equilibrium correspond to the dual variables associated with maximum and minimum active power limits, respectively. The control actions $\alpha^{+}_{\mathrm{dc}-j}$ and $\alpha^{-}_{\mathrm{dc}-j}$ are obtained from equations (4.15c) and (4.15d), respectively. In these equations, an increase in the values of the control actions is induced whenever *dc*-DG$_{\mathrm{i}}$ goes beyond its maximum or minimum active power dispatch levels, respectively. Also, control actions $\alpha^{+}_{\mathrm{dc}-j}$ and $\alpha^{-}_{\mathrm{dc}-j}$ are driven down to zero by the controller if the active power dispatch of *dc*-DG$_j$ is strictly within limits, where $k^{\mathrm{d}}_{\mathrm{dc}-j}$, $k^{\mathrm{e}}_{\mathrm{dc}-j}$, $\mu^{a}_{\mathrm{dc}-\mathrm{i}}$ and $\mu^{b}_{\mathrm{dc}-\mathrm{i}}$ are positive gains of the controllers.

In summary, the *dc*-DG$_j$ shares the following information with its neighbours:

- It sends the value of $\lambda^{\mathrm{dc}}_{j},\ j \in \mathbb{N}_{\mathrm{dc}}$, to the *dc*-DGs, *ac*-DGs and to the *IC* [see (4.12b)].
- It receives the value of $\lambda^{\mathrm{dc}}_{\mathrm{i}},\ \mathrm{i} \in \mathbb{N}_{\mathrm{dc}}$, from the *dc*-DGs [see (4.15b)].
- It receives the value of $\lambda^{\mathrm{ac}}_{\mathrm{i}},\ \mathrm{i} \in \mathbb{N}_{\mathrm{ac}}$, from the *ac*-DGs [see (4.15b)].
- It sends/receives the values of $\hat{k}^{\mathrm{IC}}_{j}$ and $\hat{\alpha}^{\mathrm{IC}}_{j}$ to the *ac*-DGs and *dc*-DGs [see (4.14)].
- It receives the values of $\alpha^{+}_{\mathrm{IC}}$ and $\alpha^{-}_{\mathrm{IC}}$ from the *IC* [see (4.16b) and (4.16c)].

### 4.3.3 Control scheme proposed for the *IC*

The control scheme proposed for the *IC* is responsible for transferring power between both sides of the hybrid *ac*/*dc*-microgrid ($P^{*}_{\mathrm{IC}-k}$), in order to help to minimize the operation cost of all the DGs (4.16). In this work, the power reference obtained from the controller corresponds to the power at the *ac*-port of the *IC* since it is the controllable power defined in section 4.2.1.

$$\tau_{\mathrm{IC}-k}\dot{P}^{*}_{\mathrm{IC}-k} = -\sum_{\mathrm{i}\in\mathbb{N}_{\mathrm{ac}}}\sum_{j\in\mathbb{N}_{\mathrm{dc}}} a_{\mathrm{i}k}a_{jk}\left(\lambda^{\mathrm{ac}}_{\mathrm{i}} - \lambda^{\mathrm{dc}}_{j}\right) \tag{4.16a}$$

$$\dot{\alpha}^{+}_{\mathrm{IC}} = \mu^{a}_{\mathrm{IC}}\max\left\{P^{\mathrm{ac}}_{\mathrm{IC}} - P^{\mathrm{ac}+}_{\mathrm{IC}} + \frac{\tau^{a}_{\mathrm{IC}}}{\mu^{a}_{\mathrm{IC}}}\alpha^{+}_{\mathrm{IC}}, 0\right\} - \tau^{a}_{\mathrm{IC}}\alpha^{+}_{\mathrm{IC}} \tag{4.16b}$$

$$\dot{\alpha}^{-}_{\mathrm{IC}} = \mu^{b}_{\mathrm{IC}}\max\left\{P^{\mathrm{ac}-}_{\mathrm{IC}} - P^{\mathrm{ac}}_{\mathrm{IC}} + \frac{\tau^{b}_{\mathrm{IC}}}{\mu^{b}_{\mathrm{IC}}}\alpha^{-}_{\mathrm{IC}}, 0\right\} - \tau^{b}_{\mathrm{IC}}\alpha^{-}_{\mathrm{IC}} \tag{4.16c}$$

The proposed controller drives the system to an optimal dispatch point transferring power between the two sides of the hybrid *ac*/*dc*-microgrid, while complying with the KKT conditions of the optimization problem. In this case, the *IC* transfers power from the cheapest side to the most expensive one by comparing the values of $\lambda^{\mathrm{ac}}_{\mathrm{i}}$ and $\lambda^{\mathrm{dc}}_{j}$, as shown in (4.16a). Variable $\tau_{\mathrm{IC}-k}$is a positive gain of the controller. Variables $\alpha^{+}_{\mathrm{IC}}$ and $\alpha^{-}_{\mathrm{IC}}$ are local control actions to keep the active power transferred through the *IC* within limits, which in equilibrium correspond to the dual variables associated with maximum and minimum active power limits, respectively.

The control actions $\alpha^{+}_{\mathrm{IC}}$ and $\alpha^{-}_{\mathrm{IC}}$ are obtained from equations (4.16b) and (4.16c), respectively. In these equations, an increase in the values of the control actions is induced whenever

the *IC* goes beyond its maximum or minimum active power levels, respectively. Also, control actions $\alpha^{+}_{\text{IC}}$ and $\alpha^{-}_{\text{IC}}$ are driven down to zero by the controller if the active power transferred through the *IC* is strictly within limits, where $\tau^{a}_{\text{IC}}$, $\tau^{b}_{\text{IC}}$, $\mu^{a}_{\text{IC}}$ and $\mu^{b}_{\text{IC}}$ are positive gains of the controllers.

In summary, the *IC* shares the following information with its neighbours:

- It sends the values of $k_{\text{IC}}$, $\alpha^{+}_{\text{IC}}$ and $\alpha^{-}_{\text{IC}}$ to the *ac*-DGs and *dc*-DGs [see (4.12a)-(4.12b)].
- It receives the value of $\lambda^{\text{ac}}_{\text{i}}$, $\text{i} \in \mathbb{N}_{\text{ac}}$ from the *ac*-DGs [see (4.16a)].
- It receives the value of $\lambda^{\text{dc}}_{j}$, $j \in \mathbb{N}_{\text{dc}}$ from the *dc*-DGs [see (4.16a)].

## 4.4 Multiple Interlinking Converters Formulation

Now, the formulation of the optimization problem considering multiple *ICs* in the hybrid *ac*/*dc*-microgrid is presented. In this case, the power transferred through each *IC* can be considered as an optimization variable since it is possible to dispatch the amount of power transferred through each one, according to their efficiency (i.e., according to the percentage of power lost in the *ac*-to-*dc* conversion). Moreover, the total amount of power transferred from one side of the microgrid to the other (i.e., the sum of the individual power transferred through each *IC*) must help to reach the least-cost dispatch of controllable DGs units as presented in Section 4.2. This is further explained in the following.

### 4.4.1 System Modelling

Fig. 4.2 shows a simplified topology for a hybrid *ac*/*dc*-microgrid, which consists of *ac*-DGs, *dc*-DGs and multiple *ICs*. The set of these devices are labelled as $\mathbb{N}_{\text{ac}} = \{1, \ldots, n\}$, $\mathbb{N}_{\text{dc}} = \{n+1, \ldots, n+m\}$, and $\mathbb{N}_{\text{IC}} = \{n+m+1, \ldots, n+m+g\}$. For simplicity, a lumped load is modelled in each side of the microgrid (*ac*-Load and *dc*-Load).

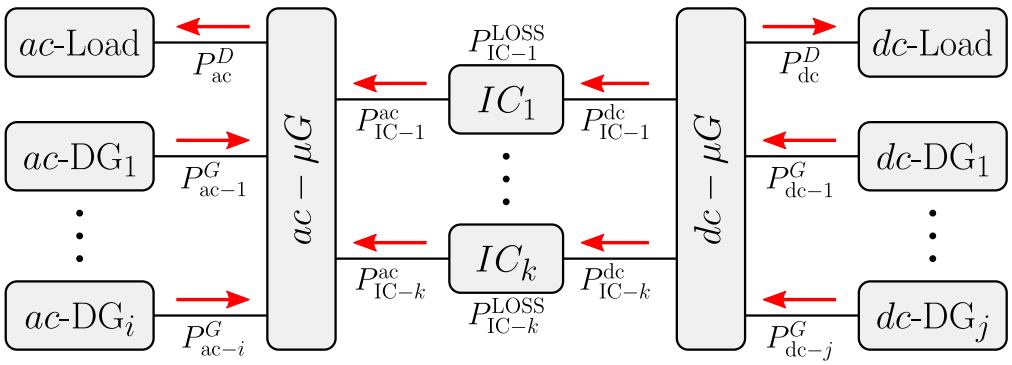


Figure 4.2: General topology for a hybrid *ac*/*dc*-microgrid with multiple *ICs*.

From Fig. 4.2 the following equations can be deduced:

$$\sum_{k\in\mathbb{N}_{\mathrm{IC}}} P^{\mathrm{ac}}_{\mathrm{IC}-k} = P^{\mathrm{D}}_{\mathrm{ac}} - \sum_{\mathrm{i}\in\mathbb{N}_{\mathrm{ac}}} P^{\mathrm{G}}_{\mathrm{ac}-\mathrm{i}} \tag{4.17a}$$

$$\sum_{k\in\mathbb{N}_{\mathrm{IC}}} P^{\mathrm{dc}}_{\mathrm{IC}-k} = \sum_{j\in\mathbb{N}_{\mathrm{dc}}} P^{\mathrm{G}}_{\mathrm{dc}-j} - P^{\mathrm{D}}_{\mathrm{dc}} \tag{4.17b}$$

where red arrows show the direction of the power flow in the microgrid: DGs supply power to the system, loads absorb power from the system, and the direction of the power flow in the *ICs* has been arbitrarily defined (it is positive from the *dc*- to the *ac*-side). In this case, the losses in the *ICs* are defined as explained in previous Section (see (4.2) and Table 4.1).

The total power transferred from the *ac*-microgrid to the *dc*-microgrid (and vice versa) can be defined as shown in (4.18). Moreover, the relationship between $P^{\mathrm{ac}}_{\mathrm{IC}}$ and $P^{\mathrm{dc}}_{\mathrm{IC}}$ can be defined as explained in previous Section [see (4.2a)].

$$P^{\mathrm{ac}}_{\mathrm{IC}} = \sum_{k\in\mathbb{N}_{\mathrm{IC}}} P^{\mathrm{ac}}_{\mathrm{IC}-k}\ , \qquad P^{\mathrm{dc}}_{\mathrm{IC}} = \sum_{k\in\mathbb{N}_{\mathrm{IC}}} P^{\mathrm{dc}}_{\mathrm{IC}-k} \tag{4.18}$$

Now, the total power transferred through multiple *ICs* ($P^{\mathrm{ac}}_{\mathrm{IC}}$) is defined as a function of the generated powers, as shown in (4.19). On the contrary, the power transferred through each *IC* ($P^{\mathrm{ac}}_{\mathrm{IC}-k}$) is not a function of the generated powers and it can be dispatched in order to reduce the losses and, therefore, minimize the operation cost of the hybrid *ac/dc*-microgrid.

$$P^{\mathrm{ac}}_{\mathrm{IC}}(\mathbf{P^G_{ac}}, \mathbf{P^G_{dc}}) = \frac{1}{1+k_{\mathrm{IC}}}\left(P^{\mathrm{D}}_{\mathrm{ac}} - \sum_{\mathrm{i}\in\mathbb{N}_{\mathrm{ac}}} P^{\mathrm{G}}_{\mathrm{ac}-\mathrm{i}} + \sum_{j\in\mathbb{N}_{\mathrm{dc}}} P^{\mathrm{G}}_{\mathrm{dc}-j} - P^{\mathrm{D}}_{\mathrm{dc}}\right) \tag{4.19}$$

where $\mathbf{P^G_{ac}} = \{P^{\mathrm{G}}_{\mathrm{ac}-\mathrm{i}} : \mathrm{i}\in\mathbb{N}_{\mathrm{ac}}\}$ and $\mathbf{P^G_{dc}} = \{P^{\mathrm{G}}_{\mathrm{dc}-j} : j\in\mathbb{N}_{\mathrm{dc}}\}$ are the set of power generated by the *ac*-DGs and *dc*-DGs, respectively.

In addition, the power transferred through the $k^{th}$ *IC* ($P^{\mathrm{ac}}_{\mathrm{IC}-k}$) is defined as a percentage ($\zeta^{\mathrm{ac}}_{\mathrm{IC}-k}$) of the total power transferred from one side of the hybrid *ac/dc*-microgrid to the other ($P^{\mathrm{ac}}_{\mathrm{IC}}$), as shown in (4.20a). Thus, the condition shown in (4.20b) must always be met.

$$P^{\mathrm{ac}}_{\mathrm{IC}-k} = \zeta^{\mathrm{ac}}_{\mathrm{IC}-k} P^{\mathrm{ac}}_{\mathrm{IC}}\ , \qquad \forall k\in\mathbb{N}_{\mathrm{IC}} \tag{4.20a}$$

$$\sum_{k\in\mathbb{N}_{\mathrm{IC}}} \zeta^{\mathrm{ac}}_{\mathrm{IC}-k} = 1 \tag{4.20b}$$

Finally, rearranging (4.20), the following expressions $\forall k\in\mathbb{N}_{\mathrm{IC}}$ are obtained for future use in the next Section:

$$P^{\mathrm{ac}}_{\mathrm{IC}} = \frac{P^{\mathrm{ac}}_{\mathrm{IC}-k}}{\zeta^{\mathrm{ac}}_{\mathrm{IC}-k}}, \quad \zeta^{\mathrm{ac}}_{\mathrm{IC}-k} = \frac{P^{\mathrm{ac}}_{\mathrm{IC}-k}}{P^{\mathrm{ac}}_{\mathrm{IC}}}, \quad \frac{\partial P^{\mathrm{ac}}_{\mathrm{IC}}}{\partial P^{\mathrm{ac}}_{\mathrm{IC}-k}} = \frac{1}{\zeta^{\mathrm{ac}}_{\mathrm{IC}-k}} \tag{4.21}$$

### 4.4.2 Optimization Problem Formulation

The optimization problem considered in this part of the work determines the least-cost dispatch of controllable DGs and *ICs* units in a hybrid *ac/dc*-microgrid while maintaining generation and transfer power within limits. Constraints impose the later condition on DGs power injections and *ICs* power transfer. The formulation is based on a system representation without line losses as follows:

$$\underset{\mathbf{P^G_{ac}}, \mathbf{P^G_{dc}}, \mathbf{P^{ac}_{IC}}}{\text{minimize}} \quad \sum_{\mathrm{i}\in\mathbb{N}_{\mathrm{ac}}} C_{\mathrm{ac-i}}\left(P^{\mathrm{G}}_{\mathrm{ac-i}}\right) + \sum_{j\in\mathbb{N}_{\mathrm{dc}}} C_{\mathrm{dc}-j}\left(P^{\mathrm{G}}_{\mathrm{dc}-j}\right) \tag{4.22a}$$

$$\text{subject to} \quad P^{\mathrm{D}}_{\mathrm{ac}} + P^{\mathrm{D}}_{\mathrm{dc}} + P^{\mathrm{LOSS}}_{\mathrm{IC}} = \sum_{\mathrm{i}\in\mathbb{N}_{\mathrm{ac}}} P^{\mathrm{G}}_{\mathrm{ac-i}} + \sum_{j\in\mathbb{N}_{\mathrm{dc}}} P^{\mathrm{G}}_{\mathrm{dc}-j}, \tag{4.22b}$$

$$P^{\mathrm{ac}}_{\mathrm{IC}} = \sum_{k\in\mathbb{N}_{\mathrm{IC}}} P^{\mathrm{ac}}_{\mathrm{IC}-k}, \tag{4.22c}$$

$$P^{\mathrm{G}-}_{\mathrm{ac-i}} \le P^{\mathrm{G}}_{\mathrm{ac-i}} \le P^{\mathrm{G}+}_{\mathrm{ac-i}}, \quad \mathrm{i}\in\mathbb{N}_{\mathrm{ac}}, \tag{4.22d}$$

$$P^{\mathrm{G}-}_{\mathrm{dc}-j} \le P^{\mathrm{G}}_{\mathrm{dc}-j} \le P^{\mathrm{G}+}_{\mathrm{dc}-j}, \quad j\in\mathbb{N}_{\mathrm{dc}}, \tag{4.22e}$$

$$P^{\mathrm{ac}-}_{\mathrm{IC}-k} \le P^{\mathrm{ac}}_{\mathrm{IC}-k} \le P^{\mathrm{ac}+}_{\mathrm{IC}-k}, \quad k\in\mathbb{N}_{\mathrm{IC}} \tag{4.22f}$$

where $\mathbf{P^{ac}_{IC}} = \{P^{\mathrm{ac}}_{\mathrm{IC}-k} : k\in\mathbb{N}_{\mathrm{IC}}\}$ is the set of power transfer through the *ICs*, (4.22b) is the power balance constraint (first equality condition), (4.22c) is the power transfer constraint (second equality condition), and (4.22d)-(4.22f) are the power limits constraints (inequality conditions). The upper limits are defined by the superscripts G+ and ac+, while the lower limits are defined by the superscripts G- and ac-. In this problem

(a) the power generated by the DGs ($P^{\mathrm{G}}_{\mathrm{ac-i}}$ and $P^{\mathrm{G}}_{\mathrm{dc}-j}$) are **optimization variables**,

(b) the power transferred through the *ICs* ($P^{\mathrm{ac}}_{\mathrm{IC}-k}$) are **optimization variables**, and

(c) the power loads ($P^{\mathrm{D}}_{\mathrm{ac}}$ and $P^{\mathrm{D}}_{\mathrm{dc}}$) are **constants** for the optimization problem.

Considering the optimization problem formulated in (4.22a)-(4.22f), the Lagrangian function can be written as follows:

$$\begin{aligned}
&\mathbb{L}\left(P^{\mathrm{G}}_{\mathrm{ac-i}}, P^{\mathrm{G}}_{\mathrm{dc}-j}, P^{\mathrm{ac}}_{\mathrm{IC}-k}, \lambda^{\mathrm{G}}, \lambda^{\mathrm{IC}}, \alpha^{+}_{\mathrm{ac-i}}, \alpha^{-}_{\mathrm{ac-i}}, \alpha^{+}_{\mathrm{dc}-j}, \alpha^{-}_{\mathrm{dc}-j}, \alpha^{+}_{\mathrm{IC}-k}, \alpha^{-}_{\mathrm{IC}-k}\right) = \\
&\quad \sum\nolimits_{\mathrm{i}\in\mathbb{N}_{\mathrm{ac}}} C_{\mathrm{ac-i}}\left(P^{\mathrm{G}}_{\mathrm{ac-i}}\right) + \sum\nolimits_{j\in\mathbb{N}_{\mathrm{dc}}} C_{\mathrm{dc}-j}\left(P^{\mathrm{G}}_{\mathrm{dc}-j}\right) \\
&\quad + \lambda^{\mathrm{G}}\left(P^{\mathrm{D}}_{\mathrm{ac}} + P^{\mathrm{D}}_{\mathrm{dc}} + P^{\mathrm{LOSS}}_{\mathrm{IC}} - \sum\nolimits_{\mathrm{i}\in\mathbb{N}_{\mathrm{ac}}} P^{\mathrm{G}}_{\mathrm{ac-i}} - \sum\nolimits_{j\in\mathbb{N}_{\mathrm{dc}}} P^{\mathrm{G}}_{\mathrm{dc}-j}\right) \\
&\quad + \lambda^{\mathrm{IC}}\left(P^{\mathrm{ac}}_{\mathrm{IC}} - \sum\nolimits_{k\in\mathbb{N}_{\mathrm{IC}}} P^{\mathrm{ac}}_{\mathrm{IC}-k}\right) \\
&\quad + \sum\nolimits_{\mathrm{i}\in\mathbb{N}_{\mathrm{ac}}} \left[\alpha^{+}_{\mathrm{ac-i}}\left(P^{\mathrm{G}}_{\mathrm{ac-i}} - P^{\mathrm{G}+}_{\mathrm{ac-i}}\right) + \alpha^{-}_{\mathrm{ac-i}}\left(P^{\mathrm{G}-}_{\mathrm{ac-i}} - P^{\mathrm{G}}_{\mathrm{ac-i}}\right)\right] \\
&\quad + \sum\nolimits_{j\in\mathbb{N}_{\mathrm{dc}}} \left[\alpha^{+}_{\mathrm{dc}-j}\left(P^{\mathrm{G}}_{\mathrm{dc}-j} - P^{\mathrm{G}+}_{\mathrm{dc}-j}\right) + \alpha^{-}_{\mathrm{dc}-j}\left(P^{\mathrm{G}-}_{\mathrm{dc}-j} - P^{\mathrm{G}}_{\mathrm{dc}-j}\right)\right] \\
&\quad + \sum\nolimits_{k\in\mathbb{N}_{\mathrm{IC}}} \left[\alpha^{+}_{\mathrm{IC}-k}\left(P^{\mathrm{ac}}_{\mathrm{IC}-k} - P^{\mathrm{ac}+}_{\mathrm{IC}-k}\right) + \alpha^{-}_{\mathrm{IC}-k}\left(P^{\mathrm{ac}-}_{\mathrm{IC}-k} - P^{\mathrm{ac}}_{\mathrm{IC}-k}\right)\right]
\end{aligned} \tag{4.23}$$

where the Lagrange multiplier $\lambda^{\mathrm{G}}$ is associated with the power balance constraint (4.22b), $\lambda^{\mathrm{IC}}$ with the power transfer constraint (4.22c), $\{\alpha^{+}_{\mathrm{ac-i}}, \alpha^{-}_{\mathrm{ac-i}}, \alpha^{+}_{\mathrm{dc}-j}, \alpha^{-}_{\mathrm{dc}-j}\}$ with the maximum and

minimum power outputs of DGs in equations (4.22d)-(4.22e), and $\{\alpha^{+}_{\mathrm{IC}-k}, \alpha^{-}_{\mathrm{IC}-k}\}$ with the power limits of the *ICs* in equation (4.22f). Since the objective function of the optimization problem is strictly convex and the constraints are linear, if the problem is feasible then it has a unique globally optimal solution.

Now, considering (4.21) and (4.23), the KKT optimality conditions of the optimization problem are as follows:

*Stationary condition* :

$$\frac{\partial \mathbb{L}}{\partial P^{\mathrm{G}}_{\mathrm{ac-i}}} = \nabla C_{\mathrm{ac-i}}\left(P^{\mathrm{G}}_{\mathrm{ac-i}}\right) - \lambda^{\mathrm{G}}\left(\frac{2k_{\mathrm{IC}}}{k_{\mathrm{IC}}+1}\right) - \lambda^{\mathrm{IC}}\left(\frac{1}{k_{\mathrm{IC}}+1}\right) + \alpha^{+}_{\mathrm{ac-i}} - \alpha^{-}_{\mathrm{ac-i}} = 0, \quad \mathrm{i} \in \mathbb{N}_{\mathrm{ac}} \tag{4.24a}$$

$$\frac{\partial \mathbb{L}}{\partial P^{\mathrm{G}}_{\mathrm{dc}-j}} = \nabla C_{\mathrm{dc}-j}\left(P^{\mathrm{G}}_{\mathrm{dc}-j}\right) - \lambda^{\mathrm{G}}\left(\frac{2}{k_{\mathrm{IC}}+1}\right) + \lambda^{\mathrm{IC}}\left(\frac{1}{k_{\mathrm{IC}}+1}\right) + \alpha^{+}_{\mathrm{dc}-j} - \alpha^{-}_{\mathrm{dc}-j} = 0, \quad j \in \mathbb{N}_{\mathrm{dc}} \tag{4.24b}$$

$$\frac{\partial \mathbb{L}}{\partial P^{\mathrm{ac}}_{\mathrm{IC}-k}} = \lambda^{\mathrm{G}} k^{\mathrm{LOSS}}_{\mathrm{IC}-k} - \lambda^{\mathrm{IC}}\left(\frac{P^{\mathrm{ac}}_{\mathrm{IC}-k} - P^{\mathrm{ac}}_{\mathrm{IC}}}{P^{\mathrm{ac}}_{\mathrm{IC}-k}}\right) + \alpha^{+}_{\mathrm{IC}-k} - \alpha^{-}_{\mathrm{IC}-k} = 0, \quad k \in \mathbb{N}_{\mathrm{IC}} \tag{4.24c}$$

*Complementary slackness* :

$$\alpha^{+}_{\mathrm{ac-i}}\left(P^{\mathrm{G}}_{\mathrm{ac-i}} - P^{\mathrm{G}+}_{\mathrm{ac-i}}\right) = 0, \quad \mathrm{i} \in \mathbb{N}_{\mathrm{ac}} \tag{4.24d}$$

$$\alpha^{-}_{\mathrm{ac-i}}\left(P^{\mathrm{G}-}_{\mathrm{ac-i}} - P^{\mathrm{G}}_{\mathrm{ac-i}}\right) = 0, \quad \mathrm{i} \in \mathbb{N}_{\mathrm{ac}} \tag{4.24e}$$

$$\alpha^{+}_{\mathrm{dc}-j}\left(P^{\mathrm{G}}_{\mathrm{dc}-j} - P^{\mathrm{G}+}_{\mathrm{dc}-j}\right) = 0, \quad j \in \mathbb{N}_{\mathrm{dc}} \tag{4.24f}$$

$$\alpha^{-}_{\mathrm{dc}-j}\left(P^{\mathrm{G}-}_{\mathrm{dc}-j} - P^{\mathrm{G}}_{\mathrm{dc}-j}\right) = 0, \quad j \in \mathbb{N}_{\mathrm{dc}} \tag{4.24g}$$

$$\alpha^{+}_{\mathrm{IC}-k}\left(P^{\mathrm{ac}}_{\mathrm{IC}-k} - P^{\mathrm{ac}+}_{\mathrm{IC}-k}\right) = 0, \quad k \in \mathbb{N}_{\mathrm{IC}} \tag{4.24h}$$

$$\alpha^{-}_{\mathrm{IC}-k}\left(P^{\mathrm{ac}-}_{\mathrm{IC}-k} - P^{\mathrm{ac}}_{\mathrm{IC}-k}\right) = 0, \quad k \in \mathbb{N}_{\mathrm{IC}} \tag{4.24i}$$

*Primal feasibility* :

(4.22b), (4.22c), (4.22d), (4.22e) and (4.22f)

*Dual feasibility* :

$$\alpha^{+}_{\mathrm{ac-i}}, \alpha^{-}_{\mathrm{ac-i}} \geq 0, \quad \mathrm{i} \in \mathbb{N}_{\mathrm{ac}} \tag{4.24j}$$

$$\alpha^{+}_{\mathrm{dc}-j}, \alpha^{-}_{\mathrm{dc}-j} \geq 0, \quad j \in \mathbb{N}_{\mathrm{dc}} \tag{4.24k}$$

$$\alpha^{+}_{\mathrm{IC}-k}, \alpha^{-}_{\mathrm{IC}-k} \geq 0, \quad k \in \mathbb{N}_{\mathrm{IC}} \tag{4.24l}$$

where $k_{\mathrm{IC}}$ and $P^{\mathrm{ac}}_{\mathrm{IC}}$ are variables from the group of *ICs* and will be explained in section 4.5.3.

Note that for each $\mathrm{i} \in \mathbb{N}_{\mathrm{ac}}$, $j \in \mathbb{N}_{\mathrm{dc}}$ and $k \in \mathbb{N}_{\mathrm{IC}}$, (4.24a), (4.24b) and (4.24c) can each be solved to obtain the Lagrange multipliers $\lambda^{\mathrm{G}}$ and $\lambda^{\mathrm{IC}}$; as useful notation, the corresponding solutions are denoted as

$$\lambda^{\mathrm{G}}_{\mathrm{ac-i}} := \frac{k_{\mathrm{IC}}+1}{2k_{\mathrm{IC}}}\left(\nabla C_{\mathrm{ac-i}}\left(P^{\mathrm{G}}_{\mathrm{ac-i}}\right) + \alpha^{+}_{\mathrm{ac-i}} - \alpha^{-}_{\mathrm{ac-i}}\right) - \frac{1}{2k_{\mathrm{IC}}}\lambda^{\mathrm{IC}}, \quad \forall \mathrm{i} \in \mathbb{N}_{\mathrm{ac}} \tag{4.25a}$$

$$\lambda^{\mathrm{G}}_{\mathrm{dc}-j} := \frac{k_{\mathrm{IC}}+1}{2}\left(\nabla C_{\mathrm{dc}-j}\left(P^{\mathrm{G}}_{\mathrm{dc}-j}\right) + \alpha^{+}_{\mathrm{dc}-j} - \alpha^{-}_{\mathrm{dc}-j}\right) + \frac{1}{2}\lambda^{\mathrm{IC}}, \quad \forall j \in \mathbb{N}_{\mathrm{dc}} \tag{4.25b}$$

$$\lambda^{\mathrm{IC}}_{k} := \frac{P^{\mathrm{ac}}_{\mathrm{IC}-k}}{P^{\mathrm{ac}}_{\mathrm{IC}-k} - P^{\mathrm{ac}}_{\mathrm{IC}}}\left[\left(k_{\mathrm{IC}-k}-1\right)\lambda^{\mathrm{G}} + \alpha^{+}_{\mathrm{IC}-k} - \alpha^{-}_{\mathrm{IC}-k}\right], \quad \forall k \in \mathbb{N}_{\mathrm{IC}} \tag{4.25c}$$

where, by optimality, we must have that (4.26a) and (4.26b) hold. We can interpret $\lambda^{\mathrm{G}}_{\mathrm{ac-i}}$ as a Lagrange multiplier for the i$^{th}$ DG on the *ac*-side, $\lambda^{\mathrm{G}}_{\mathrm{dc}-j}$ as a Lagrange multiplier for the $j^{th}$ DG on the *dc*-side, and $\lambda^{\mathrm{IC}}_{k}$ as a Lagrange multiplier of the $k^{th}$ *IC*. In this formulation, the DGs receive information from the *ICs* ($k_{\mathrm{IC}}$ and $\lambda^{\mathrm{IC}}$), while the *ICs* also receive information from the DGs ($\lambda^{\mathrm{G}}$); therefore, it is necessary to have communication links between the DGs and the *ICs*. This is further explained in the next Section.

$$\lambda^{\mathrm{G}} = \lambda^{\mathrm{G}}_{\mathrm{ac-i}} = \lambda^{\mathrm{G}}_{\mathrm{dc}-j}, \quad \forall \mathrm{i} \in \mathbb{N}_{\mathrm{ac}},\ \forall j \in \mathbb{N}_{\mathrm{dc}} \tag{4.26a}$$

$$\lambda^{\mathrm{IC}} = \lambda^{\mathrm{IC}}_{k}, \qquad \forall k \in \mathbb{N}_{\mathrm{IC}} \tag{4.26b}$$

Based on the optimality conditions of the optimal dispatch problem, a distributed control strategy is designed with the objective of providing secondary variables regulation (i.e., frequency and voltage amplitude regulation in the *ac*-microgrid, and voltage regulation in the *dc*-microgrid), while driving the hybrid *ac/dc*-microgrid with multiple *ICs* to an optimal dispatch that complies with the KKT conditions (4.24).

## 4.5 Proposed Control Scheme for Multiple *ICs*

The distributed control scheme proposed in this Chapter aims to regulate the secondary variables in a hybrid *ac/dc*-microgrid, while maintaining optimality of dispatch. As described before, the control scheme is designed for the three components of the hybrid *ac/dc*-microgrid. On the other hand, the design of the control scheme is based on the convex optimization problem (4.22a), (4.22b), (4.22c), (4.22d), (4.22e) and (4.22f) presented in Section 4.4.2.

### 4.5.1 Control scheme proposed for the *ac*-DGs

As explained in Section 4.3.1, the control scheme proposed for the *ac*-DGs is responsible for regulating the frequency on the *ac*-side of the microgrid, while minimizing the operation cost of all the DGs in the hybrid *ac/dc*-microgrid (4.27). Again, the reactive power injections are not considered since it is assumed that the *ac*-DSC described in Section 3.3 is implemented. Thus, this proposal focuses on frequency and *dc*-voltage control by means of optimally dispatching of real power of DG units.

$$\omega_{\mathrm{i}} = \omega^{*} + M_{\mathrm{ac-i}} P^{\mathrm{G}}_{\mathrm{ac-i}} + \Omega^{\mathrm{G}}_{\mathrm{ac-i}} \tag{4.27a}$$

$$\begin{aligned}\dot{\Omega}^{\mathrm{G}}_{\mathrm{ac-i}} = &-k^{a}_{\mathrm{ac-i}} \left(\omega_{\mathrm{i}} - \omega^{*}\right) - k^{b}_{\mathrm{ac-i}} \sum_{j \in \mathbb{N}_{\mathrm{ac}}} a_{\mathrm{i}j} \left(\lambda^{\mathrm{G}}_{\mathrm{ac-i}} - \lambda^{\mathrm{G}}_{\mathrm{ac}-j}\right) \\ &- k^{c}_{\mathrm{ac-i}} \sum_{j \in \mathbb{N}_{\mathrm{dc}}} a_{\mathrm{i}j} \left(\lambda^{\mathrm{G}}_{\mathrm{ac-i}} - \lambda^{\mathrm{G}}_{\mathrm{dc}-j}\right)\end{aligned} \tag{4.27b}$$

$$\dot{\alpha}^{+}_{\mathrm{ac-i}} = \mu^{a}_{\mathrm{ac-i}} \max\left\{ P^{\mathrm{G}}_{\mathrm{ac-i}} - P^{\mathrm{G}+}_{\mathrm{ac-i}} + \frac{k^{\mathrm{d}}_{\mathrm{ac-i}}}{\mu^{a}_{\mathrm{ac-i}}} \alpha^{+}_{\mathrm{ac-i}}, 0 \right\} - k^{\mathrm{d}}_{\mathrm{ac-i}} \alpha^{+}_{\mathrm{ac-i}} \tag{4.27c}$$

$$\dot{\alpha}^{-}_{\mathrm{ac-i}} = \mu^{b}_{\mathrm{ac-i}} \max\left\{ P^{\mathrm{G}-}_{\mathrm{ac-i}} - P^{\mathrm{G}}_{\mathrm{ac-i}} + \frac{k^{\mathrm{e}}_{\mathrm{ac-i}}}{\mu^{b}_{\mathrm{ac-i}}} \alpha^{-}_{\mathrm{ac-i}}, 0 \right\} - k^{\mathrm{e}}_{\mathrm{ac-i}} \alpha^{-}_{\mathrm{ac-i}} \tag{4.27d}$$

$$\lambda^{\mathrm{G}}_{\mathrm{ac-i}} = \frac{\hat{k}^{\mathrm{IC}}_{\mathrm{i}} + 1}{2\hat{k}^{\mathrm{IC}}_{\mathrm{i}}} \left(\nabla C_{\mathrm{ac-i}} \left(P^{\mathrm{G}}_{\mathrm{ac-i}}\right) + \alpha^{+}_{\mathrm{ac-i}} - \alpha^{-}_{\mathrm{ac-i}}\right) - \frac{1}{2\hat{k}^{\mathrm{IC}}_{\mathrm{i}}} \hat{\lambda}^{\mathrm{IC}}_{\mathrm{i}} \tag{4.27e}$$

The proposed controller is similar to the one described in Section 4.3.1; therefore, the terms in (4.27) can be found in the aforementioned Section. The main change with respect to the controller proposed for the case with a single *IC* is in (4.27e). Here, the estimates of the variables from the *ICs* (i.e., $\hat{k}_{\mathrm{i}}^{\mathrm{IC}}$ and $\hat{\lambda}_{\mathrm{i}}^{\mathrm{IC}}$) are calculated with the observers shown in (4.28), where variables $\hat{k}_{\mathrm{IC}-k}$ and $\lambda_k^{\mathrm{IC}}$ are received from the *ICs* and will be explained in Section 4.5.3. The term $\lambda^{\mathrm{IC}}$ corresponds to the (unique) dual variable associated with the power transfer through the *ICs* (4.22c).

$$\dot{\hat{k}}_{\mathrm{i}}^{\mathrm{IC}} = -\sum_{j\in\mathbb{N}_{\mathrm{ac}}} a_{\mathrm{i}j}\left(\hat{k}_{\mathrm{i}}^{\mathrm{IC}} - \hat{k}_j^{\mathrm{IC}}\right) - \sum_{j\in\mathbb{N}_{\mathrm{dc}}} a_{\mathrm{i}j}\left(\hat{k}_{\mathrm{i}}^{\mathrm{IC}} - \hat{k}_j^{\mathrm{IC}}\right) - \sum_{k\in\mathbb{N}_{\mathrm{IC}}} a_{\mathrm{i}k}\left(\hat{k}_{\mathrm{i}}^{\mathrm{IC}} - \hat{k}_{\mathrm{IC}-k}\right) \tag{4.28a}$$

$$\dot{\hat{\lambda}}_{\mathrm{i}}^{\mathrm{IC}} = -\sum_{j\in\mathbb{N}_{\mathrm{ac}}} a_{\mathrm{i}j}\left(\hat{\lambda}_{\mathrm{i}}^{\mathrm{IC}} - \hat{\lambda}_j^{\mathrm{IC}}\right) - \sum_{j\in\mathbb{N}_{\mathrm{dc}}} a_{\mathrm{i}j}\left(\hat{\lambda}_{\mathrm{i}}^{\mathrm{IC}} - \hat{\lambda}_j^{\mathrm{IC}}\right) - \sum_{k\in\mathbb{N}_{\mathrm{IC}}} a_{\mathrm{i}k}\left(\hat{\lambda}_{\mathrm{i}}^{\mathrm{IC}} - \lambda_k^{\mathrm{IC}}\right) \tag{4.28b}$$

In summary, the *ac*-DG$_{\mathrm{i}}$ shares the following information with its neighbours:

- It sends the value of $\lambda_{\mathrm{ac}-\mathrm{i}}^{\mathrm{G}},\ \mathrm{i}\in\mathbb{N}_{\mathrm{ac}}$ to the *ac*-DGs, *dc*-DGs and *ICs* [see (4.27e)].
- It receives the value of $\lambda_{\mathrm{ac}-j}^{\mathrm{G}},\ j\in\mathbb{N}_{\mathrm{ac}}$, from the *ac*-DGs [see (4.27b)].
- It receives the value of $\lambda_{\mathrm{dc}-j}^{\mathrm{G}},\ j\in\mathbb{N}_{\mathrm{dc}}$, from the *dc*-DGs [see (4.27b)].
- It sends/receives the values of $\hat{k}_{\mathrm{i}}^{\mathrm{IC}}$ and $\hat{\lambda}_{\mathrm{i}}^{\mathrm{IC}}$ to the *ac*-DGs and *dc*-DGs [see (4.28)].
- It receives the values of $\lambda_k^{\mathrm{IC}}$ and $\hat{k}_{\mathrm{IC}-k}$ from the *ICs* [see (4.30d) and (4.35)].

### 4.5.2 Control scheme proposed for the *dc*-DGs

As explained in Section 4.3.2, the control scheme proposed for the *dc*-DGs is responsible for regulating the voltage of the *dc*-side of the microgrid, while minimizing the operation cost of all the DGs in the hybrid *ac*/*dc*-microgrid (4.15).

$$V_j = V^* + M_{\mathrm{dc}-j}P_{\mathrm{dc}-j}^{\mathrm{G}} + \Omega_{\mathrm{dc}-j}^{\mathrm{G}} \tag{4.29a}$$

$$\begin{aligned}\dot{\Omega}_{\mathrm{dc}-j}^{\mathrm{G}} = {} & -k_{\mathrm{dc}-j}^{a}\left(V_j - V^*\right) - k_{\mathrm{dc}-j}^{b}\sum_{\mathrm{i}\in\mathbb{N}_{\mathrm{dc}}} a_{\mathrm{i}j}\left(\lambda_{\mathrm{dc}-j}^{\mathrm{G}} - \lambda_{\mathrm{dc}-\mathrm{i}}^{\mathrm{G}}\right) \\ & - k_{\mathrm{dc}-j}^{c}\sum_{\mathrm{i}\in\mathbb{N}_{\mathrm{ac}}} a_{\mathrm{i}j}\left(\lambda_{\mathrm{dc}-j}^{\mathrm{G}} - \lambda_{\mathrm{ac}-\mathrm{i}}^{\mathrm{G}}\right)\end{aligned} \tag{4.29b}$$

$$\dot{\alpha}_{\mathrm{dc}-j}^{+} = \mu_{\mathrm{dc}-j}^{a}\max\left\{P_{\mathrm{dc}-j}^{\mathrm{G}} - P_{\mathrm{dc}-j}^{\mathrm{G}+} + \frac{k_{\mathrm{dc}-j}^{\mathrm{d}}}{\mu_{\mathrm{dc}-j}^{a}}\alpha_{\mathrm{dc}-j}^{+}, 0\right\} - k_{\mathrm{dc}-j}^{\mathrm{d}}\alpha_{\mathrm{dc}-j}^{+} \tag{4.29c}$$

$$\dot{\alpha}_{\mathrm{dc}-j}^{-} = \mu_{\mathrm{dc}-j}^{b}\max\left\{P_{\mathrm{dc}-j}^{\mathrm{G}-} - P_{\mathrm{dc}-j}^{\mathrm{G}} + \frac{k_{\mathrm{dc}-j}^{\mathrm{e}}}{\mu_{\mathrm{dc}-j}^{b}}\alpha_{\mathrm{dc}-j}^{-}, 0\right\} - k_{\mathrm{dc}-j}^{\mathrm{e}}\alpha_{\mathrm{dc}-j}^{-} \tag{4.29d}$$

$$\lambda_{\mathrm{dc}-j}^{\mathrm{G}} = \frac{\hat{k}_j^{\mathrm{IC}}+1}{2}\left(\nabla C_{\mathrm{dc}-j}\left(P_{\mathrm{dc}-j}^{\mathrm{G}}\right) + \alpha_{\mathrm{dc}-j}^{+} - \alpha_{\mathrm{dc}-j}^{-}\right) + \frac{1}{2}\hat{\lambda}_j^{\mathrm{IC}} \tag{4.29e}$$

The proposed controller is similar to the one described in Section 4.3.2; therefore, the terms in (4.29) can be found in the aforementioned Section. The main change with respect to the controller proposed for the case with a single *IC* is in (4.29e). Here, the estimates of the variables from the *ICs* (i.e., $\hat{k}_j^{\mathrm{IC}}$ and $\hat{\lambda}_j^{\mathrm{IC}}$) are calculated with the observers shown in (4.28), where variables $\hat{k}_{\mathrm{IC}-k}$ and $\lambda_k^{\mathrm{IC}}$ are received from the *ICs* and will be explained in Section 4.5.3. The term $\lambda^{\mathrm{IC}}$ corresponds to the (unique) dual variable associated with the power transfer through the *ICs* (4.22c).

In summary, the *dc*-DG$_j$ shares the following information with its neighbours:

- It sends the value of $\lambda_{\mathrm{dc}-j}^{\mathrm{G}},\ j \in \mathbb{N}_{\mathrm{dc}}$, to the *dc*-DGs, *ac*-DGs and *ICs* [see (4.29e)].
- It receives the value of $\lambda_{\mathrm{dc}-\mathrm{i}}^{\mathrm{G}},\ \mathrm{i} \in \mathbb{N}_{\mathrm{dc}}$, from the *dc*-DGs [see (4.29b)].
- It receives the value of $\lambda_{\mathrm{ac}-\mathrm{i}}^{\mathrm{G}},\ \mathrm{i} \in \mathbb{N}_{\mathrm{ac}}$, from the *ac*-DGs [see (4.29b)].
- It sends/receives the values of $\hat{k}_j^{\mathrm{IC}}$ and $\hat{\lambda}_j^{\mathrm{IC}}$ to the *dc*-DGs and *ac*-DGs [see (4.28)].
- It receives the values of $\lambda_k^{\mathrm{IC}}$ and $\hat{k}_{\mathrm{IC}-k}$ from the *ICs* [see (4.30d) and (4.35)].

### 4.5.3 Control scheme proposed for the *ICs*

In addition to contribute to the minimization of the operation cost by transferring power between both sides of the hybrid *ac/dc*-microgrid, now the *ICs* must dispatch the power being transferred in order to minimize the losses in this stage and, therefore, contribute to reach the optimal dispatch point. For achieving the two aforementioned control tasks, the following controller is proposed:

$$\dot{P}_{\mathrm{IC}-k}^{*} = -\tau_{\mathrm{IC}-k}^{a} \sum_{\mathrm{i}\in\mathbb{N}_{\mathrm{ac}}} \sum_{j\in\mathbb{N}_{\mathrm{dc}}} a_{\mathrm{i}k} a_{jk} \left(\lambda_{\mathrm{ac}-\mathrm{i}}^{\mathrm{G}} - \lambda_{\mathrm{dc}-j}^{\mathrm{G}}\right) - \tau_{\mathrm{IC}-k}^{b} \sum_{h\in\mathbb{N}_{\mathrm{IC}}} a_{kh} \left(\lambda_k^{\mathrm{IC}} - \lambda_h^{\mathrm{IC}}\right) \tag{4.30a}$$

$$\dot{\alpha}_{\mathrm{IC}-k}^{+} = \mu_{\mathrm{IC}-k}^{a} \max\left\{ P_{\mathrm{IC}-k}^{\mathrm{ac}} - P_{\mathrm{IC}-k}^{\mathrm{ac}+} + \frac{\tau_{\mathrm{IC}-k}^{a}}{\mu_{\mathrm{IC}-k}^{a}} \alpha_{\mathrm{IC}-k}^{+},\ 0 \right\} - \tau_{\mathrm{IC}-k}^{a} \alpha_{\mathrm{IC}-k}^{+} \tag{4.30b}$$

$$\dot{\alpha}_{\mathrm{IC}-k}^{-} = \mu_{\mathrm{IC}-k}^{b} \max\left\{ P_{\mathrm{IC}-k}^{\mathrm{ac}-} - P_{\mathrm{IC}-k}^{\mathrm{ac}} + \frac{\tau_{\mathrm{IC}-k}^{b}}{\mu_{\mathrm{IC}-k}^{b}} \alpha_{\mathrm{IC}-k}^{-},\ 0 \right\} - \tau_{\mathrm{IC}-k}^{b} \alpha_{\mathrm{IC}-k}^{-} \tag{4.30c}$$

$$\lambda_k^{\mathrm{IC}} = \frac{P_{\mathrm{IC}-k}^{\mathrm{ac}}}{P_{\mathrm{IC}-k}^{\mathrm{ac}} - P_{\mathrm{IC}}^{\mathrm{ac}}} \left[ \left(k_{\mathrm{IC}-k} - 1\right) \overline{\lambda^{\mathrm{G}}} + \alpha_{\mathrm{IC}-k}^{+} - \alpha_{\mathrm{IC}-k}^{-} \right] \tag{4.30d}$$

where $P_{\mathrm{IC}-k}^{*}$ is the power transferred through the $k^{th}$ *IC*, which is positive when transferred from the *dc*-side to the *ac*-side, and negative in the opposite direction, $\overline{\lambda^{\mathrm{G}}}$ is the average value of the variables $\lambda_{\mathrm{ac}}^{\mathrm{G}}$ and $\lambda_{\mathrm{dc}}^{\mathrm{G}}$ received from the DGs communicating with $IC_k$. The control actions $\alpha_{\mathrm{IC}-k}^{+}$ and $\alpha_{\mathrm{IC}-k}^{-}$ were already explained in Section 4.3.3 and are used to maintain the power transferred through $IC_k$ within limits. The first term at the right-hand side in (4.30a) produces a power transfer from the cheapest side to the most expensive one by comparing the value of $\lambda_{\mathrm{ac}}^{\mathrm{G}}$ and $\lambda_{\mathrm{dc}}^{\mathrm{G}}$. The second term at the right-hand side in (4.30a) changes the dispatch of the *ICs* until they reach the same value of $\lambda^{\mathrm{IC}}$ ($\lambda^{\mathrm{IC}} = \lambda_k^{\mathrm{IC}},\ \forall k \in \mathbb{N}_{\mathrm{IC}}$), which

corresponds to the (unique) dual variable associated with the power transfer equation of the hybrid *ac/dc*-microgrid's optimal dispatch problem, (4.22c).

For the implementation of the controllers proposed in (4.27e) and (4.29e), it is necessary to know a constant related to the power transferred through the *ICs* in a hybrid *ac/dc*-microgrid with multiple *ICs*. Specifically, the constant $k_{\mathrm{IC}}$ must be known by all the *ac*-DGs [see (4.27e)], by all the *dc*-DGs [see (4.29e)] and by all the *ICs* [see (4.30d)]. This constant can be easily calculated in a hybrid *ac/dc*-microgrid with a single *IC* as the power in the *dc*-side of the *IC* over that at the *ac*-side, as described in (4.2a) and repeated in (4.31) for reader's convenience. However, the calculation of $k_{\mathrm{IC}}$ is more complicated when multiple *ICs* and a distributed communication network are considered since each *IC* does not know the amount of power being transferred through all the others.

$$k_{\mathrm{IC}} = \frac{P_{\mathrm{IC}}^{\mathrm{dc}}}{P_{\mathrm{IC}}^{\mathrm{ac}}} \tag{4.31}$$

where $P_{\mathrm{IC}}^{\mathrm{dc}}$ is the total power at the *dc*-side of the *ICs*, $P_{\mathrm{IC}}^{\mathrm{ac}}$ is the total power at the *ac*-side of the *ICs*, and $k_{\mathrm{IC}}$ is the relationship between the two aforementioned variables.

In this case, the total power transferred through the *ICs* in a hybrid *ac/dc*-microgrid can be estimated with local information from the $IC_k$ ($k \in \mathbb{N}_{\mathrm{IC}} = \{n+m+1, \ldots, n+m+g\}$) and its neighbouring *ICs* [94, 137, 138]. Let $\hat{\Gamma}_k$ be the estimate of the variable $\Gamma$ (e.g., the total power transferred through the *ICs* at the *ac*-side $P_{\mathrm{IC}}^{\mathrm{ac}}$ or the *dc*-side $P_{\mathrm{IC}}^{\mathrm{dc}}$), let $\gamma_k$ be the local variable ($P_{\mathrm{IC}-k}^{\mathrm{ac}}$ or $P_{\mathrm{IC}-k}^{\mathrm{dc}}$), let $a_{kh}$ be the element of the adjacency matrix which represent the communication channel between $IC_k$ and $IC_h$ ($k, h \in \mathbb{N}_{\mathrm{IC}} = \{n+m+1, \ldots, n+m+g\}$), and let $g$ be the total number of *ICs* in the hybrid *ac/dc*-microgrid. Then, the total power transferred through the *ICs* can be estimated with a distributed observer [137], as follows:

$$\hat{\Gamma}_k = g \cdot \gamma_k + \int \sum_{h \in \mathbb{N}_{\mathrm{IC}}} a_{kh} \left( \hat{\Gamma}_k(\tau) - \hat{\Gamma}_h(\tau) \right) \mathrm{d}\tau \tag{4.32}$$

Considering the observer in (4.32), the following observers are proposed to estimate the total power transferred between the two sides of the hybrid microgrid with multiple *ICs*.

$$\hat{P}_{\mathrm{IC}-k}^{\mathrm{ac}} = g \cdot P_{\mathrm{IC}-k}^{\mathrm{ac}} + \int \sum_{h \in \mathbb{N}_{\mathrm{IC}}} a_{kh} \left( \hat{P}_{\mathrm{IC}-k}^{\mathrm{ac}}(\tau) - \hat{P}_{\mathrm{IC}-h}^{\mathrm{ac}}(\tau) \right) \mathrm{d}\tau \tag{4.33a}$$

$$\hat{P}_{\mathrm{IC}-k}^{\mathrm{dc}} = g \cdot P_{\mathrm{IC}-k}^{\mathrm{dc}} + \int \sum_{h \in \mathbb{N}_{\mathrm{IC}}} a_{kh} \left( \hat{P}_{\mathrm{IC}-k}^{\mathrm{dc}}(\tau) - \hat{P}_{\mathrm{IC}-h}^{\mathrm{dc}}(\tau) \right) \mathrm{d}\tau \tag{4.33b}$$

According to [138], all estimates would converge to a consensus value as follows:

$$\hat{P}_{\mathrm{IC}-1}^{\mathrm{ac}} = \hat{P}_{\mathrm{IC}-2}^{\mathrm{ac}} = \cdots = \hat{P}_{\mathrm{IC}-g}^{\mathrm{ac}} = \sum_{k \in \mathbb{N}_{\mathrm{IC}}} P_{\mathrm{IC}-k}^{\mathrm{ac}} \tag{4.34a}$$

$$\hat{P}_{\mathrm{IC}-1}^{\mathrm{dc}} = \hat{P}_{\mathrm{IC}-2}^{\mathrm{dc}} = \cdots = \hat{P}_{\mathrm{IC}-g}^{\mathrm{dc}} = \sum_{k \in \mathbb{N}_{\mathrm{IC}}} P_{\mathrm{IC}-k}^{\mathrm{dc}} \tag{4.34b}$$

Therefore, the $k^{th}$ *IC* can estimate the constant $\hat{k}_{\mathrm{IC}-k}$ for implementing the controller proposed in (4.32) as follows:

$$\hat{k}_{\mathrm{IC}-k} = \frac{\hat{P}^{\mathrm{dc}}_{\mathrm{IC}-k}}{\hat{P}^{\mathrm{ac}}_{\mathrm{IC}-k}}, \qquad \forall k \in \mathbb{N}_{\mathrm{IC}} \tag{4.35}$$

The *ICs* share the following information with its neighbours:

- It sends the values of $\lambda^{\mathrm{IC}}_k$ and $\hat{k}_{\mathrm{IC}-k}$ to the *ac*-DGs and *dc*-DGs [see (4.27e) and (4.29e)].
- It receives the value of $\lambda^{\mathrm{ac}}_{\mathrm{i}},\ \mathrm{i} \in \mathbb{N}_{\mathrm{ac}}$ from the *ac*-DGs [see (4.30a)].
- It receives the value of $\lambda^{\mathrm{dc}}_j,\ j \in \mathbb{N}_{\mathrm{dc}}$ from the *dc*-DGs [see (4.30a)].
- It receives/sends the value of $\lambda^{\mathrm{IC}}_h$, $h \in \mathbb{N}_{\mathrm{IC}}$ from/to the *ICs* [see (4.30a)].
- It receives/sends the values of $\hat{P}^{\mathrm{ac}}_{\mathrm{IC}-k}$ and $\hat{P}^{\mathrm{dc}}_{\mathrm{IC}-k}$, $h \in \mathbb{N}_{\mathrm{IC}}$ from/to the *ICs* [see (4.34)].

## 4.6 Summary

In this Chapter, a new consensus-based distributed secondary control strategy for hybrid *ac/dc*-microgrids has been proposed. In the same way as the control strategy proposed in Chapter 3, this strategy also considers the hybrid *ac/dc*-microgrid as a single entity. The strategy is capable of restoring the variables modified by the primary control loop to their nominal values, while optimizing the dispatch of the DGs, in order to minimize the operation cost of the hybrid *ac/dc*-microgrid. Additionally, when the hybrid *ac/dc*-microgrid has multiple *ICs*, the power transfer is also dispatched between them for contributing to the total cost minimization.

The proposed strategy also considers a reduced communication layer, as each agent in the hybrid *ac/dc*-microgrid (i.e., DGs and *ICs*) is communicating only with its neighbouring DGs and *ICs*. The proposed controller is capable of driving the microgrid to the optimal operation point while considering the output limits of DGs and *ICs*. The tuning of the controllers proposed in this Chapter is addressed in Chapter 6. The validation of the proposed control strategy is performed in Chapter 8 using a simulated hybrid *ac/dc*-microgrid.

# Chapter 5

# Experimental *ac/dc*-Microgrid

## 5.1 Introduction

This Chapter describes the design and construction of the experimental hybrid *ac/dc*-microgrid used for validating the distributed secondary control strategies for power-sharing proposed in this thesis (see Section 3). Details of the different components of the microgrid are presented with emphasis on the DGs, *ICs* and loads[1]. The emulation of DGs is performed by real-time controlled power units whose manufacturer is the company *Triphase*, part of National Instruments. Each *Triphase* unit consists of two voltage-source converters (VSCs) connected in back-to-back configuration through a DC-Link, fed by the main grid through an isolation transformer [29].

This Chapter is organized as follows: Section 5.2 details the main characteristics of the *ac*-side of the microgrid, while the *dc*-side is described in Section 5.3. The *IC* for connecting the two sides is described in Section 5.4. Finally, Section 5.5 presents the experimental hybrid *ac/dc*-microgrid built to carry out the studies reported in this thesis and Section 5.6 provides a summary of the Chapter.

[1] https://www.die.cl/sitio/home/investigacion/laboratorios/laboratorio-de-control-de-micro-redes/

## 5.2 *ac*-Microgrid

The *ac*-microgrid is emulated using the Triphase units shown in Fig. 5.1, which are called "PM15F120C" and "PM5F60R". The first unit is composed of 4 VSCs (VSC1, VSC2, VSC3, VSC4) as shown in Fig. 5.1a. This unit allows to emulate 2 independent three-phase *ac*-DGs utilizing VSC3 and VSC4. The second unit is composed of 2 inverters (VSC1, VSC2) as shown in Fig. 5.1b. This unit allows to emulate 1 three-phase *ac*-DG utilizing VSC2. Therefore, it is possible to emulate a three-phase three-wire *ac*-microgrid composed of three *ac*-DGs, as explained in next section.

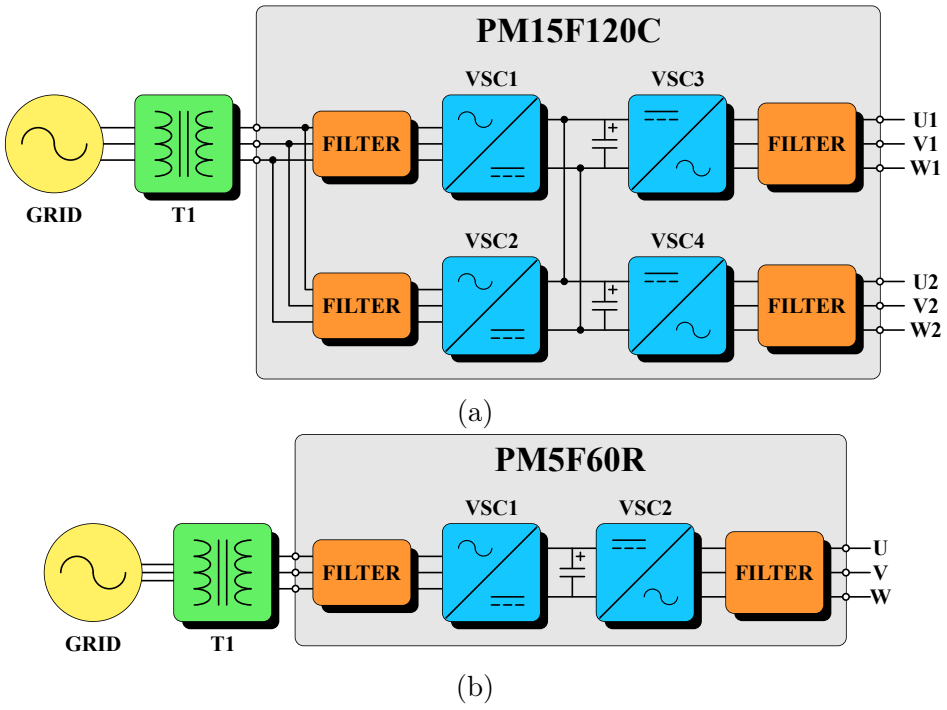


Figure 5.1: Topology of Triphase units PM15F120C and PM5F60R utilized to emulate the *ac*-microgrid.

### 5.2.1 Topology

Considering an *ac*-microgrid composed of three *ac*-DGs (each DG has its own *ac*-Filter), the topology shown in Fig. 5.2a is proposed. It is important to note that *ac*-Lines are emulated with inductors; therefore, the resistive component of the *ac*-Lines is small and corresponds to the inductor's resistance.

The loads include both controllable ($Z_1; Z_3$) and fixed ($Z_2; Z_4; Z_5$) loads. Controllable loads are emulated using back-to-back converters (Triphase unit "PM15I30F60") to be able to produce active and reactive load impacts, while the fixed loads are resistive load banks.

The orange box indicates the connection point for the *IC*, which is connected to node 2 of the *ac*-microgrid. The *IC* is connected through an *ac* circuit breaker (small black box in Fig. 5.2a); thus, it is possible to disconnect it from the *ac*-microgrid. The *IC* will be further explained in Section 5.4.

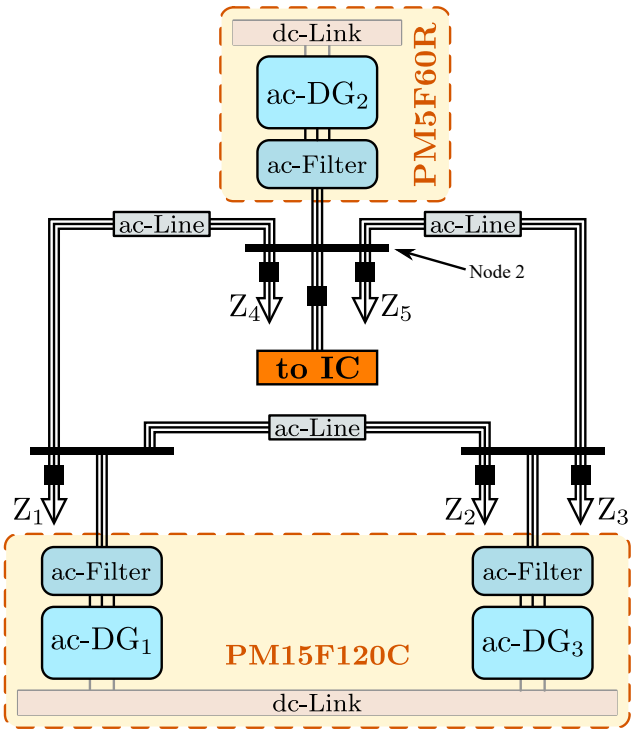


(a) Proposed topology of an *ac*-microgrid composed of three *ac*-DGs.

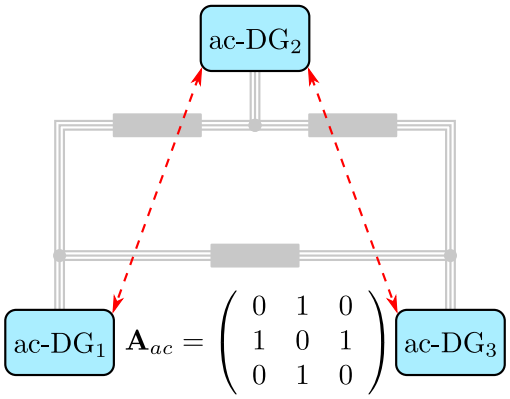


(b) Communication network of the *ac*-microgrid proposed in Fig. 5.2a.

Figure 5.2: Proposed *ac*-microgrid.

### 5.2.2 Communication Network

In Fig. 5.2b the distributed communication network is shown and the communication links have been arbitrarily assigned. The bidirectional communication links are depicted by the red arrows. The adjacency matrix for this topology ($\mathbf{A}_{ac}$) is also shown in the Fig. In addition, *ac*-DG$_1$ and *ac*-DG$_3$ have communication links to the *IC*, and to *dc*-DG$_2$ and *dc*-DG$_4$, respectively, while *ac*-DG$_2$ has communication link to *dc*-DG$_6$ only, as will be explained in Section 5.5. The communication links between *ac*-DGs and *dc*-DGs (or *ICs*) are not shown in Fig. 5.2b.

## 5.3 *dc*-Microgrid

The *dc*-microgrid is emulated using the Triphase unit called "PM15I60F06". This unit is composed of 2 VSC (VSC1 and VSC2) and 2 DC/DC converters (DCDC1 and DCDC2), each composed of three channels, as shown in Fig. 5.3. This unit allows to emulate 6 independent *dc*-DGs utilizing DCDC1 and DCDC2 (*DC*i$\pm$, i $\in \{1, \ldots, 6\}$). Therefore, it is possible to emulate a *dc*-microgrid composed of six *dc*-DGs, as explained in the following.

### 5.3.1 Topology

Considering a *dc*-microgrid composed of six *dc*-DGs (each DG has its own *dc*-Filter), the topology shown in Fig. 5.4 is proposed. It is important to note that *dc*-Lines are mainly resistive; however, in this experimental rig, inductors in series with the resistors were also

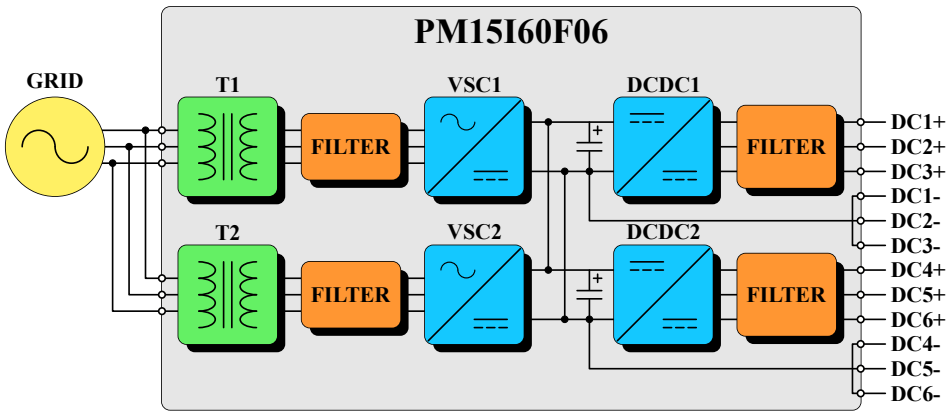


Figure 5.3: Topology of Triphase unit PM15I60F06 utilized to emulate the *dc*-microgrid.

considered to avoid current peaks due to the switching of power converters. In this case, all the loads $(R_1, \ldots, R_6)$ are fixed resistive load banks.

The *IC* is connected to node 4 of the *dc*-microgrid (orange box) through a *dc* circuit breaker (small black box); thus, it is possible to disconnect it from the *dc*-microgrid. The *IC* is further explained in Section 5.4.

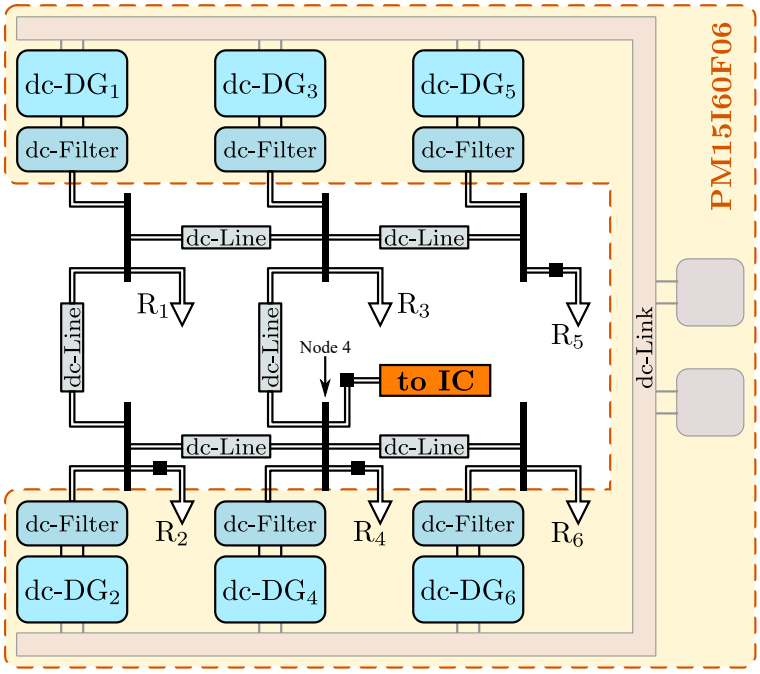


Figure 5.4: Proposed topology of a *dc*-microgrid composed of six *dc*-DGs.

### 5.3.2 Communication Network

In Fig. 5.5, it can be seen that the distributed communication network has been arbitrarily assigned (see red arrows). The adjacency matrix for this topology ($\mathbf{A}_{dc}$) is also shown in the same Fig. Additionally, *dc*-DG$_2$, *dc*-DG$_4$ and *dc*-DG$_6$ have communication links to the *IC* and to *ac*-DG$_1$, *ac*-DG$_2$ and *ac*-DG$_3$, respectively, as will be explained in Section 5.5. The communication links between *dc*-DGs and *ac*-DGs (or *ICs*) are not shown in Fig. 5.5.

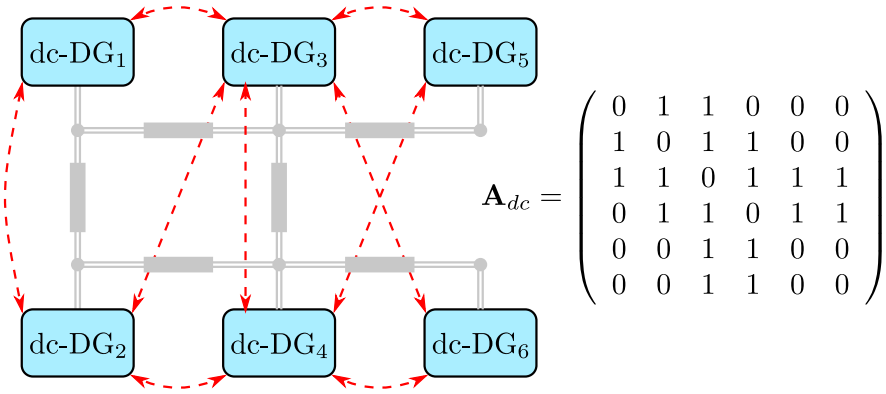


Figure 5.5: Communication network of the *dc*-microgrid proposed in Fig. 5.4.

## 5.4 Interlinking Converter (*IC*)

The *IC* is emulated using the Triphase unit shown in Fig. 5.6, which is called "PM5F42R". This unit is composed of one VSC (VSC1), one DC/DC converter (DCDC1), and 2 diode rectifiers for black starting the module, as shown in Fig. 5.6. This unit has one *ac*-port (U1,V1,W1) and two *dc*-ports (D1±,D2±), which allows to emulate an *ac*/*dc* back-to-back converter. The *ac*-port is connected to the *ac*-microgrid, while the two *dc*-ports are connected (in parallel) to the *dc*-microgrid. Therefore, it is possible to emulate an *IC* and to interconnect the *ac*- and *dc*-side of the hybrid *ac*/*dc*-microgrid.

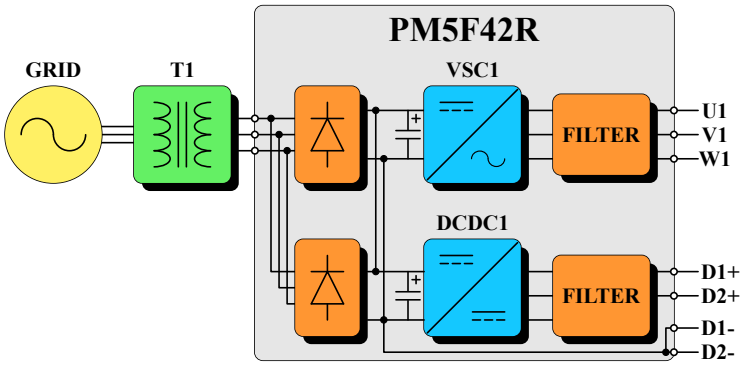


Figure 5.6: Topology of Triphase unit PM5F42R utilized to emulate the *IC*.

### 5.4.1 Topology and Communication Network

As mentioned before, the *IC* is connected to node 2 of the *ac*-microgrid and to node 4 of the *dc*-microgrid, as shown in Fig. 5.7. Moreover, the *IC* has communication links to *dc*-DG$_2$, *dc*-DG$_4$, *dc*-DG$_6$, *ac*-DG$_1$ and *ac*-DG$_2$ (see red arrows).

## 5.5 Hybrid *ac*/*dc*-Microgrid

With the information provided in Sections 5.2, 5.3 and 5.4, it is possible to build a 24.0$kW$ hybrid *ac*/*dc*-experimental microgrid. This microgrid has three main stages:

- One *ac*-microgrid composed of 3 *ac*-DGs.

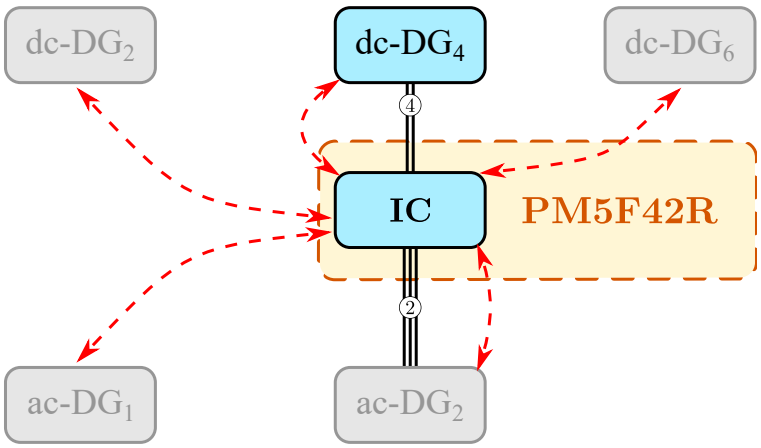


Figure 5.7: Proposed topology and communication network of the *IC*.

- One *dc*-microgrid composed of 6 *dc*-DGs.
- One *IC* to connect the two sub-microgrids.

### 5.5.1 Topology

A simplified diagram of the hybrid *ac*/*dc*-microgrid implemented in the Microgrid's Control Laboratory, University of Chile, is presented in Fig. 5.8, and a photograph of it is depicted in Fig. 5.9. General parameters for the hybrid *ac*/*dc*-microgrid are given in Table 5.1 and Table 5.2, while the parameters of the controllers are given in Table 5.3 (for the power-sharing strategy) and Table 5.4 (for the operation cost minimization strategy). The parameters of the controllers were tuned following the procedure described in Chapter 6.

Table 5.1: Experimental *ac*/*dc*-microgrid, general parameters.

| **Description** | ***dc*** | ***ac*** | ***IC*** |
|---|---|---|---|
| # of DGs | 6 | 3 | 1 |
| Nominal Voltage (V) | 150 | 110* | - |
| Frequency (Hz) | - | 50 | - |
| Nominal Power (kW/unit) | 2.5 | 3.0 | 3.0 |
| Switching frequency (kHz) | | 16 | |
| Communication rate (Hz) | | 100 | |

* *Phase-to-neutral RMS voltage*

Table 5.2: Experimental *ac*/*dc*-microgrid, parameters of the lines.

| Line | Ω | Line | Ω | Line | Ω |
|---|---|---|---|---|---|
| $R_{12}$ | 0.67 | $R_{34}$ | 0.50 | $Z_{12}$ | $0.10 + j0.79$ |
| $R_{13}$ | 0.78 | $R_{35}$ | 0.94 | $Z_{13}$ | $0.10 + j0.79$ |
| $R_{24}$ | 0.50 | $R_{46}$ | 0.47 | $Z_{23}$ | $0.10 + j0.79$ |

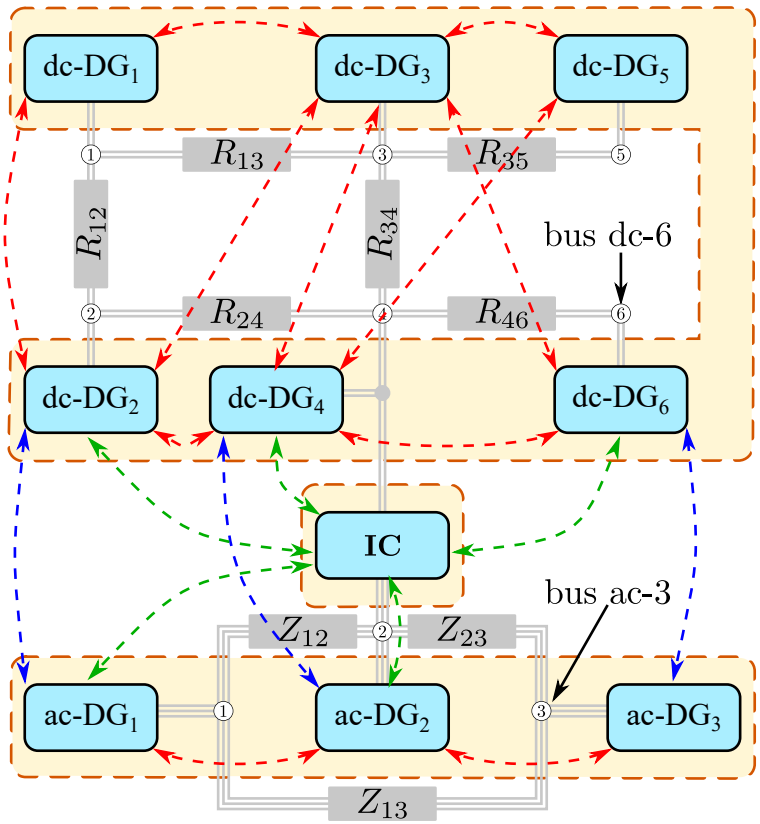


Figure 5.8: Topology of the hybrid *ac/dc*-microgrid under study, including the communication channels among DGs.


Figure 5.9: Experimental system based on five Triphase power converters, nominal powers 5-30kW (each one). They are configured to emulate the topology of Fig. 5.8.

Table 5.3: Parameter of the controllers for power-sharing strategy.

| **Param.** | ***dc*-DGs** | (3.9) |
|---|---|---|
| $\gamma_{\mathrm{i}}$ | 12.0 | (1/s) |
| $c_{\mathrm{i}}$ | 50.0 | (V/s) |
| $M_{\mathrm{dc-i}}$ | -3E-3 | (V/W) |
| $\omega_c$ | 12.566 | (rad/s) |
| **Param.** | ***IC*** | (3.10) |
| $1/\tau_{\mathrm{i}}$ | 50.0 | (1/W) |

| **Param.** | ***ac*-DGs** | (3.4)-(3.5) |
|---|---|---|
| $1/\sigma_{\mathrm{i}}$ | 50.0 | (s) |
| $\beta_{\mathrm{i}}$ | 12.0 | (1/s) |
| $b_{\mathrm{i}}$ | 500.0 | (V/s) |
| $M_{\mathrm{ac-i}}$ | -2.1E-3 | (rad/sW) |
| $N_{\mathrm{ac-i}}$ | -1.8E-3 | (V/VAr) |
| $\omega_c$ | 12.566 | (rad/s) |

Table 5.4: Parameter of the controllers for cost minimization strategy.

| **Param.** | ***dc*-DGs** | (4.15) |
|---|---|---|
| $k^a_{\mathrm{dc}-j}$ | 0.1 | (1/s) |
| $k^b_{\mathrm{dc}-j}, k^c_{\mathrm{dc}-j}$ | 1.0 | (1/s) |
| $k^{\mathrm{d}}_{\mathrm{dc}-j}, k^{\mathrm{e}}_{\mathrm{dc}-j}$ | 0.2 | |
| $\mu^a_{\mathrm{dc}-j}, \mu^b_{\mathrm{dc}-j}$ | 2.5E-3 | |
| $M_{\mathrm{dc-i}}$ | -3E-3 | (V/W) |
| **Param.** | ***IC*** | (4.16) |
| $1/\tau_{\mathrm{IC}}$ | 250.0 | (1/W) |
| $\tau^a_{\mathrm{IC}}, \tau^b_{\mathrm{IC}}$ | 0.2 | |
| $\mu^a_{\mathrm{IC}}, \mu^b_{\mathrm{IC}}$ | 2.5E-3 | |

| **Param.** | ***ac*-DGs** | (4.13) |
|---|---|---|
| $k^a_{\mathrm{ac-i}}$ | 0.1 | (1/s) |
| $k^b_{\mathrm{ac-i}}, k^c_{\mathrm{ac-i}}$ | 0.1 | (1/s) |
| $k^{\mathrm{d}}_{\mathrm{ac-i}}, k^{\mathrm{e}}_{\mathrm{ac-i}}$ | 0.2 | |
| $\mu^a_{\mathrm{ac-i}}, \mu^b_{\mathrm{ac-i}}$ | 2.5E-3 | |
| $M_{\mathrm{ac-i}}$ | -2.1E-3 | (rad/sW) |
| $\beta_{\mathrm{i}}$ | 12.0 | (1/s) |
| $b_{\mathrm{i}}$ | 50.0 | (V/s) |
| $N_{\mathrm{ac-i}}$ | -1.8E-3 | (V/VAr) |
| $\omega_c$ | 12.566 | (rad/s) |

### 5.5.2 Communication Network

Considering the communication links described before, the *adjacency matrix* (**A**) for the hybrid *ac/dc*-microgrid is shown in (5.1).

The adjacency matrix is composed of nine sub-matrices. The communication links for units within the sub-microgrids, i.e., *ac*-DGs and *dc*-DGs, are shown in sub-matrices $[\mathbf{ac}]_{3\times3}$ and $[\mathbf{dc}]_{6\times6}$, respectively, while the communication links between units from different sub-microgrids are described in sub-matrices $[\mathbf{ac\text{-}dc}]_{3\times6}$ and $[\mathbf{dc\text{-}ac}]_{6\times3}$.

In this case, the hybrid *ac/dc*-microgrid has a single *IC*. However, in case more *ICs* are considered in the microgrid, the communication links between the *ICs* are represented in sub-matrix $[\mathbf{ic}]_{1\times1}$. Finally, the communication links between the *ICs* and the DGs are shown in sub-matrices $[\mathbf{ac\text{-}ic}]_{3\times1}$, $[\mathbf{dc\text{-}ic}]_{6\times1}$, $[\mathbf{ic\text{-}ac}]_{1\times3}$ and $[\mathbf{ic\text{-}dc}]_{1\times6}$.

$$\mathbf{A} = \left(\begin{array}{cccccc|ccc|c} 0 & 1 & 1 & 0 & 0 & 0 & 0 & 0 & 0 & 0 \\ 1 & 0 & 1 & 1 & 0 & 0 & 1 & 0 & 0 & 1 \\ 1 & 1 & 0 & 1 & 1 & 1 & 0 & 0 & 0 & 0 \\ 0 & 1 & 1 & 0 & 1 & 1 & 0 & 1 & 0 & 1 \\ 0 & 0 & 1 & 1 & 0 & 0 & 0 & 0 & 0 & 0 \\ 0 & 0 & 1 & 1 & 0 & 0 & 0 & 0 & 1 & 1 \\ \hline 0 & 1 & 0 & 0 & 0 & 0 & 0 & 1 & 0 & 1 \\ 0 & 0 & 0 & 1 & 0 & 0 & 1 & 0 & 1 & 1 \\ 0 & 0 & 0 & 0 & 0 & 1 & 0 & 1 & 0 & 0 \\ \hline 0 & 1 & 0 & 1 & 0 & 1 & 1 & 1 & 0 & 0 \end{array}\right) = \left(\begin{array}{c|c|c} \mathbf{[dc]_{6\times 6}} & \mathbf{[dc\text{-}ac]_{6\times 3}} & \mathbf{[dc\text{-}ic]_{6\times 1}} \\ \hline \mathbf{[ac\text{-}dc]_{3\times 6}} & \mathbf{[ac]_{3\times 3}} & \mathbf{[ac\text{-}ic]_{3\times 1}} \\ \hline \mathbf{[ic\text{-}dc]_{1\times 6}} & \mathbf{[ic\text{-}ac]_{1\times 3}} & \mathbf{[ic]_{1\times 1}} \end{array}\right) \quad (5.1)$$

## 5.6 Summary

This Chapter has presented the design and implementation of a $24.0kW$ experimental hybrid *ac/dc*-microgrid. This prototype is used to validate the consensus-based distributed secondary control systems proposed in Chapter 3 and Chapter 4.

The main characteristics of the elements making the hybrid *ac/dc*-microgrid have been described, including information regarding the parameters of the microgrid and the controllers. Furthermore, the communication links between the DGs and the *IC* were also identified, summarized in the adjacency matrix (5.1).

In the next Chapter, an analytical model of the closed-loop system of the microgrid described in this Chapter is presented.

# Chapter 6

# Closed-loop Model of a Hybrid *ac/dc*-Microgrid with the Proposed Controllers

In this Chapter, an analytical model of the closed-loop system of the microgrid presented in Chapter 5 is derived. This model is utilized for performing a small-signal analysis of the consensus-based distributed control strategies proposed in Chapter 3 for power-sharing and Chapter 4 for operation cost minimization. The following simplifications were considered since their high-bandwidth dynamics are not relevant on the time-scale of the proposed controllers:

- The inner control loop (voltage/current controllers) is not considered.
- The modulation technique of the converters (PWM, SVM) is not considered.
- The switching of the power converter devices (IGBTs, Mosfets) is not considered.

Chapter 6 is organized as follows: Section 6.1 presents the closed-loop model for the hybrid *ac/dc*-microgrid with a single $IC$. Then, the control strategies proposed in this thesis are applied to the model of the microgrid: firstly, the closed-loop model of the control strategy for power-sharing is presented in Section 6.2; secondly, the control strategy for operation cost minimization is explained in Section 6.3, and small-signal analysis of the control strategies proposed in this thesis is performed in Section 6.4 and Section 6.5.

## 6.1 Closed-loop model for a Hybrid *ac/dc*-Microgrid

In this Section, the analytical model of the closed-loop system considering a consensus-based distributed control strategy proposed for power-sharing in a hybrid *ac/dc*-microgrid (see Chapter 3) is presented. The experimental hybrid *ac/dc*-microgrid built in the Microgrid's Control Laboratory[1] (University of Chile) is considered (see Chapter 5), i.e., the topology

[1]https://www.die.cl/sitio/home/investigacion/laboratorios/laboratorio-de-control-de-micro-redes/

with a single *IC* is analyzed [29]. In the following, the procedure for obtaining the closed-loop model is described and its most relevant equations are depicted. The complete description of this methodology is explained in Appendix A and Appendix B.

A general model for a hybrid *ac*/*dc*-microgrid, which is composed of $\mathbb{N}_{\text{ac}}$ *ac*-DGs, $\mathbb{N}_{\text{dc}}$ *dc*-DGs and a single *IC*, with a consensus-based distributed secondary control strategy is defined by the equations (6.1), (6.2), (6.3) and (6.5), and it is illustrated in Fig. 6.1. Since the microgrid model analyzed is a general model, the closed-loop model is independent of the objective of the controller; therefore, it works for either the power-sharing strategy (in green boxes) or the operation cost minimization strategy (in orange boxes).

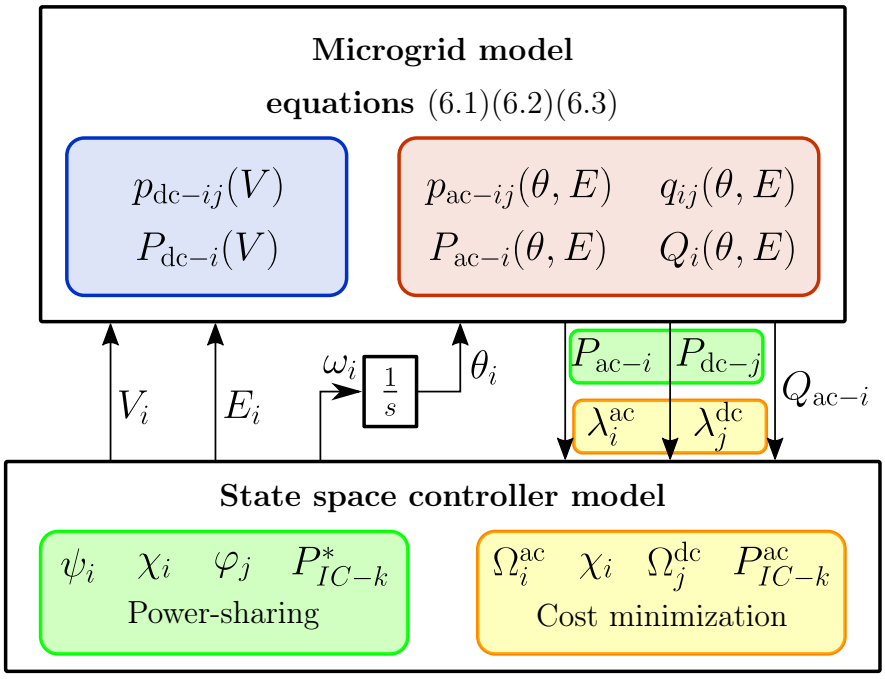


Figure 6.1: Closed-loop system of the hybrid *ac*/*dc*-microgrid.

The active power flows in the *ac*-microgrid are characterized by:

$$p_{\text{ac}-\text{i}j}(\theta, E) = \frac{R_{\text{i}j}E_{\text{i}}^2 - R_{\text{i}j}\Theta_{\text{i}j} + X_{\text{i}j}\Omega_{\text{i}j}}{R_{\text{i}j}^2 + X_{\text{i}j}^2} \tag{6.1a}$$

$$p_{\text{ac}-\text{i}}(\theta, E) = p_{\text{ac}-D\text{i}} + \sum\nolimits_{j\in\mathbb{N}_{\text{ac}}} p_{\text{ac}-\text{i}j}(\theta, E) - s_{\text{i}}P_{\text{IC}} \tag{6.1b}$$

$$\dot{\theta}_{\text{i}} = \omega_{\text{i}} \tag{6.1c}$$

$$\Theta_{\text{i}j} \coloneqq E_{\text{i}}E_j\cos(\theta_{\text{i}} - \theta_j) \tag{6.1d}$$

$$\Omega_{\text{i}j} \coloneqq E_{\text{i}}E_j\sin(\theta_{\text{i}} - \theta_j) \tag{6.1e}$$

where $p_{\text{ac}-\text{i}j}(\theta, E)$ is the active power flow in the line from bus $i$ to bus $j$, $R_{\text{i}j}$ and $X_{\text{i}j}$ are the line resistance and reactance, respectively, and $\Theta_{\text{i}j}$ and $\Omega_{\text{i}j}$ are defined in (6.1d) and (6.1e), respectively. Finally, $E_{\text{i}}$, $\theta_{\text{i}}$ and $\omega_{\text{i}}$ are the *ac*-voltage amplitude, angle and frequency at *ac*-bus $i$. The active power supplied by the $\text{i}^{th}$ *ac*-DG ($p_{\text{ac}-\text{i}}$) is given by (6.1b), where $p_{\text{ac}-D\text{i}}$ corresponds to the active power required by the local load connected to bus $i$, respectively.

The reactive power flows in the *ac*-microgrid are given by:

$$q_{ij}(\theta, E) = \frac{X_{ij}E_i^2 - X_{ij}\Theta_{ij} - R_{ij}\Omega_{ij}}{R_{ij}^2 + X_{ij}^2} \tag{6.2a}$$

$$q_i = q_{Di} + \sum\nolimits_{j \in \mathbb{N}_{ac}} q_{ij}(\theta, E) \tag{6.2b}$$

where $q_{ij}(\theta, E)$ is the reactive power flow in the line from bus $i$ to bus $j$ and the remaining variables were previously explained. The reactive power supplied by the i$^{th}$ *ac*-DG ($q_i$) is given by (6.2b), where $q_{Di}$ corresponds to the reactive power required by the local load connected to bus $i$.

The power flows in the *dc*-microgrid (blue box in Fig. 6.1) are described by:

$$p_{dc-ji}(V) = y_{ji}V_j(V_j - V_i) \tag{6.3a}$$

$$p_{dc-j}(V) = p_{dc-Dj} + \sum\nolimits_{i \in \mathbb{N}_{dc}} p_{dc-ji}(V) + s_j P_{IC} \tag{6.3b}$$

where $p_{dc-ji}(V)$ is the power flow in the *dc*-line from bus $j$ to bus $i$, $y_{ji}$ the line conductance, and $V_j$ and $V_i$ the *dc*-voltages at buses $j$ and $i$, respectively. The active power supplied by the $j^{th}$ *dc*-DG ($p_{dc-j}$) is given by (6.3b), where $p_{dc-Dj}$ corresponds to the power required by the local load connected to bus $j$.

The active power contribution of the *IC* is reflected in (6.1b) and (6.3b) by the inclusion of the variable $s_i$, which is 1 if the *IC* is connected to bus i and 0 otherwise.

Now, using the equations obtained for the power injections of the DGs, i.e., (6.1b), (6.2b) and (6.3b), a linearized model of the closed-loop system is derived. The operating point used for the linearization is obtained from a case study in which the DGs and the *IC* are within limits, and the power through the *IC* is not *zero*. In vector notation we have:

$$\Delta p_{ac} = G_1^{ac}\Delta E + G_2^{ac}\Delta\theta + G_0^{ac}\Delta P_{IC} \tag{6.4a}$$

$$\Delta q_{ac} = G_3^{ac}\Delta E + G_4^{ac}\Delta\theta \tag{6.4b}$$

$$\Delta p_{dc} = G_1^{dc}\Delta V + G_0^{dc}\Delta P_{IC} \tag{6.4c}$$

where $p_{ac}, q_{ac} \in \mathbb{R}^n$ are the vectors of active and reactive power generated by the *ac*-DGs (respectively), $p_{dc} \in \mathbb{R}^m$ is the vector of power generated by the *dc*-DGs, $E \in \mathbb{R}^n$ is the vector of bus potentials in the *ac*-microgrid, $\theta \in \mathbb{R}^n$ is the vector of bus angles, $V \in \mathbb{R}^m$ is the vector of bus potentials in the *dc*-microgrid, and $P_{IC}$ is the power flow through the *IC*, which is positive when it flows from the *dc*-microgrid to the *ac*-microgrid.

Matrices $G_1^{ac}, G_2^{ac}, G_3^{ac}, G_4^{ac} \in \mathbb{R}^{n\times n}$ are composed of partial derivatives of $p_{ac}$ and $q_{ac}$ with respect to $E$ and $\theta$, and depend on both the operating point $(E^0, \theta^0)$ and the admittance matrix of the *ac* electrical system ($Y^{ac}$). Matrix $G_1^{dc} \in \mathbb{R}^{m\times m}$ is composed of partial derivatives of $p_{dc}$ with respect to $V$, and depend on both the operating point ($V^0$) and the conductance matrix of the *dc* electrical system ($Y^{dc}$). Finally, $G_0^{ac} = (0\ \text{-}1\ 0)^T$ is the vector describing the electrical connection of the *ac*-microgrid and the *IC*, and $G_0^{dc} = (0\ 0\ 0\ 1\ 0\ 0)^T$ is the vector describing the electrical connection of the *dc*-microgrid and the *IC*.

The low-pass-filter (LPF) measurements typically utilized in the primary (droop) control loop are considered in this closed-loop model, with cut-off frequencies of $\omega_{c-\mathrm{i}}$ and $\omega_{c-j}$:

$$\dot{P}_{\mathrm{ac-i}} = -\omega_{c-\mathrm{i}}(P_{\mathrm{ac-i}} - p_{\mathrm{ac-i}}) \tag{6.5a}$$

$$\dot{Q}_{\mathrm{ac-i}} = -\omega_{c-\mathrm{i}}(Q_{\mathrm{ac-i}} - q_{\mathrm{ac-i}}) \tag{6.5b}$$

$$\dot{P}_{\mathrm{dc-}j} = -\omega_{c-j}(P_{\mathrm{dc-}j} - p_{\mathrm{dc-}j}) \tag{6.5c}$$

where $p_{\mathrm{ac-i}}$, $q_{\mathrm{ac-i}}$ and $p_{\mathrm{dc-}j}$ are the instantaneous power to be filtered out by the LPFs, and $P_{\mathrm{ac-i}}$, $Q_{\mathrm{ac-i}}$ and $P_{\mathrm{dc-}j}$ are the output of the LPFs.

Linearizing (6.5) and using (6.4), in vector notation we obtain:

$$\Delta\dot{P}_{\mathrm{ac}} = [\omega_c]G_1^{\mathrm{ac}}\Delta E + [\omega_c]G_2^{\mathrm{ac}}\Delta\theta + [\omega_c]G_0^{\mathrm{ac}}\Delta P_{\mathrm{IC}} - [\omega_c]\Delta P_{\mathrm{ac}} \tag{6.6a}$$

$$\Delta\dot{Q}_{\mathrm{ac}} = [\omega_c]G_3^{\mathrm{ac}}\Delta E + [\omega_c]G_4^{\mathrm{ac}}\Delta\theta - [\omega_c]\Delta Q_{\mathrm{ac}} \tag{6.6b}$$

$$\Delta\dot{P}_{\mathrm{dc}} = [\omega_c]G_1^{\mathrm{dc}}\Delta V + [\omega_c]G_0^{\mathrm{dc}}\Delta P_{\mathrm{IC}} - [\omega_c]\Delta P_{\mathrm{dc}} \tag{6.6c}$$

where $\omega_c \in \mathbb{R}^n$ is the vector of cutoff frequencies, and $[\omega_c] \in \mathbb{R}^{n\times n}$ denotes the diagonal matrix with $\omega_c$ on the diagonal. This notation is used in the rest of the Chapter for referring to diagonal matrices. The expressions obtained for the power injections (6.6) will be used in the following Sections to obtain the closed-loop model for the hybrid *ac/dc*-microgrid with the proposed control strategies.

## 6.2 Control Strategy Proposed for Power-sharing

Now, the consensus-based distributed secondary control strategy for power-sharing is applied to the hybrid *ac/dc*-microgrid with a single *IC*. The process for obtaining the analytical closed-loop model is detailed in Appendix A.

The controllers proposed in Chapter 3 are applied to the hybrid *ac/dc*-microgrid model obtained in (6.6) to later derive the closed-loop model for the proposed control strategy. The expressions for the controllers are repeated for reader convenience.

**Controller for the i$^{th}$ *ac*-DG $\forall \mathbf{i} \in \mathbb{N}_{\mathbf{ac}}$:**

*Frequency reference* (3.4a) :

$$\dot{\theta}_{\mathrm{i}} = \omega_{\mathrm{i}} = \omega^* + M_{\mathrm{ac-i}}P_{\mathrm{ac-i}} + \psi_{\mathrm{i}} \tag{6.7a}$$

*Frequency secondary control* (3.4b) :

$$\dot{\psi}_{\mathrm{i}} = -\sigma_{\mathrm{i}}\left(\omega_{\mathrm{i}} - \omega^*\right) - \sigma_{\mathrm{i}}\sum_{j\in\mathbb{N}_{\mathrm{ac}}} a_{\mathrm{i}j}\left(P_{\mathrm{ac-i}} - P_{\mathrm{ac-}j}\right) - \sigma_{\mathrm{i}}\sum_{j\in\mathbb{N}_{\mathrm{dc}}} a_{\mathrm{i}j}\left(P_{\mathrm{ac-i}} - P_{\mathrm{dc-}j}\right) \tag{6.7b}$$

*Voltage reference* (3.5a) :

$$E_{\mathrm{i}} = E^* + N_{\mathrm{ac-i}}\cdot Q_{\mathrm{ac-i}} + \chi_{\mathrm{i}} \tag{6.7c}$$

*Voltage secondary control* (3.5b) :

$$\dot{\chi}_{\mathrm{i}} = -\beta_{\mathrm{i}}\left(E_{\mathrm{i}} - E^*\right) - b_{\mathrm{i}}\sum\nolimits_{j\in\mathbb{N}_{\mathrm{ac}}} a_{\mathrm{i}j}\left(Q_{\mathrm{ac-i}} - Q_{\mathrm{ac-}j}\right) \tag{6.7d}$$

**Controller for the $j^{th}$ *dc*-DG $\forall j \in \mathbb{N}_{\mathbf{dc}}$:**

*Voltage reference* (3.9a) :

$$V_j = V^* + M_{\mathrm{dc}-j} \cdot P_{\mathrm{dc}-j} + \varphi_j \tag{6.8a}$$

*Voltage secondary control* (3.9b) :

$$\dot{\varphi}_j = -\gamma_j \left(V_j - V^*\right) - c_j \sum_{\mathrm{i} \in \mathbb{N}_{\mathrm{dc}}} a_{j\mathrm{i}} \left(P_{\mathrm{dc}-j} - P_{\mathrm{dc}-\mathrm{i}}\right) - c_j \sum_{\mathrm{i} \in \mathbb{N}_{\mathrm{ac}}} a_{j\mathrm{i}} \left(P_{\mathrm{dc}-j} - P_{\mathrm{ac}-\mathrm{i}}\right) \tag{6.8b}$$

**Controller for the *IC*:**

*Secondary controller*(3.10) :

$$\dot{P}_{\mathrm{IC}-k} = -\tau_k \sum_{\mathrm{i} \in \mathbb{N}_{\mathrm{ac}}} \sum_{j \in \mathbb{N}_{\mathrm{dc}}} a_{\mathrm{i}k} a_{jk} \left(P_{\mathrm{ac}-\mathrm{i}} - P_{\mathrm{dc}-j}\right) \tag{6.9a}$$

Based on the equations for the microgrid (6.1), (6.2) and (6.3), and the controllers (6.7), (6.8) and (6.9) (see Appendix A), the closed-loop model for the studied hybrid *ac/dc*-microgrid with the proposed control strategy has 28 state variables, as follows:

- 3 angles from the *ac*-microgrid ($\theta_{\mathrm{i}},\ \forall \mathrm{i} \in \mathbb{N}_{\mathrm{ac}}$).
- 3 active powers from the *ac*-microgrid ($P_{\mathrm{ac}-\mathrm{i}},\ \forall \mathrm{i} \in \mathbb{N}_{\mathrm{ac}}$).
- 3 reactive powers from the *ac*-microgrid ($Q_{\mathrm{ac}-\mathrm{i}},\ \forall \mathrm{i} \in \mathbb{N}_{\mathrm{ac}}$).
- 3 frequency secondary control variables from the *ac*-microgrid ($\psi_{\mathrm{i}},\ \forall \mathrm{i} \in \mathbb{N}_{\mathrm{ac}}$).
- 3 voltage secondary control variables from the *ac*-microgrid ($\chi_{\mathrm{i}},\ \forall \mathrm{i} \in \mathbb{N}_{\mathrm{ac}}$).
- 6 active powers from the *dc*-microgrid ($P_{\mathrm{dc}-j},\ \forall j \in \mathbb{N}_{\mathrm{dc}}$).
- 6 voltage secondary control variables from the *dc*-microgrid ($\varphi_j,\ \forall j \in \mathbb{N}_{\mathrm{dc}}$).
- 1 *IC* power ($P_{\mathrm{IC}}$)

Then, the state equations for the closed-loop model of the studied hybrid *ac/dc*-microgrid with the proposed control strategy are:

$$\begin{aligned}
\Delta\dot{\theta} &= G_8^{\mathrm{ac}} \Delta P_{\mathrm{ac}} + \Delta\psi \\
\Delta\dot{P}_{\mathrm{ac}} &= G_9^{\mathrm{ac}} \Delta Q_{\mathrm{ac}} + G_{10}^{\mathrm{ac}} \Delta\chi + G_{11}^{\mathrm{ac}} \Delta\theta + G_{12}^{\mathrm{ac}} \Delta P_{\mathrm{IC}} + G_{13}^{\mathrm{ac}} \Delta P_{\mathrm{ac}} \\
\Delta\dot{Q}_{\mathrm{ac}} &= G_5^{\mathrm{ac}} \Delta Q_{\mathrm{ac}} + G_6^{\mathrm{ac}} \Delta\chi + G_7^{\mathrm{ac}} \Delta\theta \\
\Delta\dot{\psi} &= G_{14}^{\mathrm{ac}} \Delta P_{\mathrm{ac}} + G_{15}^{\mathrm{ac}} \Delta\psi + G_{16}^{\mathrm{ac}} \Delta P_{\mathrm{dc}} \\
\Delta\dot{\chi} &= G_{17}^{\mathrm{ac}} \Delta Q_{\mathrm{ac}} + G_{18}^{\mathrm{ac}} \Delta\chi \\
\Delta\dot{P}_{\mathrm{dc}} &= G_2^{\mathrm{dc}} \Delta P_{\mathrm{dc}} + G_3^{\mathrm{dc}} \Delta\varphi + G_4^{\mathrm{dc}} \Delta P_{\mathrm{IC}} \\
\Delta\dot{\varphi} &= G_5^{\mathrm{dc}} \Delta P_{\mathrm{dc}} + G_6^{\mathrm{dc}} \Delta\varphi + G_7^{\mathrm{dc}} \Delta P_{\mathrm{ac}} \\
\Delta\dot{P}_{\mathrm{IC}} &= G_1^{\mathrm{IC}} \Delta P_{\mathrm{ac}} + G_2^{\mathrm{IC}} \Delta P_{\mathrm{dc}}
\end{aligned} \tag{6.10}$$

where matrices $G$ are calculated in a steady-state operating point and can be found in Appendix A.

The closed-loop model for the hybrid *ac/dc*-microgrid with the control strategy for power-sharing from (6.10) is used to validate the tuning of the controllers and to perform a small-signal stability analysis in Section 6.4.

## 6.3 Control Strategy Proposed for Operation Cost Minimization

In this section, the consensus-based distributed secondary control strategy for operation cost minimization is applied to the hybrid *ac/dc*-microgrid with a single *IC*. In this case, to obtain the closed-loop model for this controller, we assume all the units (i.e., *ac*-DGs, *dc*-DGs and *IC*) are operating within limits; therefore, the equations which enforce unit constraints are ignored. The process for obtaining the analytical closed-loop model is detailed in Appendix B.

The controllers proposed in Chapter 4 are applied to the hybrid *ac/dc*-microgrid model obtained in (6.6) to later derive the closed-loop model for the proposed control strategy. The expressions for the controllers are repeated for reader convenience.

**Controller for the $\mathbf{i}^{th}$ *ac*-DG $\forall \mathbf{i} \in \mathbb{N}_{\mathbf{ac}}$:**

*Frequency reference* (4.13a) :

$$\dot{\theta}_{\mathrm{i}} = \omega_{\mathrm{i}} = \omega^* + M_{\mathrm{ac-i}} P^{\mathrm{G}}_{\mathrm{ac-i}} + \Omega^{\mathrm{ac}}_{\mathrm{i}} \tag{6.11a}$$

*Frequency secondary control* (4.13b) :

$$\dot{\Omega}^{\mathrm{ac}}_{\mathrm{i}} = -k^{a}_{\mathrm{ac-i}} \left(\omega_{\mathrm{i}} - \omega^*\right) - k^{b}_{\mathrm{ac-i}} \sum_{j \in \mathbb{N}_{\mathrm{ac}}} a_{\mathrm{i}j} \left(\lambda^{\mathrm{ac}}_{\mathrm{i}} - \lambda^{\mathrm{ac}}_{j}\right) - k^{c}_{\mathrm{ac-i}} \sum_{j \in \mathbb{N}_{\mathrm{dc}}} a_{\mathrm{i}j} \left(\lambda^{\mathrm{ac}}_{\mathrm{i}} - \lambda^{\mathrm{dc}}_{j}\right) \tag{6.11b}$$

*Voltage reference* (3.5a) :

$$E_{\mathrm{i}} = E^* + N_{\mathrm{ac-i}} \cdot Q^{\mathrm{G}}_{\mathrm{ac-i}} + \chi_{\mathrm{i}} \tag{6.11c}$$

*Voltage secondary control* (3.5b) :

$$\dot{\chi}_{\mathrm{i}} = -\beta_{\mathrm{i}} \left(E_{\mathrm{i}} - E^*\right) - b_{\mathrm{i}} \sum\nolimits_{j \in \mathbb{N}_{\mathrm{ac}}} a_{\mathrm{i}j} \left(Q^{\mathrm{G}}_{\mathrm{ac-i}} - Q^{\mathrm{G}}_{\mathrm{ac-}j}\right) \tag{6.11d}$$

**Controller for the $j^{th}$ *dc*-DG $\forall j \in \mathbb{N}_{\mathbf{dc}}$:**

*Voltage reference* (4.15a) :

$$V_j = V^* + M_{\mathrm{dc-}j} P^{\mathrm{G}}_{\mathrm{dc-}j} + \Omega^{\mathrm{dc}}_{j} \tag{6.12a}$$

*Voltage secondary control* (4.15b) :

$$\dot{\Omega}^{\mathrm{dc}}_{j} = -k^{a}_{\mathrm{dc-}j} \left(V_j - V^*\right) - k^{b}_{\mathrm{dc-}j} \sum_{\mathrm{i} \in \mathbb{N}_{\mathrm{dc}}} a_{\mathrm{i}j} \left(\lambda^{\mathrm{dc}}_{j} - \lambda^{\mathrm{dc}}_{\mathrm{i}}\right) - k^{c}_{\mathrm{dc-}j} \sum_{\mathrm{i} \in \mathbb{N}_{\mathrm{ac}}} a_{\mathrm{i}j} \left(\lambda^{\mathrm{dc}}_{j} - \lambda^{\mathrm{ac}}_{\mathrm{i}}\right) \tag{6.12b}$$

**Controller for the *IC*:**

*Secondary controller*(4.16a) :

$$\dot{P}^{*}_{\mathrm{IC}-k} = -\tau_{\mathrm{IC}-k} \sum_{\mathrm{i}\in\mathbb{N}_{\mathrm{ac}}} \sum_{j\in\mathbb{N}_{\mathrm{dc}}} a_{\mathrm{i}k} a_{jk} \left(\lambda^{\mathrm{ac}}_{\mathrm{i}} - \lambda^{\mathrm{dc}}_{j}\right) \tag{6.13a}$$

Based on the equations for the microgrid (6.1), (6.2) and (6.3), and the controllers (6.11), (6.12) and (6.13) (see Appendix B), the closed-loop model for the studied hybrid *ac/dc*-microgrid with the proposed control strategy has 28 state variables, as follows:

- 3 angles from the *ac*-microgrid ($\theta_{\mathrm{i}}, \forall \mathrm{i} \in \mathbb{N}_{\mathrm{ac}}$).
- 3 active powers from the *ac*-microgrid ($P^{\mathrm{G}}_{\mathrm{ac}-\mathrm{i}}, \forall \mathrm{i} \in \mathbb{N}_{\mathrm{ac}}$).
- 3 reactive powers from the *ac*-microgrid ($Q^{\mathrm{G}}_{\mathrm{ac}-\mathrm{i}}, \forall \mathrm{i} \in \mathbb{N}_{\mathrm{ac}}$).
- 3 frequency secondary control variables from the *ac*-microgrid ($\Omega^{\mathrm{ac}}_{\mathrm{i}}, \forall \mathrm{i} \in \mathbb{N}_{\mathrm{ac}}$).
- 3 voltage secondary control variables from the *ac*-microgrid ($\chi_{\mathrm{i}}, \forall \mathrm{i} \in \mathbb{N}_{\mathrm{ac}}$).
- 6 active powers from the *dc*-microgrid ($P^{\mathrm{G}}_{\mathrm{dc}-j}, \forall j \in \mathbb{N}_{\mathrm{dc}}$).
- 6 voltage secondary control variables from the *dc*-microgrid ($\Omega^{\mathrm{dc}}_{j}, \forall j \in \mathbb{N}_{\mathrm{dc}}$).
- 1 *IC* power ($P^{\mathrm{ac}}_{\mathrm{IC}}$).

Then, the state equations for the closed-loop model of the studied hybrid *ac/dc*-microgrid with the proposed control strategy are:

$$\begin{aligned}
\Delta\dot{\theta} &= G^{\mathrm{ac}}_{8}\Delta P^{\mathrm{G}}_{\mathrm{ac}} + \Delta\Omega^{\mathrm{ac}} \\
\Delta\dot{P}^{\mathrm{G}}_{\mathrm{ac}} &= G^{\mathrm{ac}}_{9}\Delta Q^{\mathrm{G}}_{\mathrm{ac}} + G^{\mathrm{ac}}_{10}\Delta\chi + G^{\mathrm{ac}}_{11}\Delta\theta + G^{\mathrm{ac}}_{12}\Delta P^{\mathrm{ac}}_{\mathrm{IC}} + G^{\mathrm{ac}}_{13}\Delta P^{\mathrm{G}}_{\mathrm{ac}} \\
\Delta\dot{Q}^{\mathrm{G}}_{\mathrm{ac}} &= G^{\mathrm{ac}}_{5}\Delta Q^{\mathrm{G}}_{\mathrm{ac}} + G^{\mathrm{ac}}_{6}\Delta\chi + G^{\mathrm{ac}}_{7}\Delta\theta \\
\Delta\dot{\Omega}^{\mathrm{ac}} &= G^{\mathrm{ac}}_{14}\Delta P^{\mathrm{G}}_{\mathrm{ac}} + G^{\mathrm{ac}}_{15}\Delta\Omega^{\mathrm{ac}} + G^{\mathrm{ac}}_{16}\Delta P^{\mathrm{G}}_{\mathrm{dc}} \\
\Delta\dot{\chi} &= G^{\mathrm{ac}}_{17}\Delta Q^{\mathrm{G}}_{\mathrm{ac}} + G^{\mathrm{ac}}_{18}\Delta\chi \\
\Delta\dot{P}^{\mathrm{G}}_{\mathrm{dc}} &= G^{\mathrm{dc}}_{2}\Delta P^{\mathrm{G}}_{\mathrm{dc}} + G^{\mathrm{dc}}_{3}\Delta\Omega^{\mathrm{dc}} + G^{\mathrm{dc}}_{4}\Delta P^{\mathrm{ac}}_{\mathrm{IC}} \\
\Delta\dot{\Omega}^{\mathrm{dc}} &= G^{\mathrm{dc}}_{5}\Delta P^{\mathrm{G}}_{\mathrm{dc}} + G^{\mathrm{dc}}_{6}\Delta\Omega^{\mathrm{dc}} + G^{\mathrm{dc}}_{7}\Delta P^{\mathrm{G}}_{\mathrm{ac}} \\
\Delta\dot{P}^{\mathrm{ac}}_{\mathrm{IC}} &= G^{\mathrm{IC}}_{1}\Delta P^{\mathrm{G}}_{\mathrm{ac}} + G^{\mathrm{IC}}_{2}\Delta P^{\mathrm{G}}_{\mathrm{dc}}
\end{aligned} \tag{6.14}$$

The closed-loop model for the hybrid *ac/dc*-microgrid with the control strategy for operation cost minimization from (6.14) is used to validate the tuning of the controllers and to perform a small-signal stability analysis in Section 6.5.

## 6.4 Small-signal Analysis of the Control Strategy for Power-sharing

In this Section, a small-signal stability analysis is performed to the closed-loop model for the hybrid *ac/dc*-microgrid with the control strategy for power-sharing obtained in Section 6.2. Now, the closed-loop model is used to derive the stable limits for gains of the proposed controller and verify their tuning. Moreover, a sensitivity analysis for parameters of the controllers is performed.

### 6.4.1 Eigenvalues and Participation Factors

The eigenvalues obtained for the linearized closed-loop system obtained in Section 6.2 are plotted in Fig. 6.2 and their coordinates, natural frequency $\omega_n$ and damping ratio $\zeta$ are shown in Table 6.1. The steady-state operating point conditions at the operating point determined by the loading conditions in Table 6.2 were obtained from a system simulation, and the parameters of the controllers are the ones shown in Table 5.3. Since the secondary control strategy for power-sharing is active, all the DGs are generating 79% of their maximum active power (i.e., $P_{\text{dc}}^{\text{max}} = 2.5\text{kW}$ and $P_{\text{ac}}^{\text{max}} = 3.0$ kVA). It is important to emphasize that the conclusions drawn regarding stability and participation factors and sensitivity are, strictly speaking, valid only for the tuning and the operating point described in this Section.

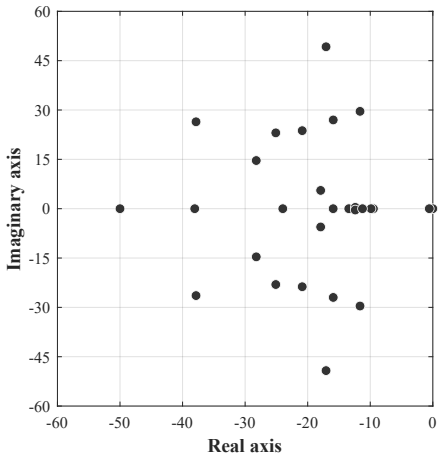


Figure 6.2: Eigenvalues of the system, strategy for power-sharing.

| Eigenvalues | | | | | |
|---|---|---|---|---|---|
| Real | | Complex | | $\omega_n$(Hz) | $\zeta$(%) |
| $\lambda_1$ | 0.0 | $\lambda_{6,7}$ | $-11.6 \pm j29.6$ | 5.1 | 36.5 |
| $\lambda_2$ | $-0.6$ | $\lambda_{8,9}$ | $-12.4 \pm j\ 0.4$ | 2.0 | 99.9 |
| $\lambda_3$ | $-9.5$ | $\lambda_{11,12}$ | $-15.9 \pm j27.0$ | 5.0 | 50.7 |
| $\lambda_4$ | $-9.9$ | $\lambda_{14,15}$ | $-17.1 \pm j49.2$ | 8.3 | 32.8 |
| $\lambda_5$ | $-11.2$ | $\lambda_{16,17}$ | $-17.9 \pm j\ 5.6$ | 3.0 | 95.4 |
| $\lambda_{10}$ | $-13.4$ | $\lambda_{18,19}$ | $-20.9 \pm j23.7$ | 5.0 | 66.1 |
| $\lambda_{13}$ | $-15.9$ | $\lambda_{21,22}$ | $-25.1 \pm j23.1$ | 5.4 | 73.6 |
| $\lambda_{20}$ | $-24.0$ | $\lambda_{23,24}$ | $-28.2 \pm j14.6$ | 5.1 | 88.8 |
| $\lambda_{27}$ | $-38.1$ | $\lambda_{25,26}$ | $-37.8 \pm j26.4$ | 7.3 | 82.0 |
| $\lambda_{28}$ | $-50.0$ | | | | |

Table 6.1: Eigenvalues coordinates of the system, strategy for power-sharing.

Table 6.2: Load conditions for base-case with control strategy for power-sharing.

| Load | $kW$ | Load | $kW$ | Load | $kVA$ |
|---|---|---|---|---|---|
| $R_1$ | 2.05 | $R_4$ | 2.05 | $Z_1$ | $1.7 + j0.8$ |
| $R_2$ | 2.05 | $R_5$ | 2.05 | $Z_2$ | $4.2 + j0.0$ |
| $R_3$ | 1.37 | $R_6$ | 2.05 | $Z_3$ | $3.3 + j1.1$ |

The following approach was used for tuning the gains of the controllers. First, all the controllers were active, and full-load conditions were assumed. Second, the root locus method using the closed-loop model derived in Section 6.2 was applied to the aforementioned operat-

ing condition. The following parameters were sequentially tuned: 1) the parameters related to the local voltages ($\beta_{\mathrm{i}}, \gamma_{\mathrm{i}}$) considering the other parameters are *zero*, 2) the parameters associated with the active power consensus ($\sigma_{\mathrm{i}}, c_{\mathrm{i}}, \tau_{\mathrm{i}}$) considering ($\beta_{\mathrm{i}}, \gamma_{\mathrm{i}}$) as defined in 1), and 3) the parameters from the reactive power consensus ($b_{\mathrm{i}}$) considering parameters obtained in 1) and 2). Third, several simulation scenarios were carried out to fine-tune the gains, changing the operating points to different loading conditions in order to analyze the bidirectionality of the power in the *IC*, and the results were satisfactory. If a more refined tuning of the controllers is desired, meta-heuristic optimization techniques can be considered [139]; however, this is out of the scope of this work.

From Fig. 6.2 and Table 6.1, it can be noted that, since all the eigenvalues have a negative real part (except the eigenvalue at *zero*), the system is asymptotically stable for the nominal values of the gains shown in Table 5.3. Moreover, there are 9 real eigenvalues (see left column in Table 6.1), 18 complex (9 conjugate pairs) eigenvalues (see right column in Table 6.1), and one eigenvalue at the origin ($\lambda_1$), which is related to the angle-frequency relationship in the *ac*-microgrid ($\dot{\theta} = \omega$). The real eigenvalues are completely damped (by definition). On the other hand, it can be seen that the complex eigenvalues $\lambda_{14,15}$, $\lambda_{6,7}$ and $\lambda_{11,12}$, have a damping ratio equal to 32.8%, 36.5% and 50.7%, respectively. Although these modes are very oscillatory, they are fast ($\omega_n > 5$Hz) and the system's stability is not affected. The damping ratio of the other conjugate pairs is higher than 66%, thus, it can be concluded that they are well damped. The slowest eigenvalue ($\lambda_2 = -0.563$) is strongly related to the power flow through the *IC*, as will be explained in the following by analyzing the participation factors.

The participation factors ($p_{\mathrm{i}j}$) are a measure of the relative participation of the i$^{th}$ state variable in the $j^{th}$ eigenvalue (or mode), and vice versa [140]. Fig. 6.3 is presented to analyze the participation factors. Here, the eigenvalues for the base case discussed before are plotted, and the ones with the highest participation factors with respect to the state variables are highlighted.

The eigenvalues with the highest participation of the state variables related to the secondary controller for the *dc*-DGs ($\Delta\varphi$) are highlighted in green (see Fig. 6.3a). It can be seen that $\Delta\varphi$ participates mainly in real eigenvalues and in two conjugate pairs ($\lambda_{20,21}$, $\lambda_{25,26}$), which damping ratios are 73.6% and 82.0%, respectively. The frequency of oscillation for these conjugate pairs is also similar, which helps to understand the secondary control dynamics for the *dc*-DGs. The state variables for the power generated by the *dc*-DGs ($\Delta P_{\mathrm{dc}}$) have a strong participation in the eigenvalues highlighted in red (see Fig. 6.3b). Comparing Fig. 6.3a and Fig. 6.3b, it is clear that a strong relation between $\Delta P_{\mathrm{dc}}$ and $\Delta\varphi$ exists, since they participate in almost the same eigenvalues. Therefore, it is possible to conclude that the dynamics for these two variables is similar.

The eigenvalues with the highest participation of the state variables for the power generated by the *ac*-DGs ($\Delta P_{\mathrm{ac}}$) are highlighted in blue (see Fig. 6.3c). It can be seen that $\Delta P_{\mathrm{ac}}$ participates mostly in real eigenvalues and in one conjugate pair ($\lambda_{6,7}$), which are the complex eigenvalues with the smallest damping ratio (36.5%). Therefore, if a higher damping ratio in the power generated by the *ac*-DGs is desired, the tuning of the controllers should be adjusted as will be described in next Section with the sensitivity analysis.

Fig. 6.3d shows the participation of the other state variables in the eigenvalues, highlighted

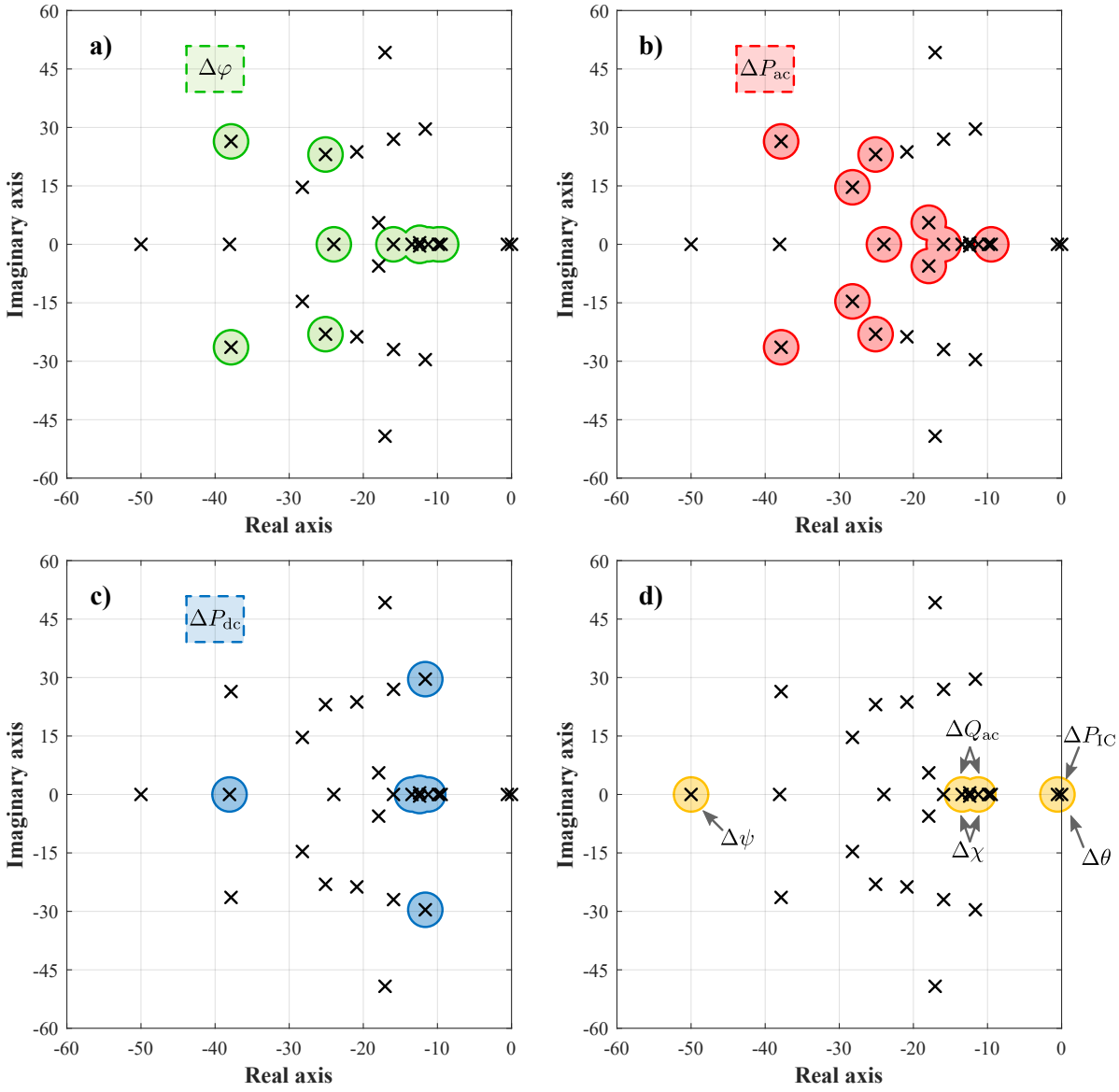


Figure 6.3: Participation factors for the eigenvalues of the system with the strategy for power-sharing.

in yellow. From the Figure it is possible to state that the eigenvalue at the origin ($\lambda_1$) is highly sensitive to the state variable of the angles in the *ac*-microgrid ($\Delta\omega$). On the other hand, the slowest eigenvalue ($\lambda_2$) is highly sensitive to the power in the *IC* ($\Delta P_{\mathrm{IC}}$). The eigenvalues marked with $\lambda_{10}, \lambda_{13}$ are highly sensitive to the reactive power-sharing, i.e., to the state variables of the reactive power ($\Delta Q_{\mathrm{ac}}$) and the voltage secondary controller of the *ac*-DGs ($\Delta\chi$). Finally, the eigenvalue with the fastest dynamic ($\lambda_{28}$) is strongly sensitive to the frequency secondary controller of the *ac*-DGs ($\Delta\psi$).

### 6.4.2 Sensitivity Analysis

Now, a sensitivity analysis is performed to the closed-loop system obtained in Section 6.2 for the hybrid *ac*/*dc*-microgrid with the control strategy proposed for power-sharing. The

sensitivity analysis helps to understand how the parameters of the controllers affect the dynamics of the system, in the vicinity of the operating point. Specifically, four control objectives are analyzed: *(i)* *dc*-voltage regulation, *(ii)* *ac*-voltage regulation, *(iii)* active power consensus, and *(iv)* reactive power consensus. In all cases, the linearized model from Section 6.2 is considered at the original operating point and the parameters of the controllers are modified from 50% (in blue) to 150% (in red) of the value shown in Table 5.3 (identified with a black '**x**'). The results for the sensitivity analysis are shown in Fig. 6.4.

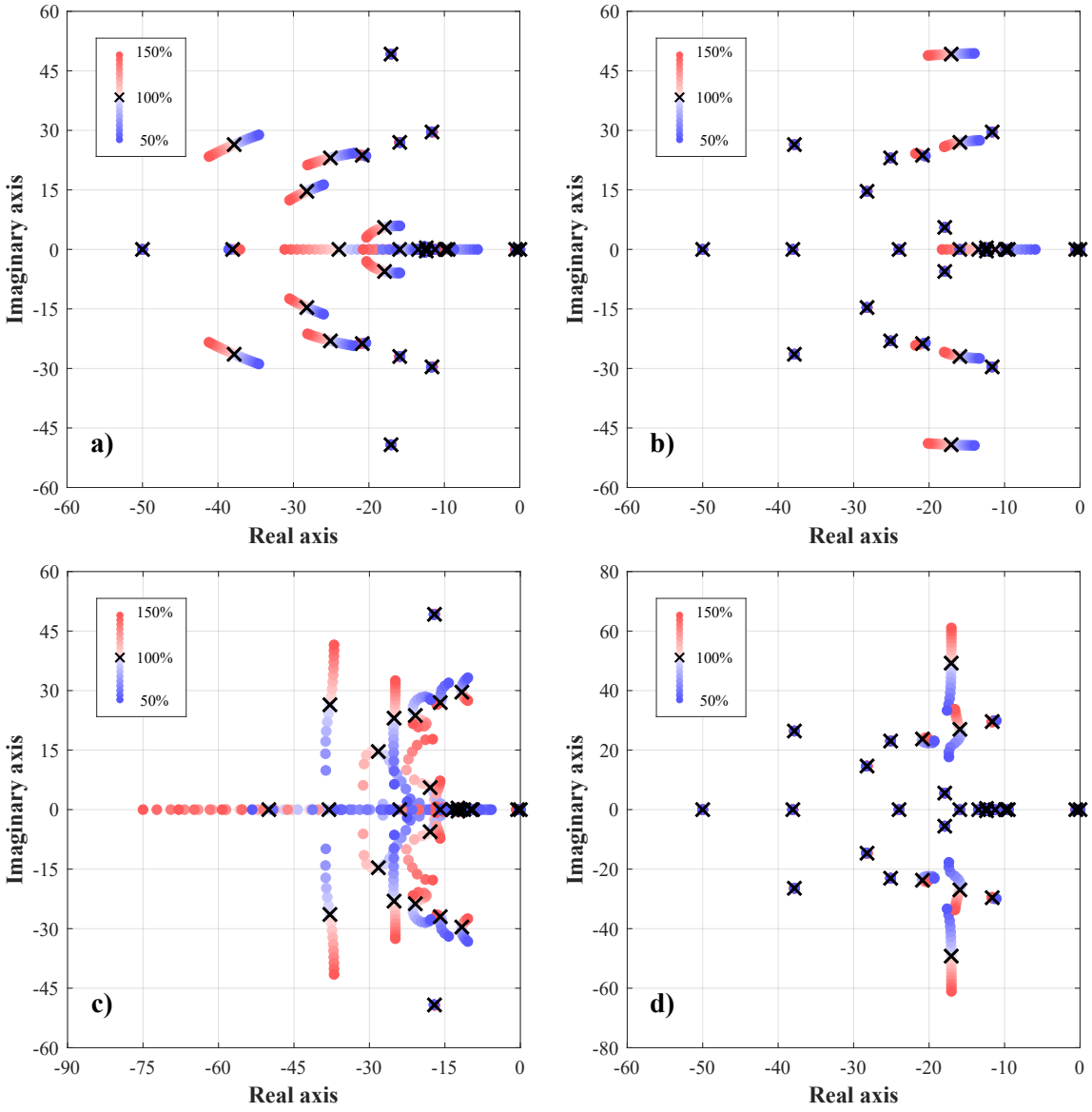


Figure 6.4: Sensitivity analysis for the eigenvalues of the system with the strategy for power-sharing. a) *dc*-voltage regulation. b) *ac*-voltage regulation. c) Active power consensus. d) Reactive power consensus.

First, Fig. 6.4a shows the trajectories of the eigenvalues when a sweep is applied to the gain for *dc*-voltage regulation ($6.0 < \gamma_i < 18.0$). The expression for the *dc*-DG's secondary controller is repeated in (6.15) for the convenience of the reader, and the modified gain is highlighted in red. Using the information from the participation factors analyzed in the

previous Section (see Fig. 6.3), it is possible to conclude that the eigenvalues affected by the modification in the gains for *dc*-voltage regulation are the ones that are more sensitive to the secondary controller of the *dc*-DGs (see Fig. 6.3a) and to the power generated by the *dc*-DGs (see Fig. 6.3b). On the other hand, from the trajectories of the complex eigenvalues, we can conclude that frequency and damping ratio of these modes increase for an increase in $\gamma_{\mathrm{i}}$.

$$\rho_{\mathrm{i}}\dot{\varphi}_{\mathrm{i}} = -\boldsymbol{\gamma_{\mathrm{i}}}(V_{\mathrm{i}} - V^{*}) - c_{\mathrm{i}} \sum_{j \in \mathbb{N}_{\mathrm{dc}}} a_{\mathrm{i}j} \left(P_{\mathrm{dc-i}} - P_{\mathrm{dc}-j}\right) - c_{\mathrm{i}} \sum_{j \in \mathbb{N}_{\mathrm{ac}}} a_{\mathrm{i}j} \left(P_{\mathrm{dc-i}} - P_{\mathrm{ac}-j}\right) \tag{6.15}$$

Second, Fig. 6.4b shows the trajectories of the eigenvalues when a sweep is applied to the gain for *ac*-voltage regulation ($6.0 < \beta_{\mathrm{i}} < 18.0$). The expression for the *ac*-DG's secondary controller is repeated in (6.16) for the convenience of the reader, and the modified gain is highlighted in red. Comparing with the information from the participation factors (see Fig. 6.3) it can be concluded that the eigenvalues affected by the sweep in the gain are not strictly related to a state variable. Moreover, the trajectories show that the eigenvalues move along the real-axis; however, they are maintained within the stable region of the complex plane (left semi-plane).

$$\varrho_{\mathrm{i}}\dot{\chi}_{\mathrm{i}} = -\boldsymbol{\beta_{\mathrm{i}}}(E_{\mathrm{i}} - E^{*}) - b_{\mathrm{i}} \sum_{j \in \mathbb{N}_{\mathrm{ac}}} a_{\mathrm{i}j} \left(Q_{\mathrm{i}} - Q_{j}\right) \tag{6.16}$$

Third, Fig. 6.4c shows the trajectories of the eigenvalues when a sweep is simultaneously applied to the gains for the active power consensus ($25.0 < c_{\mathrm{i}}, \sigma_{\mathrm{i}}, \tau_{k} < 75.0$). The expressions for the secondary controller of the *dc*-DGs, *ac*-DGs and *IC* are repeated in (6.17), respectively, for the convenience of the reader, and the modified gains are highlighted in red. It is evident that the active power consensus affects almost all the eigenvalues from the system. Moreover, it can be noted that the eigenvalues that have a longer trajectory are those that are more sensitive to the state variables of the active power. On the other hand, the complex eigenvalues with the smallest damping ratio tend to move to the right-hand side; however, they remain in the stable region for the range of the gains considered in this analysis. It can also be noted that some complex eigenvalues move away from the real-axis, while others move closer. Thus, the increase/reduction of the gains improves or worsens the damping ratio of different oscillatory modes. What is clear is that an increase in gains also increases the natural frequency of the eigenvalues.

$$\rho_{\mathrm{i}}\dot{\varphi}_{\mathrm{i}} = -\gamma_{\mathrm{i}} \left(V_{\mathrm{i}} - V^{*}\right) - \boldsymbol{c_{\mathrm{i}}} \sum_{j \in \mathbb{N}_{\mathrm{dc}}} a_{\mathrm{i}j} \left(P_{\mathrm{dc-i}} - P_{\mathrm{dc}-j}\right) - \boldsymbol{c_{\mathrm{i}}} \sum_{j \in \mathbb{N}_{\mathrm{ac}}} a_{\mathrm{i}j} \left(P_{\mathrm{dc-i}} - P_{\mathrm{ac}-j}\right) \tag{6.17a}$$

$$\dot{\psi}_{\mathrm{i}} = -\boldsymbol{\sigma_{\mathrm{i}}} \left[ \left(\omega_{\mathrm{i}} - \omega^{*}\right) + \sum_{j \in \mathbb{N}_{\mathrm{ac}}} a_{\mathrm{i}j} \left(P_{\mathrm{ac-i}} - P_{\mathrm{ac}-j}\right) + \sum_{j \in \mathbb{N}_{\mathrm{dc}}} a_{\mathrm{i}j} \left(P_{\mathrm{ac-i}} - P_{\mathrm{dc}-j}\right) \right] \tag{6.17b}$$

$$\dot{P}^{*}_{\mathrm{IC}-k} = -\boldsymbol{\tau_{k}} \sum_{\mathrm{i} \in \mathbb{N}_{\mathrm{ac}}} \sum_{j \in \mathbb{N}_{\mathrm{dc}}} a_{\mathrm{i}k} a_{jk} \left(P_{\mathrm{ac-i}} - P_{\mathrm{dc}-j}\right) \tag{6.17c}$$

Finally, Fig. 6.4d shows the trajectories of the eigenvalues when a sweep is applied to the gain for the reactive power consensus ($250.0 < b_{\mathrm{i}} < 750.0$). The expressions for the secondary

controller of the *ac*-DGs is repeated in (6.18) for the convenience of the reader, and the modified gain is highlighted in red. Comparing with the information from the participation factors (see Fig. 6.3) it can be concluded that the eigenvalues affected by the sweep in the gain $b_{\mathrm{i}}$ are not strictly related to a state variable. Moreover, the trajectories show that the eigenvalues move along the imaginary-axis. On the other hand, the eigenvalues affected by the change in the gain related to the reactive power consensus are the same affected by the *ac*-voltage regulation (see Fig. 6.4b), which is explained by the $Q$-$E$ relation in the *ac*-microgrid.

$$\varrho_{\mathrm{i}}\dot{\chi}_{\mathrm{i}} = -\beta_{\mathrm{i}}\left(E_{\mathrm{i}} - E^{*}\right) - \boldsymbol{b_{\mathrm{i}}}\sum_{j\in\mathbb{N}_{\mathrm{ac}}} a_{\mathrm{i}j}\left(Q_{\mathrm{i}} - Q_{j}\right) \tag{6.18}$$

## 6.5 Small-signal Analysis of the Control Strategy for Operation Cost Minimization

In this Section, a small-signal stability analysis is performed to the closed-loop model for the hybrid *ac*/*dc*-microgrid with the control strategy for operation cost minimization obtained in Section 6.3. The closed-loop model is used to derive the stable limits for gains of the proposed controller and verify their tuning. Moreover, a sensitivity analysis for parameters of the controllers is performed.

### 6.5.1 Eigenvalues and Participation Factors

The eigenvalues obtained for the linearized closed-loop system derived in Section 6.3 are plotted in Fig. 6.5 and their coordinates, natural frequency $\omega_n$ and damping ratio $\zeta$ are shown in Table 6.3. The steady-state operating point conditions at the operating point determined by the loading conditions in Table 6.4 were obtained from a system simulation, and the parameters of the controllers are the ones shown in Table 5.4. The power generated by the DGs (in p.u.) is shown in Table 6.5. It is important to emphasize that the conclusions drawn regarding stability and participation factors and sensitivity are, strictly speaking, valid only for the tuning and the operating point described in this Section.

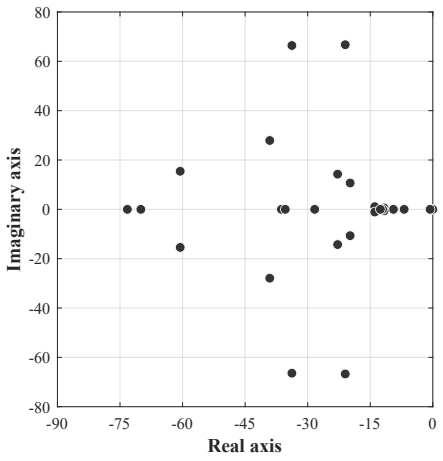


Figure 6.5: Eigenvalues of the system, strategy for cost minimization.

| Eigenvalues | | | | | |
|---|---|---|---|---|---|
| Real | | Complex | | $\omega_n$(Hz) | $\zeta$(%) |
| $\lambda_1$ | 0.0 | $\lambda_{6,7}$ | $-11.7 \pm j\ 0.6$ | 1.9 | 99.9 |
| $\lambda_2$ | $-0.7$ | $\lambda_{10,11}$ | $-13.9 \pm j\ 1.1$ | 2.2 | 99.7 |
| $\lambda_3$ | $-6.9$ | $\lambda_{12,13}$ | $-19.8 \pm j10.7$ | 3.6 | 88.0 |
| $\lambda_4$ | $-9.3$ | $\lambda_{14,15}$ | $-21.0 \pm j66.7$ | 11.1 | 30.0 |
| $\lambda_5$ | $-9.5$ | $\lambda_{16,17}$ | $-22.8 \pm j14.3$ | 4.3 | 84.8 |
| $\lambda_8$ | $-12.0$ | $\lambda_{19,20}$ | $-33.8 \pm j66.4$ | 11.9 | 45.3 |
| $\lambda_9$ | $-12.6$ | $\lambda_{23,24}$ | $-39.1 \pm j27.9$ | 7.6 | 81.4 |
| $\lambda_{18}$ | $-28.3$ | $\lambda_{25,26}$ | $-60.6 \pm j15.4$ | 9.9 | 96.9 |
| $\lambda_{21}$ | $-35.4$ | | | | |
| $\lambda_{22}$ | $-36.3$ | | | | |
| $\lambda_{27}$ | $-70.0$ | | | | |
| $\lambda_{28}$ | $-73.2$ | | | | |

Table 6.3: Eigenvalues coordinates of the system, strategy for cost minimization.

Table 6.4: Load conditions for base-case with control strategy for cost minimization.

| Load | $kW$ | Load | $kW$ | Load | $kW$ |
|---|---|---|---|---|---|
| $R_1$ | 1.03 | $R_4$ | 1.02 | $Z_1$ | 1.90 |
| $R_2$ | 1.57 | $R_5$ | 1.02 | $Z_2$ | 2.57 |
| $R_3$ | 1.37 | $R_6$ | 1.02 | $Z_3$ | 2.64 |

Table 6.5: Power generated by the DGs, in p.u.

| $dc$-DG$_1$ | $dc$-DG$_2$ | $dc$-DG$_3$ | $dc$-DG$_4$ | $dc$-DG$_5$ | $dc$-DG$_6$ | $ac$-DG$_1$ | $ac$-DG$_2$ | $ac$-DG$_3$ |
|---|---|---|---|---|---|---|---|---|
| 0.631 | 0.864 | 0.993 | 0.268 | 0.175 | 0.654 | 0.985 | 0.520 | 0.284 |

The following approach was used for tuning the gains of the controllers. First, all the controllers were considered active, and full-load conditions were assumed. Second, the root locus method using the closed-loop model derived in Section 6.3 was applied to the aforementioned operating condition. The following parameters were sequentially tuned: 1) the parameters related to the local voltages ($\beta_{\rm i}, k^a_{{\rm dc}-j}$) considering the other parameters are *zero*, 2) the parameters associated with the $\lambda$ consensus ($k^{b,c}_{{\rm dc}-j}, k^{b,c}_{{\rm ac}-{\rm i}}, \tau_{{\rm IC}-k}$) considering ($\beta_{\rm i}, k^a_{{\rm dc}-j}$) as defined in 1), and 3) the parameters corresponding to the reactive power consensus ($b_{\rm i}$) considering parameters obtained in 1) and 2). Third, several simulation scenarios were carried out to fine-tune the gains, changing the operating points to different loading conditions in order to analyze the bidirectionality of the power in the $IC$, and the results were satisfactory. If a more refined tuning of the controllers is required, meta-heuristic optimization techniques can be considered; however, this is out of the scope of this work.

From Fig. 6.5 and Table 6.3, it can be noted that, since all the eigenvalues have a negative real part (except the eigenvalue at *zero*), the system is asymptotically stable for the nominal values of the gains shown in Table 5.4. Moreover, there are 11 real eigenvalues (see left column in Table 6.3), 16 complex (8 conjugate pairs) eigenvalues (see right column in Table 6.3), and one eigenvalue at the origin ($\lambda_1$), which is related to the angle-frequency relationship in the $ac$-microgrid ($\dot{\theta} = \omega$). Although the real eigenvalues are completely damped (by definition), it can be seen that the complex eigenvalues are also mostly well damped. Complex pairs

$\lambda_{14,15}$ and $\lambda_{19,20}$, have a damping ratio equal to 30.0% and 45.3%, respectively, while the damping ratio of the other conjugate pairs is higher than 81%. On the other hand, the slowest eigenvalue ($\lambda_2 = -0.655$) is strongly related to the power flow through the *IC*, as will be explained in the following by analyzing the participation factors.

The Fig. 6.6 is presented for analyzing the participation factors. Here, the eigenvalues for the base case discussed before are plotted, and the ones with the highest participation factors with respect to the state variables are highlighted.

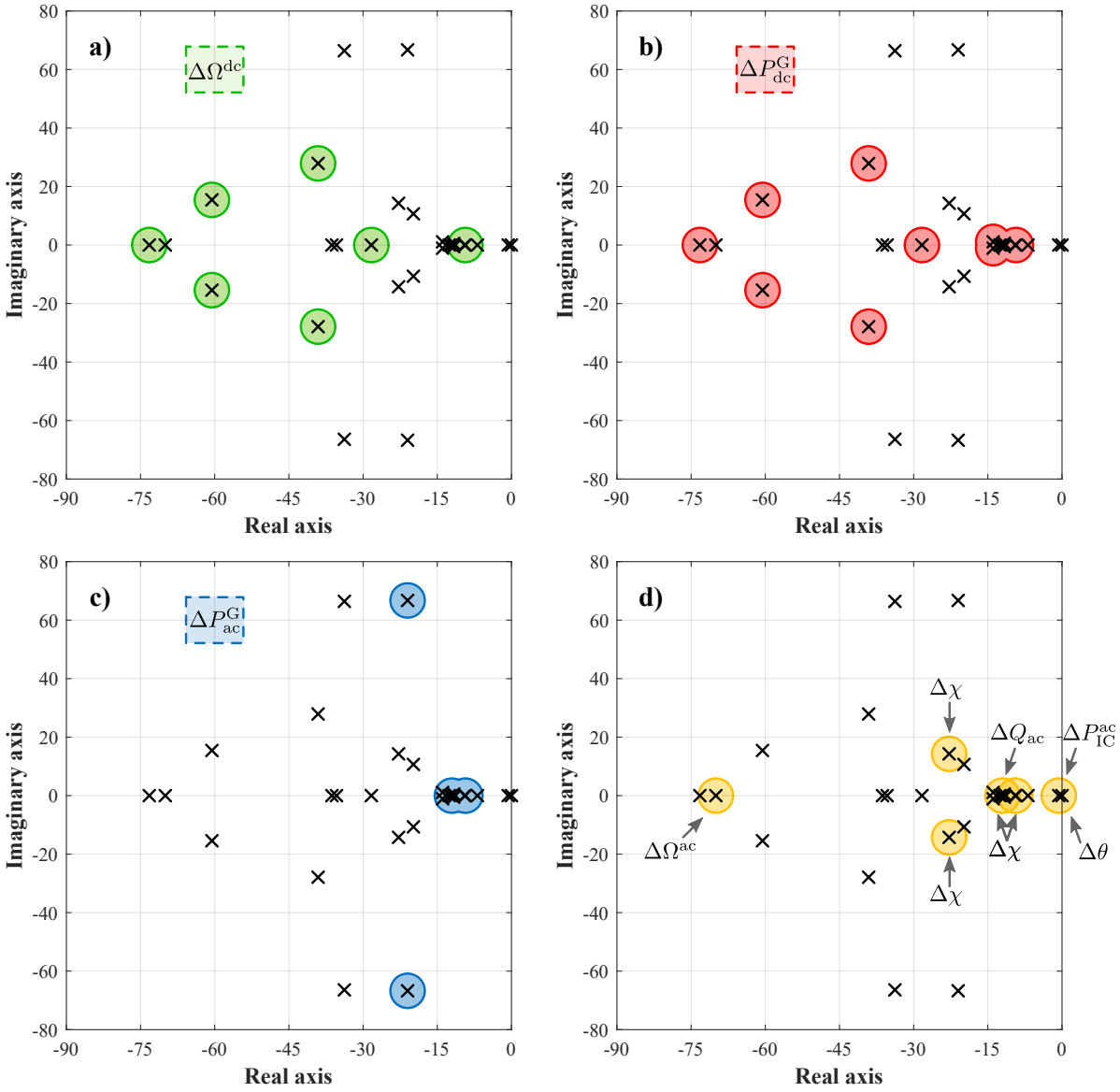


Figure 6.6: Participation factors for the eigenvalues of the system with the strategy for cost minimization.

The eigenvalues with the highest participation of the state variables related to the secondary controller for the *dc*-DGs ($\Delta\Omega^{dc}$) are highlighted in green (see Fig. 6.6a). It can be seen that $\Delta\Omega^{dc}$ participates mostly in real eigenvalues and in two conjugate pairs ($\lambda_{23,24}$, $\lambda_{25,26}$), which damping ratio is 81.4% and 96.9%, respectively. The frequency of oscillation

for these conjugate pairs is also similar (7.6Hz and 9.9Hz, respectively), which give us an insight of the secondary control dynamics for the *dc*-DGs.

The state variables for the power generated by the *dc*-DGs ($\Delta P_{\text{dc}}^{\text{G}}$) have a strong participation in the eigenvalues highlighted in red (see Fig. 6.6b). Comparing Fig. 6.6a and Fig. 6.6b, it is clear that a strong relation between $\Delta P_{\text{dc}}^{\text{G}}$ and $\Delta\Omega^{\text{dc}}$ exists, since they participate in almost the same eigenvalues. Therefore, it is possible to conclude that the dynamics for these two variables is similar, as described before for the control strategy for power-sharing.

The eigenvalues with the highest participation of the state variables for the power generated by the *ac*-DGs ($\Delta P_{\text{ac}}^{\text{G}}$) are highlighted in blue (see Fig. 6.6c). It can be seen that $\Delta P_{\text{ac}}^{\text{G}}$ participates mostly in real eigenvalues and in one conjugate pair ($\lambda_{14,15}$), which are the complex eigenvalues with the smallest damping ratio (30.0%). Therefore, if a higher damping ratio in the power generated by the *ac*-DGs is desired, the tuning of the controllers should be adjusted as will be described in next Section with the sensitivity analysis.

Fig. 6.6d shows the participation of the other state variables in the eigenvalues, highlighted in yellow. From the Figure it is possible to state that the eigenvalue at the origin ($\lambda_1$) is highly sensitive to the state variable of the angles in the *ac*-microgrid ($\Delta\omega$). On the other hand, the slowest eigenvalue ($\lambda_2$) is highly sensitive to the power in the *IC* ($\Delta P_{\text{IC}}^{\text{ac}}$). The eigenvalue marked with $\lambda_9$ is highly sensitive to the reactive power ($\Delta Q_{\text{ac}}^{\text{G}}$), while the eigenvalues marked with $\lambda_5, \lambda_9, \lambda_{16,17}$ are highly sensitive to the voltage secondary controller of the *ac*-DGs ($\Delta\chi$). Finally, the eigenvalue with the fastest dynamic ($\lambda_{27}$) is strongly sensitive to the frequency secondary controller of the *ac*-DGs ($\Delta\Omega^{\text{ac}}$).

### 6.5.2 Sensitivity Analysis

Now, a sensitivity analysis is performed on the closed-loop system obtained in Section 6.3 for the hybrid *ac/dc*-microgrid with the control strategy proposed for cost minimization. The sensitivity analysis helps to understand how the parameters of the controllers affect the dynamics of the system, in the vicinity of the operating point. Specifically, four control objectives are analyzed: *(i) dc*-voltage regulation, *(ii) ac*-voltage regulation, *(iii)* incremental cost ($\lambda$) consensus, and *(iv)* reactive power consensus. In all cases, the linearized model from Section 6.3 is considered at the original operating point and the parameters of the controllers are modified from 50% (in blue) to 150% (in red) of the value shown in Table 5.4 (black '$\mathbf{x}$'). The results for the sensitivity analysis are shown in Fig. 6.7.

First, Fig. 6.7a shows the trajectories of the eigenvalues when a sweep is applied to the gain for *dc*-voltage regulation ($0.05 < k_{\text{dc}-j}^{a} < 0.15$). The expression for the *dc*-DG's secondary controller is repeated in (6.19) for the convenience of the reader, and the modified gain is highlighted in red. Using the information from the participation factors analyzed in the previous Section (see Fig. 6.6), it is possible to conclude that the eigenvalues affected by the modification in the gains for *dc*-voltage regulation are the ones that are more sensitive to the secondary controller of the *dc*-DGs (see Fig. 6.6a) and to the power generated by the *dc*-DGs (see Fig. 6.6b). On the other hand, from the trajectories of the complex eigenvalues, we can

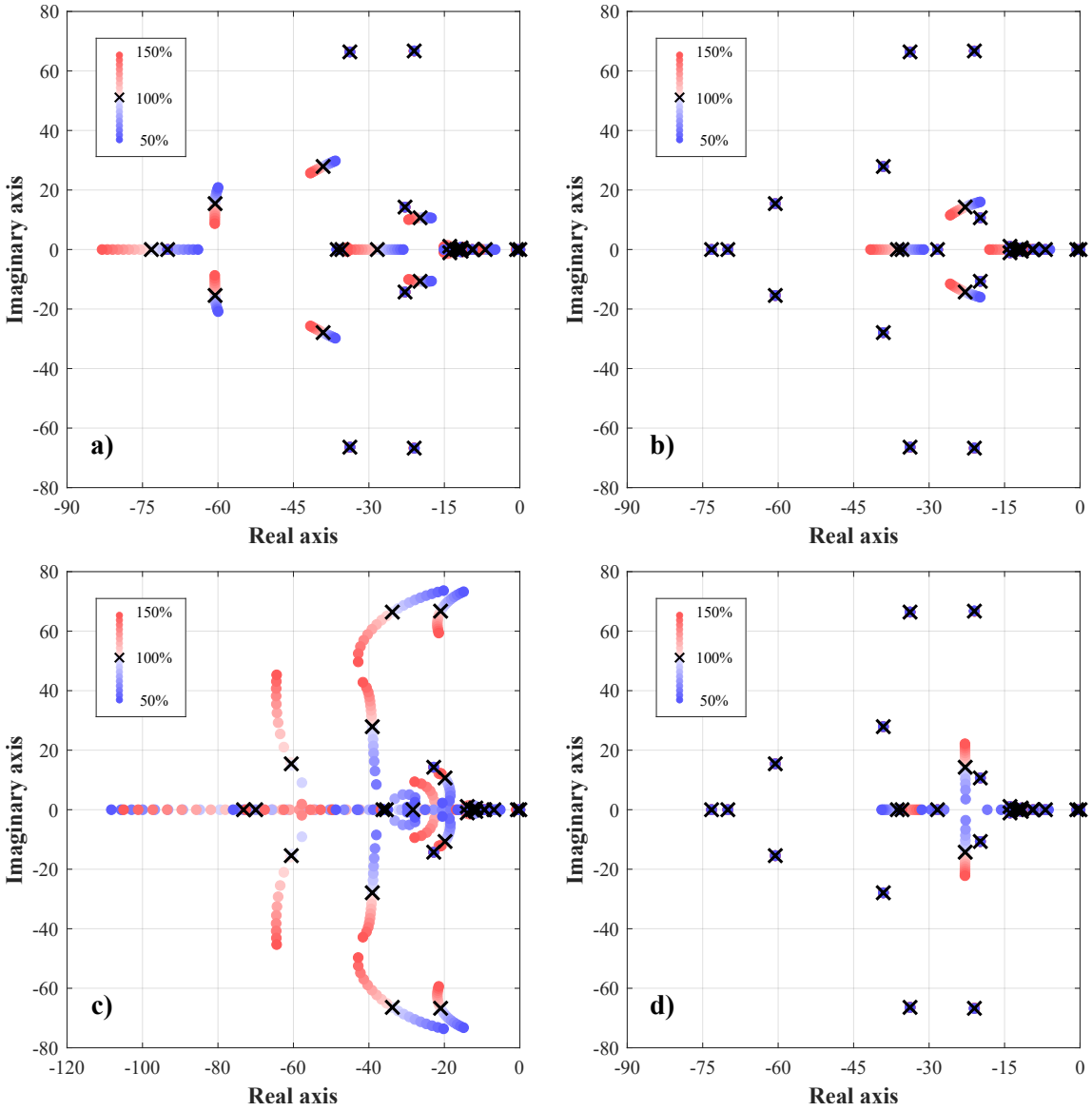


Figure 6.7: Sensitivity analysis for the eigenvalues of the system with the strategy for cost minimization. a) *dc*-voltage regulation. b) *ac*-voltage regulation. c) Incremental cost ($\lambda$) consensus. d) Reactive power consensus.

conclude that frequency and damping ratio of these modes increase for an increase in $k^{a}_{\mathrm{dc}-j}$.

$$\dot{\Omega}^{\mathrm{dc}}_{j} = -\boldsymbol{k^{a}_{\mathrm{dc}-j}}(V_j - V^{*}) - k^{b}_{\mathrm{dc}-j}\sum_{\mathrm{i}\in\mathbb{N}_{\mathrm{dc}}} a_{\mathrm{ij}}\left(\lambda^{\mathrm{dc}}_{j} - \lambda^{\mathrm{dc}}_{\mathrm{i}}\right) - k^{c}_{\mathrm{dc}-j}\sum_{\mathrm{i}\in\mathbb{N}_{\mathrm{ac}}} a_{\mathrm{ij}}\left(\lambda^{\mathrm{dc}}_{j} - \lambda^{\mathrm{ac}}_{\mathrm{i}}\right) \tag{6.19}$$

Secondly, Fig. 6.7b shows the trajectories of the eigenvalues when a sweep is applied to the gain for *ac*-voltage regulation ($6.0 < \beta_{\mathrm{i}} < 18.0$). The expression for the *ac*-DG's secondary controller is repeated in (6.20) for the convenience of the reader, and the modified gain is highlighted in red. Comparing with the information from the participation factors (see Fig. 6.6) it can be concluded that the eigenvalues affected by the sweep in $\beta_{\mathrm{i}}$ are highly

sensitive to the state variables for the voltage secondary controller in the *ac*-DGs ($\Delta\chi$) and for the reactive power($\Delta Q^{\mathrm{G}}_{\mathrm{ac}}$), as shown in Fig. 6.6d. Moreover, the trajectories show that the eigenvalues mainly move along the real-axis; however, they are maintained within the stable region of the complex plane (left semi-plane).

$$\varrho_{\mathrm{i}}\dot{\chi}_{\mathrm{i}} = -\boldsymbol{\beta_{\mathrm{i}}}(E_{\mathrm{i}} - E^*) - b_{\mathrm{i}} \sum_{j\in\mathbb{N}_{\mathrm{ac}}} a_{ij}\left(Q^{\mathrm{G}}_{\mathrm{ac-i}} - Q^{\mathrm{G}}_{\mathrm{ac}-j}\right) \tag{6.20}$$

Thirdly, Fig. 6.7c shows the trajectories of the eigenvalues when a sweep is simultaneously applied to the gains for the incremental cost consensus ($0.5 < k^{b,c}_{\mathrm{dc}-j} < 1.5$, $0.05 < k^{b,c}_{\mathrm{ac-i}} < 0.15$, $125 < \tau_{\mathrm{IC}} < 375$). The expressions for the secondary controller of the *dc*-DGs, *ac*-DGs and *IC* are repeated in (6.21), respectively, and the modified gains are highlighted in red. It is evident that the incremental cost consensus affects almost all the eigenvalues from the system. Moreover, it can be noted that the eigenvalues that have a longer trajectory are those that are more sensitive to the state variables of the active power due to the cost is a function of the power. On the other hand, the complex eigenvalues with the smallest damping ratio tend to move to the right-hand side when the gains decrease; however, they remain in the stable region for the range of the gains considered in this analysis. It can also be noted that some complex eigenvalues move away from the real-axis, while others move closer. Thus, it is not possible to conclude if the increase/reduction of the gains improves or worsens the damping ratio of the oscillatory modes. What is clear is that an increase in gains also increases the natural frequency of eigenvalues.

$$\dot{\Omega}^{\mathrm{dc}}_{j} = -k^{a}_{\mathrm{dc}-j}\left(V_j - V^*\right) - \boldsymbol{k^{b}_{\mathrm{dc}-j}} \sum_{\mathrm{i}\in\mathbb{N}_{\mathrm{dc}}} a_{\mathrm{i}j}\left(\lambda^{\mathrm{dc}}_{j} - \lambda^{\mathrm{dc}}_{\mathrm{i}}\right) - \boldsymbol{k^{c}_{\mathrm{dc}-j}} \sum_{\mathrm{i}\in\mathbb{N}_{\mathrm{ac}}} a_{\mathrm{i}j}\left(\lambda^{\mathrm{dc}}_{j} - \lambda^{\mathrm{ac}}_{\mathrm{i}}\right) \tag{6.21a}$$

$$\dot{\Omega}^{\mathrm{ac}}_{\mathrm{i}} = -k^{a}_{\mathrm{ac-i}}\left(\omega_{\mathrm{i}} - \omega^*\right) - \boldsymbol{k^{b}_{\mathrm{ac-i}}} \sum_{j\in\mathbb{N}_{\mathrm{ac}}} a_{\mathrm{i}j}\left(\lambda^{\mathrm{ac}}_{\mathrm{i}} - \lambda^{\mathrm{ac}}_{j}\right) - \boldsymbol{k^{c}_{\mathrm{ac-i}}} \sum_{j\in\mathbb{N}_{\mathrm{dc}}} a_{\mathrm{i}j}\left(\lambda^{\mathrm{ac}}_{\mathrm{i}} - \lambda^{\mathrm{dc}}_{j}\right) \tag{6.21b}$$

$$\dot{P}^{*}_{\mathrm{IC}-k} = -\boldsymbol{\tau_{\mathrm{IC}-k}} \sum_{\mathrm{i}\in\mathbb{N}_{\mathrm{ac}}} \sum_{j\in\mathbb{N}_{\mathrm{dc}}} a_{\mathrm{i}k}a_{jk}\left(\lambda_{\mathrm{ac-i}} - \lambda_{\mathrm{dc}-j}\right) \tag{6.21c}$$

Finally, Fig. 6.7d shows the trajectories of the eigenvalues when a sweep is applied to the gain for the reactive power consensus ($250 < b_{\mathrm{i}} < 750$). The expressions for the secondary controller of the *ac*-DGs is repeated in (6.22) for the convenience of the reader, and the modified gain is highlighted in red. Comparing with the information from the participation factors (see Fig. 6.6) it can be concluded that the eigenvalues affected by the sweep in the gain $b_{\mathrm{i}}$ are highly sensitive to the state variables for the voltage secondary controller in the *ac*-DGs ($\Delta\chi$) and for the reactive power($\Delta Q^{\mathrm{G}}_{\mathrm{ac}}$), as shown in Fig. 6.6d. Moreover, the trajectories show that the complex eigenvalues move along the imaginary-axis. On the other hand, the eigenvalues affected by the change in the gain related to the reactive power consensus are the same affected by the *ac*-voltage regulation (see Fig. 6.7b), which is explained by the *Q*-*E* relation in the *ac*-microgrid.

$$\varrho_{\mathrm{i}}\dot{\chi}_{\mathrm{i}} = -\beta_{\mathrm{i}}\left(E_{\mathrm{i}} - E^*\right) - \boldsymbol{b_{\mathrm{i}}} \sum_{j\in\mathbb{N}_{\mathrm{ac}}} a_{\mathrm{i}j}\left(Q^{\mathrm{G}}_{\mathrm{ac-i}} - Q^{\mathrm{G}}_{\mathrm{ac}-j}\right) \tag{6.22}$$

## 6.6 Summary

In this Chapter, the closed-loop model for a hybrid *ac/dc*-microgrid with a single *IC* was obtained. The model was augmented with the two consensus based distributed secondary controllers proposed in this thesis. First, the control strategy proposed for power-sharing between the DGs was included, obtaining an analytical closed-loop model composed by 28 state variables. Secondly, the control strategy proposed for operation cost minimization was included, obtaining again an analytical closed-loop model composed by 28 state variables. The state variables were the same for the two analyzed cases. The obtained closed-loop model for the hybrid *ac/dc*-microgrid was used to derive the stable limits for gains of proposed controllers and verify their tuning.

Later, a small-signal analysis was performed for the two closed-loop models obtained. The eigenvalues from the characteristic equation were extensively analyzed, identifying their sensitivity with respect to the state variables. The later was performed using the participation factors. Moreover, a sensitivity analysis was also performed to identify how the increase or decrease of controller's gains affects the state variables. Four cases were analyzed for each control strategy proposed in this thesis, identifying the effect of the gains in the oscillatory modes.

In the next Chapter, the distributed secondary control strategy for power-sharing proposed in Chapter 3 is validated through experimental and simulation tests.

# Chapter 7

# Validation of the Strategy Proposed for Power-Sharing

## 7.1 Introduction

This Chapter presents the experimental and simulation tests performed for validating the distributed secondary control strategy for power-sharing proposed in Chapter 3. For the experimental tests, the experimental rig described in Chapter 5 is considered. For the simulation tests two systems were considered: the system described in Chapter 5 for the first simulation test and a modified microgrid considering multiple *ICs* for the second simulation test. This could not be experimentally implemented in the lab, because a single *IC* was available in the *Triphase* microgrid. For all tests, all the control layers of the microgrid (i.e., inner, primary and secondary control loops) are active.

This Chapter is organized as follows: experimental tests are presented in Sections 7.2 to 7.5. Specifically, the tests were performed for validating the operation of the proposed control strategy against load impacts (Section 7.2), connection/disconnection of DGs (Section 7.3) and communication issues such as loss of communication links (Section 7.4) and communication delays (7.5). Simulation tests are presented in Sections 7.6 and 7.7 to compare the performance of the proposed strategy against those achieved by the control strategies presented in [21] and [134], and analyze the performance of the proposed strategy considering a hybrid *ac/dc*-microgrid with multiple *ICs*, respectively.

## 7.2 Experimental Test #1: Load Steps

The structure of the system under study is shown in Fig. 7.1. In this test, load changes are applied to both sides of the hybrid *ac/dc*-microgrid in order to validate:

(i) the proposed DSC,

(ii) power-sharing among all DGs, and

(iii) bidirectional power flow through the *IC*.

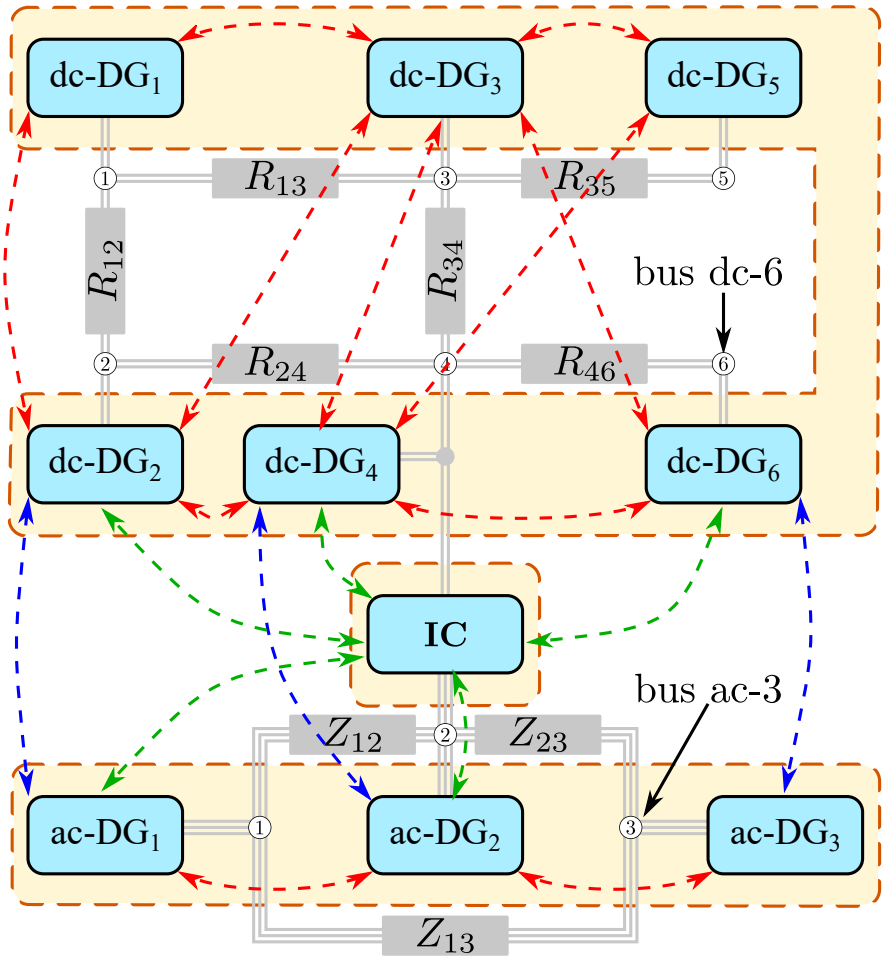


Figure 7.1: Topology of the hybrid *ac*/*dc*-microgrid under study.

For this test, the local load condition of the 9 DGs is summarized in Table 7.1, where the load steps applied are highlighted in black. The total load of the hybrid *ac*/*dc*-microgrid is 15.3kW (9.6kW on *dc*-side and 5.7kW on *ac*-side) and 1.9kVAr, i.e., 63.75% of the nominal active power (24.0kW) and 21.1% of the nominal reactive power (9.0kVAr). The power on the *dc*-side is 64.0% of the nominal power of this side (15.0kW); meanwhile, the active power on the *ac*-side corresponds to 63.3% of 9.0kW. The results are shown in Fig. 7.2.

Table 7.1: Experimental *ac*/*dc*-microgrid, load conditions for test #1.

| | *dc*-side loads, in kW | | | | | | *ac*-side loads, in kVA | | |
|---|---|---|---|---|---|---|---|---|---|
| Time | $R_1$ | $R_2$ | $R_3$ | $R_4$ | $R_5$ | $R_6$ | $Z_1$ | $Z_2$ | $Z_3$ |
| $0s < t < 30s$ | 2.05 | 0.00 | 1.37 | 2.05 | 2.05 | 2.05 | 0.0+$j$0.8 | 2.4+$j$0.0 | 3.3+$j$1.1 |
| $30s < t < 60s$ | 2.05 | **2.05** | 1.37 | 2.05 | 2.05 | 2.05 | 0.0+$j$0.8 | 2.4+$j$0.0 | **1.8+$j$0.0** |
| $60s < t < 90s$ | 2.05 | 0.00 | 1.37 | 2.05 | 2.05 | 2.05 | 0.0+$j$0.8 | 2.4+$j$0.0 | 3.3+$j$1.1 |
| $90s < t < 120s$ | 2.05 | 0.00 | 1.37 | 2.05 | **0.00** | 2.05 | **1.7+$j$0.8** | 2.4+$j$0.0 | 3.3+$j$1.1 |
| $120s < t < 150s$ | 2.05 | 0.00 | 1.37 | 2.05 | 2.05 | 2.05 | 0.0+$j$0.8 | 2.4+$j$0.0 | 3.3+$j$1.1 |

Because the secondary control loop is enabled, both *ac*-DGs and *dc*-DGs share almost perfectly the per unit (p.u.) power generated. The p.u. active powers of the nine DGs

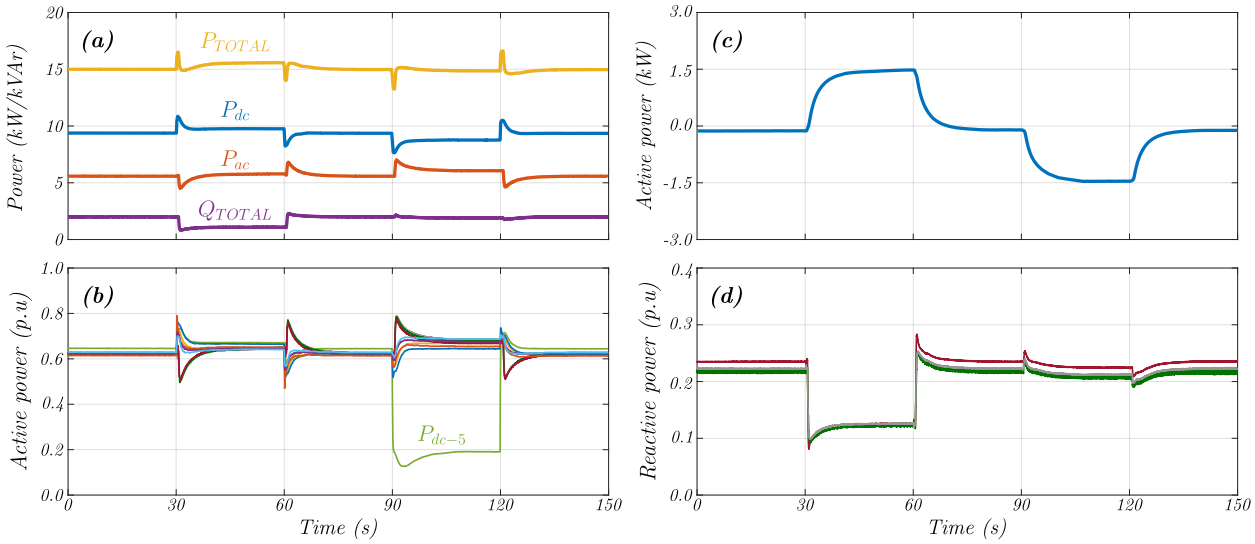


Figure 7.2: Power in the hybrid *ac*/*dc*-microgrid for Test #1. (a) Total power (active and reactive). (b) Active power generated by *ac*-DGs ($P_{\text{ac}-\text{i}}, \text{i} = 1, 2, 3$) and *dc*-DGs ($P_{\text{dc}-j}, j = 1, \ldots, 6$), in p.u. (c) Active power through the *IC* ($P_{\text{IC}}$). (d) Reactive power generated by *ac*-DGs ($Q_{\text{ac}-\text{i}}, \text{i} = 1, 2, 3$), in p.u.

are shown in Fig. 7.2b. As it is well known, the sharing of active power in the *dc*-side is compromised by the voltage regulation [see (3.9b)]. However, for $t < 30s$, the power-sharing of each *dc*-DG is still very good, with values between 0.646p.u. (*dc*-$\text{DG}_5$) and 0.615p.u. (*dc*-$\text{DG}_2$) and a total average (*dc*-side) of 0.628p.u. On the *ac*-side, the sharing of active power is almost perfect [see (3.4b)] with a value of about 0.624p.u. in each DG.

The power transferred through the *IC* is shown in Fig. 7.2c. For $t < 30$ the active powers (in p.u.) on two sides of the microgrid are almost identical (64.0% *dc* and 63.3% *ac*). Therefore, the power transferred through the *IC* is negligible [see Fig. 7.2c]. The reactive power-sharing on the *ac*-side is shown in Fig. 7.2d. In this case, there is a compromise between voltage regulation and reactive power-sharing [see (3.5b)]. The maximum reactive power corresponds to that of *ac*-$\text{DG}_1$ (for the whole test); meanwhile, *ac*-$\text{DG}_2$ and *ac*-$\text{DG}_3$ have almost equal values of normalized reactive power-sharing.

Secondary variables of the hybrid *ac*/*dc*-microgrid are shown in Fig. 7.3. It is concluded that the three secondary variables, i.e., the *dc*-voltage [see Fig. 7.3a], the *ac*-voltage [see Fig. 7.3b] and the frequency [see Fig. 7.3c] are maintained within the tolerance bands shown in black dashed lines (allowable range for the voltages is $V_{nom} \pm 5\%$ and for the frequency is $f_{nom} \pm 2\%$). For $t < 30s$ the lowest dc output voltage corresponds to *dc*-$\text{DG}_5$ and the highest corresponds to *dc*-$\text{DG}_2$ (no load is connected to the output of *dc*-$\text{DG}_2$).

At $t = 30s$ a load change is applied on both the *ac*-side and the *dc*-side. The load at node 2 on the *dc*-side is increased to 2.05kW, while the load at node 3 on the *ac*-side is decreased to $1.8 + j0.0$kVA. In this case, the p.u. load on the *dc*-side is higher than that on the *ac*-side. This is reflected in the power flow through the *IC*, as shown in Fig. 7.2c. For $30s < t < 60s$, the active power transferred through the *IC* is $P^*_{\text{IC}} = 1.5$kW (the reactive power-sharing does not change). At $t = 60s$, the initial loading condition is resumed, i.e., $P^*_{\text{IC}} \approx 0$kW.

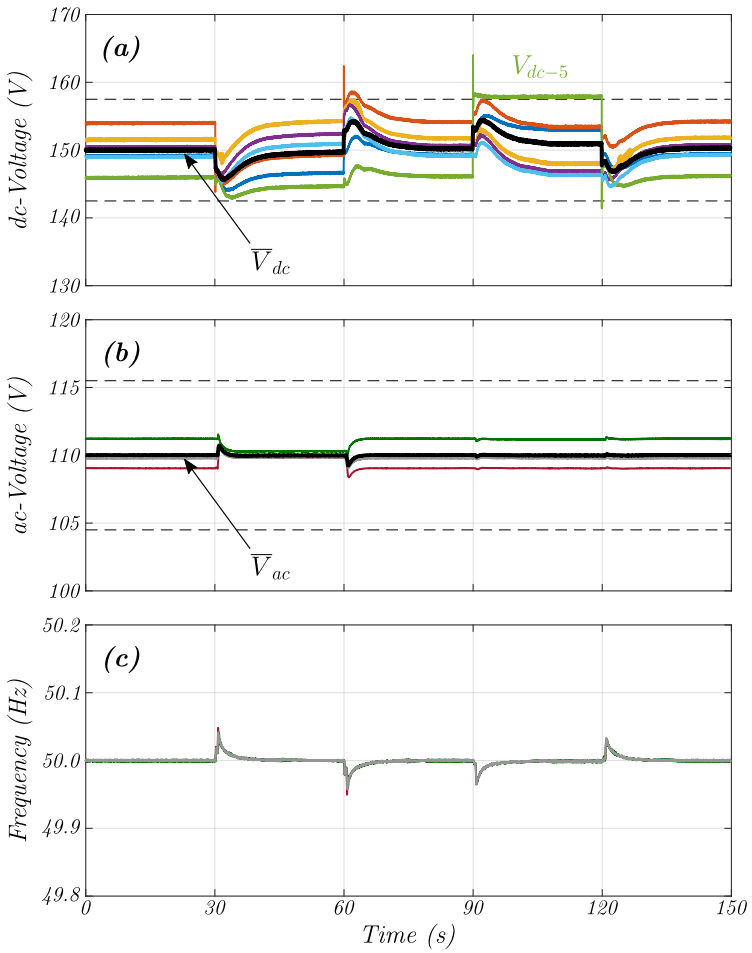


Figure 7.3: Variables of the secondary control on the hybrid $ac/dc$-microgrid for Test #1. (a) Voltages on the $dc$-DGs ($V_j, j = 1, \ldots, 6$). (b) Phase-to-neutral RMS voltages on the $ac$-DGs ($V_{\rm i}, {\rm i} = 1, 2, 3$). (c) Frequency of the voltages on the $ac$-DGs ($f_{\rm i}, {\rm i} = 1, 2, 3$).

At $t = 90s$, a new load change is applied on both $ac$- and $dc$-sides. The load at node 5 ($dc$-side) is step-decreased to 0.00kW, while the load at node 1 ($ac$-side) is step-increased to $1.7 + j0.8$kVA. Now, the percentage of $ac$-load is higher than that on the $dc$-side [see Fig. 7.2.(c)]. Therefore, for $90s < t < 120s$, $P^*_{\rm IC} = -1.5$kW and the reactive power-sharing on the $ac$-side does not change [see Fig. 7.2d].

It is important to note that, for $90s < t < 120s$, the $dc$-DG$_5$ [green line in Fig. 7.2b] is not participating in the power-sharing. In this time period, the load $R_5$ is disconnected from node 5 on the $dc$-microgrid (see Fig. 5.8). Therefore, a high voltage is obtained at the $dc$-DG$_5$ output, when (3.9a)-(3.9b) are applied. Hence, it is not possible for this DG to participate in the power-sharing without surpassing the $dc$-voltage upper limit [see Fig. 7.3a]. This problem can be solved using the tertiary control system by, for instance, changing the value of $V^*$ for all or some of the $dc$-DGs [see (3.9a)-(3.9b)]. However, tertiary control system is outside the scope of this thesis.

Finally, at $t = 120s$ the loads are step-changed back to the initial condition until the end of the test ($t = 150s$), i.e., $P^*_{\rm IC} \approx 0$kW, and all DGs participate in power-sharing.

## 7.3 Experimental Test #2: Unit Loss

In this test, the DGs on both sides of the hybrid microgrid and the *IC* are disconnected and then reconnected to test the plug-and-play capability of the proposed strategy. For this test, the load condition is summarized in Table 7.2 and it is not changed during the test. The total load of the hybrid *ac*/*dc*-microgrid is 16.5kW (9.6kW on *dc*-side and 6.9kW on *ac*-side) and 1.9kVAr, which represents 68.8% of the nominal active power (24.0kW) and 21.1% of the nominal reactive power (9.0kVAr), as shown in Fig. 7.4a. The power on the *dc*-side corresponds to 64.0% of the nominal power of this side (15.0kW), while the active power on the *ac*-side is 76.7% of the nominal power of this side (9.0kW).

Table 7.2: Experimental *ac*/*dc*-microgrid, load conditions for test #2.

| *dc*-side loads, in kW | | | | | | *ac*-side loads, in kVA | | |
|---|---|---|---|---|---|---|---|---|
| $R_1$ | $R_2$ | $R_3$ | $R_4$ | $R_5$ | $R_6$ | $Z_1$ | $Z_2$ | $Z_3$ |
| 2.05 | 0.00 | 1.37 | 2.05 | 2.05 | 2.05 | 2.2+$j$1.1 | 2.4+$j$0.0 | 2.3+$j$0.8 |

At $t = 0s$, both *ac*-DGs and *dc*-DGs are perfectly sharing the load power [see Fig. 7.4b]. Because the p.u. load on the *ac*-side is larger than that on the *dc*-side, the power flow in the *IC* is negative ($P^*_{\text{IC}} \approx -0.8$kW), as shown in Fig. 7.4c. The reactive power-sharing on the *ac*-side is shown in Fig. 7.4d. On the other hand, secondary variables of the hybrid *ac*/*dc*-microgrid are shown in Fig. 7.5. The secondary variables, i.e., *dc*-voltage [Fig. 7.5a], *ac*-voltage [Fig. 7.5b] and frequency [Fig. 7.5c] are maintained within the accepted limits.

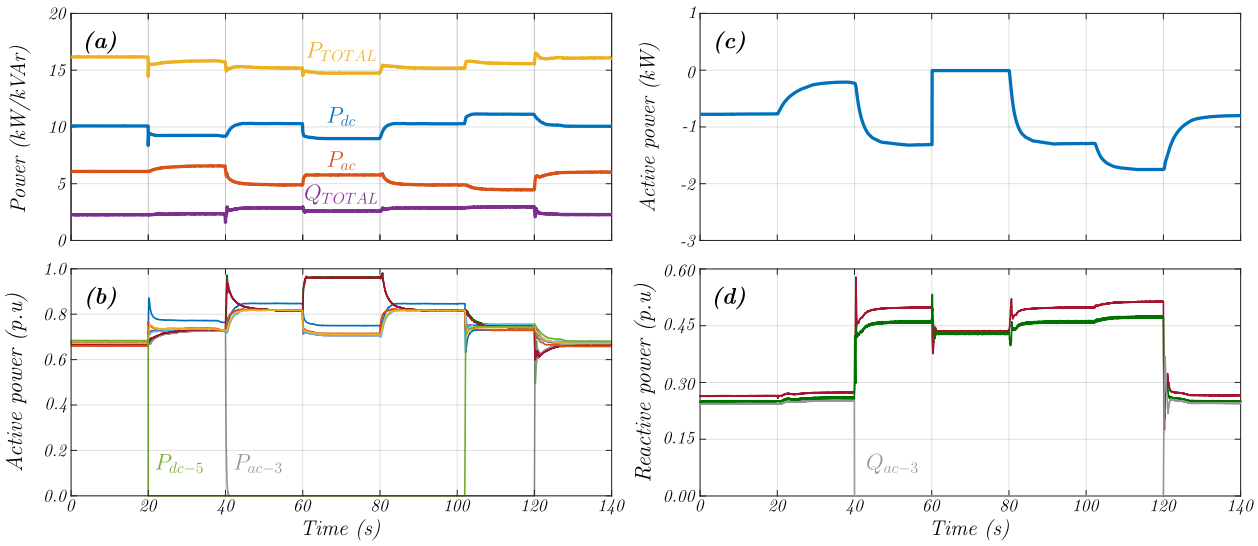


Figure 7.4: Power on the hybrid *ac*/*dc*-microgrid for Test #2. (a) Total power (active and reactive). (b) Active power generated by *ac*-DGs ($P_{\text{ac}-\text{i}}, \text{i} = 1, 2, 3$) and *dc*-DGs ($P_{\text{dc}-j}, j = 1, \ldots, 6$), in p.u. (c) Active power through the *IC* ($P_{\text{IC}}$). (d) Reactive power generated by *ac*-DGs ($Q_{\text{i}}, \text{i} = 1, 2, 3$), in p.u.

At $t = 20s$, *dc*-DG$_5$ fails and it is disconnected from both the microgrid and the communication network, and its power and voltage are reduced to zero (see green line in Fig. 7.4b and Fig. 7.5a, respectively) and the other *dc*-DGs and *ac*-DGs maintain power-sharing and restoration of the secondary variables, as shown in Fig. 7.4b, Fig. 7.4d and Fig. 7.5. Due to

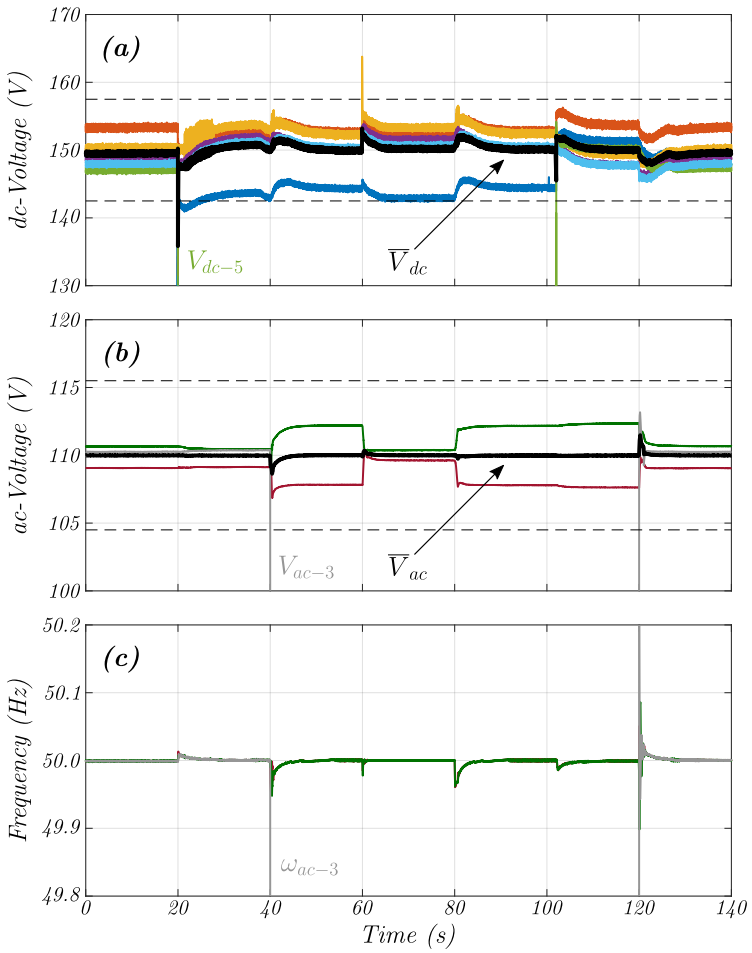


Figure 7.5: Variables of the secondary control on the hybrid *ac*/*dc*-microgrid for Test #2. (a) Voltages on the *dc*-DGs ($V_j, j = 1, \ldots, 6$). (b) Phase-to-neutral RMS voltages on the *ac*-DGs ($V_{\mathrm{i}}, \mathrm{i} = 1, 2, 3$). (c) Frequency of the voltages on the *ac*-DGs ($f_{\mathrm{i}}, \mathrm{i} = 1, 2, 3$).

the absence of *dc*-DG$_5$, the power transferred from the *dc*-side to the *ac*-side is reduced, as shown in Fig. 7.4c.

At $t = 40s$, *ac*-DG$_3$ fails and it is disconnected from both the microgrid and the communication network, and its power, voltage and frequency are all reduced to zero (see grey line in Fig. 7.4b, Fig. 7.4d, Fig. 7.5b and Fig. 7.5c, respectively) and the remaining *dc*-DGs and *ac*-DGs maintain power-sharing and restoration of the secondary variables, as shown in Fig. 7.4b, Fig. 7.4d and Fig. 7.5. Now, the absence of *ac*-DG$_3$ produces an increase in the power transferred from the *dc*-side to the *ac*-side, as shown in Fig. 7.4c.

At $t = 60s$, the *IC* fails and it is disconnected from both the microgrid and the communication network, and its power is reduced to zero [see Fig. 7.4c]. This splits the hybrid microgrid into two independent systems; therefore, the power-sharing is now performed only among the units in the same sub-microgrid, as shown in Fig. 7.4b. Because the p.u. load on the *ac*-side is higher than that on the *dc*-side, the p.u. powers generated by the *ac*-DGs are larger than those generated by the *dc*-DGs. On the other hand, the secondary variables are maintained within the operational limits all the time (see Fig. 7.5).

Finally, the failed units are reconnected to resume normal operation. The *IC* is reconnected at $t = 80s$, while *dc*-DG$_5$ is reconnected at $t = 100s$ and *ac*-DG$_3$ at $t = 120s$. The microgrid continues operating as expected after each re-connection, maintaining both power-sharing and regulation of the secondary variables.

## 7.4 Experimental Test #3: Communication Loss

In this test, the base case corresponds to the scenario where all units are connected to the communication network, as described in Fig. 7.6a. The base load condition is $6.0kW$ for the *ac*-microgrid (66.6% of its nominal power) and $9.6kW$ for the *dc*-microgrid (64.0% of its nominal power), as shown in Table 7.3. For emulating the loss of communication links between DGs, units *ac*-DG$_1$ and *dc*-DG$_2$ are disconnected from the communication network at $t = 40s$ (see Fig. 7.6b), and then re-connected to the communication network at $t = 240s$ (see Fig. 7.6a). The other DGs remain communicating for all the test.

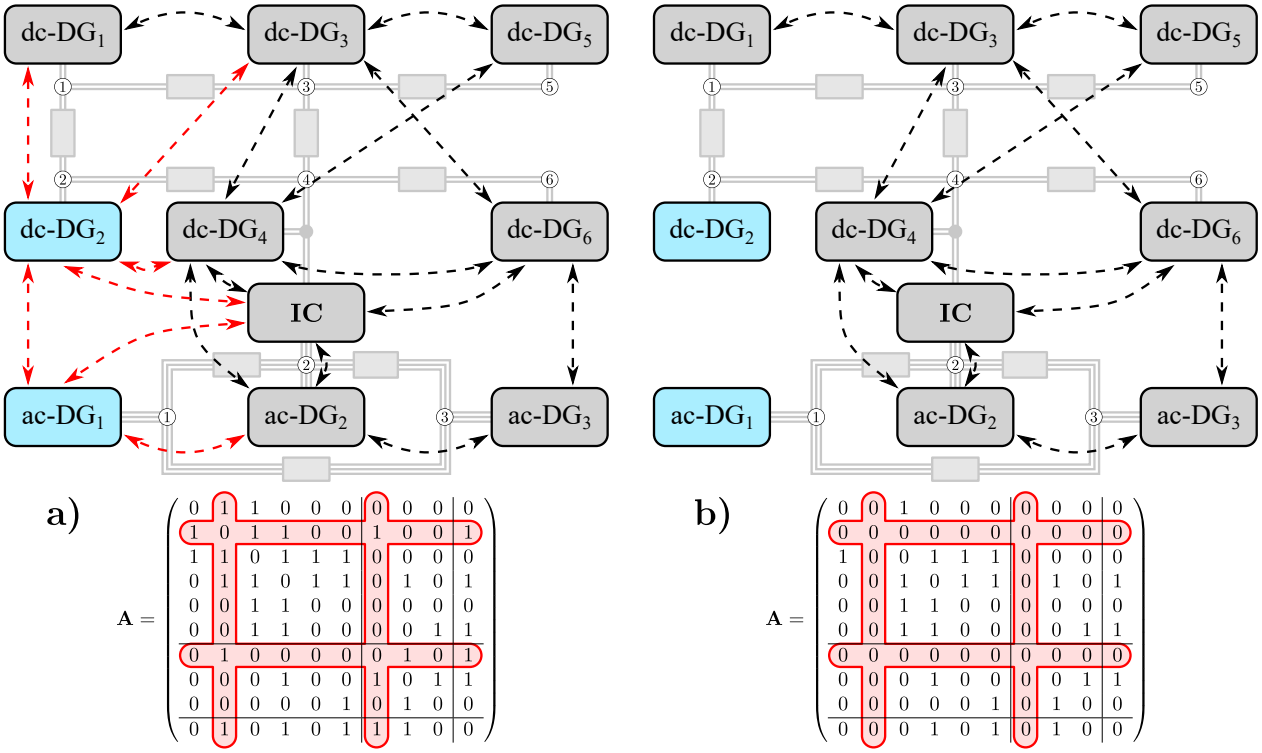


Figure 7.6: Communication network for test #3. a) Normal operation. b) Communication loss operation.

Table 7.3: Experimental *ac*/*dc*-microgrid, load conditions for test #3.

| Load | $kW$ | Load | $kW$ | Load | $kVA$ |
|---|---|---|---|---|---|
| $R_1$ | 2.05 | $R_4$ | 2.05 | $Z_1$ | $2.5 + j1.2$ |
| $R_2$ | 0.00 | $R_5$ | 2.05 | $Z_2$ | $2.4 + j0.0$ |
| $R_3$ | 1.37 | $R_6$ | 2.05 | $Z_3$ | $1.1 + j0.0$ |

The total power generated in this test is shown in 7.7a. The test begins with all the control loops activated; therefore, all the DGs are sharing both the active and reactive power, as

shown in Fig. 7.7b and Fig. 7.7d, respectively. As the load (in p.u.) on the *ac*-side is different from that of the *dc*-side, there is a transfer of power through the *IC*, as shown in Fig. 7.7c.

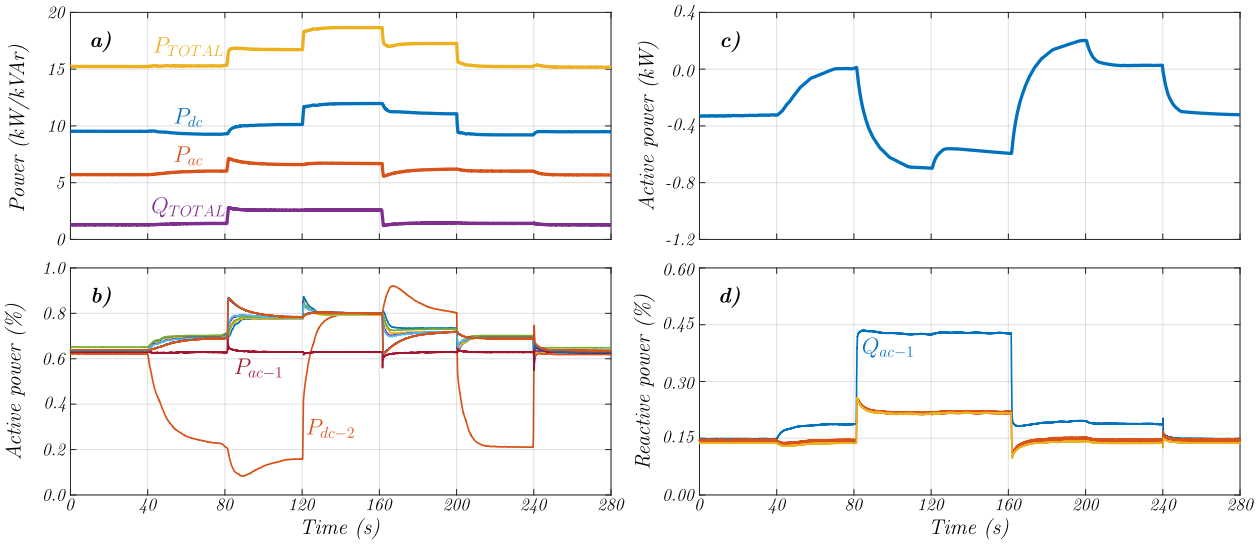


Figure 7.7: Power on the hybrid *ac*/*dc*-microgrid for Test #3. (a) Total power (active and reactive). (b) Active power generated by *ac*-DGs ($P_{\text{ac}-\text{i}}, \text{i} = 1, 2, 3$) and *dc*-DGs ($P_{\text{dc}-j}, j = 1, \ldots, 6$), in p.u. (c) Active power through the *IC* ($P_{\text{IC}}$). (d) Reactive power generated by *ac*-DGs ($Q_{\text{i}}, \text{i} = 1, 2, 3$), in p.u.

As mentioned before, in $t = 40s$ units *ac*-DG$_1$ and *dc*-DG$_2$ are disconnected from the communication network. Therefore, the disconnected units stop performing power-consensus with the other units and the distributed controllers only take care of the local variables regulation. Since the frequency is a global variable on the *ac*-side, *ac*-DG$_1$ continues supplying the same amount of power, while *dc*-DG$_2$ harshly reduces the generated power (see Fig. 7.7b) due to now it focuses on regulating the local *dc*-voltage. Results for the secondary variables are shown in Fig. 7.8. The power transferred by the *IC* also changes when the units disconnected from the communication network stop performing power-consensus, as shown in Fig. 7.7c.

Several load steps are applied on both sides of the hybrid microgrid, as follows:

- $t = \ \ 80s$ : load power in the *ac*-microgrid is increased to $8.4kW$ (93.3%).
- $t = 120s$ : load power in the *dc*-microgrid is increased to $11.65kW$ (77.3%).
- $t = 160s$ : load power in the *ac*-microgrid is decreased to $6.0kW$ (66.6%).
- $t = 200s$ : load power in the *dc*-microgrid is decreased to $9.6kW$ (64.0%).

In all cases, the units connected to the communication network continue performing the power-consensus task, while the disconnected units only regulate their local variables. The *IC* continues transferring power between the sub-microgrids, helping to the *ac*-DGs to reach the power-consensus with the *dc*-DGs, and vice versa.

As soon as the units *ac*-DG$_1$ and *dc*-DG$_2$ are re-connected to the communication network,

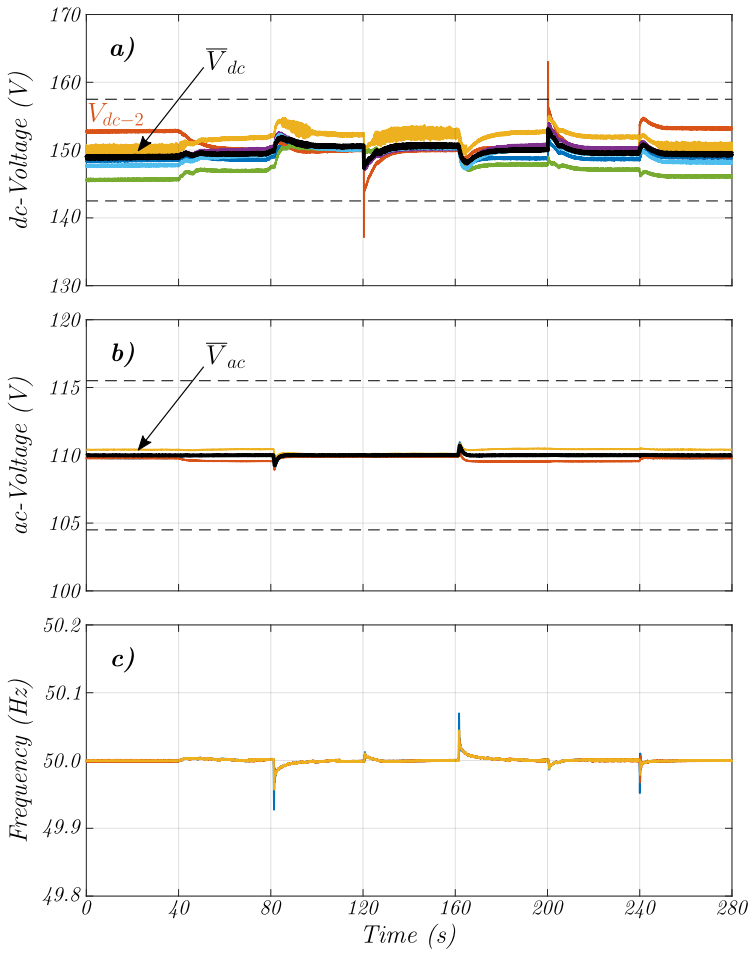


Figure 7.8: Variables of the secondary control on the hybrid *ac*/*dc*-microgrid for Test #3. (a) Voltages on the *dc*-DGs ($V_j, j = 1, \ldots, 6$). (b) Phase-to-neutral RMS voltages on the *ac*-DGs ($V_{\mathrm{i}}, \mathrm{i} = 1, 2, 3$). (c) Frequency of the voltages on the *ac*-DGs ($f_{\mathrm{i}}, \mathrm{i} = 1, 2, 3$).

at $t = 240s$, they start participating in the power consensus and they continue performing the secondary variable regulation. Therefore, the proposed control strategy is validated against communication loss issues.

## 7.5 Experimental Test #4: Communication Delays

In this test, a constant delay $\tau_{\mathrm{d}}$ is introduced in the consensus terms of the controllers for analyzing the performance of the controller against communication delays, as shown in (7.1)-(7.4). Different delays are considered in this test, which are considered as short-delay, medium delay and long delay. A delay of one second is considered to be a large delay, as described in [107, 108]; such a delay may be due to weather conditions or line of sight requirements in rural/remote areas [141]. The tested cases are:

(i) base case ($\tau_{\mathrm{d}} = 0.0s$),

(ii) small time-delay ($\tau_{\mathrm{d}} = 0.1s$),

(iii) medium time-delay ($\tau_{\rm d} = 0.5s$), and

(iv) large time-delay ($\tau_{\rm d} = 1.0s$).

$$\sigma_{\rm i}\dot{\psi}_{\rm i} = -\left(\omega_{\rm i} - \omega^*\right) + \psi_{\rm ac-i} + \psi_{\rm dc-i} \tag{7.1a}$$

$$\psi_{\rm ac-i} = -\sum\nolimits_{j\in\mathbb{N}_{\rm ac}} a_{{\rm i}j}\left(P_{\rm ac-i} - P_{{\rm ac}-j}(t-\tau_{\rm d})\right) \tag{7.1b}$$

$$\psi_{\rm dc-i} = -\sum\nolimits_{j\in\mathbb{N}_{\rm dc}} a_{{\rm i}j}\left(P_{\rm ac-i} - P_{{\rm dc}-j}(t-\tau_{\rm d})\right) \tag{7.1c}$$

$$\rho_{\rm i}\dot{\varphi}_{\rm i} = -\gamma_{\rm i}\left(V_{\rm i} - V^*\right) + \varphi_{\rm dc-i} + \varphi_{\rm ac-i} \tag{7.2a}$$

$$\varphi_{\rm dc-i} = -c_{\rm i}\sum\nolimits_{j\in\mathbb{N}_{\rm dc}} a_{{\rm i}j}\left(P_{\rm dc-i} - P_{{\rm dc}-j}(t-\tau_{\rm d})\right) \tag{7.2b}$$

$$\varphi_{\rm ac-i} = -c_{\rm i}\sum\nolimits_{j\in\mathbb{N}_{\rm ac}} a_{{\rm i}j}\left(P_{\rm dc-i} - P_{{\rm ac}-j}(t-\tau_{\rm d})\right) \tag{7.2c}$$

$$\tau_k\dot{P}^*_{{\rm IC}-k} = -\sum_{{\rm i}\in\mathbb{N}_{\rm ac}}\sum_{j\in\mathbb{N}_{\rm dc}} a_{{\rm i}k}a_{jk}\left(P_{\rm ac-i} - P_{{\rm dc}-j}(t-\tau_{\rm d})\right) \tag{7.3}$$

$$\varrho_{\rm i}\dot{\chi}_{\rm i} = -\beta_{\rm i}\left(E_{\rm i} - E^*\right) - b_{\rm i}\sum\nolimits_{j\in\mathbb{N}_{\rm ac}} a_{{\rm i}j}\left(Q_{\rm i} - Q_j(t-\tau_{\rm d})\right) \tag{7.4}$$

The base load condition is $5.9kW$ for the *ac*-microgrid (65.5% of its nominal power) and $11.6kW$ for the *dc*-microgrid (77.3% of its nominal power), as shown in Table 7.4.

Table 7.4: Experimental *ac*/*dc*-microgrid, load conditions for test #4.

| Load | $kW$ | Load | $kW$ | Load | $kVA$ |
|---|---|---|---|---|---|
| $R_1$ | 2.05 | $R_4$ | 2.05 | $Z_1$ | $1.7 + j0.0$ |
| $R_2$ | 2.05 | $R_5$ | 2.05 | $Z_2$ | $2.4 + j0.0$ |
| $R_3$ | 1.37 | $R_6$ | 2.05 | $Z_3$ | $1.8 + j0.0$ |

At $t = 0$, since all the control loops are activated and the system is at steady-state, both *ac*-DGs and *dc*-DGs are sharing the load power for all the studied values of $\tau_{\rm d}$, as shown in Fig. 7.9a-d and Fig. 7.11a-d for active and reactive power, respectively, and the power is being transferred through the *IC* as shown in Fig.7.9e-h. On the other hand, the secondary variables are also regulated within limits for all the studied values of $\tau_{\rm d}$, as shown in Fig. 7.10a-d, Fig. 7.10e-h and Fig. 7.11e-h, for frequency, *dc*-voltage and *ac*-voltage, respectively.

A load step is applied in the *ac*-side between $t = 30s$ and $t = 60s$. At $t = 30s$, loads $Z_1$ and $Z_3$ are increased to $2.9 + j1.4kVA$ and $2.8 + j1.4kVA$, respectively. The initial power load condition is resumed at $t = 60s$, i.e., $Z_1 = 1.7 + j0.0kVA$ and $Z_3 = 1.8 + j0.0kVA$.

It can be seen that the control algorithm continues working correctly for all the studied values of $\tau_{\rm d}$: the power consensus is achieved (see Fig. 7.9a-d and Fig. 7.11a-d for active and reactive power, respectively) and the secondary variables are maintained within limits (see Fig. 7.10a-d, Fig. 7.10e-h and Fig. 7.11e-h, for frequency, *dc*-voltage and *ac*-voltage,

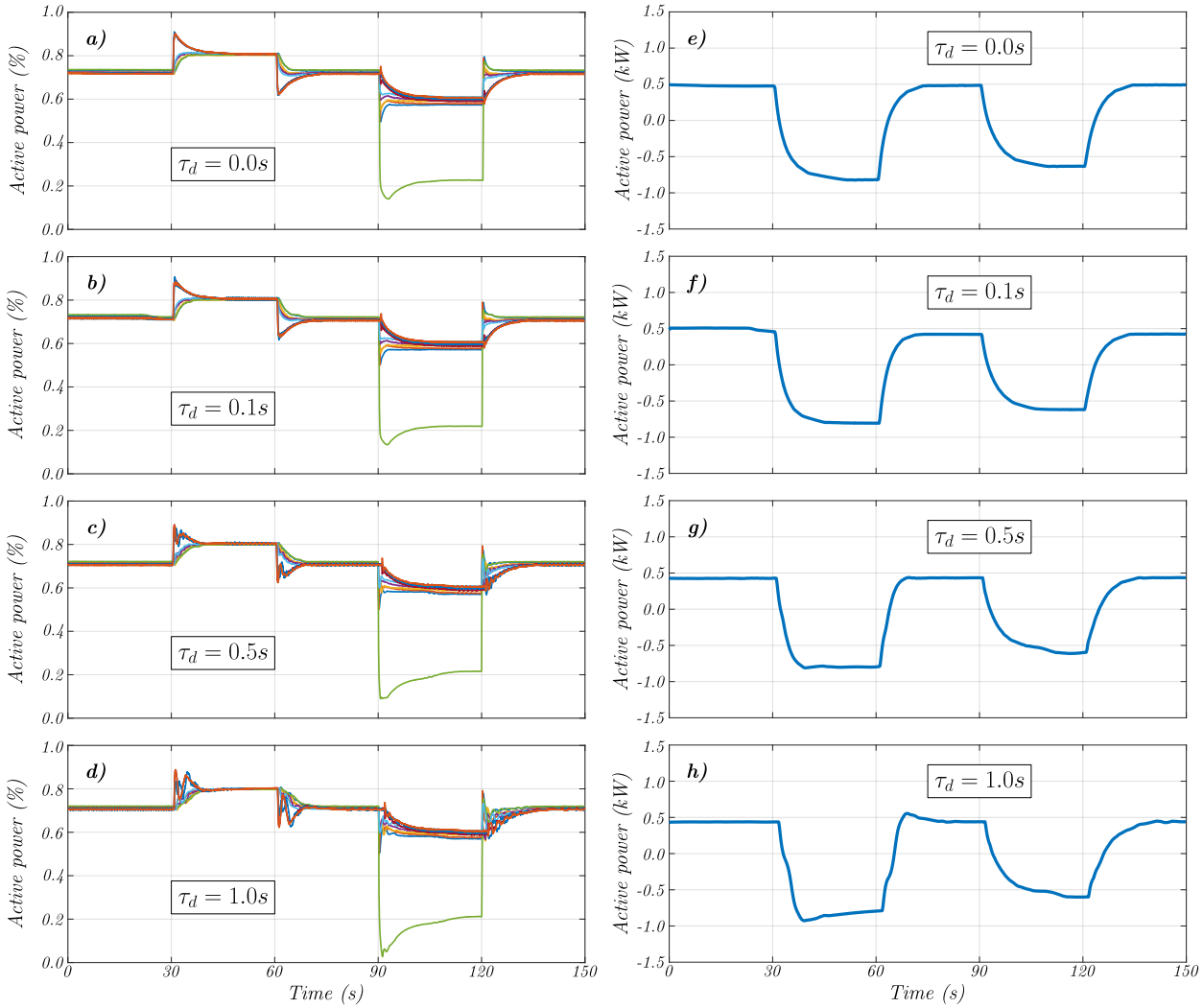


Figure 7.9: Test #4: (a-d) Active power generated by *ac*-DGs ($P_{\text{ac}-\text{i}}, \text{i} = 1, 2, 3$) and *dc*-DGs ($P_{\text{dc}-j}, j = 1, \ldots, 6$), in p.u. (e-h) Active power through the *IC* ($P_{\text{IC}}$).

respectively). On the other hand, the power transferred by the *IC* is adjusted to help maintaining the power consensus among DGs (see Fig.7.9e-h).

Between $t = 90s$ and $t = 120s$, a load step is applied in the *dc*-side. At $t = 90s$, loads $R_2$ and $R_5$ on the *dc*-side are disconnected. As discussed in test #1 (Section 7.2), *dc*-DG$_5$ is disconnected from the power-sharing controller when load $R_5$ is disconnected (see Fig. 7.9a-d), in order to maintain its voltage within limits. Then, the base load condition is resumed at $t = 120s$, i.e., $R_2 = 2.05kW$ and $R_5 = 2.05kW$. As in the previous case, the control algorithm continues working correctly for all the studied values of $\tau_{\text{d}}$.

It is worth noting that, even though the control algorithm reaches the steady-state condition after applying the load steps at both sides of the hybrid *ac*/*dc*-microgrid, the transient response becomes more oscillatory as the delay increases. Moreover, the overshoot of the transient response also becomes larger for long delays. Therefore, the proposed control scheme is able to handle communication issues as communication delays; however, special attention has to be given to the transient response in order to avoid surpassing the operational limits

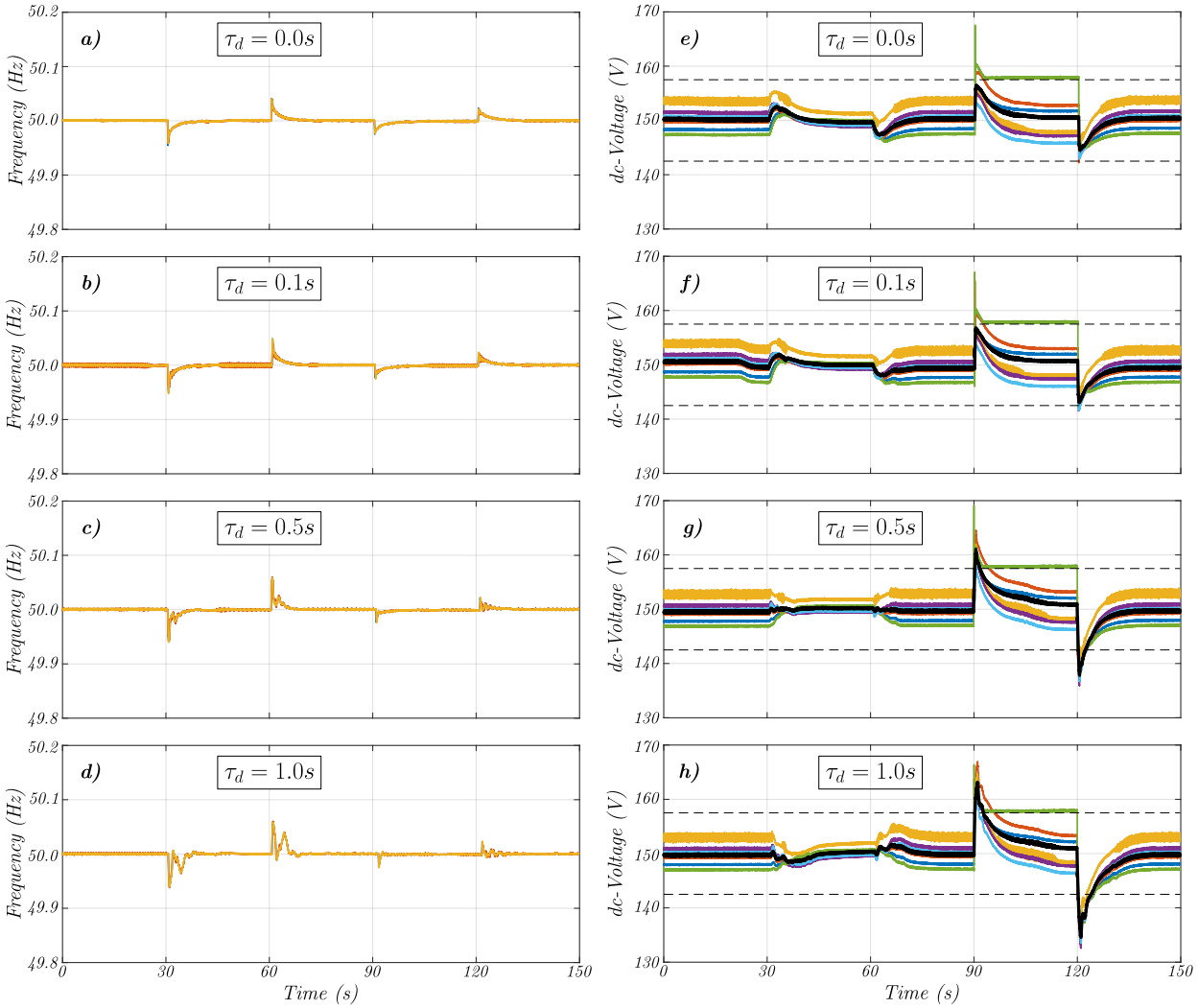


Figure 7.10: Test #4: (a-d) Frequency of the voltages on the *ac*-DGs ($f_{\mathrm{i}}, \mathrm{i} = 1, 2, 3$). (e-h) Voltages on the *dc*-DGs ($V_j, j = 1, \ldots, 6$).

of the DGs.

## 7.6 Simulation Test #5: Comparison With Performance of Other Strategies

As mentioned before, the performance of the proposed control strategy is compared to the performances obtained with strategies proposed in [21] and [134]. The strategies proposed in [21, 134] are based on normalized droop curves on both sides of the *IC* to generate the power reference for the *IC*, while the work in [134] also restores the secondary variables. Load impacts and plug-and-play capabilities are studied using simulation work. For further details about the parameters and the topology of the simulated microgrid see Section 5.5.

The results obtained using the control strategy presented in [21] are depicted in the left column of Fig. 7.12, while the results obtained with the strategy presented in [134] are shown in the central column of Fig. 7.12. The results obtained with the strategy proposed in this

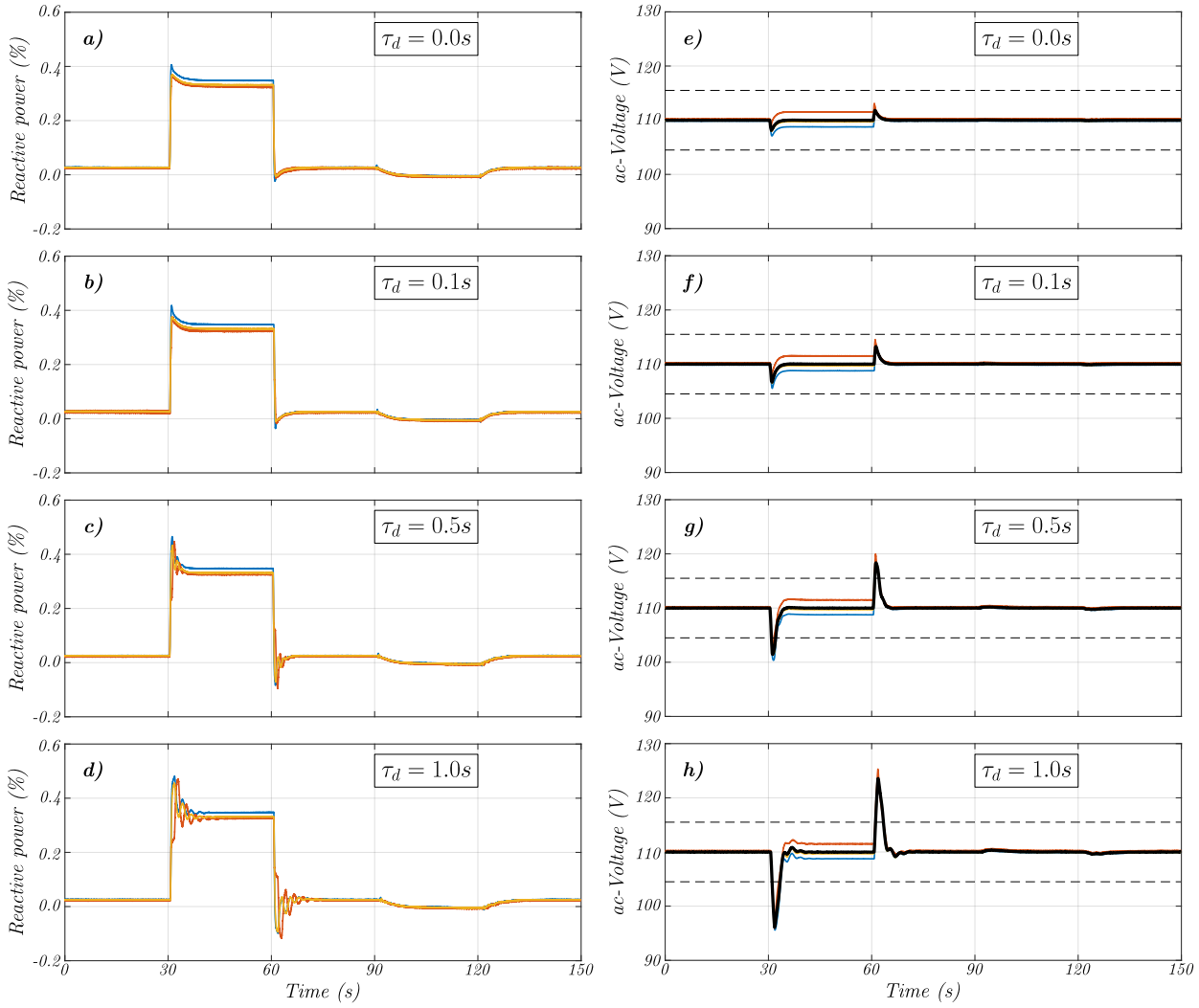


Figure 7.11: Test #4: (a-d) Reactive power generated by $ac$-DGs ($Q_{\mathrm{i}}, \mathrm{i} = 1, 2, 3$), in p.u. (e-h) Phase-to-neutral RMS voltages on the $ac$-DGs ($V_{\mathrm{i}}, \mathrm{i} = 1, 2, 3$).

work are illustrated in the right column of Fig. 7.12.

For simulation purposes, using strategies proposed in [21] and [134], each $ac$-DG and $dc$-DG is controlled using the strategies presented in Section 3.3 and Section 3.4, respectively. However, for [21] secondary control is not applied. Additionally, for [21] and [134] the elements of the adjacency matrix given in (5.1) are all zero since neither [21] nor [134] consider power consensus. On the other hand, the adjacency matrix used in the proposed strategy is shown in (5.1).

To check the effects produced by the connection and disconnection of the $IC$, it is disconnected from the microgrid in two periods of time, $35s < t < 75s$ and $115s < t < 155s$. Additionally, there are three load power scenarios in this test:

- $P_{\mathrm{dc}} < P_{ac}$ : $15s < t < 55s$
- $P_{\mathrm{dc}} > P_{ac}$ : $95s < t < 135s$

- $P_{\text{dc}} \approx P_{ac}$ : for the rest of the time

First, when the *IC* is controlled using the strategy presented in [21], the power-sharing is not achieved between DGs located on different sides of the hybrid *ac*/*dc*-microgrid, even when the *IC* is connected [see Fig. 7.12a], and the secondary variables are not restored [see Fig. 7.12c and (7.5)]. Therefore, the power transferred through the *IC* [see Fig. 7.12b] is not utilized to achieve sharing of the per unit power on both sides.

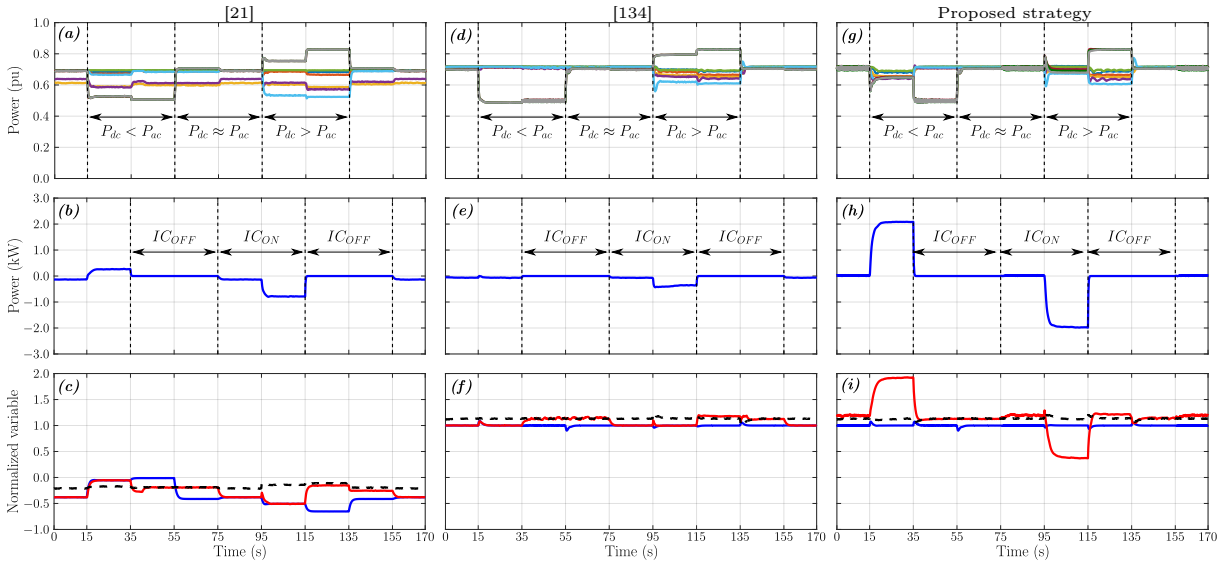


Figure 7.12: Test #5: *Top row:* Active power in p.u. generated by *ac*-DGs and *dc*-DGs. *Middle row:* Active power transferred by the *IC*. *Bottom row:* Normalized *dc*-voltage (in red) and normalized frequency (in blue) on both sides of the *IC*, the black dashed lines show the *normalized* average *dc*-voltage in the *dc*-microgrid.

Second, when the *IC* is controlled using the strategy proposed on [134], power-sharing is not achieved among DGs located on different sides of the hybrid *ac*/*dc*-microgrid [see Fig. 7.12d] although the secondary variables are restored to their nominal values [see Fig. 7.12(f)]. Furthermore, after the secondary variables are restored to their nominal values, the power transferred through the *IC* [see Fig. 7.12(e)] is negligible (the difference between the normalized values tends to be zero due to the secondary controllers).

Finally, if the *IC* is controlled using the strategy proposed in this work, it is capable of achieving good power-sharing among the *ac*- and *dc*-DGs [see Fig. 7.12(g)] while the *IC* is connected. If the *IC* is disconnected, the power-sharing is achieved within each sub-microgrid, dividing the controller into two independent sub-controllers. The *IC* and the proposed control system make it possible to achieve power-sharing between the *ac*-side and the *dc*-side, as shown in Fig. 7.12(h), while the secondary variables are well regulated [see Fig. 7.12(i)]. Although the normalized average voltage on the *dc*-side (see black dashed lines in the bottom row of Fig. 7.12) is not equal to the nominal value, the voltages are maintained within the operation limits due to the compromise between power consensus and voltage regulation.

The normalized frequencies ($f_{pu}$) and voltages ($V_{pu}$) shown in the bottom row of Fig. 7.12

are calculated using:

$$f_{\text{pu}}=\frac{f-\frac{1}{2}(f_{\max}+f_{\min})}{\frac{1}{2}(f_{\max}-f_{\min})},\ V_{\text{pu}}=\frac{V-\frac{1}{2}(V_{\max}+V_{\min})}{\frac{1}{2}(V_{\max}-V_{\min})}. \tag{7.5}$$

A summary of the comparison tests for strategies proposed in [21], [134] and the proposed strategy (P. S.) is shown in Table 7.5. By using [21], it is not possible to address the same control tasks that can be addressed by the proposed strategy. This is evident since [21] only equalizes the normalized *dc*-voltage and frequency at two ports of the *IC* without any secondary control strategy. Therefore, the *IC* only cares about its local variables and the power-sharing solely depends on the droop controls applied, which is a drawback when microgrids have a large number of buses. By using [134], the secondary control is applied restoring the secondary variables. However, the power consensus between *ac*- and *dc*-DGs is not achieved since the *IC* only equalizes its local normalized variables. In contrast, the proposed strategy restores secondary variables while achieving power consensus between *ac*- and *dc*-DGs. This power consensus is reached as long the *IC* is working, i.e., as long as the path for transferring energy exists.

Table 7.5: Comparison test summary.

| | [21] | [134] | P. S. |
|---|---|---|---|
| Power-consensus, *IC* working | ✗ | ✗ | ✓ |
| Frequency restoration | ✗ | ✓ | ✓ |
| *dc*-voltage restoration | ✗ | ✓ | ✓ |

## 7.7 Simulation Test #6: Multiple *ICs* Operation

In this subsection, the performance of the proposed control methodology is evaluated when three *ICs* and six DGs, on each side of the hybrid *ac*/*dc*-microgrid, are considered. The studied topology is shown in Fig. 7.13.

Two scenarios are analyzed. Firstly, the operation of the proposed controller presented in Section 3.5 is evaluated (left column in Fig. 7.14), i.e., power-consensus among *ICs* is not considered in this test. Secondly, the proposed control methodology presented in Section 3.6 (including power-consensus among *ICs*), is simulated with the results being shown in the right column of Fig. 7.14.

For $t < 10s$, the *ICs* are not connected to the hybrid *ac*/*dc*-microgrid, i.e., the *ac*-side is not connected to the *dc*-side and the power-sharing among DGs on both sides of the microgrid is not active. Note that for $t < 60s$, the load power on the *ac*-side is higher than the load power on the *dc*-side [see Fig. 7.14a&d]. At $t = 10s$, $IC_1$ is connected and active power is transferred from the *dc*-side to *ac*-side initiating power-consensus between the *ac*- and *dc*-DGs. In this case, the control system performance is similar for both scenarios, considering that a single *IC* is connected.

At $t = 20s$, $IC_2$ is connected. The power-consensus among *ac*- and *dc*-DGs is maintained but the power-consensus between $IC_1$ and $IC_2$ is not achieved in the first scenario, but

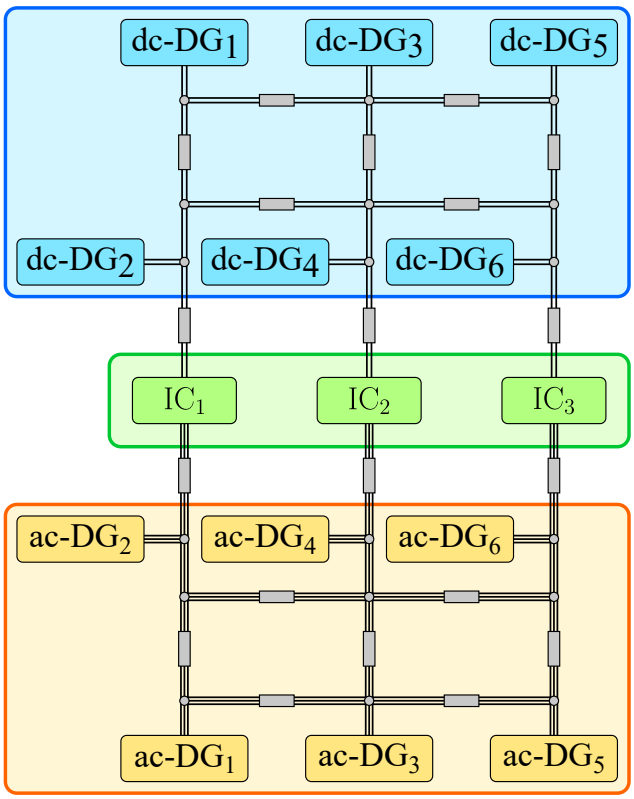


Figure 7.13: Test #6: Topology of the simulated microgrid.

it is achieved in the second one (see Fig. 7.14b&e. At $t = 30s$, $IC_3$ is activated and the same results in terms of power-sharing among the *ICs* are obtained. The power-consensus among *ICs* in the first scenario is not achieved because, when the *IC* is connected, the power-consensus among DGs on both sides has already been achieved. Therefore $P_{\text{IC}}{}^*$ is not modified for $IC_1$ (see (3.10)).

Then, $IC_1$, $IC_2$ and $IC_3$ are disconnected at $t = 40s$, $t = 50s$ and $t = 60s$, respectively. In both scenarios the power-consensus among DGs is maintained and the power-sharing among *ICs* is also achieved. In the first scenario, the latter is achieved because the parameters of the controllers are the same for each *IC*; otherwise power-sharing among *ICs* is not ensured. Finally, at $t = 70s$, a load impact is applied and the load power on the *dc*-side is higher than the load power on the *ac*-side. At $t = 80s$, all the *ICs* are connected at the same time and both power-consensuses are achieved. Note that, in both scenarios, the secondary variables are correctly regulated, as shown in Fig. 7.14c&f.

It is important to clarify that the proposed power consensus strategy for the *ICs* [see (3.12)] does not produce a circulating current/power between them. Therefore, it is not necessary to utilize auxiliary *ac* control signals as it is discussed in [82]. The methodology utilized to achieve power-consensus among the *ICs* eliminate any possible mismatch in the power flow transferred through the *ICs*.

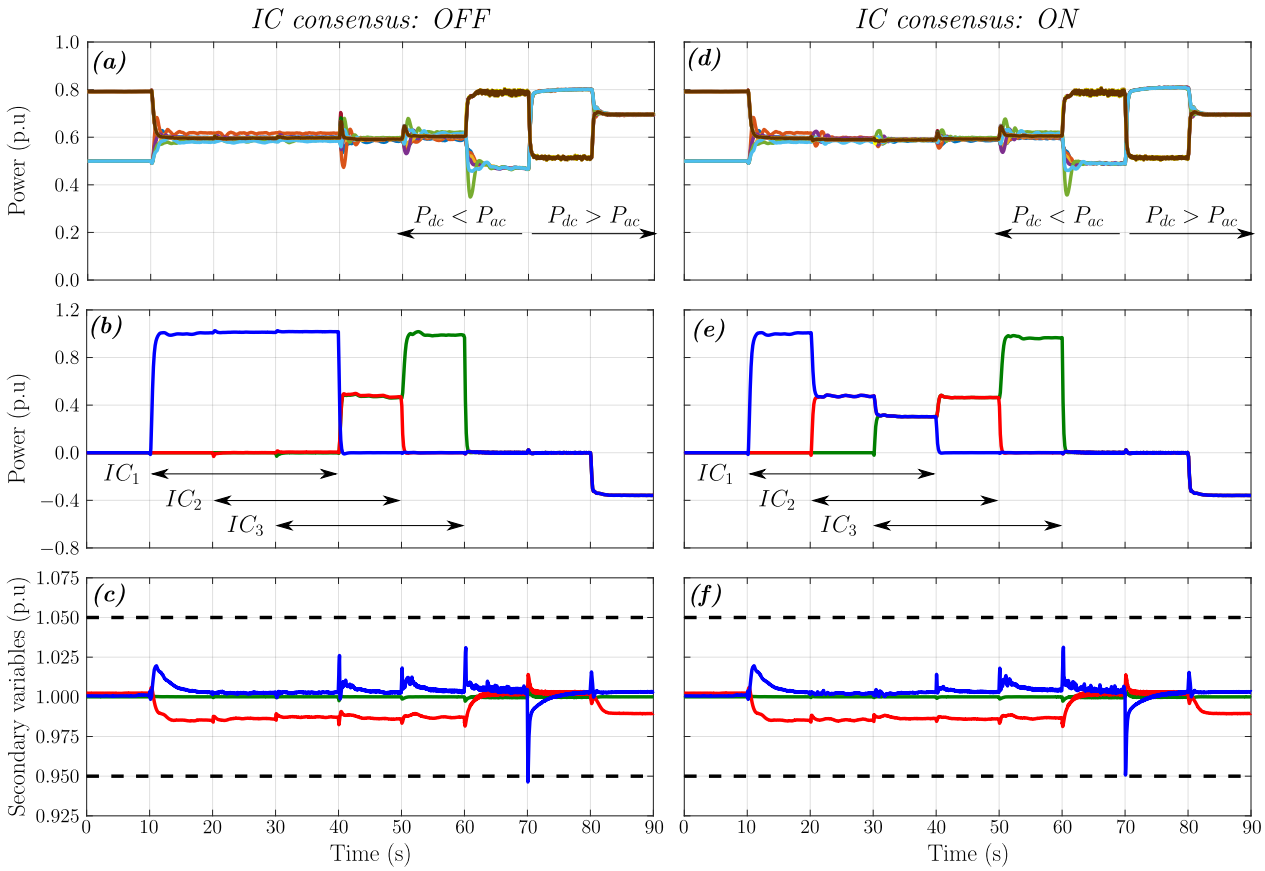


Figure 7.14: Test #6: (a)&(d) Active power in p.u. generated by the *ac*- and *dc*-DGs. (b)&(e) Active power in p.u. transferred through the *ICs*. (c)&(f) Secondary variables in per unit, *ac*-side frequency (green), *ac*-voltage (red) and *dc*-voltage (blue).

## 7.8 Summary

In this Chapter, experimental and simulation results were presented to validate the distributed consensus-based secondary control strategy for power-sharing proposed in this thesis. The experimental validation was performed on a $24kW$ scaled-down prototype of a hybrid *ac*/*dc*-microgrid, while the validation through simulation was performed in the same system and in a new one based on the experimental prototype.

In summary, the experimental and simulation results demonstrated the advantages of the proposed method, which are:

- Active power consensus is achieved among the *ac*-DGs and *dc*-DGs when a load impact is applied on either side of the hybrid *ac*/*dc*-microgrid and when a DG is connected/disconnected to/from the microgrid.
- The secondary control variables, i.e., average *dc*- and *ac*-voltages, and frequency, are restored to their nominal values in steady-state under all the analyzed cases.
- The *IC* participates actively in the proposed secondary control strategy, transferring power from the *dc*-side to the *ac*-side (or vice versa) according to the loading of the

sub-microgrids.

- The DGs can be easily connected to or disconnected from the microgrid as well as the distributed secondary control system, demonstrating the plug-and-play capability of the proposed strategy (see Test #2 results).

- The proposed scheme is able to handle some of the most common communication issues that can be found in a microgrid, such as the loss of communication channels or communication delays (see Test #3 and Test #4 results).

- Since the consensus-based control strategy proposed in this work considers the hybrid *ac/dc*-microgrid as a single entity, it behaviour is better than the ones reported in the literature that consider the hybrid *ac/dc*-microgrid as three independent systems which interact between them [21, 134] (see Test #5 results).

- By including the power-consensus term among the *ICs* it is possible to avoid unnecessary losses and saturation of the *ICs* due to the circulating currents (see Test #6 results).

# Chapter 8

# Validation of the Strategy Proposed for Operation Cost Minimization

## 8.1 Introduction

In this Chapter, simulation tests are performed for validating the consensus-based distributed control strategy for operation cost minimization proposed in Chapter 4. Two systems were simulated: the system described in Section 5 for testing the strategy proposed for a microgrid with a single $IC$, and a modified microgrid for evaluating the strategy proposed for a hybrid $ac/dc$-microgrid with multiple $ICs$.

The Chapter is organized as follows: Section 8.2 presents the validation of the control strategy for a hybrid $ac/dc$-microgrid with a single $IC$ proposed in Section 4.3; the cost function and the constraints defined in the formulation of the optimization problem are successfully analyzed. The performance of the aforementioned control strategy against load steps is validated in Section 8.3. Then, Section 8.4 shows the validation of the control strategy proposed for a microgrid with multiple $ICs$ proposed in Section 4.5; the cost function and the power limit constraints defined in the formulation of the optimization problem are successfully analyzed. The validation of the control strategy mentioned before against multiple load changes is presented in Section 8.5. Finally, a comparison between the two consensus-based distributed secondary control strategies proposed in this work is depicted in Section 8.6.

## 8.2 Simulation Test #7: Single *IC* Performance

First, the control strategy proposed for minimizing the operation cost in a microgrid with a single *IC* is analyzed (see Section 4.3). The microgrid presented in Chapter 5 is simulated, maintaining the parameters (Table 5.4) and communication network (adjacency matrix) (5.1) described in that Chapter. Due to the control strategy analyzed in this Chapter is focused on minimizing the operation cost of the hybrid *ac/dc*-microgrid, the parameters for the cost functions of the DGs [see (4.4)] are depicted in Table 8.1 (for the *ac*-DGs) and Table 8.2 (for the *dc*-DGs). On the other hand, the operation limits for the DGs are:

$$\begin{aligned} &\bullet\ P_{\mathrm{ac-i}}^{\mathrm{G-}} = 0.0kW, \qquad P_{\mathrm{ac-i}}^{\mathrm{G+}} = 3.0kW, \qquad \forall \mathrm{i} \in \mathbb{N}_{\mathrm{ac}} \\ &\bullet\ P_{\mathrm{dc-}j}^{\mathrm{G-}} = 0.0kW, \qquad P_{\mathrm{dc-}j}^{\mathrm{G+}} = 2.5kW, \qquad \forall j \in \mathbb{N}_{\mathrm{dc}} \end{aligned} \tag{8.1}$$

Table 8.1: Parameters for the cost functions of the *ac*-DGs [eq. (4.4a)].

| **Unit** | $\boldsymbol{a_{\mathrm{ac-i}}}$ | $\boldsymbol{b_{\mathrm{ac-i}}}$ | $\boldsymbol{c_{\mathrm{ac-i}}}$ |
|---|---|---|---|
| *ac*-DG$_1$ | 0.44 | 1.1 | 70 |
| *ac*-DG$_2$ | 0.49 | 2.1 | 60 |
| *ac*-DG$_3$ | 0.31 | 3.1 | 55 |

Table 8.2: Parameters for the cost functions of the *dc*-DGs [eq. (4.4b)].

| **Unit** | $\boldsymbol{a_{\mathrm{dc-}j}}$ | $\boldsymbol{b_{\mathrm{dc-}j}}$ | $\boldsymbol{c_{\mathrm{dc-}j}}$ | **Unit** | $\boldsymbol{a_{\mathrm{dc-}j}}$ | $\boldsymbol{b_{\mathrm{dc-}j}}$ | $\boldsymbol{c_{\mathrm{dc-}j}}$ |
|---|---|---|---|---|---|---|---|
| *dc*-DG$_1$ | 0.28 | 2.6 | 57 | *dc*-DG$_4$ | 0.51 | 2.8 | 68 |
| *dc*-DG$_2$ | 0.39 | 1.8 | 64 | *dc*-DG$_5$ | 0.21 | 3.3 | 61 |
| *dc*-DG$_3$ | 0.46 | 1.2 | 58 | *dc*-DG$_6$ | 0.79 | 0.9 | 62 |

The losses in the *IC* are assumed by $k^{\mathrm{LOSS}} = 4\%$ (see Section 4.2.1), and its operation limits are given by (8.2). For simplicity, losses are assumed constant for the entire operating range.

$$\bullet\ P_{\mathrm{IC}}^{\mathrm{ac-}} = -2.0kW, \qquad P_{\mathrm{IC}}^{\mathrm{ac+}} = 2.0kW \tag{8.2}$$

The local-load of the 9 DGs remains constant during this test, and it is summarized in Table 8.3. The total load of the hybrid *ac/dc*-microgrid is 18.48kW (9.55kW on *dc*-side and 8.93kW on *ac*-side) and 1.9kVAr, i.e., 77% of the nominal active power (24.0kW) and 21.1% of the nominal reactive power (9.0kVAr). The power on the *dc*-side is 63.7% of the nominal power of this side (15.0kW); meanwhile, the active power on the *ac*-side corresponds to 99.2% of 9.0kW. The operating conditions analyzed in this test are summarized in Table 8.4, and the results are shown in Fig. 8.1 and Fig. 8.2.

Table 8.3: Hybrid *ac/dc*-microgrid with a single *IC*, load conditions for test #7.

| Load | $kW$ | Load | $kW$ | Load | $kVA$ |
|---|---|---|---|---|---|
| $R_1$ | 2.05 | $R_4$ | 1.03 | $Z_1$ | $2.22 + j0.8$ |
| $R_2$ | 2.05 | $R_5$ | 1.02 | $Z_2$ | $4.07 + j0.0$ |
| $R_3$ | 1.37 | $R_6$ | 2.05 | $Z_3$ | $2.64 + j1.1$ |

Table 8.4: Summary for the operating conditions analyzed in simulation test #7.

| **Operating condition** | **Time** |
|---|---|
| No optimization | 0s - 100s |
| Optimization within microgrids | 100s - 200s |
| Full optimization enabled | 200s - 300s |
| *ac*-DGs limits constraint active | 300s - 400s |
| *dc*-DGs limits constraint active | 400s - 500s |
| *IC* limits constraint active | 500s - 600s |

The simulation starts with the inner, primary and secondary controllers enabled. Regarding the distributed secondary control loop, only the terms responsible for the secondary variables restoration are not equal to zero, i.e., the optimization is not enabled; thus, the parameters for the controllers under the *no optimization* condition are:

$$\begin{aligned} &\bullet \text{ In (4.13b)}: \quad k^a_{\text{ac}-\text{i}} > 0, \quad k^b_{\text{ac}-\text{i}} = k^c_{\text{ac}-\text{i}} = 0, \quad \forall \text{i} \in \mathbb{N}_{\text{ac}} \\ &\bullet \text{ In (4.15b)}: \quad k^a_{\text{dc}-j} > 0, \quad k^b_{\text{dc}-j} = k^c_{\text{dc}-j} = 0, \quad \forall j \in \mathbb{N}_{\text{dc}} \\ &\bullet \text{ In (4.16a)}: \quad 1/\tau_{\text{IC}} = 0 \end{aligned} \tag{8.3}$$

At $t = 0s$, due to the droop controllers are independently operating within each microgrid, the *ac*-DGs are perfectly sharing the active power generated while the frequency is maintained at the nominal value (see Fig. 8.1a and Fig. 8.1c, respectively). On the other hand, it is not possible to achieve an accurate power-sharing for the *dc*-DGs while regulating the *dc*-voltages (see Fig. 8.1d and Fig. 8.1f, respectively). Since the microgrids are working independently, the power through the *IC* is zero (see Fig. 8.2a). The objective function for the minimization problem is the total operating cost of the microgrid ($C_T$), given by (8.4). Under this scenario, the total operating cost is $C_T = 611.28$ ($\$/h$), as shown in Fig. 8.2c.

$$C_T\ (\$/h) = \sum\nolimits_{\text{i}\in\mathbb{N}_{\text{ac}}} C_{\text{ac}-\text{i}}\left(P^{\text{G}}_{\text{ac}-\text{i}}\right) + \sum\nolimits_{j\in\mathbb{N}_{\text{dc}}} C_{\text{dc}-j}\left(P^{\text{G}}_{\text{dc}-j}\right) \tag{8.4}$$

At $t = 100s$, the *optimization within each microgrid* operating condition is enabled (independently); therefore, now the parameters for the controllers are:

$$\begin{aligned} &\bullet \text{ In (4.13b)}: \quad k^a_{\text{ac}-\text{i}}, k^b_{\text{ac}-\text{i}} > 0, \quad k^c_{\text{ac}-\text{i}} = 0, \quad \forall \text{i} \in \mathbb{N}_{\text{ac}} \\ &\bullet \text{ In (4.15b)}: \quad k^a_{\text{dc}-j}, k^b_{\text{dc}-j} > 0, \quad k^c_{\text{dc}-j} = 0, \quad \forall j \in \mathbb{N}_{\text{dc}} \\ &\bullet \text{ In (4.16a)}: \quad 1/\tau_{\text{IC}} = 0 \end{aligned} \tag{8.5}$$

The generated power changes with respect to the previous condition (see Fig. 8.1a and Fig. 8.1d). Moreover, now the *ac*-DGs and *dc*-DGs achieve a $\lambda$ consensus with the units within the same microgrid, as shown in Fig. 8.2d. It can be seen that the cheapest microgrid corresponds to the *dc*-microgrid ($\lambda^{\text{ac}} > \lambda^{\text{dc}}$). Since the *IC* is not participating in the control task, the power transfer remains equal to zero (see Fig. 8.2a). On the other hand, the optimization reduces the total operating cost of the microgrid [$C_T = 609.78$ ($\$/h$)].

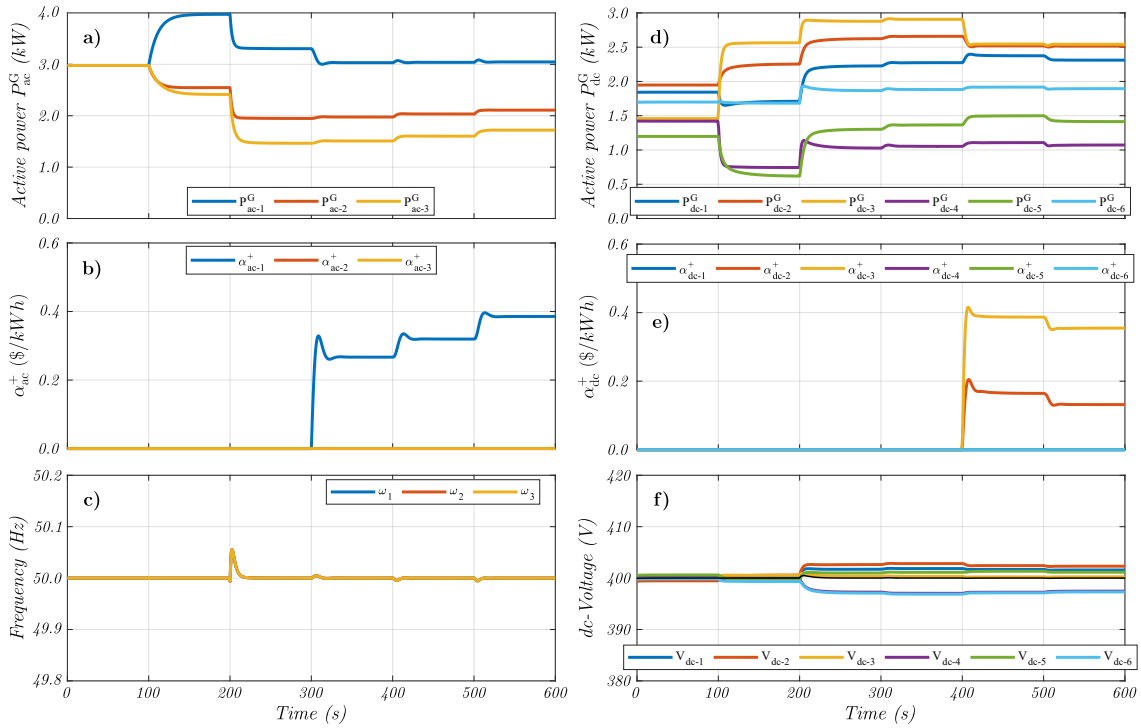


Figure 8.1: Simulation Test #7: (a)&(d) Active power generated by *ac*-DGs ($P^{\mathrm{G}}_{\mathrm{ac-i}}$) and *dc*-DGs ($P^{\mathrm{G}}_{\mathrm{dc}-j}$). (b)&(e) Lagrange multiplier for generated power constraints ($\alpha^+_{\mathrm{ac-i}}$ and $\alpha^+_{\mathrm{dc}-j}$). (c)&(f) Secondary variables (frequency and *dc*-voltage).

The *full optimization* operating condition is enabled at $t = 200s$. The parameters for the controllers are:

$$\begin{aligned}
&\bullet \text{ In (4.13b)}: \quad k^a_{\mathrm{ac-i}}, k^b_{\mathrm{ac-i}}, k^c_{\mathrm{ac-i}} > 0, \quad \forall \mathrm{i} \in \mathbb{N}_{\mathrm{ac}} \\
&\bullet \text{ In (4.15b)}: \quad k^a_{\mathrm{dc}-j}, k^b_{\mathrm{dc}-j}, k^c_{\mathrm{dc}-j} > 0, \quad \forall j \in \mathbb{N}_{\mathrm{dc}} \\
&\bullet \text{ In (4.16a)}: \quad 1/\tau_{\mathrm{IC}} > 0
\end{aligned} \tag{8.6}$$

Now, the power generated in the cheapest microgrid ($P^{\mathrm{G}}_{\mathrm{dc}-j}$) increases and the power generated in the most expensive microgrid ($P^{\mathrm{G}}_{\mathrm{ac-i}}$) decreases (see Fig. 8.1d and Fig. 8.1a, respectively). The *IC* starts transferring power from the cheapest microgrid to the most expensive one in order to maintain the power-balance constraint and to minimize the total operating cost [$C_T = 608.93$ ($/h$)], as shown in Fig. 8.2c. The change in the generated powers produces a $\lambda$ consensus between the two microgrids ($\lambda^{\mathrm{ac}} \approx \lambda^{\mathrm{dc}}$), as shown in Fig. 8.2d.

Since the power limit constraints for the DGs and the *IC* have not been enabled yet, some units are working above their maximum allowed capacities (see Fig. 8.1a for *ac*-DG$_1$, Fig. 8.1d for *dc*-DG$_2$ and *dc*-DG$_3$, and Fig. 8.2a for the *IC*). Therefore, the constraints for the *ac*-DGs, *dc*-DGs and *IC* are enabled at $t = 300s$, $t = 400s$ and $t = 500s$, respectively. It can be seen in Fig. 8.1b that the Lagrange multiplier ($\alpha^+_{\mathrm{ac}-1}$) associated with the power limit constraint for the $P^{\mathrm{G}}_{\mathrm{ac}-1}$ increases its value when this constraint is enabled ($t = 300s$), which produces a decrease in $P^{\mathrm{G}}_{\mathrm{ac}-1}$ and fixes it to the upper limit ($P^{\mathrm{G}}_{\mathrm{ac}-1} = P^{\mathrm{G}+}_{\mathrm{ac}-1} = 3kW$). As a new constraint has been enabled, the total operating cost for the microgrid is $C_T = 608.99$ ($/h$).

The same behaviour described before can be seen in Fig. 8.1e for *dc*-DG$_2$ and *dc*-DG$_3$.

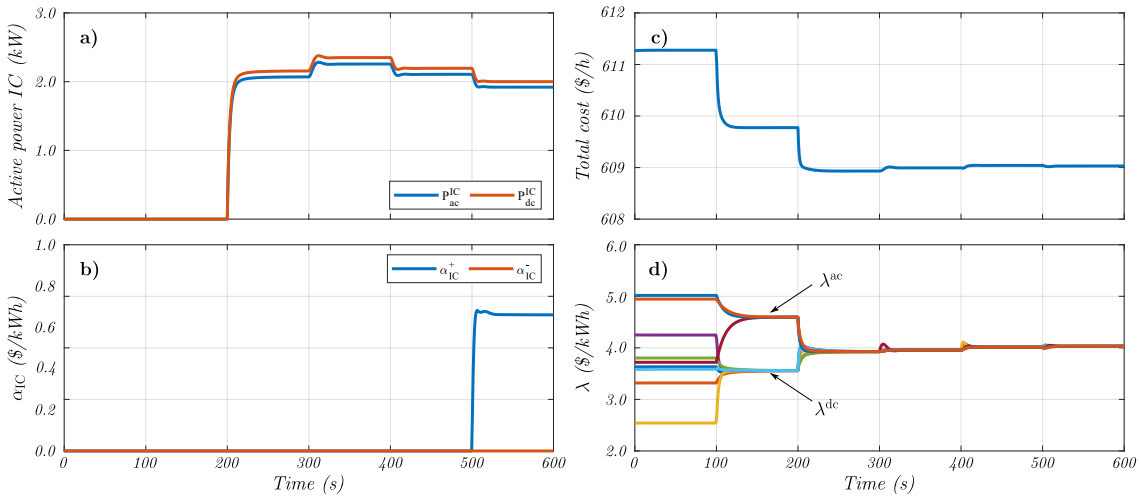


Figure 8.2: Simulation Test #7: (a) Active power through the *IC*. (b) Lagrange multiplier for transfer power constraints ($\alpha_{\text{IC}}^{\text{ac}+}$). (c) Total operating cost. (d) Lagrange multiplier $\lambda$.

Here, the Lagrange multipliers ($\alpha^{+}_{\text{dc}-2}$ and $\alpha^{+}_{\text{dc}-3}$) increase their values when the constraints are activated ($t = 400s$), which produces a decrease in those powers until they touch the upper limit ($P^{\text{G}}_{\text{dc}-2} = P^{\text{G}}_{\text{dc}-3} = P^{\text{G}+}_{\text{dc}-2} = P^{\text{G}+}_{\text{dc}-3} = 2.5kW$), and an increase in the total operating cost [$C_T = 609.04$ ($/h$)].

Finally, the Lagrange multiplier associated with the power transfer constraint for the *IC* ($\alpha^{+}_{\text{IC}}$) can be seen in Fig. 8.2b; it also increases its value when the constraint is activated ($t = 500s$), until the power through the *IC* touches the upper limit. In this case, since the power through the *IC* flows from the *dc*-side to the *ac*-side ($P^{\text{ac}}_{\text{IC}} > 0$), the power on the *dc*-side of the *IC* is higher than that on the *ac*-side of the *IC* ($P^{\text{dc}}_{\text{IC}} > P^{\text{ac}}_{\text{IC}}$); therefore, the power constraint is considered on the side with the highest power ($P^{\text{dc}}_{\text{IC}} = P^{\text{dc}+}_{\text{IC}} = 2kW$). The total operating cost of the microgrid also slightly increases since a new constraint has been activated [$C_T = 609.06$ ($/h$)].

The secondary variables are restored and maintained within limits during all the test, as shown in Fig. 8.1c for the frequency in the *ac*-microgrid and in Fig. 8.1f for the average voltage in the *dc*-microgrid.

Summarizing, Table 8.5 shows the total operating cost for the hybrid *ac*/*dc*-microgrid under all the studied scenarios. It can be seen that, as expected, the minimum operating cost is achieved when the full optimization is enabled and the constraints are not being considered. On the other hand, the total operating cost increases as new constraints are being incorporated to the controller.

## 8.3 Simulation Test #8: Single *IC* With Load Steps

Now, the performance of the proposed control strategy against load steps is analyzed. The microgrid used in the previous Section is simulated, maintaining the parameters and communication network (adjacency matrix) described before. The parameters for the cost functions of the DGs [see (4.4)] are also the same as before (see Table 8.1 and Table 8.2). The operation

Table 8.5: Summary for the total operating cost under the studied scenarios.

| **Operating condition** | **Time** | **Cost ($/h)** |
|---|---|---|
| No optimization | 0s - 100s | 611.28 |
| Opt. within microgrids | 100s - 200s | 609.78 |
| **Full optimization** | 200s - 300s | **608.93** |
| *ac*-DGs limits constraint | 300s - 400s | 608.99 |
| *dc*-DGs limits constraint | 400s - 500s | 609.04 |
| *IC* limits constraint | 500s - 600s | 609.06 |

limits for the DGs are also maintained (see (8.1) and (8.2)). The losses in the *IC* are assumed by $k^{\text{LOSS}} = 4\%$ (see Section 4.2.1).

The initial local-load of the 9 DGs is summarized in Table 8.6. The total load of the microgrid is 13.11kW (8.55kW on *dc*-side and 4.56kW on *ac*-side), i.e., 54.6% of the nominal active power. The power on the *dc*-side is 57.0% of the nominal power of this side; meanwhile, the active power on the *ac*-side corresponds to 50.7%. In this case, the reactive power loads are not considered since the proposed control strategy is not affecting the reactive power on the *ac*-microgrid. The results are shown in Fig. 8.3 and Fig. 8.4.

Table 8.6: Hybrid *ac/dc*-microgrid with a single *IC*, load conditions for test #8.

| Load | $kW$ | Load | $kW$ | Load | $kVA$ |
|---|---|---|---|---|---|
| $R_1$ | 1.03 | $R_4$ | 1.03 | $Z_1$ | $1.90 + j0.0$ |
| $R_2$ | 2.05 | $R_5$ | 1.02 | $Z_2$ | $1.65 + j0.0$ |
| $R_3$ | 1.37 | $R_6$ | 2.05 | $Z_3$ | $1.01 + j0.0$ |

The simulation starts with all the controllers and the limit constraints enabled, i.e., the full optimization is active and the parameters for the controllers are as depicted in (8.6). For $0 < t < 50s$, the DGs are achieving a $\lambda$ consensus (see Fig. 8.4d) and the total operating cost of the microgrid (see Fig. 8.4c) is minimum [$C_T = 588.66$ ($/h$)]. The power through the *IC* (see Fig. 8.4a) is negligible ($P_{\text{IC}}^{\text{ac}} \approx 0$) and the DGs are operating within limits (see Fig. 8.3a for $P_{\text{ac}-\text{i}}^{\text{G}}$, Fig. 8.3d for $P_{\text{dc}-j}^{\text{G}}$, Fig. 8.3b for $\alpha_{\text{ac}-\text{i}}^{+}$, and Fig. 8.3e for $\alpha_{\text{dc}-j}^{+}$), while the secondary variables are restored (see Fig. 8.3c for frequency and Fig. 8.3f for *dc*-voltage).

At $t = 50s$, a load step is applied in the *ac*-microgrid. The *ac*-load is step-increased to 8.91kW (99.0% of the nominal power at this side). Due to the increase in the load power, the generators increase their generated power (see Fig. 8.3a for $P_{\text{ac}-\text{i}}^{\text{G}}$ and Fig. 8.3d for $P_{\text{dc}-j}^{\text{G}}$) and the *IC* transfers power from the *dc*-side to the *ac*-side (see Fig. 8.4a). The cheapest generators touch the upper limits (see Fig. 8.3b and Fig. 8.3e for the Lagrangian multipliers $\alpha_{\text{ac}-1}^{+}$ and $\alpha_{\text{dc}-3}^{+}$, respectively), and the *IC* transfers the maximum allowed power ($P_{\text{IC}}^{\text{dc}+} = 2kW$), as explained by the increase in the Lagrange multiplier $\alpha_{\text{IC}}^{+}$ shown in Fig. 8.4b. The secondary variables are maintained in the allowed range and the $\lambda$ consensus is maintained by the DGs (see Fig. 8.4d). The total operating cost for the new load condition is $C_T = 605.09$ ($/h$). At $t = 200s$, the initial loading condition is resumed, i.e., $P_{\text{IC}}^{\text{dc}} \approx P_{\text{IC}}^{\text{ac}} \approx 0kW$.

A load change is applied at both sides at $t = 350s$. The *ac*-load is step-decreased to 3.66kW (40.7% of 9.0kW), while the *dc*-load is step-increased to 15.00kW (100.0% of the

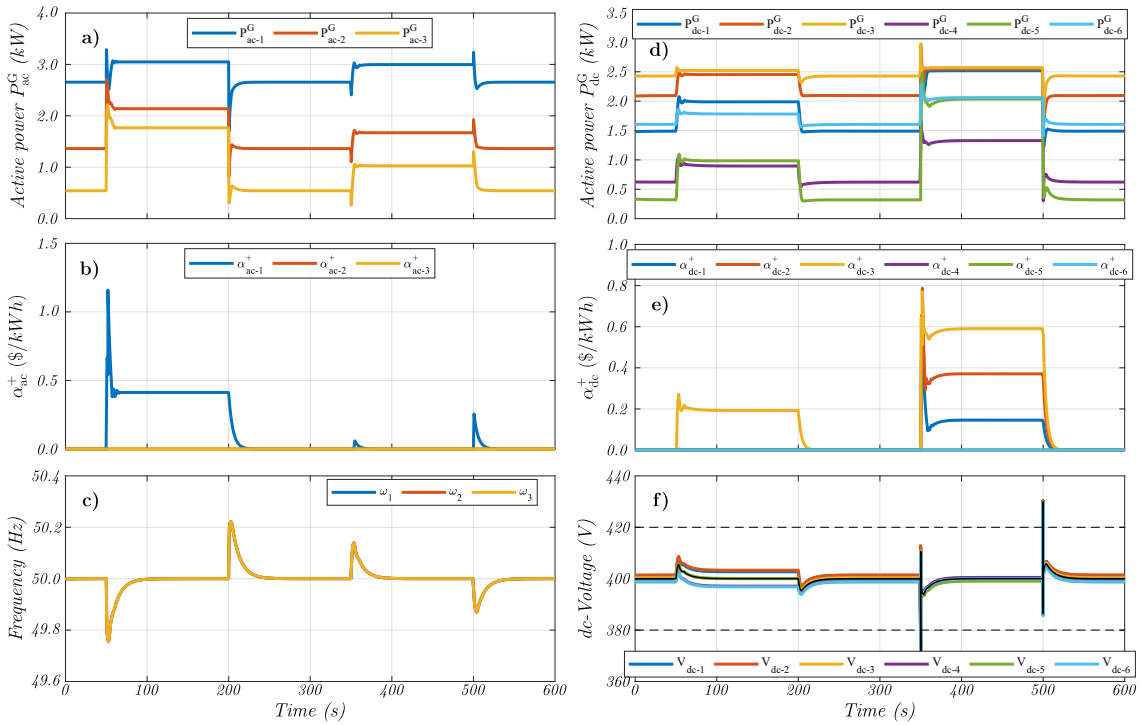


Figure 8.3: Simulation Test #8: (a)&(d) Active power generated by *ac*-DGs ($P^{\mathrm{G}}_{\mathrm{ac-i}}$) and *dc*-DGs ($P^{\mathrm{G}}_{\mathrm{dc}-j}$). (b)&(e) Lagrange multiplier for generated power constraints ($\alpha^{+}_{\mathrm{ac-i}}$ and $\alpha^{+}_{\mathrm{dc}-j}$). (c)&(f) Secondary variables (frequency and *dc*-voltage).

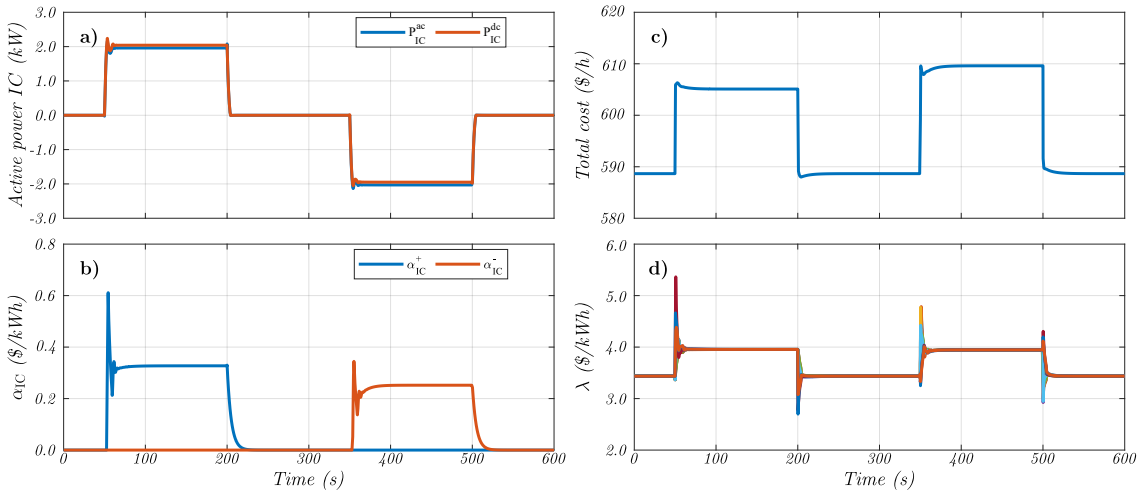


Figure 8.4: Simulation Test #8: (a) Active power through the *IC*. (b) Lagrange multiplier for transfer power constraints ($\alpha^{\mathrm{ac}+}_{\mathrm{IC}}$). (c) Total operating cost. (d) Lagrange multiplier $\lambda$.

nominal power at this side). The power generated at both sides is increased; however, only that of the *dc*-microgrid touch the upper limits of the generators (see Fig. 8.3d for $P^{\mathrm{G}}_{\mathrm{dc}-j}$ and Fig. 8.3e for the Lagrangian multipliers $\alpha^{+}_{\mathrm{dc}-1}$, $\alpha^{+}_{\mathrm{dc}-2}$ and $\alpha^{+}_{\mathrm{dc}-3}$). The power through the *IC* is now from the *ac*-side to the *dc*-side. Therefore, the power is now negative and it touches the lower limit ($P^{\mathrm{ac}-}_{\mathrm{IC}} = -2kW$), as shown in Fig. 8.4b for the $P^{\mathrm{ac}}_{\mathrm{IC}}$ and Fig. 8.4b for $\alpha^{-}_{\mathrm{IC}}$. The secondary variables are within limits and the $\lambda$ consensus is maintained by the DGs (see Fig. 8.4d). The total operating cost for the new load condition is $C_T = 609.61$ ($/h). At

$t = 500s$, the initial loading condition is resumed, i.e., $P_{\text{IC}}^{\text{dc}} \approx P_{\text{IC}}^{\text{ac}} \approx 0kW$.

## 8.4 Simulation Test #9: Multiple *ICs* Performance

Now, the control strategy proposed for minimizing the operation cost in a microgrid with multiple *ICs* is analyzed (see Section 4.5). The microgrid used in Section 7.7 is considered for this part of the work (see Fig. 7.13), maintaining the parameters and communication network (adjacency matrix) described there. Due the strategy analyzed in this Chapter is focused on minimizing the operation cost of the hybrid *ac/dc*-microgrid, the parameters for the cost functions of the DGs [see (4.4)] are depicted in Table 8.7. On the other hand, the operation limits for the DGs are given by:

$$\begin{aligned} &\bullet\ P_{\text{ac}-\text{i}}^{\text{G}-} = 0.0kW, \qquad P_{\text{ac}-\text{i}}^{\text{G}+} = 3.0kW, \qquad \forall \text{i} \in \mathbb{N}_{\text{ac}} \\ &\bullet\ P_{\text{dc}-j}^{\text{G}-} = 0.0kW, \qquad P_{\text{dc}-j}^{\text{G}+} = 2.5kW, \qquad \forall j \in \mathbb{N}_{\text{dc}} \end{aligned} \tag{8.7}$$

Table 8.7: Parameters for the cost functions of the DGs [eq. (4.4)].

| **Unit** | $\boldsymbol{a_{\text{ac}-\text{i}}}$ | $\boldsymbol{b_{\text{ac}-\text{i}}}$ | $\boldsymbol{c_{\text{ac}-\text{i}}}$ | **Unit** | $\boldsymbol{a_{\text{dc}-j}}$ | $\boldsymbol{b_{\text{dc}-j}}$ | $\boldsymbol{c_{\text{dc}-j}}$ |
|---|---|---|---|---|---|---|---|
| *ac*-DG$_1$ | 0.55 | 1.5 | 70 | *dc*-DG$_1$ | 0.31 | 2.4 | 57 |
| *ac*-DG$_2$ | 0.49 | 2.4 | 60 | *dc*-DG$_2$ | 0.52 | 1.6 | 64 |
| *ac*-DG$_3$ | 0.44 | 2.3 | 55 | *dc*-DG$_3$ | 0.46 | 2.0 | 58 |
| *ac*-DG$_4$ | 0.66 | 1.9 | 67 | *dc*-DG$_4$ | 0.51 | 2.6 | 68 |
| *ac*-DG$_5$ | 0.39 | 2.9 | 43 | *dc*-DG$_5$ | 0.21 | 3.2 | 61 |
| *ac*-DG$_6$ | 0.27 | 3.2 | 76 | *dc*-DG$_6$ | 0.79 | 0.9 | 62 |

The losses in the *ICs* and their operation limits are assumed by:

$$\begin{aligned} &\bullet\ k_1^{\text{LOSS}} = 4\%, \qquad P_{\text{IC}-1}^{\text{ac}-} = -1.2kW, \qquad P_{\text{IC}-1}^{\text{ac}+} = 1.2kW \\ &\bullet\ k_2^{\text{LOSS}} = 6\%, \qquad P_{\text{IC}-2}^{\text{ac}-} = -1.2kW, \qquad P_{\text{IC}-2}^{\text{ac}+} = 1.2kW \\ &\bullet\ k_3^{\text{LOSS}} = 2\%, \qquad P_{\text{IC}-3}^{\text{ac}-} = -1.2kW, \qquad P_{\text{IC}-3}^{\text{ac}+} = 1.2kW \end{aligned} \tag{8.8}$$

The local-load of the 12 DGs remains constant during this test, and it is summarized in Table 8.8. The total load of the hybrid *ac/dc*-microgrid is 24.6kW (9.9kW on *dc*-side and 14.7kW on *ac*-side), i.e., 74.5% of the nominal active power (33.0kW). The load power on the *dc*-side $(R_1, \ldots, R_6)$ is 66.0% of the nominal power of this side (15.0kW); meanwhile, the active load power on the *ac*-side $(Z_1, \ldots, Z_6)$ corresponds to 81.7% of 18.0kW. In this case, the reactive power loads are not considered since the proposed control strategy is not affecting the reactive power on the *ac*-microgrid. The operating conditions analyzed in this test are summarized in Table 8.9, and the results for this test are shown in Fig. 8.5 and Fig. 8.6.

The simulation starts with the inner, primary and secondary controllers enabled. Regarding the distributed secondary control loop, only the optimization within each microgrid considering the operation limit constraints and the restoring terms are enabled (independently); thus, the parameters for the controllers under the *optimization within microgrids*

Table 8.8: Hybrid *ac/dc*-microgrid with multiple *ICs*, load conditions for test #9.

| Load | $kW$ | Load | $kW$ | Load | $kW$ | Load | $kW$ |
|---|---|---|---|---|---|---|---|
| $R_1$ | 0.9 | $R_4$ | 2.4 | $Z_1$ | 2.5 | $Z_4$ | 2.4 |
| $R_2$ | 1.3 | $R_5$ | 1.5 | $Z_2$ | 1.7 | $Z_5$ | 2.1 |
| $R_3$ | 2.1 | $R_6$ | 1.7 | $Z_3$ | 2.3 | $Z_6$ | 3.7 |

Table 8.9: Summary for the operating conditions analyzed in simulation test #9.

| **Operating condition** | **Time** |
|---|---|
| Optimization within microgrids | 0s - 50s |
| Full optimization enabled | 50s - 150s |
| $\lambda^{\mathrm{IC}}$ consensus active | 150s - 250s |
| *ICs* limits constraint enabled | 250s - 400s |

operating condition are as follows:

$$\begin{aligned}
&\bullet \text{ In (4.27b)}: \quad k^a_{\mathrm{ac-i}}, k^b_{\mathrm{ac-i}} > 0, \quad k^c_{\mathrm{ac-i}} = 0, \quad \forall \mathrm{i} \in \mathbb{N}_{\mathrm{ac}} \\
&\bullet \text{ In (4.29b)}: \quad k^a_{\mathrm{dc}-j}, k^b_{\mathrm{dc}-j} > 0, \quad k^c_{\mathrm{dc}-j} = 0, \quad \forall j \in \mathbb{N}_{\mathrm{dc}} \\
&\bullet \text{ In (4.30a)}: \quad \tau^a_{\mathrm{IC}-k}, \tau^b_{\mathrm{IC}-k} = 0, \quad \forall k \in \mathbb{N}_{\mathrm{IC}}
\end{aligned} \tag{8.9}$$

For $0s < t < 50s$, the DGs are operating within limits (see Fig. 8.5a for $P^{\mathrm{G}}_{\mathrm{ac-i}}$ and Fig. 8.5d for $P^{\mathrm{G}}_{\mathrm{dc}-j}$), and the Lagrange multipliers associated to the power limits constraint are zero (see Fig. 8.5b for $\alpha^{+}_{\mathrm{ac-i}}$ and Fig. 8.5e for $\alpha^{+}_{\mathrm{dc}-j}$). The secondary variables are properly regulated (see Fig. 8.5c for frequency and Fig. 8.5f for *dc*-voltage). On the other hand, the power through the *ICs* is zero (see Fig. 8.6a) and, therefore, the losses in the *ICs* are also null (see Fig. 8.6c). The $\lambda^{\mathrm{G}}$ consensus is achieved within each microgrid (see Fig. 8.6e) and the total operating cost is shown in Fig. 8.6d [$C_T = 820.55$ ($/h$)].

At $t = 50s$, the *full optimization* operating condition of the microgrid is enabled. However, the $\lambda^{\mathrm{IC}}$ consensus and the *ICs* limit constraints are maintained deactivated. Thus, the parameters for the controllers for $50s < t < 150s$ are as follows:

$$\begin{aligned}
&\bullet \text{ In (4.27b)}: \quad k^a_{\mathrm{ac-i}}, k^b_{\mathrm{ac-i}}, k^c_{\mathrm{ac-i}} > 0, \quad \forall \mathrm{i} \in \mathbb{N}_{\mathrm{ac}} \\
&\bullet \text{ In (4.29b)}: \quad k^a_{\mathrm{dc}-j}, k^b_{\mathrm{dc}-j}, k^c_{\mathrm{dc}-j} > 0, \quad \forall j \in \mathbb{N}_{\mathrm{dc}} \\
&\bullet \text{ In (4.30a)}: \quad \tau^a_{\mathrm{IC}-k} > 0, \quad \tau^b_{\mathrm{IC}-k} = 0, \quad \forall k \in \mathbb{N}_{\mathrm{IC}}
\end{aligned} \tag{8.10}$$

Enabling the $\lambda^{\mathrm{G}}$ consensus produces an increase in the power generated in the cheapest microgrid (*dc*-microgrid, see Fig. 8.5d) and a decrease in that of the most expensive one (*ac*-microgrid, see Fig. 8.5a). Furthermore, *dc*-$\mathrm{DG}_1$ and *dc*-$\mathrm{DG}_2$ touch the upper limit but, in steady-state, only the former one is fixed at the maximum value ($P^{\mathrm{G}}_{\mathrm{dc}-1} = P^{\mathrm{G}+}_{\mathrm{dc}-1} = 2.5kW$), as explained by the Lagrange multiplier associated to the limits constraint (see Fig. 8.5e). The secondary variables are restored after the transient and maintained within limits (see Fig. 8.5c for frequency and Fig. 8.5f for *dc*-voltage).

Since the power through the *ICs* flows from the *dc*-microgrid to the *ac*-microgrid, the power transfer is positive, as depicted in Fig. 8.6a. On the other hand, since the $\lambda^{\mathrm{IC}}$ consensus

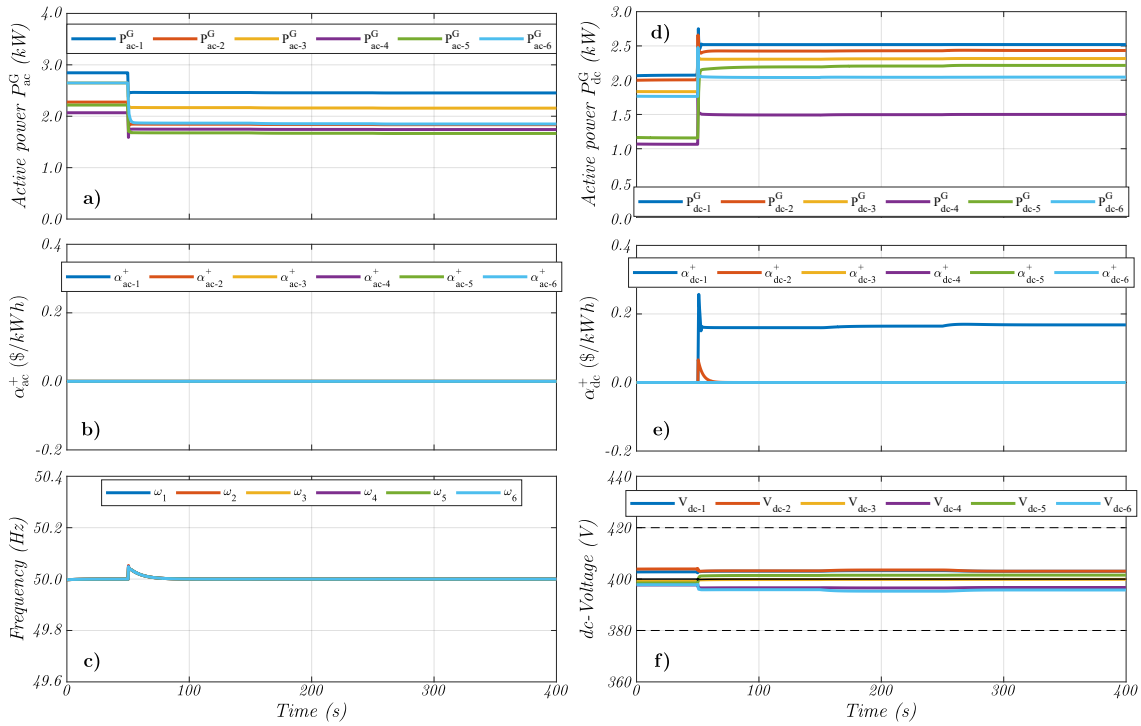


Figure 8.5: Simulation Test #9: (a)&(d) Active power generated by *ac*-DGs ($P^{\mathrm{G}}_{\mathrm{ac-i}}$) and *dc*-DGs ($P^{\mathrm{G}}_{\mathrm{dc}-j}$). (b)&(e) Lagrange multiplier for generated power constraints ($\alpha^{+}_{\mathrm{ac-i}}$ and $\alpha^{+}_{\mathrm{dc}-j}$). (c)&(f) Secondary variables (frequency and *dc*-voltage).

is not active (see Fig. 8.6f), the *ICs* only share the power for achieving $\lambda^{\mathrm{G}}$ consensus. In this scenario, all the *ICs* are within limits and the Lagrange multiplier associated to this constraint is zero (see Fig. 8.6b). It is important to highlight that the Lagrange multiplier $\lambda_{\mathrm{IC}}$ can be positive or negative (depending on the direction of the power through the *ICs*) since it shifts the incremental cost function ($\lambda^{G}$) from the DGs (see (4.27e) and (4.29e)). The total operating cost of the microgrid is reduced when activating the full optimization [$C_T = 819.55$ ($/h$), see Fig. 8.6d].

The $\lambda^{\mathrm{IC}}$ consensus is activated at $t = 150s$, and the parameters for the controllers are as shown in (8.11). It can be seen that the *ICs* begin to work collaboratively and they reach the same value of $\lambda^{\mathrm{IC}}$, as depicted in Fig. 8.6f. Moreover, a re-dispatch of the power through the *ICs* is produced (see Fig. 8.6a) and, therefore, the losses in the *ICs* change as well (see Fig. 8.6c). The re-dispatch of the power through the *ICs* very subtly affects the operation of the DGs (see Fig. 8.5). On the other hand, since all the optimization is now active, the total operating cost of the microgrid decreases again [$C_T = 819.50$ ($/h$), see Fig. 8.6d].

$$\begin{aligned}
&\bullet \ \text{In (4.27b)}: \quad k^{a}_{\mathrm{ac-i}}, k^{b}_{\mathrm{ac-i}}, k^{c}_{\mathrm{ac-i}} > 0, \qquad \forall \mathrm{i} \in \mathbb{N}_{\mathrm{ac}} \\
&\bullet \ \text{In (4.29b)}: \quad k^{a}_{\mathrm{dc}-j}, k^{b}_{\mathrm{dc}-j}, k^{c}_{\mathrm{dc}-j} > 0, \qquad \forall j \in \mathbb{N}_{\mathrm{dc}} \\
&\bullet \ \text{In (4.30a)}: \quad \tau^{a}_{\mathrm{IC}-k}, \tau^{b}_{\mathrm{IC}-k} > 0, \qquad \forall k \in \mathbb{N}_{\mathrm{IC}}
\end{aligned} \tag{8.11}$$

Finally, the limit constraints for the power transfer through the *ICs* are activated at $t = 250s$. The power through the *IC* with the lowest losses is decreased and that of the other two is increased (see Fig. 8.6a). The Lagrange multiplier associated to this constraint can be

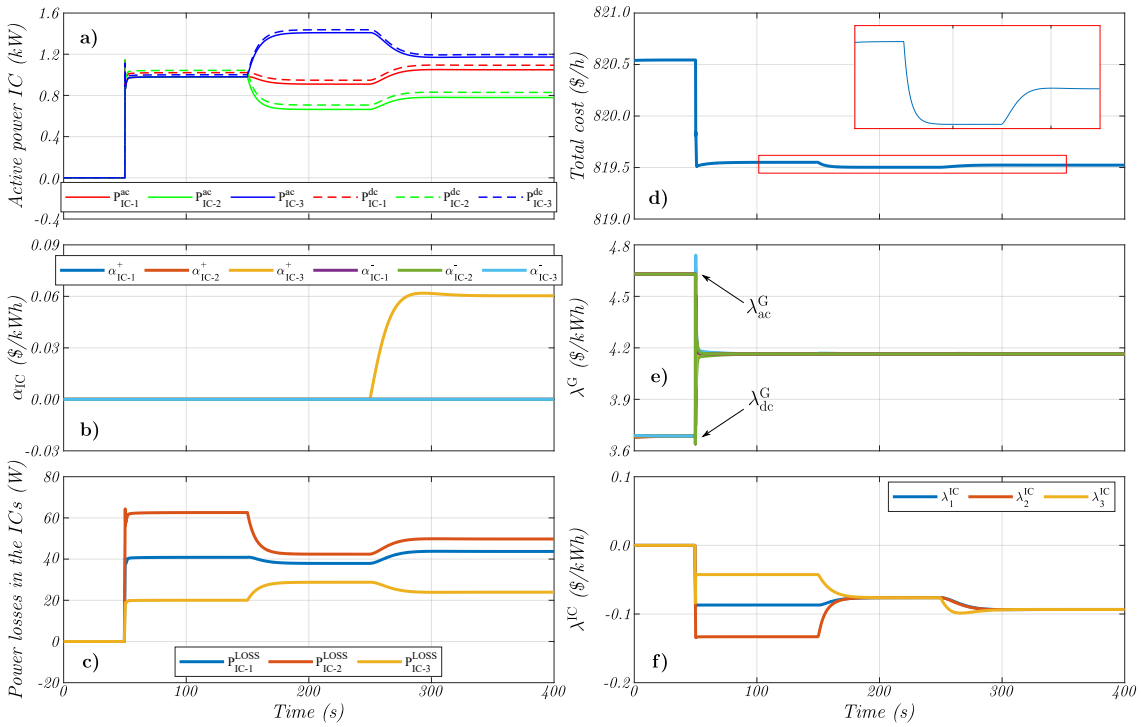


Figure 8.6: Simulation Test #9: (a) Active power through the *ICs*. (b) Lagrange multiplier for transfer power constraints ($\alpha^{\text{ac}+}_{\text{IC}-k}$ and $\alpha^{\text{ac}-}_{\text{IC}-k}$). (c) Power losses in the *ICs*. (d) Total operating cost. (e) Lagrange multiplier $\lambda^{\text{G}}$. (f) Lagrange multiplier $\lambda^{\text{IC}}$.

seen in Fig. 8.6b. Again, the inclusion of the power transfer limit constraints slightly increase the total operating cost of the microgrid [$C_T = 819.52$ ($/h$), see Fig. 8.6d] and marginally affects the operation of the DGs (see Fig. 8.5).

In summary, Table 8.10 shows the total operating cost for the hybrid *ac/dc*-microgrid under all the studied scenarios. It can be seen that, as expected, the minimum operating cost is achieved when the full optimization is enabled and the $\lambda^{\text{IC}}$ consensus is being considered. On the other hand, the total operating cost increases as new constraints are being incorporated to the controller.

Table 8.10: Summary for the total operating cost under the studied scenarios.

| **Operating condition** | **Time** | **Cost ($/h)** |
|---|---|---|
| Opt. within microgrids | 0s - 50s | 820.55 |
| Full optimization | 50s - 150s | 819.55 |
| **$\boldsymbol{\lambda}^{\text{IC}}$ consensus** | 150s - 250s | **819.50** |
| *ICs* limits constraint | 250s - 400s | 819.52 |

## 8.5 Simulation Test #10: Multiple *ICs* With Load Steps

Now, the performance of the proposed control strategy against load steps is analyzed. The microgrid used in the previous Section is simulated, maintaining the parameters and commu-

nication network (adjacency matrix) described before. The parameters for the cost functions of the DGs [see (4.4)] are also the same as before (see Table 8.7). The operation limits for the DGs are also maintained [see (8.7) and (8.8)]. The losses in the *ICs* are given by (8.8). The initial local-load of the 12 DGs is the same as in the previous test (see Table 8.8). The results for this test are shown in Fig. 8.7 and Fig. 8.8.

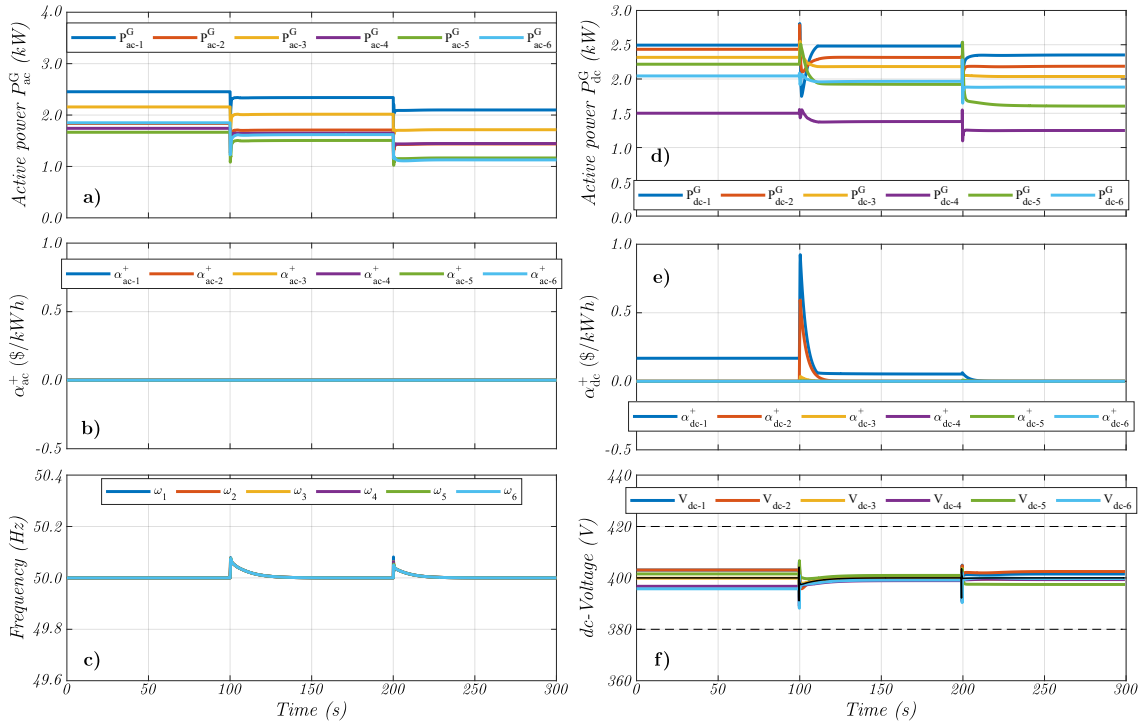


Figure 8.7: Simulation Test #10: (a)&(d) Active power generated by *ac*-DGs ($P^{\mathrm{G}}_{\mathrm{ac-i}}$) and *dc*-DGs ($P^{\mathrm{G}}_{\mathrm{dc}-j}$). (b)&(e) Lagrange multiplier for generated power constraints ($\alpha^{+}_{\mathrm{ac-i}}$ and $\alpha^{+}_{\mathrm{dc}-j}$). (c)&(f) Secondary variables (frequency and *dc*-voltage).

The simulation begins with all the controllers and the power limit constraints enabled, i.e., the full optimization of the microgrid is active and the parameters for the controllers are as depicted in (8.11). For $0s < t < 100s$, the DGs are achieving a $\lambda^{\mathrm{G}}$ consensus (see Fig. 8.8e) and the *ICs* are achieving $\lambda^{\mathrm{IC}}$ consensus (see Fig. 8.8f).

The total operating cost of the microgrid (see Fig. 8.8d) is minimum in this scenario [$C_T = 819.52$ ($/$h$)], and the power through the $IC_3$ is touching the upper limit (see Fig. 8.8a for $P^{\mathrm{dc}}_{\mathrm{IC}-3}$ and Fig. 8.8b for $\alpha^{+}_{\mathrm{IC}-3}$). On the other hand, the *dc*-DG$_1$ is generating its maximum power and the other DGs are operating within limits (see Fig. 8.7a for $P^{\mathrm{G}}_{\mathrm{ac-i}}$, Fig. 8.7d for $P^{\mathrm{G}}_{\mathrm{dc}-j}$, Fig. 8.7b for $\alpha^{+}_{\mathrm{ac-i}}$, and Fig. 8.7e for $\alpha^{+}_{\mathrm{dc}-j}$), while the secondary variables are regulated (see Fig. 8.7c for frequency and Fig. 8.7f for *dc*-voltage).

At $t = 100s$, a load step is applied at both sides of the hybrid *ac*/*dc*-microgrid. The load at the *ac*-side is step-decreased to 13.7kW (76.1% of the nominal power at this side), while the load power at the *dc*-side is step-increased to 12.1kW (80.7% of the nominal power at this side). Due to the change in the power load, the power through the *ICs* decreases until it is negligible ($P^{\mathrm{ac}}_{\mathrm{IC}-k} \approx 0$), as shown in Fig. 8.8a. Moreover, the Lagrange multiplier associated to the power transfer limit ($\alpha^{+}_{\mathrm{IC}-3}$) slowly decreases until it becomes zero (see

Fig. 8.8b). The only element that remains touching its upper operation limit is the $dc$-DG$_1$, which corresponds to the cheapest generator in the microgrid.

Despite the transient response, the secondary variables are maintained within limits all the time (see Fig. 8.7c for frequency and Fig. 8.7f for $dc$-voltage), and the $\lambda$ consensuses are achieved by the DGs (see Fig. 8.8e for $\lambda^{\mathrm{G}}$) and by the *ICs* (see Fig. 8.8f for $\lambda^{\mathrm{IC}}$). The total operating cost for the new load condition is $C_T = 812.85$ ($\$/h$), as shown in Fig. 8.8d.

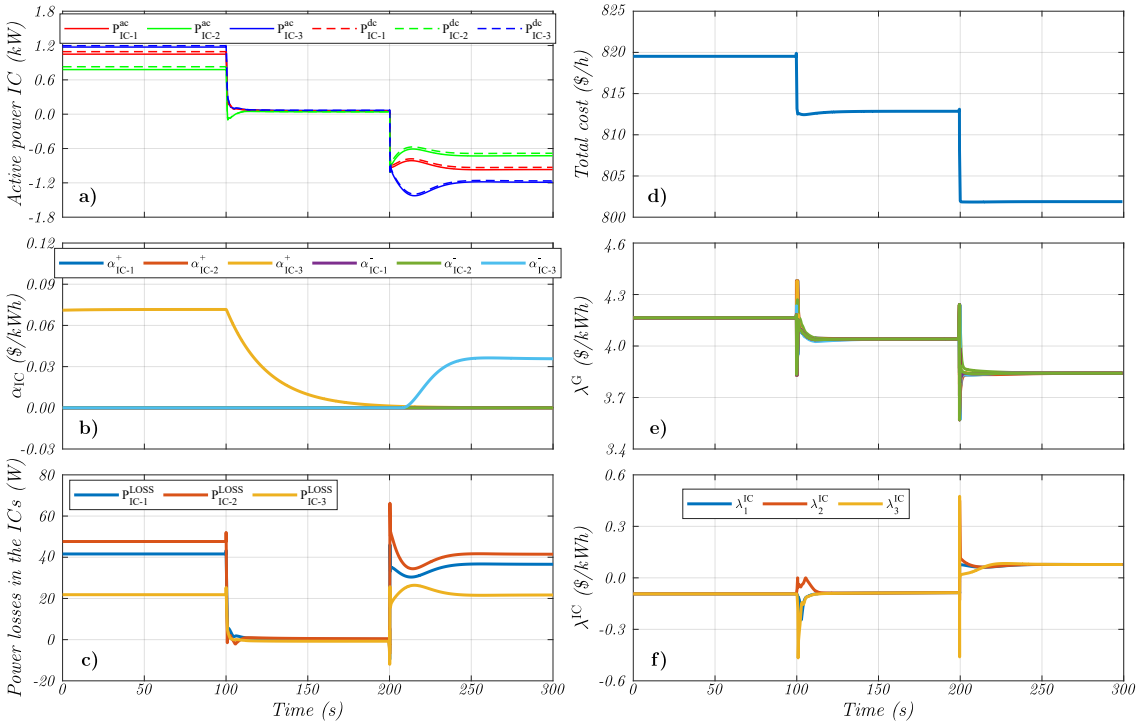


Figure 8.8: Simulation Test #10: (a) Active power through the *ICs*. (b) Lagrange multiplier for transfer power constraints ($\alpha^{\mathrm{ac}+}_{\mathrm{IC}-k}$ and $\alpha^{\mathrm{ac}-}_{\mathrm{IC}-k}$). (c) Power losses in the *ICs*. (d) Total operating cost. (e) Lagrange multiplier $\lambda^{\mathrm{G}}$. (f) Lagrange multiplier $\lambda^{\mathrm{IC}}$.

At $t = 200s$, a new load step is applied at both sides of the hybrid $ac/dc$-microgrid; the load on the $ac$-side is step-decreased to 11.7kW (65.0% of the nominal power at this side), while the load power on the $dc$-side is step-increased to 13.1kW (87.3% of the nominal power at this side). Due to the change in the load, the power through the *ICs* now flows from the $ac$-microgrid to the $dc$-microgrid, as depicted in Fig. 8.8a. One more time, the *IC* with the lowest losses ($IC_3$) touches its operation limits and the Lagrange multiplier associated to this constraint is increased (see Fig. 8.8b for $\alpha^{-}_{\mathrm{IC}-3}$).

All DGs now are working within limits (see Fig. 8.7a for $P^{\mathrm{G}}_{\mathrm{ac-i}}$, and Fig. 8.7d for $P^{\mathrm{G}}_{\mathrm{dc}-j}$), which is reflected in the Lagrange multipliers associated to these constraints (see Fig. 8.7b for $\alpha^{+}_{\mathrm{ac-i}}$, and Fig. 8.7e for $\alpha^{+}_{\mathrm{dc}-j}$). On the other hand, all the secondary variables remain regulated within limits (see Fig. 8.7c for frequency and Fig. 8.7f for $dc$-voltage). One more time, the $\lambda$ consensuses are achieved by the DGs (see Fig. 8.8e for $\lambda^{\mathrm{G}}$) and by the *ICs* (see Fig. 8.8f for $\lambda^{\mathrm{IC}}$) all the time, and the total operating cost for the new load condition is $C_T = 801.89$ ($\$/h$), as shown in Fig. 8.8d.

## 8.6 Simulation Test #11: Comparison

Finally, a comparison of the two control strategies proposed in this thesis is presented, i.e., the scheme for power-sharing presented in Chapter 3 (henceforth called *DSC-I*) and the algorithm for operation cost minimization depicted in Chapter 4 (called *DSC-II* from now on). The control strategies are applied to the two microgrids utilized in this thesis, i.e., to the one with a single *IC* (see Fig. 5.8) and to the other with multiple *ICs* (see Fig. 7.13). The parameters for the controllers are those used in Chapters 7 and 8.

The power loads remain constant during this test, and are summarized in Table 8.11 for the two topologies simulated in these tests. Furthermore, the loading condition of the hybrid *ac/dc*-microgrid was designed to avoid the DGs' and *ICs*' overload, in order to make a clean comparison without the limit constraints which penalizes the cost in the second strategy (*DSC-II*). Since both the reactive power consensus and the *ac*-voltage regulation are achieved using the same control strategy in both cases (see Section 3.3), only active power loads are considered in the *ac*-side. The results for these tests are shown in Fig. 8.9 and Fig. 8.10. In the figures, the results for the microgrid with a single *IC* are depicted in the column on the left side while the results for the microgrid with multiple *ICs* are presented in the column on the right side.

Table 8.11: Hybrid *ac/dc*-microgrid, load conditions for test #11.

**Topology with a single *IC***

| Load | *kW* | Load | *kW* |
|---|---|---|---|
| $R_1$ | 1.02 | $Z_1$ | 1.90 |
| $R_2$ | 1.55 | $Z_2$ | 2.57 |
| $R_3$ | 1.37 | $Z_3$ | 2.64 |
| $R_4$ | 1.03 | | |
| $R_5$ | 1.03 | | |
| $R_6$ | 1.03 | | |

**Topology with multiple *ICs***

| Load | *kW* | Load | *kW* |
|---|---|---|---|
| $R_1$ | 1.9 | $Z_1$ | 2.1 |
| $R_2$ | 1.3 | $Z_2$ | 1.7 |
| $R_3$ | 1.1 | $Z_3$ | 2.3 |
| $R_4$ | 1.4 | $Z_4$ | 2.1 |
| $R_5$ | 1.5 | $Z_5$ | 2.1 |
| $R_6$ | 1.7 | $Z_6$ | 1.7 |

In the single *IC* case, the total load of the hybrid *ac/dc*-microgrid is 14.14kW (7.03kW on *dc*-side and 7.11kW on *ac*-side), i.e., 58.9% of the nominal active power of this microgrid (24.0kW). The load power on the *dc*-side ($R_1, \ldots, R_6$) is 46.9% of the nominal power of this side (15.0kW); meanwhile, the active load power on the *ac*-side ($Z_1, Z_2, Z_3$) corresponds to 79.0% of 9.0kW. On the other hand, in the multiple *ICs* case, the total load of the hybrid *ac/dc*-microgrid is 20.9kW (8.9kW on *dc*-side and 12.0kW on *ac*-side), i.e., 63.3% of the nominal active power of this microgrid (33.0kW). The load power on the *dc*-side ($R_1, \ldots, R_6$) is 59.3% of the nominal power of this side (15.0kW); meanwhile, the active load power on the *ac*-side ($Z_1, \ldots, Z_6$) corresponds to 66.7% of 18.0kW.

The simulations begin with all the controllers enabled, i.e., the inner, primary and secondary control loops are active. Specifically, in both cases, for $t < 100s$ the *DSC-I* strategy is working and the DGs are achieving an accurate power consensus, as depicted in Fig. 8.9a for the single *IC* case and Fig. 8.9d for the multiple *ICs* case. The power generated by the *ac*-DGs ($P^{\mathrm{G}}_{\mathrm{ac-i}}$, $\forall \mathrm{i} \in \mathbb{N}_{\mathrm{ac}}$) is shown in red while the power generated by the *dc*-DGs ($P^{\mathrm{G}}_{\mathrm{dc}-j}$, $\forall j \in \mathbb{N}_{\mathrm{dc}}$) is shown in blue.

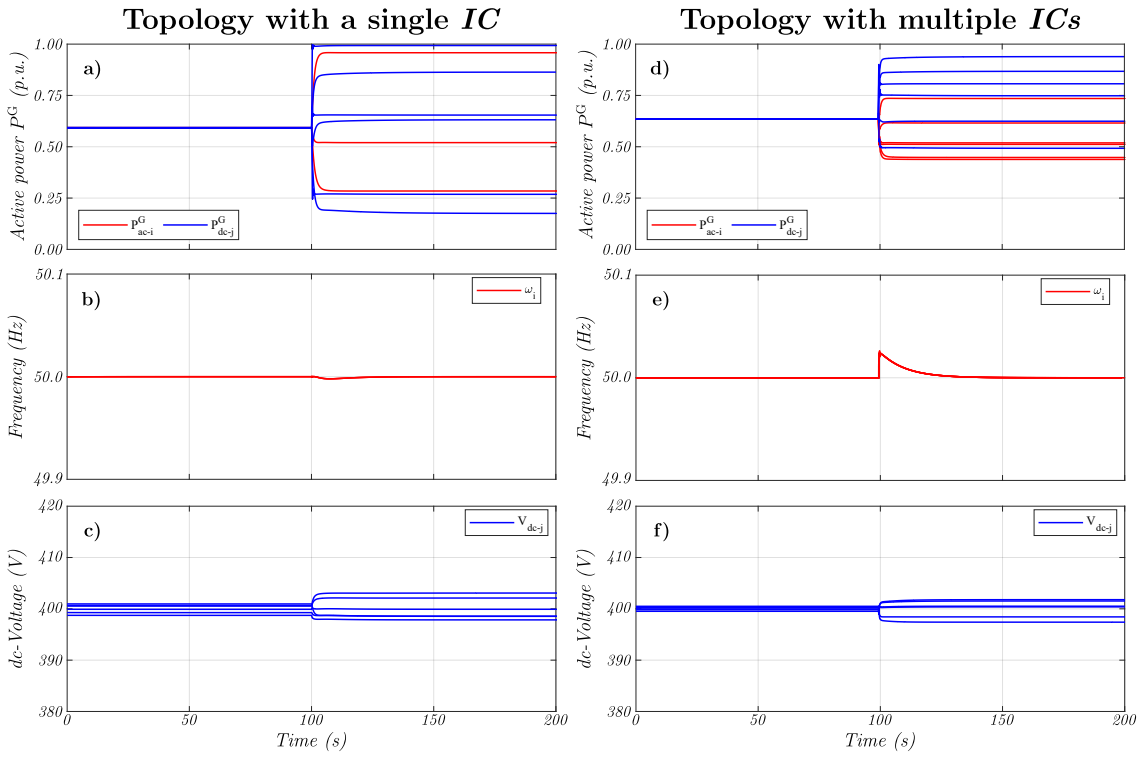


Figure 8.9: Simulation Test #11: (a)&(d) Power generated by *ac*-DGs ($P^{\mathrm{G}}_{\mathrm{ac-i}},\ \mathrm{i} \in \mathbb{N}_{\mathrm{ac}}$) and *dc*-DGs ($P^{\mathrm{G}}_{\mathrm{dc}-j},\ j \in \mathbb{N}_{\mathrm{dc}}$). (b)&(e) Frequency of the voltages in the *ac*-microgrid ($\omega_{\mathrm{i}},\ \mathrm{i} \in \mathbb{N}_{\mathrm{ac}}$). (c)&(f) Voltage magnitudes in the *dc*-microgrid ($V_{\mathrm{dc}-j},\ j \in \mathbb{N}_{\mathrm{dc}}$).

As described before, in both cases, the power load (in p.u.) in the *ac*-side is higher than that in the *dc*-side. Therefore, the *ICs* transfer power from the *dc*-side to the *ac*-side ($P^{\mathrm{ac}}_{\mathrm{IC}-k} > 0,\ \forall k \in \mathbb{N}_{\mathrm{IC}}$), as shown in Fig. 8.10a and Fig. 8.10d. Moreover, since the power consensus (*DSC-I*) strategy is operating, the *ICs* are sharing the power in the case with multiple *ICs* (see Fig. 8.10d). The Lagrange multipliers of the DGs ($\lambda^{\mathrm{G}}$) are not being shared in any case (see Fig. 8.10b and Fig. 8.10e). On the other hand, the Lagrange multipliers of the *ICs* ($\lambda^{\mathrm{IC}}$) are not shared in the case with multiple *ICs* (see Fig. 8.10e).

The *DSC-II* strategy is activated at $t = 100s$. It can be seen that both the DGs and the *ICs* immediately start to share the Lagrange multipliers (see Fig. 8.10d and Fig. 8.10e). Therefore, in order to minimize the total operating cost of the microgrid, the power generated by the DGs is re-dispatched (see Fig. 8.10a and Fig. 8.10d), increasing the amount of power being transferred through the *ICs*. Moreover, the power in the *ICs* is also re-dispatched to reduce the total operating cost, as shown in Fig. 8.10d.

At this point, it is important to remember that the main objective of the secondary control loop is to restore the variables modified by the primary control loop to their nominal values, i.e., the frequency of the voltages in the *ac*-microgrid and the magnitude of the voltages in the *dc*-microgrid. The two control strategies proposed in this work fulfill this objective, and successfully restore the secondary variables to their nominal values, as depicted in Fig. 8.9b and Fig. 8.9e for the frequency ($\omega_{\mathrm{i}},\ \forall \mathrm{i} \in \mathbb{N}_{\mathrm{ac}}$), and in Fig. 8.9c and Fig. 8.9f for the *dc*-voltages ($V_{\mathrm{dc}-j},\ \forall j \in \mathbb{N}_{\mathrm{dc}}$).

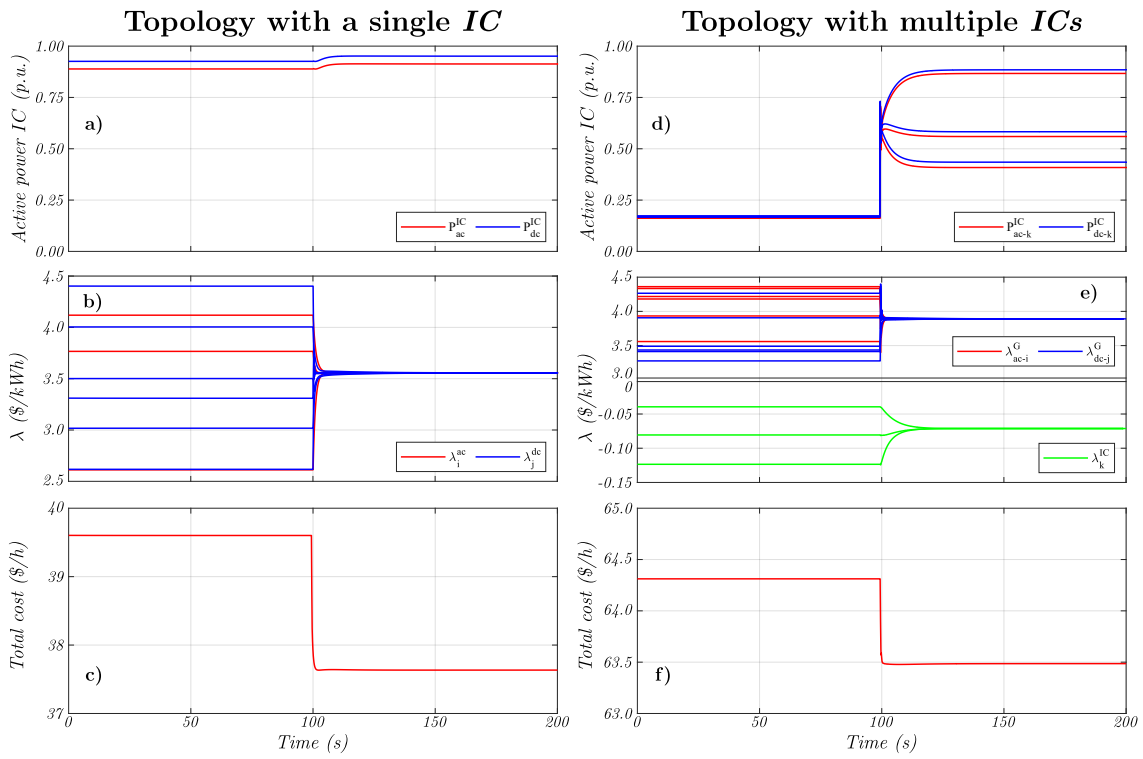


Figure 8.10: Simulation Test #11: (a)&(d) Active power through the *ICs*. (b)&(e) Lagrange multipliers ($\lambda$). (c)&(f) Total operating cost.

From Fig. 8.10c and Fig. 8.10f it is clear that the *DSC-II* strategy minimizes the total operation cost of the hybrid *ac/dc*-microgrid. In this case, since the fixed cost in the quadratic cost function [parameters $c_{\mathrm{ac-i}}$ and $c_{\mathrm{dc}-j}$ in (4.4)] are the same when applying the two control strategies, the total cost ($\$/h$) shown in the Figs. corresponds to the operation cost which depends on the amount of power generated by the DGs (i.e., $c_{\mathrm{ac-i}} = c_{\mathrm{dc}-j} = 0$ is considered in the calculation). Thus, it is possible to analyze the real effect of re-dispatching the power supplied by the DGs and transferred by the *ICs* on the operation cost.

A summary for the total operation cost of the hybrid *ac/dc*-microgrid under the cases analyzed in this test is presented in Table 8.12. The total variable cost of the single *IC* topology is reduced by 4.97% when the *DSC-II* strategy is applied, i.e., it is reduced from 39.601($/h) to 37.364($/h). On the other hand, the application of the *DSC-II* strategy reduces the total variable cost of the multiple *ICs* topology from 64.312($/h) to 63.486($/h), i.e., it is reduced by 1.28%. Although the savings are not that significant in monetary terms (dollars), they can be important in percentage terms even though the microgrids are small.

Finally, these tests allow to identify two possibilities to minimize the total operating cost of the microgrids, which can be applied independently or together. First, it is possible to re-dispatch the power generated by the DGs within each microgrid, with a small variation of the power transferred through the *IC*, as in the single *IC* topology. Secondly, as shown in the multiple *ICs* topology, it is possible to increase the amount of power transferred from the cheapest microgrid (*dc*-microgrid in this case) to the most expensive one (*ac*-microgrid in this case), while re-dispatching the power generated by the DGs.

Table 8.12: Total operation cost of the hybrid *ac/dc*-microgrid for test #11.

| **Microgrid Topology** | **Power-sharing (*DSC-I*)** | **Cost minimization (*DSC-II*)** | **Savings %** |
|---|---|---|---|
| Single *IC* | 39.601 ($/h) | 37.364 ($/h) | 4.97 |
| Multiple *ICs* | 64.312 ($/h) | 63.486 ($/h) | 1.28 |

## 8.7 Summary

In this Chapter, simulation results were presented to validate the distributed consensus-based secondary control strategy for operating cost minimization (with a single or multiple *ICs*) proposed in this thesis. The validation through simulation was performed in two prototypes of a hybrid *ac/dc*-microgrid; the first one corresponds to a $24kW$ downscale prototype with a single *IC*, and the second one in a $33kW$ downscale prototype of a hybrid *ac/dc*-microgrid with multiple *ICs*.

Summarizing, the simulation results demonstrated the advantages of the proposed method, which are:

- It is possible to minimize the total operating cost in a microgrid with one or multiple *ICs*, by solving an optimization problem online and in a distributed way.
- The DGs in a hybrid *ac/dc*-microgrid can be dispatched according to a global objective, which is to minimize the total operating cost.
- For the DGs or the *ICs*, it is not necessary to have the full information of the microgrid to solve the optimization problem.
- It is possible to limit either the power generated by the DGs or the power transfer through the *ICs* by implementing constraints to the optimization problem.
- The secondary control variables, i.e., average *dc*-voltages and frequency, are restored to their nominal values in steady-state under all the analyzed cases.
- The *IC* participates actively in the proposed secondary control strategy, helping to minimize the total operating cost of the microgrid by regulating the power transfer from the *dc*-side to the *ac*-side (or vice versa) according to the incremental cost of the sub-microgrids.

# Chapter 9

# Conclusions and Future Work

## 9.1 Conclusions

Continuous improvement in distributed generation technologies and energy storage systems (specifically, more efficient and economical devices) is driving the electrical systems (at the distribution level) towards microgrids. On the other hand, in order to avoid unnecessary *ac*-to-*dc* and *dc*-to-*ac* conversions, much effort has been carried out to investigate hybrid *ac*/*dc*-microgrids. Accordingly, the main goal of this thesis was to propose consensus-based distributed secondary control strategies for hybrid *ac*/*dc*-microgrids, which treat the microgrid as a single entity and not as three independent ones interacting with each other (i.e., *ac*, *dc*, and *IC*).

Owing to the results obtained in this thesis, it can be stated that the proposed control schemes simultaneously regulate *ac*-voltage magnitude and frequency, as well as the *dc*-voltage magnitude via a distributed consensus approach, which can be augmented with an additional control objective such as active power consensus between *ac*-DGs and *dc*-DGs (and *ICs*) or operation cost minimization of the complete microgrid. In addition, the major findings of this Ph.D. project are highlighted below:

**Secondary variables restoration**

- As the research work demonstrated, the secondary variables modified by the primary control loop (droop control) in a hybrid *ac*/*dc*-microgrid can be simultaneously restored to their nominal values with a global distributed secondary control strategy.

- Due to the characteristics of each variable, it is possible to restore the frequency of all the *ac*-DGs in the *ac*-microgrid to the nominal value. On the other hand, it is possible to restore the average value of the voltages at each side of the hybrid *ac*/*dc*-microgrid to their nominal values, while the voltages in each *ac*-DG and *dc*-DG are spread within an acceptable range. The experimental and simulation tests carried out in this research effort exhibited a fast and smooth restoration of the variables mentioned above.

**Active power consensus**

- In this thesis, a new control algorithm to achieve active power consensus among the *ac*-DGs and *dc*-DGs in a hybrid *ac/dc*-microgrid has been proposed. Moreover, the control algorithm also achieves active power consensus among the *ICs*, avoiding circulating currents in the *dc*-side. The control task is performed jointly with the secondary variables restoration.

- The novel control scheme is based on the consensus strategy from the multiagent theory, and therefore the DGs need to be communicated with, at least, one neighbouring unit. Several tests were carried out in a hybrid *ac/dc*-microgrid prototype (24kW), such as load-steps, connection/disconnection of DGs, and communication issues. Both experimental and simulation results demonstrated the effectiveness of the proposed control scheme.

**Real-time operation cost minimization**

- In this thesis, a new control algorithm to achieve an online minimization of the operation cost in a hybrid *ac/dc*-microgrid, by re-dispatching the *ac*-DGs and *dc*-DGs, has been proposed. Moreover, the control algorithm also re-dispatched the power transferred by the *ICs*, reducing the power losses in the *ac*-to *dc* (and vice versa) conversion. The control task is performed jointly with the secondary variables restoration.

- The novel control scheme is based on the consensus strategy from the multiagent theory, and therefore the DGs need to be communicated with, at least, one neighbouring unit. Several tests were carried out in a hybrid *ac/dc*-microgrid prototype. Simulation results demonstrated the effectiveness of the proposed control scheme.

**Reduced communication layer**

- The proposed control schemes consider a reduced communication layer, as each DG is communicating only with its neighbouring DGs. Due to the fact that *ICs* also participate in the communication layer, the secondary control strategies can be adapted to each side separately in case the *ICs* are not available, i.e, if there is not possible to transfer power from one side to the other side. Moreover, with the control scheme for operation cost minimization, this feature allows to maintain the *ICs* operating within limits by including them as constraints in the optimization problem, without affecting neither the secondary variables restoration nor the operation cost minimization.

**Analytical closed-loop model**

- An analytical model of the closed-loop system of a hybrid *ac/dc*-microgrid with the proposed consensus-based secondary control strategies was derived for analyzing small-signal stability and tuning of the parameters of proposed controllers. The models were derived with the hybrid *ac/dc*-microgrid as a single entity, considering the interaction of the *ac*-DGs and *dc*-DGs via the power transfer through the *IC*.

## 9.2 Future Work

The following are some interesting topics in which further research can be undertaken to extend the scope of this project:

- Additional objective functions could be included in the optimization problem. For example, an energy management system could be formulated in the hybrid *ac/dc*-microgrid: energy storage systems with renewable energies could be added to the objective function.
- Further stability analyses could be performed to the hybrid *ac/dc*-microgrid with the proposed controllers (e.g., large-signal stability).
- Different methodologies for improving the tuning of the parameters could be proposed.
- The theoretical stability limits for the parameters of the controllers found with the small-signal model could be experimentally tested.

## 9.3 Publications

The details of the publications from the work developed during this project and other contributions to papers related to microgrids are listed in the following.

### 9.3.1 Papers related to this Ph.D. Project

**Journal Papers**

1. **E. Espina**, R. Cárdenas-Dobson, J. W. Simpson-Porco, D. Sáez and M. Kazerani, "A Consensus-Based Secondary Control Strategy for Hybrid ac/dc Microgrids with Experimental Validation," in IEEE Transactions on Power Electronics, doi: 10.1109/TPEL.2020.3031539.
2. **E. Espina**, J. Llanos, C. Burgos-Mellado, R. Cárdenas-Dobson, M. Martínez-Gómez and D. Sáez, "Distributed Control Strategies for Microgrids: An Overview," in IEEE Access, vol. 8, pp. 193412-193448, 2020, doi: 10.1109/ACCESS.2020.3032378.
3. **E. Espina**, R. Cárdenas-Dobson, M. Espinoza-B., C. Burgos-Mellado and D. Sáez, "Cooperative Regulation of Imbalances in Three-Phase Four-Wire Microgrids Using Single-Phase Droop Control and Secondary Control Algorithms," in IEEE Transactions on Power Electronics, vol. 35, no. 2, pp. 1978-1992, Feb. 2020, doi: 10.1109/TPEL.2019.2917653.
4. C. Burgos-Mellado, J. Llanos, **E. Espina**, D. Sáez, R. Cárdenas, M. Sumner, A. Watson, "Single-Phase Consensus-Based Control for Regulating Voltage and Sharing Unbalanced Currents in 3-Wire Isolated AC Microgrids," in IEEE Access, vol. 8, pp. 164882-164898, 2020, doi: 10.1109/ACCESS.2020.3022488.

**Conference Papers**

5. **E. Espina**, R. Cárdenas-Dobson, D. Saez, J. W. Simpson-Porco, M. Kazerani, J. Gómez, A. Navas, "Experimental Performance Evaluation of a Distributed Secondary Control Strategy for Hybrid *ac/dc*-Microgrids in the event of Communication Loss/Delay," 2021 23rd European Conference on Power Electronics and Applications (EPE'21 ECCE Europe), Ghent, Belgium, 2021

6. **E. Espina**, C. Burgos-Mellado, J. Gómez, J. Llanos, E. Rute, A. Navas, M. Martínez-Gómez, R. Cárdenas, D. Sáez, "Experimental Hybrid AC/DC-Microgrid Prototype for Laboratory Research," 2020 22nd European Conference on Power Electronics and Applications (EPE'20 ECCE Europe), Lyon, France, 2020, pp. 1-9, doi: 10.23919/EPE20ECCEEurope43536.2020.9215751.

7. **E. Espina**, R. Cárdenas, F. Donoso, M. Urrutia and M. Espinoza, "A Novel Distributed Secondary Control Strategy Applied to Hybrid AC/DC Microgrids," 2019 21st European Conference on Power Electronics and Applications (EPE '19 ECCE Europe), Genova, Italy, 2019, pp. P.1-P.9, doi: 10.23919/EPE.2019.8915135.

### 9.3.2 Participation in other publications

**Journal Papers**

8. M. Espinoza, R. Cárdenas, J. Clare, D. Soto-Sánchez, M. Díaz, **E. Espina**, "An Integrated Converter and Machine Control System for MMC-Based High-Power Drives," in IEEE Transactions on Industrial Electronics, vol. 66, no. 3, pp. 2343-2354, March 2019, doi: 10.1109/TIE.2018.2801839.

**Conference Papers**

9. J. S. Gómez, J. Llanos, C. Burgos, **E. Espina**, and J. Rodriguez, "CooperativePower Conditioners for Microgrids in Mining," 2021 23rd European Conference on Power Electronics and Applications (EPE'21 ECCE Europe), Ghent, Belgium, 2021

10. A. Navas-Fonseca, C. Burgos-Mellado, J. Gómez, J. Llanos, **E. Espina**, D. Sáez, M. Sumner, "Distributed Predictive Control using Frequency and Voltage Soft Constraints in AC Microgrids including Economic Dispatch of Generation," 2021 47th Annual Conference of the IEEE Industrial Electronics Society (IECON), Toronto, Canada, 2021

11. A. Navas-Fonseca, C. Burgos-Mellado, **E. Espina**, E. Rute, J. Gómez, D. Sáez, M. Sumner, "Distributed Predictive Secondary Control for Voltage Restoration and Economic Dispatch of Generation for DC Microgrids," the 4th IEEE International Conference on DC Microgrids (ICDCM), USA, 2021

12. **E. Espina**, M. Espinoza and R. Cárdenas, "Active power angle droop control per phase for unbalanced 4-wire microgrids," 2017 IEEE Southern Power Electronics Conference (SPEC), Puerto Varas, 2017, pp. 1-6, doi: 10.1109/SPEC.2017.8333637.

13. M. Malhue, M. Díaz, F. Rojas, **E. Espina** and R. Cárdenas, "A Parallel Fast Delayed Signal Cancellation PLL for Unbalanced and Distorted Grid Applications," 2019 IEEE CHILEAN Conference on Electrical, Electronics Engineering, Information and Communication Technologies (CHILECON), Valparaiso, Chile, 2019, pp. 1-6, doi: 10.1109/CHILECON47746.2019.8988085.

14. F.Donoso, A.Mora, M.Espinoza, M.Urrutia, **E. Espina** and R.Cárdenas, "Predictive-based Modulation Schemes for the Hybrid Modular Multilevel Converter," 2019 21st European Conference on Power Electronics and Applications (EPE '19 ECCE Europe), Genova, Italy, 2019, pp. P.1-P.9, doi: 10.23919/EPE.2019.8914876.

15. M. Espinoza, R. Cárdenas, M. Díaz, F. Donoso, **E. Espina**, A. Letelier, A. Mora, "Effects of a Variable dc-Port Voltage on the Half-Bridge-Based Modular Multilevel Converter for Drive Systems," 2019 21st European Conference on Power Electronics and Applications (EPE '19 ECCE Europe), Genova, Italy, 2019, pp. P.1-P.10, doi: 10.23919/EPE.2019.8915500.

16. M. Urrutia, F. Donoso, A. Mora, **E. Espina**, M. Díaz and R. Cárdenas, "Enhanced Circulating-current Control for the Modular Multilevel Matrix Converter Based on Model Predictive Control," 2019 21st European Conference on Power Electronics and Applications (EPE '19 ECCE Europe), Genova, Italy, 2019, pp. 1-9.

17. M. Espinoza, F. Donoso, **E. Espina**, M. Díaz and R. Cárdenas, "A Novel Control Strategy for Modular Multilevel-Based Drives Considering the System Operating Point," 2018 20th European Conference on Power Electronics and Applications (EPE'18 ECCE Europe), Riga, 2018, pp. P.1-P.10.

18. M. Espinoza, M. Díaz, **E. Espina**, C. M. Hackl and R. Cárdenas, "Control strategies for modular multilevel converters driving cage machines," 2017 IEEE Southern Power Electronics Conference (SPEC), Puerto Varas, 2017, pp. 1-6,
doi: 10.1109/SPEC.2017.8333628.

# Bibliography


[1] R. Lasseter, "Microgrids," in *2002 IEEE Power Engineering Society Winter Meeting. Conference Proceedings (Cat. No.02CH37309)*, vol. 1, pp. 305–308 vol.1, 2002.

[2] D. E. Olivares, A. Mehrizi-Sani, A. H. Etemadi, C. A. Cañizares, R. Iravani, M. Kazerani, A. H. Hajimiragha, O. Gomis-Bellmunt, M. Saeedifard, R. Palma-Behnke, G. A. Jiménez-Estévez, and N. D. Hatziargyriou, "Trends in microgrid control," *IEEE Transactions on Smart Grid*, vol. 5, no. 4, pp. 1905–1919, 2014.

[3] N. Hatziargyriou, H. Asano, R. Iravani, and C. Marnay, "Microgrids," *IEEE Power and Energy Magazine*, vol. 5, no. 4, pp. 78–94, 2007.

[4] H. Farhangi, "The path of the smart grid," *IEEE Power and Energy Magazine*, vol. 8, no. 1, pp. 18–28, 2010.

[5] J. M. Guerrero, J. C. Vasquez, J. Matas, L. G. de Vicuna, and M. Castilla, "Hierarchical control of droop-controlled ac and dc microgrids—a general approach toward standardization," *IEEE Transactions on Industrial Electronics*, vol. 58, no. 1, pp. 158–172, 2011.

[6] N. Eghtedarpour and E. Farjah, "Power control and management in a hybrid ac/dc microgrid," *IEEE Transactions on Smart Grid*, vol. 5, no. 3, pp. 1494–1505, 2014.

[7] S. Parhizi, H. Lotfi, A. Khodaei, and S. Bahramirad, "State of the art in research on microgrids: A review," *IEEE Access*, vol. 3, pp. 890–925, 2015.

[8] X. Wang, J. M. Guerrero, Z. Chen, and F. Blaabjerg, "Distributed energy resources in grid interactive ac microgrids," in *The 2nd International Symposium on Power Electronics for Distributed Generation Systems*, pp. 806–812, 2010.

[9] O. Palizban and K. Kauhaniemi, "Hierarchical control structure in microgrids with distributed generation: Island and grid-connected mode," *Renewable and Sustainable Energy Reviews*, vol. 44, pp. 797–813, 04 2015.

[10] L. Che and M. Shahidehpour, "Dc microgrids: Economic operation and enhancement of resilience by hierarchical control," *IEEE Transactions on Smart Grid*, vol. 5, no. 5, pp. 2517–2526, 2014.

[11] T. Dragičević, X. Lu, J. C. Vasquez, and J. M. Guerrero, "Dc microgrids—part i: A

review of control strategies and stabilization techniques," *IEEE Transactions on Power Electronics*, vol. 31, no. 7, pp. 4876–4891, 2016.

[12] T. Dragičević, X. Lu, J. C. Vasquez, and J. M. Guerrero, "Dc microgrids—part ii: A review of power architectures, applications, and standardization issues," *IEEE Transactions on Power Electronics*, vol. 31, no. 5, pp. 3528–3549, 2016.

[13] D. Kumar, F. Zare, and A. Ghosh, "Dc microgrid technology: System architectures, ac grid interfaces, grounding schemes, power quality, communication networks, applications, and standardizations aspects," *IEEE Access*, vol. 5, pp. 12230–12256, 2017.

[14] F. Gao, R. Kang, J. Cao, and T. Yang, "Primary and secondary control in dc microgrids: a review," *Journal of Modern Power Systems and Clean Energy*, vol. 7, no. 2, pp. 227–242, 2019.

[15] J. M. Guerrero, P. C. Loh, T.-L. Lee, and M. Chandorkar, "Advanced control architectures for intelligent microgrids—part ii: Power quality, energy storage, and ac/dc microgrids," *IEEE Transactions on Industrial Electronics*, vol. 60, no. 4, pp. 1263–1270, 2013.

[16] X. Liu, P. Wang, and P. C. Loh, "A hybrid ac/dc microgrid and its coordination control," *IEEE Transactions on Smart Grid*, vol. 2, no. 2, pp. 278–286, 2011.

[17] F. Nejabatkhah and Y. W. Li, "Overview of power management strategies of hybrid ac/dc microgrid," *IEEE Transactions on Power Electronics*, vol. 30, no. 12, pp. 7072–7089, 2015.

[18] S. K. Sahoo, A. K. Sinha, and N. K. Kishore, "Control techniques in ac, dc, and hybrid ac–dc microgrid: A review," *IEEE Journal of Emerging and Selected Topics in Power Electronics*, vol. 6, no. 2, pp. 738–759, 2018.

[19] A. Gupta, S. Doolla, and K. Chatterjee, "Hybrid ac–dc microgrid: Systematic evaluation of control strategies," *IEEE Transactions on Smart Grid*, vol. 9, no. 4, pp. 3830–3843, 2018.

[20] J. A. Lopes, N. Hatziargyriou, J. Mutale, P. Djapic, and N. Jenkins, "Integrating distributed generation into electric power systems: A review of drivers, challenges and opportunities," *Electric Power Systems Research*, vol. 77, pp. 1189–1203, 07 2007.

[21] P. C. Loh, D. Li, Y. K. Chai, and F. Blaabjerg, "Autonomous Control of Interlinking Converter With Energy Storage in Hybrid AC-DC Microgrid," *IEEE Trans. Ind. Appl.*, vol. 49, pp. 1374–1382, May 2013.

[22] P. C. Loh, D. Li, Y. K. Chai, and F. Blaabjerg, "Autonomous operation of hybrid microgrid with ac and dc subgrids," *IEEE Transactions on Power Electronics*, vol. 28, no. 5, pp. 2214–2223, 2013.

[23] P. Wang, C. Jin, D. Zhu, Y. Tang, P. C. Loh, and F. H. Choo, "Distributed control for autonomous operation of a three-port ac/dc/ds hybrid microgrid," *IEEE Transactions*

*on Industrial Electronics*, vol. 62, no. 2, pp. 1279–1290, 2015.

[24] P. C. Loh, D. Li, Y. K. Chai, and F. Blaabjerg, "Hybrid ac–dc microgrids with energy storages and progressive energy flow tuning," *IEEE Transactions on Power Electronics*, vol. 28, no. 4, pp. 1533–1543, 2013.

[25] M. H. Cintuglu, T. Youssef, and O. A. Mohammed, "Development and application of a real-time testbed for multiagent system interoperability: A case study on hierarchical microgrid control," *IEEE Transactions on Smart Grid*, vol. 9, no. 3, pp. 1759–1768, 2018.

[26] E. Espina, J. Llanos, C. Burgos-Mellado, R. Cárdenas-Dobson, M. Martínez-Gómez, and D. Sáez, "Distributed control strategies for microgrids: An overview," *IEEE Access*, vol. 8, pp. 193412–193448, 2020.

[27] Q. Zhou, M. Shahidehpour, A. Paaso, S. Bahramirad, A. Alabdulwahab, and A. Abusorrah, "Distributed control and communication strategies in networked microgrids," *IEEE Communications Surveys Tutorials*, vol. 22, no. 4, pp. 2586–2633, 2020.

[28] E. Espina, R. Cárdenas, F. Donoso, M. Urrutia, and M. Espinoza, "A novel distributed secondary control strategy applied to hybrid ac/dc microgrids," in *2019 21st European Conference on Power Electronics and Applications (EPE '19 ECCE Europe)*, pp. P.1–P.9, 2019.

[29] E. Espina, C. Burgos-Mellado, J. S. Gomez, J. Llanos, E. Rute, A. Navas F., M. Martínez-Gómez, R. Cárdenas, and D. Sáez, "Experimental hybrid ac/dc-microgrid prototype for laboratory research," in *2020 22nd European Conference on Power Electronics and Applications (EPE'20 ECCE Europe)*, pp. 1–9, 2020.

[30] E. Espina, R. Cárdenas-Dobson, D. Sáez, J. Simpson-Porco, M. Kazerani, J. Gómez, and A. Navas, "Experimental performance evaluation of a distributed secondary control strategy for hybrid *ac/dc*-microgrids in the event of communication loss/delay," in *2021 23nd European Conference on Power Electronics and Applications (EPE'21 ECCE Europe)*, 2021.

[31] E. Espina, R. Cárdenas-Dobson, J. W. Simpson-Porco, D. Sáez, and M. Kazerani, "A consensus-based secondary control strategy for hybrid ac/dc microgrids with experimental validation," *IEEE Transactions on Power Electronics*, vol. 36, no. 5, pp. 5971–5984, 2021.

[32] E. Espina, R. Cárdenas-Dobson, M. Espinoza-B., C. Burgos-Mellado, and D. Sáez, "Cooperative regulation of imbalances in three-phase four-wire microgrids using single-phase droop control and secondary control algorithms," *IEEE Transactions on Power Electronics*, vol. 35, no. 2, pp. 1978–1992, 2020.

[33] C. Burgos-Mellado, J. Llanos, E. Espina, D. Sáez, R. Cárdenas, M. Sumner, and A. Watson, "Single-phase consensus-based control for regulating voltage and sharing unbalanced currents in 3-wire isolated ac microgrids," *IEEE Access*, vol. 8, pp. 164882–164898, 2020.

[34] J. Gómez, J. Llanos, C. Burgos-Mellado, E. Espina, and J. Rodríguez, "Cooperative-power conditioners for microgrids in mining," in *2021 23nd European Conference on Power Electronics and Applications (EPE'21 ECCE Europe)*, 2021.

[35] A. Navas-Fonseca, C. Burgos-Mellado, E. Espina, E. Rute, J. Gómez, D. Sáez, and M. Sumner, "Distributed predictive secondary control for voltage restoration and economic dispatch of generation for dc microgrids," in *The 4th IEEE International Conference on DC Microgrids (ICDCM), USA, 2021*, 2021.

[36] A. Navas-Fonseca, C. Burgos-Mellado, J. Gómez, J. Llanos, E. Espina, D. Sáez, and M. Sumner, "Distributed predictive control using frequency and voltage soft constraints in ac microgrids including economic dispatch of generation," in *2021 47th Annual Conference of the IEEE Industrial Electronics Society (IECON), Toronto, Canada, 2021*, 2021.

[37] M. Espinoza-B, R. Cárdenas, J. Clare, D. Soto-Sanchez, M. Díaz, E. Espina, and C. M. Hackl, "An integrated converter and machine control system for mmc-based high-power drives," *IEEE Transactions on Industrial Electronics*, vol. 66, no. 3, pp. 2343–2354, 2019.

[38] E. Espina, M. Espinoza, and R. Cárdenas, "Active power angle droop control per phase for unbalanced 4-wire microgrids," in *2017 IEEE Southern Power Electronics Conference (SPEC)*, pp. 1–6, 2017.

[39] M. Malhue, M. Díaz, F. Rojas, E. Espina, and R. Cardenas, "A parallel fast delayed signal cancellation pll for unbalanced and distorted grid applications," in *2019 IEEE CHILEAN Conference on Electrical, Electronics Engineering, Information and Communication Technologies (CHILECON)*, pp. 1–6, 2019.

[40] F. Donoso, A. Mora, M. Espinoza, M. Urrutia, E. Espina, and R. Cardenas, "Predictive-based modulation schemes for the hybrid modular multilevel converter," in *2019 21st European Conference on Power Electronics and Applications (EPE '19 ECCE Europe)*, pp. P.1–P.9, 2019.

[41] M. Espinoza, R. Cárdenas, M. Díaz, F. Donoso, E. Espina, A. Letelier, and A. Mora, "Effects of a variable dc-port voltage on the half-bridge-based modular multilevel converter for drive systems," in *2019 21st European Conference on Power Electronics and Applications (EPE '19 ECCE Europe)*, pp. P.1–P.10, 2019.

[42] M. Urrutia, F. Donoso, A. Mora, E. Espina, M. Díaz, and R. Cárdenas, "Enhanced circulating-current control for the modular multilevel matrix converter based on model predictive control," in *2019 21st European Conference on Power Electronics and Applications (EPE '19 ECCE Europe)*, pp. 1–9, 2019.

[43] M. Espinoza, F. Donoso, E. Espina, M. Díaz, and R. Cardenas, "A novel control strategy for modular multilevel-based drives considering the system operating point," in *2018 20th European Conference on Power Electronics and Applications (EPE'18 ECCE Europe)*, pp. P.1–P.10, 2018.

[44] M. Espinoza, M. Díaz, E. Espina, C. M. Hackl, and R. Cardenas, "Control strategies for modular multilevel converters driving cage machines," in *2017 IEEE Southern Power Electronics Conference (SPEC)*, pp. 1–6, 2017.

[45] M. Chandorkar, D. Divan, and R. Adapa, "Control of parallel connected inverters in standalone ac supply systems," *IEEE Transactions on Industry Applications*, vol. 29, no. 1, pp. 136–143, 1993.

[46] D. Shanxu, M. Yu, X. Jian, K. Yong, and C. Jian, "Parallel operation control technique of voltage source inverters in ups," in *Proceedings of the IEEE 1999 International Conference on Power Electronics and Drive Systems. PEDS'99 (Cat. No.99TH8475)*, vol. 2, pp. 883–887 vol.2, 1999.

[47] J. Guerrero, J. Matas, L. de Vicuna, N. Berbel, and J. Sosa, "Wireless-control strategy for parallel operation of distributed generation inverters," in *Proceedings of the IEEE International Symposium on Industrial Electronics, 2005. ISIE 2005.*, vol. 2, pp. 845–850 vol. 2, 2005.

[48] K. De Brabandere, B. Bolsens, J. Van den Keybus, A. Woyte, J. Driesen, and R. Belmans, "A voltage and frequency droop control method for parallel inverters," *IEEE Transactions on Power Electronics*, vol. 22, no. 4, pp. 1107–1115, 2007.

[49] N. Pogaku, M. Prodanovic, and T. C. Green, "Modeling, analysis and testing of autonomous operation of an inverter-based microgrid," *IEEE Transactions on Power Electronics*, vol. 22, no. 2, pp. 613–625, 2007.

[50] H. Nikkhajoei and R. H. Lasseter, "Distributed generation interface to the certs microgrid," *IEEE Transactions on Power Delivery*, vol. 24, no. 3, pp. 1598–1608, 2009.

[51] R. H. Lasseter, J. H. Eto, B. Schenkman, J. Stevens, H. Vollkommer, D. Klapp, E. Linton, H. Hurtado, and J. Roy, "Certs microgrid laboratory test bed," *IEEE Transactions on Power Delivery*, vol. 26, no. 1, pp. 325–332, 2011.

[52] M. Shahbazi and A. Khorsandi, "Chapter 10 - power electronic converters in microgrid applications," in *Microgrid* (M. S. Mahmoud, ed.), pp. 281–309, Butterworth-Heinemann, 2017.

[53] S. D'Arco and J. A. Suul, "Equivalence of virtual synchronous machines and frequency-droops for converter-based microgrids," *IEEE Transactions on Smart Grid*, vol. 5, no. 1, pp. 394–395, 2014.

[54] Y. Han, H. Li, P. Shen, E. A. A. Coelho, and J. M. Guerrero, "Review of active and reactive power sharing strategies in hierarchical controlled microgrids," *IEEE Transactions on Power Electronics*, vol. 32, no. 3, pp. 2427–2451, 2017.

[55] Y. Khayat, Q. Shafiee, R. Heydari, M. Naderi, T. Dragičević, J. W. Simpson-Porco, F. Dörfler, M. Fathi, F. Blaabjerg, J. M. Guerrero, and H. Bevrani, "On the secondary control architectures of ac microgrids: An overview," *IEEE Transactions on Power Electronics*, vol. 35, no. 6, pp. 6482–6500, 2020.

[56] F. Katiraei and M. Iravani, "Power management strategies for a microgrid with multiple distributed generation units," *IEEE Transactions on Power Systems*, vol. 21, no. 4, pp. 1821–1831, 2006.

[57] J. C. Vasquez, J. M. Guerrero, A. Luna, P. Rodriguez, and R. Teodorescu, "Adaptive droop control applied to voltage-source inverters operating in grid-connected and islanded modes," *IEEE Transactions on Industrial Electronics*, vol. 56, no. 10, pp. 4088–4096, 2009.

[58] Y. Li and Y. W. Li, "Power management of inverter interfaced autonomous microgrid based on virtual frequency-voltage frame," *IEEE Transactions on Smart Grid*, vol. 2, no. 1, pp. 30–40, 2011.

[59] J. Guerrero, L. de Vicuna, J. Matas, M. Castilla, and J. Miret, "A wireless controller to enhance dynamic performance of parallel inverters in distributed generation systems," *IEEE Transactions on Power Electronics*, vol. 19, no. 5, pp. 1205–1213, 2004.

[60] W. Yao, M. Chen, J. Matas, J. M. Guerrero, and Z. M. Qian, "Design and Analysis of the Droop Control Method for Parallel Inverters Considering the Impact of the Complex Impedance on the Power Sharing," *IEEE Trans. Ind. Electron.*, vol. 58, pp. 576–588, Feb 2011.

[61] J. M. Guerrero, J. C. Vasquez, J. Matas, J. L. Sosa, and L. Garcia de Vicuna, "Parallel operation of uninterruptible power supply systems in microgrids," in *2007 European Conference on Power Electronics and Applications*, pp. 1–9, 2007.

[62] Y. A.-R. I. Mohamed and E. F. El-Saadany, "Adaptive decentralized droop controller to preserve power sharing stability of paralleled inverters in distributed generation microgrids," *IEEE Transactions on Power Electronics*, vol. 23, no. 6, pp. 2806–2816, 2008.

[63] W. Haiyun, Z. Zuochun, Y. Qingfang, B. Wei, H. Guoqing, L. Guanghui, and F. Kaihui, "A hierarchical control of microgrid based on droop controlled voltage source converter," in *2013 IEEE PES Asia-Pacific Power and Energy Engineering Conference (APPEEC)*, pp. 1–4, 2013.

[64] C. Ahumada, R. Cárdenas, D. Sáez, and J. M. Guerrero, "Secondary control strategies for frequency restoration in islanded microgrids with consideration of communication delays," *IEEE Transactions on Smart Grid*, vol. 7, no. 3, pp. 1430–1441, 2016.

[65] Y. You, G. Wang, C.-h. Zhang, and J.-r. Lian, "An improved frequency control method for microgrid in islanded operation," in *2013 2nd International Symposium on Instrumentation and Measurement, Sensor Network and Automation (IMSNA)*, pp. 296–299, 2013.

[66] A. Raghami, M. T. Ameli, and M. Hamzeh, "Primary and secondary frequency control in an autonomous microgrid supported by a load-shedding strategy," in *4th Annual International Power Electronics, Drive Systems and Technologies Conference*, pp. 282–287, 2013.

[67] J. He, Y. W. Li, and F. Blaabjerg, "An enhanced islanding microgrid reactive power, imbalance power, and harmonic power sharing scheme," *IEEE Transactions on Power Electronics*, vol. 30, no. 6, pp. 3389–3401, 2015.

[68] M. Savaghebi, Q. Shafiee, J. C. Vasquez, and J. M. Guerrero, "Adaptive virtual impedance scheme for selective compensation of voltage unbalance and harmonics in microgrids," in *2015 IEEE Power Energy Society General Meeting*, pp. 1–5, 2015.

[69] Y. Zhu, B. Liu, F. Wang, F. Zhuo, and Y. Zhao, "A virtual resistance based reactive power sharing strategy for networked microgrid," in *2015 9th International Conference on Power Electronics and ECCE Asia (ICPE-ECCE Asia)*, pp. 1564–1572, 2015.

[70] H. Zeineldin, "A q-f droop curve for facilitating islanding detection of inverter-based distributed generation," *Power Electronics, IEEE Transactions on*, vol. 24, pp. 665 – 673, 04 2009.

[71] B. Johnson, R. Lasseter, F. Alvarado, and R. Adapa, "Expandable multiterminal dc systems based on voltage droop," *IEEE Transactions on Power Delivery*, vol. 8, no. 4, pp. 1926–1932, 1993.

[72] C. Jin, P. Wang, J. Xiao, Y. Tang, and F. H. Choo, "Implementation of Hierarchical Control in DC Microgrids," *IEEE Trans. Ind. Electron.*, vol. 61, pp. 4032–4042, Aug 2014.

[73] Q. Shafiee, T. Dragičević, J. C. Vasquez, and J. M. Guerrero, "Hierarchical control for multiple dc-microgrids clusters," *IEEE Transactions on Energy Conversion*, vol. 29, no. 4, pp. 922–933, 2014.

[74] L. Xu and D. Chen, "Control and operation of a dc microgrid with variable generation and energy storage," *IEEE Transactions on Power Delivery*, vol. 26, no. 4, pp. 2513–2522, 2011.

[75] B. Wang, M. Sechilariu, and F. Locment, "Intelligent dc microgrid with smart grid communications: Control strategy consideration and design," *IEEE Transactions on Smart Grid*, vol. 3, no. 4, pp. 2148–2156, 2012.

[76] X. Lu, J. M. Guerrero, K. Sun, and J. C. Vasquez, "An improved droop control method for dc microgrids based on low bandwidth communication with dc bus voltage restoration and enhanced current sharing accuracy," *IEEE Transactions on Power Electronics*, vol. 29, no. 4, pp. 1800–1812, 2014.

[77] T. Dragičević, J. M. Guerrero, J. C. Vasquez, and D. Škrlec, "Supervisory control of an adaptive-droop regulated dc microgrid with battery management capability," *IEEE Transactions on Power Electronics*, vol. 29, no. 2, pp. 695–706, 2014.

[78] H.-H. Huang, C.-Y. Hsieh, J.-Y. Liao, and K.-H. Chen, "Adaptive droop resistance technique for adaptive voltage positioning in boost dc–dc converters," *IEEE Transactions on Power Electronics*, vol. 26, no. 7, pp. 1920–1932, 2011.

[79] S. Augustine, M. K. Mishra, and N. Lakshminarasamma, "Adaptive droop control strategy for load sharing and circulating current minimization in low-voltage standalone dc microgrid," *IEEE Transactions on Sustainable Energy*, vol. 6, no. 1, pp. 132–141, 2015.

[80] M. Baharizadeh, H. Karshenas, and J. Guerrero, "New control strategy of interlinking converters as the key segment of hybrid ac-dc microgrids," *IET Generation, Transmission & Distribution*, vol. 10, 03 2016.

[81] X. Li, L. Guo, Y. Li, Z. Guo, C. Hong, Y. Zhang, and C. Wang, "A unified control for the dc–ac interlinking converters in hybrid ac/dc microgrids," *IEEE Transactions on Smart Grid*, vol. 9, no. 6, pp. 6540–6553, 2018.

[82] S. Peyghami, H. Mokhtari, and F. Blaabjerg, "Autonomous operation of a hybrid ac/dc microgrid with multiple interlinking converters," *IEEE Trans. Smart Grid*, vol. 9, pp. 6480–6488, Nov 2018.

[83] F. Lewis, H. Zhang, K. Movric, and A. Das, *Cooperative Control of Multi-Agent Systems: Optimal and Adaptive Design Approaches*. Springer International Publishing, Jan 2014.

[84] A. Bidram, V. Nasirian, A. Davoudi, and F. Lewis, *Cooperative Synchronization in Distributed Microgrid Control*. Springer International Publishing, Jan 2017.

[85] J. W. Simpson-Porco, Q. Shafiee, F. Dörfler, J. C. Vásquez, J. M. Guerrero, and F. Bullo, "Secondary Frequency and Voltage Control of Islanded Microgrids via Distributed Averaging," *IEEE Trans. Ind. Electron.*, vol. 62, pp. 7025–7038, Nov 2015.

[86] C. Godsil and G. Royle, *Algebraic Graph Theory*, vol. 207 of *Graduate Texts in Mathematics.* volume 207 of Graduate Texts in Mathematics. Springer, 2001.

[87] Q. Shafiee, J. C. Vasquez, and J. M. Guerrero, "Distributed secondary control for islanded microgrids - a networked control systems approach," in *IECON 2012 - 38th Annual Conference on IEEE Industrial Electronics Society*, pp. 5637–5642, 2012.

[88] Q. Shafiee, J. M. Guerrero, and J. C. Vasquez, "Distributed secondary control for islanded microgrids—a novel approach," *IEEE Transactions on Power Electronics*, vol. 29, no. 2, pp. 1018–1031, 2014.

[89] A. Bidram, A. Davoudi, F. Lewis, and Z. Qu, "Secondary control of microgrids based on distributed cooperative control of multi-agent systems," *IET Generation Transmission & Distribution*, vol. 7, pp. 822–831, 08 2013.

[90] F. Guo, C. Wen, J. Mao, and Y.-D. Song, "Distributed secondary voltage and frequency restoration control of droop-controlled inverter-based microgrids," *IEEE Transactions on Industrial Electronics*, vol. 62, no. 7, pp. 4355–4364, 2015.

[91] A. Bidram, A. Davoudi, F. L. Lewis, and J. M. Guerrero, "Distributed cooperative secondary control of microgrids using feedback linearization," *IEEE Transactions on*

*Power Systems*, vol. 28, no. 3, pp. 3462–3470, 2013.

[92] F. Dörfler, J. W. Simpson-Porco, and F. Bullo, "Breaking the hierarchy: Distributed control and economic optimality in microgrids," *IEEE Transactions on Control of Network Systems*, vol. 3, no. 3, pp. 241–253, 2016.

[93] L. Meng, X. Zhao, F. Tang, M. Savaghebi, T. Dragicevic, J. C. Vasquez, and J. M. Guerrero, "Distributed voltage unbalance compensation in islanded microgrids by using a dynamic consensus algorithm," *IEEE Transactions on Power Electronics*, vol. 31, no. 1, pp. 827–838, 2016.

[94] Q. Shafiee, V. Nasirian, J. C. Vasquez, J. M. Guerrero, and A. Davoudi, "A multi-functional fully distributed control framework for ac microgrids," *IEEE Transactions on Smart Grid*, vol. 9, no. 4, pp. 3247–3258, 2018.

[95] Q. Li, C. Peng, M. Wang, M. Chen, J. M. Guerrero, and D. Abbott, "Distributed secondary control and management of islanded microgrids via dynamic weights," *IEEE Transactions on Smart Grid*, vol. 10, no. 2, pp. 2196–2207, 2019.

[96] J. Zhou, M.-J. Tsai, and P.-T. Cheng, "Consensus-based cooperative droop control for accurate reactive power sharing in islanded ac microgrid," *IEEE Journal of Emerging and Selected Topics in Power Electronics*, vol. 8, no. 2, pp. 1108–1116, 2020.

[97] G. Lou, W. Gu, Y. Xu, M. Cheng, and W. Liu, "Distributed mpc-based secondary voltage control scheme for autonomous droop-controlled microgrids," in *2017 IEEE Power Energy Society General Meeting*, pp. 1–1, 2017.

[98] R. Heydari, T. Dragicevic, and F. Blaabjerg, "High-bandwidth secondary voltage and frequency control of vsc-based ac microgrid," *IEEE Transactions on Power Electronics*, vol. 34, no. 11, pp. 11320–11331, 2019.

[99] J. S. Gómez, D. Sáez, J. W. Simpson-Porco, and R. Cárdenas, "Distributed predictive control for frequency and voltage regulation in microgrids," *IEEE Trans. Smart Grid*, vol. 11, pp. 1319–1329, March 2020.

[100] X. Lu, X. Yu, J. Lai, Y. Wang, and J. M. Guerrero, "A novel distributed secondary coordination control approach for islanded microgrids," *IEEE Transactions on Smart Grid*, vol. 9, no. 4, pp. 2726–2740, 2018.

[101] A. Bidram, A. Davoudi, and F. L. Lewis, "Finite-time frequency synchronization in microgrids," in *2014 IEEE Energy Conversion Congress and Exposition (ECCE)*, pp. 2648–2654, 2014.

[102] S. Zuo, A. Davoudi, Y. Song, and F. L. Lewis, "Distributed finite-time voltage and frequency restoration in islanded ac microgrids," *IEEE Transactions on Industrial Electronics*, vol. 63, no. 10, pp. 5988–5997, 2016.

[103] N. M. Dehkordi, N. Sadati, and M. Hamzeh, "Distributed robust finite-time secondary voltage and frequency control of islanded microgrids," *IEEE Transactions on Power*

*Systems*, vol. 32, no. 5, pp. 3648–3659, 2017.

[104] C. Li, M. Savaghebi, J. C. Vasquez, and J. M. Guerrero, "Multiagent based distributed control for operation cost minimization of droop controlled ac microgrid using incremental cost consensus," in *2015 17th European Conference on Power Electronics and Applications (EPE'15 ECCE-Europe)*, pp. 1–9, 2015.

[105] G. Chen and E. Feng, "Distributed secondary control and optimal power sharing in microgrids," *IEEE/CAA Journal of Automatica Sinica*, vol. 2, no. 3, pp. 304–312, 2015.

[106] G. Chen and Z. Zhao, "Delay effects on consensus-based distributed economic dispatch algorithm in microgrid," *IEEE Transactions on Power Systems*, vol. 33, no. 1, pp. 602–612, 2018.

[107] G. Chen and Z. Guo, "Distributed secondary and optimal active power sharing control for islanded microgrids with communication delays," *IEEE Transactions on Smart Grid*, vol. 10, no. 2, pp. 2002–2014, 2019.

[108] J. Llanos, D. E. Olivares, J. W. Simpson-Porco, M. Kazerani, and D. Sáez, "A novel distributed control strategy for optimal dispatch of isolated microgrids considering congestion," *IEEE Transactions on Smart Grid*, vol. 10, no. 6, pp. 6595–6606, 2019.

[109] A. Wang and W. Liu, "Distributed incremental cost consensus-based optimization algorithms for economic dispatch in a microgrid," *IEEE Access*, vol. 8, pp. 12933–12941, 2020.

[110] M. Savaghebi, A. Jalilian, J. C. Vasquez, and J. M. Guerrero, "Secondary control scheme for voltage unbalance compensation in an islanded droop-controlled microgrid," *IEEE Transactions on Smart Grid*, vol. 3, no. 2, pp. 797–807, 2012.

[111] L. Meng, F. Tang, M. Savaghebi, J. Vasquez, and J. Guerrero, "Tertiary control of voltage unbalance compensation for optimal power quality in islanded microgrids," in *2016 IEEE Power and Energy Society General Meeting (PESGM)*, pp. 1–1, 2016.

[112] C. Burgos-Mellado, J. J. Llanos, R. Cárdenas, D. Sáez, D. E. Olivares, M. Sumner, and A. Costabeber, "Distributed control strategy based on a consensus algorithm and on the conservative power theory for imbalance and harmonic sharing in 4-wire microgrids," *IEEE Transactions on Smart Grid*, vol. 11, no. 2, pp. 1604–1619, 2020.

[113] C. Li, E. A. A. Coelho, T. Dragicevic, J. M. Guerrero, and J. C. Vasquez, "Multiagent-based distributed state of charge balancing control for distributed energy storage units in ac microgrids," *IEEE Transactions on Industry Applications*, vol. 53, no. 3, pp. 2369–2381, 2017.

[114] Y. Guan, L. Meng, C. Li, J. C. Vasquez, and J. M. Guerrero, "A dynamic consensus algorithm to adjust virtual impedance loops for discharge rate balancing of ac microgrid energy storage units," *IEEE Transactions on Smart Grid*, vol. 9, no. 5, pp. 4847–4860, 2018.

[115] A. Maknouninejad, Z. Qu, F. L. Lewis, and A. Davoudi, "Optimal, nonlinear, and distributed designs of droop controls for dc microgrids," *IEEE Transactions on Smart Grid*, vol. 5, no. 5, pp. 2508–2516, 2014.

[116] V. Nasirian, A. Davoudi, F. L. Lewis, and J. M. Guerrero, "Distributed adaptive droop control for dc distribution systems," *IEEE Transactions on Energy Conversion*, vol. 29, no. 4, pp. 944–956, 2014.

[117] V. Nasirian, S. Moayedi, A. Davoudi, and F. L. Lewis, "Distributed cooperative control of dc microgrids," *IEEE Transactions on Power Electronics*, vol. 30, no. 4, pp. 2288–2303, 2015.

[118] V. Nasirian, A. Davoudi, F. Lewis, and J. Guerrero, "Distributed adaptive droop control for dc distribution systems," in *2016 IEEE Power and Energy Society General Meeting (PESGM)*, pp. 1–1, 2016.

[119] P. Wang, X. Lu, X. Yang, W. Wang, and D. Xu, "An improved distributed secondary control method for dc microgrids with enhanced dynamic current sharing performance," *IEEE Transactions on Power Electronics*, vol. 31, no. 9, pp. 6658–6673, 2016.

[120] B. Fan, S. Guo, J. Peng, Q. Yang, W. Liu, and L. Liu, "A consensus-based algorithm for power sharing and voltage regulation in dc microgrids," *IEEE Transactions on Industrial Informatics*, vol. 16, no. 6, pp. 3987–3996, 2020.

[121] S. Peyghami, H. Mokhtari, P. C. Loh, P. Davari, and F. Blaabjerg, "Distributed primary and secondary power sharing in a droop-controlled lvdc microgrid with merged ac and dc characteristics," *IEEE Transactions on Smart Grid*, vol. 9, no. 3, pp. 2284–2294, 2018.

[122] C. Li, J. C. Vasquez, and J. M. Guerrero, "Convergence analysis of distributed control for operation cost minimization of droop controlled dc microgrid based on multiagent," in *2016 IEEE Applied Power Electronics Conference and Exposition (APEC)*, pp. 3459–3464, 2016.

[123] Z. Cheng, Z. Li, J. Liang, J. Gao, J. Si, and S. Li, "Distributed economic power dispatch and bus voltage control for droop-controlled dc microgrids," *Energies*, vol. 12, p. 1400, Apr 2019.

[124] M. Zaery, E. M. Ahmed, M. Orabi, and M. Youssef, "Operational cost reduction based on distributed adaptive droop control technique in dc microgrids," in *2017 IEEE Energy Conversion Congress and Exposition (ECCE)*, pp. 2638–2644, 2017.

[125] J. Hu, J. Duan, H. Ma, and M.-Y. Chow, "Distributed adaptive droop control for optimal power dispatch in dc microgrid," *IEEE Transactions on Industrial Electronics*, vol. 65, no. 1, pp. 778–789, 2018.

[126] S. Moayedi and A. Davoudi, "Unifying distributed dynamic optimization and control of islanded dc microgrids," *IEEE Transactions on Power Electronics*, vol. 32, no. 3, pp. 2329–2346, 2017.

[127] H. Han, H. Wang, Y. Sun, J. Yang, and Z. Liu, "A distributed control scheme on cost optimization under communication delays for dc microgrids," *IET Generation, Transmission & Distribution*, vol. 11, 07 2017.

[128] Z. Wang, W. Wu, and B. Zhang, "A distributed control method with minimum generation cost for dc microgrids," *IEEE Transactions on Energy Conversion*, vol. 31, no. 4, pp. 1462–1470, 2016.

[129] F. Guo, C. Wen, J. Mao, and Y.-D. Song, "Distributed economic dispatch for smart grids with random wind power," *IEEE Transactions on Smart Grid*, vol. 7, no. 3, pp. 1572–1583, 2016.

[130] T. R. Oliveira, W. W. A. Gonçalves Silva, and P. F. Donoso-Garcia, "Distributed secondary level control for energy storage management in dc microgrids," *IEEE Transactions on Smart Grid*, vol. 8, no. 6, pp. 2597–2607, 2017.

[131] R. Zhang, B. Hredzak, and T. Morstyn, "Distributed control with virtual capacitance for the voltage restorations, state of charge balancing, and load allocations of heterogeneous energy storages in a dc datacenter microgrid," *IEEE Transactions on Energy Conversion*, vol. 34, no. 3, pp. 1296–1308, 2019.

[132] R. Zhang and B. Hredzak, "Distributed finite-time multiagent control for dc microgrids with time delays," *IEEE Transactions on Smart Grid*, vol. 10, no. 3, pp. 2692–2701, 2019.

[133] S. Chen, X. Lu, and Q. Gong, "Soc balance and economic dispatch using distributed cooperative control for distributed energy storage systems in dc microgrid applications," in *IECON 2020 The 46th Annual Conference of the IEEE Industrial Electronics Society*, pp. 3371–3376, 2020.

[134] H.-J. Yoo, T.-T. Nguyen, and H.-M. Kim, "Consensus-based distributed coordination control of hybrid ac/dc microgrids," *IEEE Transactions on Sustainable Energy*, vol. 11, no. 2, pp. 629–639, 2020.

[135] J.-W. Chang, G.-S. Lee, S.-I. Moon, and P.-I. Hwang, "A novel distributed control method for interlinking converters in an islanded hybrid ac/dc microgrid," *IEEE Transactions on Smart Grid*, pp. 1–1, 2021.

[136] N. Ahmad Khan, "Power loss modeling of isolated ac/dc converter," Master's thesis, KTH, Electrical Energy Conversion, 2012.

[137] Z. Li, Z. Duan, G. Chen, and L. Huang, "Consensus of multiagent systems and synchronization of complex networks: A unified viewpoint," *IEEE Transactions on Circuits and Systems I: Regular Papers*, vol. 57, no. 1, pp. 213–224, 2010.

[138] D. Spanos, R. Olfati-saber, and R. Murray, "Dynamic consensus on mobile networks," *Proc. 16th Int. Fed. Autom. Control, Prague, Czech Republic*, 01 2005.

[139] K. E. Adetunji, I. W. Hofsajer, A. M. Abu-Mahfouz, and L. Cheng, "A review of meta-

heuristic techniques for optimal integration of electrical units in distribution networks," *IEEE Access*, vol. 9, pp. 5046–5068, 2021.

[140] P. Kundur and N. Balu, *Power System Stability and Control*. EPRI power system engineering series, McGraw-Hill, 1994.

[141] I. Serban, S. Céspedes, C. Marinescu, C. A. Azurdia-Meza, J. S. Gómez, and D. S. Hueichapan, "Communication requirements in microgrids: A practical survey," *IEEE Access*, vol. 8, pp. 47694–47712, 2020.

# APPENDICES

# Appendix A

# Closed-loop model for a hybrid *ac*/*dc*-microgrid with the Power-sharing Strategy

In this Appendix, the procedure for obtaining the closed-loop model for the microgrid presented in Chapter 5 is presented. This model is also utilized for performing a small-signal analysis of the consensus-based distributed control strategy proposed in Chapter 3 for power-sharing.

Due to the primary purpose for obtaining the closed-loop model of the consensus-based distributed secondary control strategy proposed for power-sharing in a hybrid *ac*/*dc*-microgrid, the following simplifications were considered since their dynamics are much faster than that of the studied controllers:

- The inner control loop (voltage/current controllers) is not considered.
- The modulation of the converters is not considered.
- The switching of the switching devices is not considered.

Appendix A is organized as follows: Section A.1 presents the closed-loop model for the *ac*-microgrid, while the closed-loop model for the *dc*-microgrid is depicted in Section A.2. The closed-loop model for the *IC* is presented in Section A.3.

## A.1 Closed-loop model for the *ac*-microgrid

In this Section, the closed-loop model for the *ac*-microgrid is obtained, including the topology and the controllers' characteristics.

### A.1.1 Power flow in the *ac*-microgrid

The topology of the *ac*-microgrid is re-presented in Fig. A.1. The set of *ac*-DGs are labelled as $\mathbb{N}_{\text{ac}} = \{1, \ldots, n\}$. Further details of the topology can be found in Section 5.2.

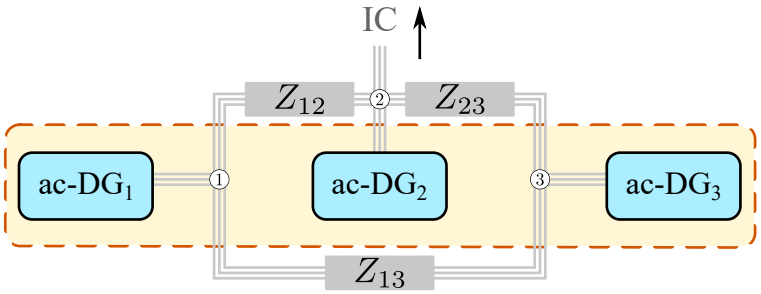


Figure A.1: Topology of the *ac*-microgrid.

The power flows between buses i and $j$ in the *ac*-microgrid $\forall \text{i}, j \in \mathbb{N}_{\text{ac}}$, are given by:

$$p_{\text{ac}-\text{i}j} = \frac{1}{R_{\text{i}j}^2 + X_{\text{i}j}^2} \left[ R_{\text{i}j} E_{\text{i}}^2 - R_{\text{i}j} E_{\text{i}} E_j \cos\left(\theta_{\text{i}} - \theta_j\right) + X_{\text{i}j} E_{\text{i}} E_j \sin\left(\theta_{\text{i}} - \theta_j\right) \right] \tag{A.1a}$$

$$q_{\text{ac}-\text{i}j} = \frac{1}{R_{\text{i}j}^2 + X_{\text{i}j}^2} \left[ X_{\text{i}j} E_{\text{i}}^2 - X_{\text{i}j} E_{\text{i}} E_j \cos\left(\theta_{\text{i}} - \theta_j\right) - R_{\text{i}j} E_{\text{i}} E_j \sin\left(\theta_{\text{i}} - \theta_j\right) \right] \tag{A.1b}$$

where $p_{\text{ac}-\text{i}j}$ ($q_{\text{ac}-\text{i}j}$) is the active (reactive) power flow from bus i to bus $j$, $R_{\text{i}j}$ and $X_{\text{i}j}$ are characteristics for the line between the two buses, $E_{\text{i}}$ is the magnitude of the voltage at bus i, and $\theta_{\text{i}}$ is its angle.

On the other hand, the power injected to the bus i is given by:

$$p_{\text{ac}-\text{i}} = p_{\text{D}\text{ac}-\text{i}} + \sum\nolimits_{j \in \mathbb{N}_{\text{ac}}} p_{\text{ac}-\text{i}j} \tag{A.2a}$$

$$q_{\text{ac}-\text{i}} = q_{\text{D}\text{ac}-\text{i}} + \sum\nolimits_{j \in \mathbb{N}_{\text{ac}}} q_{\text{ac}-\text{i}j} \tag{A.2b}$$

where $p_{\text{ac}-\text{i}}$ ($q_{\text{ac}-\text{i}}$) is the active (reactive) power injected by *ac*-DG$_{\text{i}}$ and $p_{\text{D}\text{ac}-\text{i}}$($q_{\text{D}\text{ac}-\text{i}}$) is the local active (reactive) power demanded at bus i.

Linearizing (A.2), in vector notation we have:

$$\Delta p_{\text{ac}} = G_1^{\text{ac}} \Delta E + G_2^{\text{ac}} \Delta\theta + G_0^{\text{ac}} \Delta P_{\text{IC}} \tag{A.3a}$$

$$\Delta q_{\text{ac}} = G_3^{\text{ac}} \Delta E + G_4^{\text{ac}} \Delta\theta \tag{A.3b}$$

where $p_{\text{ac}}, q_{\text{ac}} \in \mathbb{R}^n$ are the vectors of active and reactive power generation (respectively), $E \in \mathbb{R}^n$ is the vector of bus potentials, $\theta \in \mathbb{R}^n$ is the vector of bus angles, $P_{\text{IC}}$ is the power flow through the *IC*, which is positive when it flows from the *dc*-microgrid to the *ac*-microgrid. Matrices $G_1^{\text{ac}}, G_2^{\text{ac}}, G_3^{\text{ac}}, G_4^{\text{ac}} \in \mathbb{R}^{n \times n}$ are composed of partial derivatives of $p_{\text{ac}}$ and $q_{\text{ac}}$ with respect to $E$ and $\theta$, and depend on both the operating point $(E^0, \theta^0)$ and the admittance matrix of the electrical system ($Y$). Finally, $G_0^{\text{ac}} = (0\ \text{-}1\ 0)^T$ is the vector describing the electrical connection of the *ac*-microgrid and the *IC*.

### A.1.2 Voltage reference

From (3.5a), the voltage reference for the i$^{th}$ *ac*-DG ($\forall \mathrm{i} \in \mathbb{N}_{\mathrm{ac}}$) is:

$$E_{\mathrm{i}} = E^* + N_{\mathrm{ac-i}} \cdot Q_{\mathrm{ac-i}} + \chi_{\mathrm{i}} \tag{A.4}$$

where $Q_{\mathrm{ac-i}}$ is the filtered reactive power generated by the i$^{th}$ *ac*-DG, and it is given by:

$$\begin{aligned} Q_{\mathrm{ac-i}} &= \frac{\omega_{c-\mathrm{i}}}{s + \omega_{c-\mathrm{i}}} q_{\mathrm{ac-i}} \\ \dot{Q}_{\mathrm{ac-i}} &= \omega_{c-\mathrm{i}} \left( q_{\mathrm{ac-i}} - Q_{\mathrm{ac-i}} \right) \end{aligned} \tag{A.5}$$

where $\omega_{c-\mathrm{i}}$ is the cutoff frequency for the low pass filter.

Now, linearizing (A.5), the following expression for $\Delta Q_{\mathrm{ac}}$ is obtained in vector notation:

$$\Delta \dot{Q}_{\mathrm{ac}} = [\omega_c] \Delta q_{\mathrm{ac}} - [\omega_c] \Delta Q_{\mathrm{ac}} \tag{A.6}$$

where $\omega_c \in \mathbb{R}^n$ is the vector of cutoff frequencies, and $[\omega_c] \in \mathbb{R}^{n \times n}$ denotes the diagonal matrix with $\omega_c$ on the diagonal. This notation is used in the rest of the Chapter for referring to diagonal matrices.

Replacing $\Delta q_{\mathrm{ac}}$ from (A.3b), we have:

$$\begin{aligned} \Delta \dot{Q}_{\mathrm{ac}} &= [\omega_c] \left( G_3^{\mathrm{ac}} \Delta E + G_4^{\mathrm{ac}} \Delta \theta \right) - [\omega_c] \Delta Q_{\mathrm{ac}} \\ \Delta \dot{Q}_{\mathrm{ac}} &= [\omega_c] G_3^{\mathrm{ac}} \Delta E + [\omega_c] G_4^{\mathrm{ac}} \Delta \theta - [\omega_c] \Delta Q_{\mathrm{ac}} \end{aligned} \tag{A.7}$$

Now, linearizing the expression for the voltage shown in (A.4), we obtain:

$$\Delta E = [N_{\mathrm{ac}}] \Delta Q_{\mathrm{ac}} + \Delta \chi \tag{A.8}$$

Replacing $\Delta E$ from (A.8) in (A.7), we have:

$$\begin{aligned} \Delta \dot{Q}_{\mathrm{ac}} &= [\omega_c] G_3^{\mathrm{ac}} \left( [N_{\mathrm{ac}}] \Delta Q_{\mathrm{ac}} + \Delta \chi \right) + [\omega_c] G_4^{\mathrm{ac}} \Delta \theta - [\omega_c] \Delta Q_{\mathrm{ac}} \\ \Delta \dot{Q}_{\mathrm{ac}} &= [\omega_c] \left( G_3^{\mathrm{ac}} [N_{\mathrm{ac}}] - I_n \right) \Delta Q_{\mathrm{ac}} + [\omega_c] G_3^{\mathrm{ac}} \Delta \chi + [\omega_c] G_4^{\mathrm{ac}} \Delta \theta \\ \Delta \dot{Q}_{\mathrm{ac}} &= G_5^{\mathrm{ac}} \Delta Q_{\mathrm{ac}} + G_6^{\mathrm{ac}} \Delta \chi + G_7^{\mathrm{ac}} \Delta \theta \end{aligned} \tag{A.9}$$

Equation (A.9) corresponds to the state equation for the state variables $\Delta Q_{\mathrm{ac}}$.

### A.1.3 Frequency reference

From (3.4a), the frequency reference for the i$^{th}$ *ac*-DG ($\forall \mathrm{i} \in \mathbb{N}_{\mathrm{ac}}$) is:

$$\dot{\theta}_{\mathrm{i}} = \omega_{\mathrm{i}} = \omega^* + M_{\mathrm{ac-i}} P_{\mathrm{ac-i}} + \psi_{\mathrm{i}} \tag{A.10}$$

where $\Delta P_{\mathrm{ac}}$ is the filtered active power generated by the i$^{th}$ *ac*-DG, and it is given by:

$$\begin{aligned} P_{\mathrm{ac-i}} &= \frac{\omega_{c-\mathrm{i}}}{s + \omega_{c-\mathrm{i}}} p_{\mathrm{ac-i}} \\ \dot{P}_{\mathrm{ac-i}} &= \omega_{c-\mathrm{i}} \left( p_{\mathrm{ac-i}} - P_{\mathrm{ac-i}} \right) \end{aligned} \tag{A.11}$$

Linearizing (A.11), the following expression for $\Delta P_{\text{ac}}$ is obtained in vector notation:

$$\Delta \dot{P}_{\text{ac}} = [\omega_c]\Delta p_{\text{ac}} - [\omega_c]\Delta P_{\text{ac}} \tag{A.12}$$

Replacing $\Delta p_{\text{ac}}$ from (A.3a), we have:

$$\begin{aligned}\Delta \dot{P}_{\text{ac}} &= [\omega_c]\left(G_1^{\text{ac}}\Delta E + G_2^{\text{ac}}\Delta\theta + G_0^{\text{ac}}\Delta P_{\text{IC}}\right) - [\omega_c]\Delta P_{\text{ac}} \\ \Delta \dot{P}_{\text{ac}} &= [\omega_c]G_1^{\text{ac}}\Delta E + [\omega_c]G_2^{\text{ac}}\Delta\theta + [\omega_c]G_0^{\text{ac}}\Delta P_{\text{IC}} - [\omega_c]\Delta P_{\text{ac}}\end{aligned} \tag{A.13}$$

Now, replacing $\Delta E$ from (A.8):

$$\begin{aligned}\Delta \dot{P}_{\text{ac}} &= [\omega_c]G_1^{\text{ac}}\left([N_{\text{ac}}]\Delta Q_{\text{ac}} + \Delta\chi\right) + [\omega_c]G_2^{\text{ac}}\Delta\theta + [\omega_c]G_0^{\text{ac}}\Delta P_{\text{IC}} - [\omega_c]\Delta P_{\text{ac}} \\ \Delta \dot{P}_{\text{ac}} &= [\omega_c]G_1^{\text{ac}}[N_{\text{ac}}]\Delta Q_{\text{ac}} + [\omega_c]G_1^{\text{ac}}\Delta\chi + [\omega_c]G_2^{\text{ac}}\Delta\theta + [\omega_c]G_0^{\text{ac}}\Delta P_{\text{IC}} - [\omega_c]\Delta P_{\text{ac}} \\ \Delta \dot{P}_{\text{ac}} &= G_9^{\text{ac}}\Delta Q_{\text{ac}} + G_{10}^{\text{ac}}\Delta\chi + G_{11}^{\text{ac}}\Delta\theta + G_{12}^{\text{ac}}\Delta P_{\text{IC}} + G_{13}^{\text{ac}}\Delta P_{\text{ac}}\end{aligned} \tag{A.14}$$

Equation (A.14) corresponds to the state equation for the state variables $\Delta P_{\text{ac}}$.

On the other hand, linearizing (A.10), we obtain:

$$\begin{aligned}\Delta \dot{\theta} &= \Delta\omega = [M_{\text{ac}}]\Delta P_{\text{ac}} + \Delta\psi \\ \Delta \dot{\theta} &= \Delta\omega = G_8^{\text{ac}}\Delta P_{\text{ac}} + \Delta\psi\end{aligned} \tag{A.15}$$

Equation (A.15) corresponds to the state equation for the state variables $\Delta\theta$.

### A.1.4 Frequency secondary control

From (3.4b), the frequency secondary controller for the i$^{th}$ *ac*-DG ($\forall \text{i} \in \mathbb{N}_{\text{ac}}$) is:

$$\dot{\psi}_{\text{i}} = -\sigma_{\text{i}}\left(\omega_{\text{i}} - \omega^*\right) - \sigma_{\text{i}}\sum_{j\in\mathbb{N}_{\text{ac}}} a_{\text{i}j}\left(P_{\text{ac}-\text{i}} - P_{\text{ac}-j}\right) - \sigma_{\text{i}}\sum_{j\in\mathbb{N}_{\text{dc}}} a_{\text{i}j}\left(P_{\text{ac}-\text{i}} - P_{\text{dc}-j}\right) \tag{A.16}$$

To obtain the small-signal model of this controller, it is necessary to remember the adjacency matrix, which is given by:

$$A = \begin{pmatrix} A_{\text{dc}} & A_{\text{dc}-\text{ac}} & A_{\text{dc}-\text{IC}} \\ A_{\text{ac}-\text{dc}} & A_{\text{ac}} & A_{\text{ac}-\text{IC}} \\ A_{\text{IC}-\text{dc}} & A_{\text{IC}-\text{ac}} & A_{\text{IC}} \end{pmatrix} \tag{A.17}$$

The adjacency matrix (**A**) is composed by 9 sub-matrices, which describe the following characteristics of the communication network of the hybrid *ac/dc*-microgrid:

- $A_{\mathrm{dc}}$ : Communication links between *dc*-DGs.
- $A_{\mathrm{dc-ac}}$ : Communication links between *dc*-DGs and *ac*-DGs.
- $A_{\mathrm{dc-IC}}$ : Communication links between *dc*-DGs and *ICs*.
- $A_{\mathrm{ac-dc}}$ : Communication links between *ac*-DGs and *dc*-DGs.
- $A_{\mathrm{ac}}$ : Communication links between *ac*-DGs.
- $A_{\mathrm{ac-IC}}$ : Communication links between *ac*-DGs and *ICs*.
- $A_{\mathrm{IC-dc}}$ : Communication links between *ICs* and *dc*-DGs.
- $A_{\mathrm{IC-ac}}$ : Communication links between *ICs* and *ac*-DGs.
- $A_{\mathrm{IC}}$ : Communication links between *ICs* (0, in this case is only one).

Therefore, to describe the communication network for this controller we must focus only in the communication links between *ac*-DGs and *dc*-DGs, i.e., in sub-matrices $A_{\mathrm{ac}}$ and $A_{\mathrm{ac-dc}}$.

The weighted in-degree ($\mathrm{d_i}$) of node $v_{\mathrm{i}}$ is defined in the literature as the $\mathrm{i}^{th}$ row sum of the adjacency matrix A, as follows:

$$\mathrm{d_i} = \sum\nolimits_{j=1}^{N} a_{\mathrm{i}j} \tag{A.18}$$

In this thesis, I define a **modified in-degree** to represent the interaction between elements within each sub-matrix. Thus, the modified in-degrees for node $v_{\mathrm{i}}$ are given by:

$$\mathrm{d}_{(\mathrm{ac-ac})-\mathrm{i}} = \sum\nolimits_{j\in\mathbb{N}_{\mathrm{ac}}} a_{\mathrm{i}j} = a_{\mathrm{i}1} + a_{\mathrm{i}2} + \cdots + a_{\mathrm{i}n} \tag{A.19a}$$

$$\mathrm{d}_{(\mathrm{ac-dc})-\mathrm{i}} = \sum\nolimits_{j\in\mathbb{N}_{\mathrm{dc}}} a_{\mathrm{i}j} = a_{\mathrm{i}1} + a_{\mathrm{i}2} + \cdots + a_{\mathrm{i}m} \tag{A.19b}$$

In vector notation, we have:

$$D_{\mathrm{ac-ac}} = \mathrm{d}iag(\mathrm{d}_{(\mathrm{ac-ac})-\mathrm{i}}) \tag{A.20a}$$

$$D_{\mathrm{ac-dc}} = \mathrm{d}iag(\mathrm{d}_{(\mathrm{ac-dc})-\mathrm{i}}) \tag{A.20b}$$

Additionally, the Laplacian matrix ($L_{\mathrm{ac}}$) for the *ac*-microgrid is defined as:

$$L_{\mathrm{ac}} = D_{\mathrm{ac-ac}} + D_{\mathrm{ac-dc}} - A_{\mathrm{ac-ac}} \tag{A.21}$$

Now, linearizing the controller from (A.16), we obtain:

$$\Delta\dot{\psi} = -[\sigma]\Delta\omega - [\sigma]L_{\mathrm{ac}}\frac{1}{S^{+}_{\mathrm{ac}}}\Delta P_{\mathrm{ac}} + [\sigma]A_{\mathrm{ac-dc}}\frac{1}{P^{+}_{\mathrm{dc}}}\Delta P_{\mathrm{dc}} \tag{A.22}$$

Considering the expression for $\Delta\omega$ from (A.15), we have:

$$\begin{aligned}
\Delta\dot{\psi} &= -[\sigma]\left(G^{\mathrm{ac}}_{8}\Delta P_{\mathrm{ac}} + \Delta\psi\right) - [\sigma]L_{\mathrm{ac}}\frac{1}{S^{+}_{\mathrm{ac}}}\Delta P_{\mathrm{ac}} + [\sigma]A_{\mathrm{ac-dc}}\frac{1}{P^{+}_{\mathrm{dc}}}\Delta P_{\mathrm{dc}} \\
\Delta\dot{\psi} &= -[\sigma]\left(G^{\mathrm{ac}}_{8} + L_{\mathrm{ac}}\frac{1}{S^{+}_{\mathrm{ac}}}\right)\Delta P_{\mathrm{ac}} - [\sigma]\Delta\psi + [\sigma]A_{\mathrm{ac-dc}}\frac{1}{P^{+}_{\mathrm{dc}}}\Delta P_{\mathrm{dc}} \\
\Delta\dot{\psi} &= G^{\mathrm{ac}}_{14}\Delta P_{\mathrm{ac}} + G^{\mathrm{ac}}_{15}\Delta\psi + G^{\mathrm{ac}}_{16}\Delta P_{\mathrm{dc}}
\end{aligned} \tag{A.23}$$

Equation (A.23) corresponds to the state equation for the state variables $\Delta\psi$.

### A.1.5 Voltage secondary control

From (3.5b), the voltage secondary controller for the i$^{th}$ *ac*-DG ($\forall \mathrm{i} \in \mathbb{N}_{\mathrm{ac}}$) is:

$$\dot{\chi}_{\mathrm{i}} = -\beta_{\mathrm{i}} \left(E_{\mathrm{i}} - E^{*}\right) - b_{\mathrm{i}} \sum\nolimits_{j \in \mathbb{N}_{\mathrm{ac}}} a_{\mathrm{i}j} \left(Q_{\mathrm{ac-i}} - Q_{\mathrm{ac}-j}\right) \tag{A.24}$$

Now, linearizing the controller and considering the modified in-degree explained before:

$$\Delta\dot{\chi} = -[\beta]\Delta E - [b]L_{\mathrm{ac}}^{'}\frac{1}{S_{\mathrm{ac}}^{+}}\Delta Q_{\mathrm{ac}} \tag{A.25}$$

where:

$$L_{\mathrm{ac}}^{'} = D_{\mathrm{ac-ac}} - A_{\mathrm{ac-ac}} \tag{A.26}$$

Replacing the expression for $\Delta E$ from (A.8), we obtain:

$$\begin{aligned}
\Delta\dot{\chi} &= -[\beta]\left([N_{\mathrm{ac}}]\Delta Q_{\mathrm{ac}} + \Delta\chi\right) - [b]L_{\mathrm{ac}}^{'}\frac{1}{S_{\mathrm{ac}}^{+}}\Delta Q_{\mathrm{ac}} \\
\Delta\dot{\chi} &= -\left([\beta][N_{\mathrm{ac}}] + [b]L_{\mathrm{ac}}^{'}\frac{1}{S_{\mathrm{ac}}^{+}}\right)\Delta Q_{\mathrm{ac}} - [\beta]\Delta\chi \\
\Delta\dot{\chi} &= G_{17}^{\mathrm{ac}}\Delta Q_{\mathrm{ac}} + G_{18}^{\mathrm{ac}}\Delta\chi
\end{aligned} \tag{A.27}$$

Equation (A.27) corresponds to the state equation for the state variables $\Delta\chi$.

## A.2 Closed-loop model for the *dc*-microgrid

In this Section, the closed-loop model for the *dc*-microgrid is obtained, including the topology and the controllers' characteristics.

### A.2.1 Power flow in the *dc*-microgrid

The topology of the *dc*-microgrid is re-presented in Fig. A.2. The set of *dc*-DGs are labelled as $\mathbb{N}_{\text{dc}} = \{n+1, \ldots, n+m\}$. Further details of the topology can be found in Section 5.3.

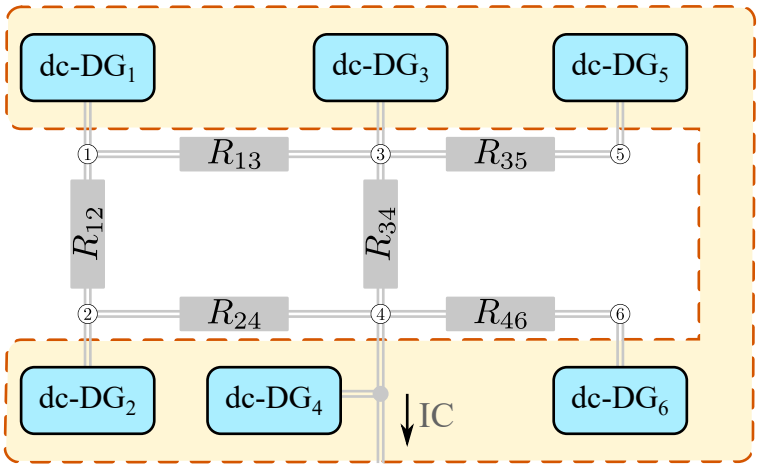


Figure A.2: Topology of the *dc*-microgrid.

The power injections for bus $j$ in the *dc*-microgrid $\forall j \in \mathbb{N}_{\text{dc}}$, are given by:

$$p_{\text{dc}-j} = p_{\text{Ddc}-j} + \sum\nolimits_{\text{i}\in\mathbb{N}_{\text{dc}}} p_{j\text{i}}, \quad \forall j \in \mathbb{N}_{\text{dc}} \tag{A.28}$$

where $p_{\text{Ddc}-j}$ is the local load at bus $j$, $p_{j\text{i}}$ is the power flow between buses $j$ and i, and $p_{\text{dc}-j}$ is the power generated by the $j^{th}$ *dc*-DG.

In vector notation, the power injections can be written as follows:

$$p_{\text{dc}} = [V]YV + G_0^{\text{dc}} P_{\text{IC}} \tag{A.29}$$

where $p_{\text{dc}} \in \mathbb{R}^m$ is the vector of power generation, $V \in \mathbb{R}^m$ is the vector of bus potentials, $Y \in \mathbb{R}^{m\times m}$ is the admittance matrix, $P_{\text{IC}}$ is the power in the *IC* and $G_0^{\text{dc}} = (0\ 0\ 0\ 1\ 0\ 0)^T$ is the vector describing the electrical connection of the *dc*-microgrid and the *IC*.

Linearizing the power injections, we have:

$$\begin{aligned} \Delta p_{\text{dc}} &= \left([V_0]Y + [YV_0]\right)\Delta V + G_0^{\text{dc}} \Delta P_{\text{IC}} \\ \Delta p_{\text{dc}} &= G_1^{\text{dc}} \Delta V + G_0^{\text{dc}} \Delta P_{\text{IC}} \end{aligned} \tag{A.30}$$

### A.2.2 Voltage reference

From (3.9a), the voltage reference for the $j^{th}$ *dc*-DG ($\forall j \in \mathbb{N}_{\text{dc}}$) is:

$$V_j = V^* + M_{\text{dc}-j} \cdot P_{\text{dc}-j} + \varphi_j \tag{A.31}$$

where $P_{\mathrm{dc}}$ is the filtered power generated by the $j^{th}$ *dc*-DG, and it is given by:

$$\begin{aligned} P_{\mathrm{dc}-j} &= \frac{\omega_c}{s+\omega_c} p_{\mathrm{dc}-j} \\ \dot{P}_{\mathrm{dc}-j} &= \omega_c \left(p_{\mathrm{dc}-j} - P_{\mathrm{dc}-j}\right) \end{aligned} \tag{A.32}$$

Now, linearizing (A.32), the following expression for $\Delta\dot{P}_{\mathrm{dc}}$ is obtained in vector notation:

$$\Delta\dot{P}_{\mathrm{dc}} = [\omega_c]\Delta p_{\mathrm{dc}} - [\omega_c]\Delta P_{\mathrm{dc}} \tag{A.33}$$

Replacing $\Delta p_{\mathrm{dc}}$ from (A.30), we have:

$$\begin{aligned} \Delta\dot{P}_{\mathrm{dc}} &= [\omega_c]\left(G_1^{\mathrm{dc}}\Delta V + G_0^{\mathrm{dc}}\Delta P_{\mathrm{IC}}\right) - [\omega_c]\Delta P_{\mathrm{dc}} \\ \Delta\dot{P}_{\mathrm{dc}} &= [\omega_c]G_1^{\mathrm{dc}}\Delta V + [\omega_c]G_0^{\mathrm{dc}}\Delta P_{\mathrm{IC}} - [\omega_c]\Delta P_{\mathrm{dc}} \end{aligned} \tag{A.34}$$

Now, linearizing the expression for the voltage (A.31), we obtain:

$$\Delta V = [M_{\mathrm{dc}}]\Delta P_{\mathrm{dc}} + \Delta\varphi \tag{A.35}$$

Replacing (A.35) in (A.34), we have:

$$\begin{aligned} \Delta\dot{P}_{\mathrm{dc}} &= [\omega_c]G_1^{\mathrm{dc}}\left([M_{\mathrm{dc}}]\Delta P_{\mathrm{dc}} + \Delta\varphi\right) + [\omega_c]G_0^{\mathrm{dc}}\Delta P_{\mathrm{IC}} - [\omega_c]\Delta P_{\mathrm{dc}} \\ \Delta\dot{P}_{\mathrm{dc}} &= [\omega_c]G_1^{\mathrm{dc}}[M_{\mathrm{dc}}]\Delta P_{\mathrm{dc}} + [\omega_c]G_1^{\mathrm{dc}}\Delta\varphi + [\omega_c]G_0^{\mathrm{dc}}\Delta P_{\mathrm{IC}} - [\omega_c]\Delta P_{\mathrm{dc}} \\ \Delta\dot{P}_{\mathrm{dc}} &= [\omega_c]\left(G_1^{\mathrm{dc}}[M_{\mathrm{dc}}] - I_m\right)\Delta P_{\mathrm{dc}} + [\omega_c]G_1^{\mathrm{dc}}\Delta\varphi + [\omega_c]G_0^{\mathrm{dc}}\Delta P_{\mathrm{IC}} \\ \Delta\dot{P}_{\mathrm{dc}} &= G_2^{\mathrm{dc}}\Delta P_{\mathrm{dc}} + G_3^{\mathrm{dc}}\Delta\varphi + G_4^{\mathrm{dc}}\Delta P_{\mathrm{IC}} \end{aligned} \tag{A.36}$$

Equation (A.36) corresponds to the state equation for the state variables $\Delta P_{\mathrm{dc}}$.

### A.2.3 Secondary control loop

From (3.9b), the voltage secondary controller for the $j^{th}$ *dc*-DG ($\forall j \in \mathbb{N}_{\mathrm{dc}}$) is:

$$\dot{\varphi}_j = -\gamma_j\left(V_j - V^*\right) - c_j\sum_{\mathrm{i}\in\mathbb{N}_{\mathrm{dc}}} a_{j\mathrm{i}}\left(P_{\mathrm{dc}-j} - P_{\mathrm{dc}-\mathrm{i}}\right) - c_j\sum_{\mathrm{i}\in\mathbb{N}_{\mathrm{ac}}} a_{j\mathrm{i}}\left(P_{\mathrm{dc}-j} - P_{\mathrm{ac}-\mathrm{i}}\right) \tag{A.37}$$

The modified in-degrees for node $v_j$ are given by:

$$\mathrm{d}_{(\mathrm{dc}-\mathrm{dc})-j} = \sum\nolimits_{\mathrm{i}\in\mathbb{N}_{\mathrm{dc}}} a_{j\mathrm{i}} = a_{j1} + a_{j2} + \cdots + a_{jm} \tag{A.38a}$$

$$\mathrm{d}_{(\mathrm{dc}-\mathrm{ac})-j} = \sum\nolimits_{\mathrm{i}\in\mathbb{N}_{\mathrm{ac}}} a_{j\mathrm{i}} = a_{j1} + a_{j2} + \cdots + a_{jn} \tag{A.38b}$$

In vector notation, we have:

$$D_{\mathrm{dc}-\mathrm{dc}} = \mathrm{d}iag(\mathrm{d}_{(\mathrm{dc}-\mathrm{dc})-j}) \tag{A.39a}$$

$$D_{\mathrm{dc}-\mathrm{ac}} = \mathrm{d}iag(\mathrm{d}_{(\mathrm{dc}-\mathrm{ac})-j}) \tag{A.39b}$$

In addition, the Laplacian matrix ($L_{\mathrm{dc}}$) for the *dc*-microgrid is defined as:

$$L_{\mathrm{dc}} = D_{\mathrm{dc-dc}} + D_{\mathrm{dc-ac}} - A_{\mathrm{dc-dc}} \tag{A.40}$$

Now, linearizing the controller from (A.37), we obtain:

$$\Delta\dot{\varphi} = -[\gamma]\Delta V - [c]L_{\mathrm{dc}}\frac{1}{P_{\mathrm{dc}}^{+}}\Delta P_{\mathrm{dc}} + [c]A_{\mathrm{dc-ac}}\frac{1}{P_{\mathrm{ac}}^{+}}\Delta P_{\mathrm{ac}} \tag{A.41}$$

Using the expression for $\Delta V$ obtained in (A.35):

$$\begin{aligned}
\Delta\dot{\varphi} &= -[\gamma]\left([M_{\mathrm{dc}}]\Delta P_{\mathrm{dc}} + \Delta\varphi\right) - [c]L_{\mathrm{dc}}\frac{1}{P_{\mathrm{dc}}^{+}}\Delta P_{\mathrm{dc}} + [c]A_{\mathrm{dc-ac}}\frac{1}{P_{\mathrm{ac}}^{+}}\Delta P_{\mathrm{ac}} \\
\Delta\dot{\varphi} &= -\left([\gamma][M_{\mathrm{dc}}] + [c]L_{\mathrm{dc}}\frac{1}{P_{\mathrm{dc}}^{+}}\right)\Delta P_{\mathrm{dc}} - [\gamma]\Delta\varphi + [c]A_{\mathrm{dc-ac}}\frac{1}{P_{\mathrm{ac}}^{+}}\Delta P_{\mathrm{ac}} \\
\Delta\dot{\varphi} &= G_5^{\mathrm{dc}}\Delta P_{\mathrm{dc}} + G_6^{\mathrm{dc}}\Delta\varphi + G_7^{\mathrm{dc}}\Delta P_{\mathrm{ac}}
\end{aligned} \tag{A.42}$$

Equation (A.42) corresponds to the state equation for the state variables $\Delta\varphi$.

## A.3 Closed-loop model for the *IC*

In this Section, the closed-loop model for the *IC* is obtained, including the controllers' characteristics.

### A.3.1 Secondary control loop

From (3.10), the voltage secondary controller for the $k^{th}$ *IC* is:

$$\dot{P}_{\mathrm{IC}-k} = -\tau_k \sum_{\mathrm{i}\in\mathbb{N}_{\mathrm{ac}}}\sum_{j\in\mathbb{N}_{\mathrm{dc}}} a_{\mathrm{i}k}a_{jk}\left(P_{\mathrm{ac-i}} - P_{\mathrm{dc}-j}\right) \tag{A.43}$$

Using the same procedure described before, the modified in-degrees for node $v_{\mathrm{i}}$ are:

$$\mathrm{d}_{(\mathrm{IC-ac})-k} = \sum\nolimits_{\mathrm{i}\in\mathbb{N}_{\mathrm{ac}}} a_{k\mathrm{i}} = a_{k1} + a_{k2} + \cdots + a_{kn} \tag{A.44a}$$

$$\mathrm{d}_{(\mathrm{IC-dc})-k} = \sum\nolimits_{j\in\mathbb{N}_{\mathrm{dc}}} a_{kj} = a_{k1} + a_{k2} + \cdots + a_{km} \tag{A.44b}$$

In vector notation, we have:

$$D_{\mathrm{IC-ac}} = \mathrm{d}iag(\mathrm{d}_{(\mathrm{IC-ac})-\mathrm{i}}) \tag{A.45a}$$

$$D_{\mathrm{IC-dc}} = \mathrm{d}iag(\mathrm{d}_{(\mathrm{IC-dc})-\mathrm{i}}) \tag{A.45b}$$

Now, linearizing the controller from (A.43), we have:

$$\begin{aligned}
\Delta\dot{P}_{\mathrm{IC}} &= -[\tau]D_{\mathrm{IC-dc}}A_{\mathrm{IC-ac}}\frac{1}{S_{\mathrm{ac}}^{+}}\Delta P_{\mathrm{ac}} + [\tau]D_{\mathrm{IC-ac}}A_{\mathrm{IC-dc}}\frac{1}{P_{\mathrm{dc}}^{+}}\Delta P_{\mathrm{dc}} \\
\Delta\dot{P}_{\mathrm{IC}} &= G_1^{\mathrm{IC}}\Delta P_{\mathrm{ac}} + G_2^{\mathrm{IC}}\Delta P_{\mathrm{dc}}
\end{aligned} \tag{A.46}$$

Equation (A.46) corresponds to the state equation for the state variable $\Delta P_{\mathrm{IC}}$.

## A.4 Summary

In the following, a summary of the state variables and state equations are presented.

### A.4.1 State variables

The closed-loop model for the studied hybrid *ac/dc*-microgrid with the proposed control strategy has 28 state variables, as follows:

- 3 angles from the *ac*-microgrid ($\theta_{\rm i}, \forall {\rm i} \in \mathbb{N}_{\rm ac}$).
- 3 active powers from the *ac*-microgrid ($P_{\rm ac}, \forall {\rm i} \in \mathbb{N}_{\rm ac}$).
- 3 reactive powers from the *ac*-microgrid ($Q_{\rm ac}, \forall {\rm i} \in \mathbb{N}_{\rm ac}$).
- 3 frequency secondary control variables from the *ac*-microgrid ($\psi_{\rm i}, \forall {\rm i} \in \mathbb{N}_{\rm ac}$).
- 3 voltage secondary control variables from the *ac*-microgrid ($\chi_{\rm i}, \forall {\rm i} \in \mathbb{N}_{\rm ac}$).
- 6 active powers from the *dc*-microgrid ($P_{\rm dc}, \forall j \in \mathbb{N}_{\rm dc}$).
- 6 voltage secondary control variables from the *dc*-microgrid ($\varphi_j, \forall j \in \mathbb{N}_{\rm dc}$).
- 1 *IC* power ($P_{\rm IC}$)

### A.4.2 State equations

The state equations for the closed-loop model of the studied hybrid *ac/dc*-microgrid with the proposed control strategy are repeated below:

$$\begin{aligned}
\Delta\dot{\theta} &= G_8^{\rm ac}\Delta P_{\rm ac} + \Delta\psi && \text{(A.15)}\\
\Delta\dot{P}_{\rm ac} &= G_9^{\rm ac}\Delta Q_{\rm ac} + G_{10}^{\rm ac}\Delta\chi + G_{11}^{\rm ac}\Delta\theta + G_{12}^{\rm ac}\Delta P_{\rm IC} + G_{13}^{\rm ac}\Delta P_{\rm ac} && \text{(A.14)}\\
\Delta\dot{Q}_{\rm ac} &= G_5^{\rm ac}\Delta Q_{\rm ac} + G_6^{\rm ac}\Delta\chi + G_7^{\rm ac}\Delta\theta && \text{(A.9)}\\
\Delta\dot{\psi} &= G_{14}^{\rm ac}\Delta P_{\rm ac} + G_{15}^{\rm ac}\Delta\psi + G_{16}^{\rm ac}\Delta P_{\rm dc} && \text{(A.23)}\\
\Delta\dot{\chi} &= G_{17}^{\rm ac}\Delta Q_{\rm ac} + G_{18}^{\rm ac}\Delta\chi && \text{(A.27)}\\
\Delta\dot{P}_{\rm dc} &= G_2^{\rm dc}\Delta P_{\rm dc} + G_3^{\rm dc}\Delta\varphi + G_4^{\rm dc}\Delta P_{\rm IC} && \text{(A.36)}\\
\Delta\dot{\varphi} &= G_5^{\rm dc}\Delta P_{\rm dc} + G_6^{\rm dc}\Delta\varphi + G_7^{\rm dc}\Delta P_{\rm ac} && \text{(A.42)}\\
\Delta\dot{P}_{\rm IC} &= G_1^{\rm IC}\Delta P_{\rm ac} + G_2^{\rm IC}\Delta P_{\rm dc} && \text{(A.46)}
\end{aligned}$$

# Appendix B

# Closed-loop Model for a Hybrid *ac/dc*-Microgrid with the Operation Cost Minimization Strategy

In this Appendix, the procedure for obtaining the closed-loop model for the microgrid presented in Chapter 5 is presented. This model is also utilized for performing a small-signal analysis of the consensus-based distributed control strategy proposed in Chapter 4 for operation cost minimization.

Due to the primary purpose for obtaining the closed-loop model of the consensus-based distributed secondary control strategy proposed for operation cost minimization in a hybrid *ac/dc*-microgrid, the following simplifications were considered since their dynamics are much faster than that of the studied controllers:

- The inner control loop (voltage/current controllers) is not considered.
- The modulation techniques (PWM, SVM) of the converters is not considered.
- The switching of the switching devices is not considered.

Appendix B is organized as follows: Section B.1 presents the closed-loop model for the *ac*-microgrid, while the closed-loop model for the *dc*-microgrid is depicted in Section B.2. The closed-loop model for the *IC* is presented in Section B.3.

## B.1 Closed-loop model for the *ac*-microgrid

In this Section, the closed-loop model for the *ac*-microgrid is obtained, including the topology and the controllers' characteristics. Since the topology of the *ac*-microgrid is the same as the one considered for the consensus-based distributed secondary strategy for power-sharing (see Section A.1), the explanation is focused in the inclusion of the consensus-based distributed secondary controller for operation cost minimization. In this case, to obtain the closed-loop model for this controller, we assume all the units (i.e., *ac*-DGs, *dc*-DGs and *IC*) are operating

within limits.

### B.1.1 Power flow in the *ac*-microgrid

The topology of the *ac*-microgrid can be seen in Fig. A.1. The set of *ac*-DGs are labelled as $\mathbb{N}_{\text{ac}} = \{1, \ldots, n\}$. Further details of the topology can be found in Section 5.2. As shown in (A.3), the power generated by the *ac*-DGs can be expressed in vector notation as follows:

$$\Delta p_{\text{ac}}^{\text{G}} = G_1^{\text{ac}} \Delta E + G_2^{\text{ac}} \Delta\theta + G_0^{\text{ac}} \Delta P_{\text{IC}}^{\text{ac}} \tag{B.1a}$$

$$\Delta q_{\text{ac}}^{\text{G}} = G_3^{\text{ac}} \Delta E + G_4^{\text{ac}} \Delta\theta \tag{B.1b}$$

where $p_{\text{ac}}^{\text{G}}, q_{\text{ac}}^{\text{G}} \in \mathbb{R}^n$ are the vectors of active and reactive power generation (respectively), the other matrices were already explained.

### B.1.2 Voltage reference

From (3.5a), the voltage reference for the i$^{th}$ *ac*-DG ($\forall \text{i} \in \mathbb{N}_{\text{ac}}$) is:

$$E_{\text{i}} = E^* + N_{\text{ac}-\text{i}} \cdot Q_{\text{ac}-\text{i}}^{\text{G}} + \chi_{\text{i}} \tag{B.2}$$

where $Q_{\text{ac}-\text{i}}^{\text{G}}$ is the filtered reactive power generated by the i$^{th}$ *ac*-DG. Then, as described in (A.9), in vector notation we have:

$$\begin{aligned} \Delta\dot{Q}_{\text{ac}} &= [\omega_c] \left( G_3^{\text{ac}} [N_{\text{ac}}] - I_n \right) \Delta Q_{\text{ac}} + [\omega_c] G_3^{\text{ac}} \Delta\chi + [\omega_c] G_4^{\text{ac}} \Delta\theta \\ \Delta\dot{Q}_{\text{ac}}^{\text{G}} &= G_5^{\text{ac}} \Delta Q_{\text{ac}} + G_6^{\text{ac}} \Delta\chi + G_7^{\text{ac}} \Delta\theta \end{aligned} \tag{B.3}$$

Equation (B.3) corresponds to the state equation for the state variables $\Delta Q_{\text{ac}}^{\text{G}}$.

### B.1.3 Frequency reference

From (4.13a), the frequency reference for the i$^{th}$ *ac*-DG ($\forall \text{i} \in \mathbb{N}_{\text{ac}}$) is:

$$\dot{\theta}_{\text{i}} = \omega_{\text{i}} = \omega^* + M_{\text{ac}-\text{i}} P_{\text{ac}-\text{i}}^{\text{G}} + \Omega_{\text{i}}^{\text{ac}} \tag{B.4}$$

Following the procedure described before (see Section A.1), in vector notation we have:

$$\begin{aligned} \Delta\dot{P}_{\text{ac}}^{\text{G}} &= [\omega_c] G_1^{\text{ac}} [N_{\text{ac}}] \Delta Q_{\text{ac}}^{\text{G}} + [\omega_c] G_1^{\text{ac}} \Delta\chi + [\omega_c] G_2^{\text{ac}} \Delta\theta + [\omega_c] G_0^{\text{ac}} \Delta P_{\text{IC}}^{\text{ac}} - [\omega_c] \Delta P_{\text{ac}}^{\text{G}} \\ \Delta\dot{P}_{\text{ac}}^{\text{G}} &= G_9^{\text{ac}} \Delta Q_{\text{ac}}^{\text{G}} + G_{10}^{\text{ac}} \Delta\chi + G_{11}^{\text{ac}} \Delta\theta + G_{12}^{\text{ac}} \Delta P_{\text{IC}}^{\text{ac}} + G_{13}^{\text{ac}} \Delta P_{\text{ac}}^{\text{G}} \end{aligned} \tag{B.5}$$

Equation (B.5) corresponds to the state equation for the state variables $\Delta P_{\text{ac}}^{\text{G}}$.

On the other hand, linearizing (B.4), we obtain:

$$\begin{aligned} \Delta\dot{\theta} &= \Delta\omega = [M_{\text{ac}}] \Delta P_{\text{ac}}^{\text{G}} + \Delta\Omega^{\text{ac}} \\ \Delta\dot{\theta} &= \Delta\omega = G_8^{\text{ac}} \Delta P_{\text{ac}}^{\text{G}} + \Delta\Omega^{\text{ac}} \end{aligned} \tag{B.6}$$

Equation (B.6) corresponds to the state equation for the state variables $\Delta\theta$.

### B.1.4 Frequency secondary control

Since the *ac*-DGs and the *IC* are operating within limits, the Lagrange multipliers associated to the power limit constraints are zero ($\alpha^{+}_{\mathrm{ac-i}} = \alpha^{-}_{\mathrm{ac-i}} = \alpha^{+}_{\mathrm{IC}} = \alpha^{-}_{\mathrm{IC}} = 0$). Thus, from (4.13b), the frequency secondary controller for the i$^{th}$ *ac*-DG ($\forall \mathrm{i} \in \mathbb{N}_{\mathrm{ac}}$) is:

$$\dot{\Omega}^{\mathrm{ac}}_{\mathrm{i}} = -k^{a}_{\mathrm{ac-i}} \left(\omega_{\mathrm{i}} - \omega^{*}\right) - k^{b}_{\mathrm{ac-i}} \sum_{j \in \mathbb{N}_{\mathrm{ac}}} a_{\mathrm{i}j} \left(\lambda^{\mathrm{ac}}_{\mathrm{i}} - \lambda^{\mathrm{ac}}_{j}\right) - k^{c}_{\mathrm{ac-i}} \sum_{j \in \mathbb{N}_{\mathrm{dc}}} a_{\mathrm{i}j} \left(\lambda^{\mathrm{ac}}_{\mathrm{i}} - \lambda^{\mathrm{dc}}_{j}\right) \tag{B.7}$$

On the other hand, from (4.12a) and (4.12b), for $\lambda^{\mathrm{ac}}_{\mathrm{i}}$ and $\lambda^{\mathrm{dc}}_{j}$ we have:

$$\lambda^{\mathrm{ac}}_{\mathrm{i}} = \left(\frac{k_{\mathrm{IC}} + 1}{2k_{\mathrm{IC}}}\right) \left(2a_{\mathrm{ac-i}} P^{\mathrm{G}}_{\mathrm{ac-i}} + b_{\mathrm{ac-i}}\right) \tag{B.8a}$$

$$\lambda^{\mathrm{dc}}_{j} = \left(\frac{k_{\mathrm{IC}} + 1}{2}\right) \left(2a_{\mathrm{dc}-j} P^{\mathrm{G}}_{\mathrm{dc}-j} + b_{\mathrm{dc}-j}\right) \tag{B.8b}$$

Linearizing (B.8), in vector notation we have:

$$\Delta\lambda^{\mathrm{ac}} = \left(\frac{k_{\mathrm{IC}} + 1}{k_{\mathrm{IC}}}\right) [a_{\mathrm{ac}}] \Delta P^{\mathrm{G}}_{\mathrm{ac}} = [a^{k}_{\mathrm{ac}}] \Delta P^{\mathrm{G}}_{\mathrm{ac}} \tag{B.9a}$$

$$\Delta\lambda^{\mathrm{dc}} = \left(k_{\mathrm{IC}} + 1\right) [a_{\mathrm{dc}}] \Delta P^{\mathrm{G}}_{\mathrm{dc}} = [a^{k}_{\mathrm{dc}}] \Delta P^{\mathrm{G}}_{\mathrm{dc}} \tag{B.9b}$$

Now, if the **modified in-degree** defined in (A.19) is considered, linearizing the controller from (B.7), in vector notation we obtain:

$$\Delta\dot{\Omega}^{\mathrm{ac}} = -[k^{\mathrm{a}}_{\mathrm{ac}}] \Delta\omega - \left\{[k^{\mathrm{b}}_{\mathrm{ac}}] \left(D_{\mathrm{ac-ac}} - A_{\mathrm{ac-ac}}\right) + [k^{\mathrm{c}}_{\mathrm{ac}}] D_{\mathrm{ac-dc}}\right\} \Delta\lambda^{\mathrm{ac}} + [k^{\mathrm{c}}_{\mathrm{ac}}] A_{\mathrm{ac-dc}} \Delta\lambda^{\mathrm{dc}} \tag{B.10}$$

Considering the expressions for $\Delta\omega$, $\Delta\lambda^{\mathrm{ac}}$ and $\Delta\lambda^{\mathrm{dc}}$, we have:

$$\begin{aligned}
\Delta\dot{\Omega}^{\mathrm{ac}} =& - \left\{[k^{\mathrm{b}}_{\mathrm{ac}}] \left(D_{\mathrm{ac-ac}} - A_{\mathrm{ac-ac}}\right) + [k^{\mathrm{c}}_{\mathrm{ac}}] D_{\mathrm{ac-dc}}\right\} [a^{k}_{\mathrm{ac}}] \Delta P^{\mathrm{G}}_{\mathrm{ac}} \\
& - [k^{\mathrm{a}}_{\mathrm{ac}}] \left(G^{\mathrm{ac}}_{8} \Delta P^{\mathrm{G}}_{\mathrm{ac}} + \Delta\Omega^{\mathrm{ac}}\right) + [k^{\mathrm{c}}_{\mathrm{ac}}] A_{\mathrm{ac-dc}} [a^{k}_{\mathrm{dc}}] \Delta P^{\mathrm{G}}_{\mathrm{dc}} \\
\Delta\dot{\Omega}^{\mathrm{ac}} =& - \left\{[k^{\mathrm{a}}_{\mathrm{ac}}] G^{\mathrm{ac}}_{8} + [k^{\mathrm{b}}_{\mathrm{ac}}] \left(D_{\mathrm{ac-ac}} - A_{\mathrm{ac-ac}}\right) [a^{k}_{\mathrm{ac}}] + [k^{\mathrm{c}}_{\mathrm{ac}}] D_{\mathrm{ac-dc}} [a^{k}_{\mathrm{ac}}]\right\} \Delta P^{\mathrm{G}}_{\mathrm{ac}} \\
& - [k^{\mathrm{a}}_{\mathrm{ac}}] \Delta\Omega^{\mathrm{ac}} + [k^{\mathrm{c}}_{\mathrm{ac}}] A_{\mathrm{ac-dc}} [a^{k}_{\mathrm{dc}}] \Delta P^{\mathrm{G}}_{\mathrm{dc}} \\
\Delta\dot{\Omega}^{\mathrm{ac}} =& G^{\mathrm{ac}}_{14} \Delta P^{\mathrm{G}}_{\mathrm{ac}} + G^{\mathrm{ac}}_{15} \Delta\Omega^{\mathrm{ac}} + G^{\mathrm{ac}}_{16} \Delta P^{\mathrm{G}}_{\mathrm{dc}}
\end{aligned} \tag{B.11}$$

Equation (B.11) corresponds to the state equation for the state variables $\Delta\Omega^{\mathrm{ac}}$.

### B.1.5 Voltage secondary control

Following the procedure described before (see Section A.1), in vector notation we have:

$$\begin{aligned}
\Delta\dot{\chi} =& - \left([\beta][N_{\mathrm{ac}}] + [b] \left(D_{\mathrm{ac-ac}} - A_{\mathrm{ac-ac}}\right) \frac{1}{S^{+}_{\mathrm{ac}}}\right) \Delta Q^{\mathrm{G}}_{\mathrm{ac}} - [\beta] \Delta\chi \\
\Delta\dot{\chi} =& G^{\mathrm{ac}}_{17} \Delta Q^{\mathrm{G}}_{\mathrm{ac}} + G^{\mathrm{ac}}_{18} \Delta\chi
\end{aligned} \tag{B.12}$$

Equation (B.12) corresponds to the state equation for the state variables $\Delta\chi$.

## B.2 Closed-loop model for the *dc*-microgrid

In this Section, the closed-loop model for the *dc*-microgrid is obtained, including the topology and the controllers' characteristics. Since the topology of the *dc*-microgrid is the same as the one considered for the consensus-based distributed secondary strategy for power-sharing (see Section A.2), the explanation is focused in the inclusion of the consensus-based distributed secondary controller for operation cost minimization. In this case, to obtain the closed-loop model for this controller, we assume all the units (i.e., *ac*-DGs, *dc*-DGs and *IC*) are operating within limits.

### B.2.1 Power flow in the *dc*-microgrid

The topology of the *dc*-microgrid can be seen in Fig. A.2. The set of *dc*-DGs are labelled as $\mathbb{N}_{\text{dc}} = \{n+1, \ldots, n+m\}$. Further details of the topology can be found in Section 5.3. As shown in (A.30), the power generated by the *dc*-DGs can be expressed in vector notation as follows:

$$\begin{aligned} \Delta p_{\text{dc}}^{\text{G}} &= \left([V_0]Y + [YV_0]\right)\Delta V + (0\ 0\ 0\ 1/k_{\text{IC}}\ 0\ 0)^T \Delta P_{\text{IC}}^{\text{ac}} \\ \Delta p_{\text{dc}}^{\text{G}} &= G_1^{\text{dc}} \Delta V + G_0^{\text{dc}} \Delta P_{\text{IC}}^{\text{ac}} \end{aligned} \tag{B.13}$$

### B.2.2 Voltage reference

From (4.15a), the voltage reference for the $j^{th}$ *dc*-DG ($\forall j \in \mathbb{N}_{\text{dc}}$) is:

$$V_j = V^* + M_{\text{dc}-j} P_{\text{dc}-j}^{\text{G}} + \Omega_j^{\text{dc}} \tag{B.14}$$

where $P_{\text{dc}}^{\text{G}}$ is the filtered power generated by the $j^{th}$ *dc*-DG. Then, as described in (A.36), in vector notation we have:

$$\begin{aligned} \Delta \dot{P}_{\text{dc}}^{\text{G}} &= [\omega_c]\left(G_1^{\text{dc}}[M_{\text{dc}}] - I_m\right)\Delta P_{\text{dc}}^{\text{G}} + [\omega_c] G_1^{\text{dc}} \Delta\Omega^{\text{dc}} + [\omega_c] G_0^{\text{dc}} \Delta P_{\text{dc}}^{\text{G}} \\ \Delta \dot{P}_{\text{dc}}^{\text{G}} &= G_2^{\text{dc}} \Delta P_{\text{IC}}^{\text{ac}} + G_3^{\text{dc}} \Delta\Omega^{\text{dc}} + G_4^{\text{dc}} \Delta P_{\text{IC}}^{\text{ac}} \end{aligned} \tag{B.15}$$

Equation (B.15) corresponds to the state equation for the state variables $\Delta P_{\text{dc}}^{\text{G}}$.

Linearizing (B.14), we obtain an expression for $\Delta V$:

$$\Delta V = [M_{\text{dc}}]\Delta P_{\text{dc}}^{\text{G}} + \Delta\Omega^{\text{dc}} \tag{B.16}$$

### B.2.3 Secondary control loop

Since the *dc*-DGs and the *IC* are operating within limits, the Lagrange multipliers associated to the power limit constraints are zero ($\alpha_{\text{dc}-j}^{+} = \alpha_{\text{dc}-j}^{-} = \alpha_{\text{IC}}^{+} = \alpha_{\text{IC}}^{-} = 0$). Thus, from (4.15b), the voltage secondary controller for the $j^{th}$ *dc*-DG ($\forall j \in \mathbb{N}_{\text{dc}}$) is:

$$\dot{\Omega}_j^{\text{dc}} = -k_{\text{dc}-j}^{a}\left(V_j - V^*\right) - k_{\text{dc}-j}^{b} \sum_{\text{i}\in\mathbb{N}_{\text{dc}}} a_{\text{ij}} \left(\lambda_j^{\text{dc}} - \lambda_{\text{i}}^{\text{dc}}\right) - k_{\text{dc}-j}^{c} \sum_{\text{i}\in\mathbb{N}_{\text{ac}}} a_{\text{ij}} \left(\lambda_j^{\text{dc}} - \lambda_{\text{i}}^{\text{ac}}\right) \tag{B.17}$$

Now, if the **modified in-degree** defined in (A.19) is considered, linearizing the controller from (B.17), in vector notation we obtain:

$$\Delta\dot{\Omega}^{\mathrm{dc}} = -[k^a_{\mathrm{dc}}]\Delta V - \left\{[k^b_{\mathrm{dc}}]\left(D_{\mathrm{dc-dc}} - A_{\mathrm{dc-dc}}\right) + [k^c_{\mathrm{dc}}]D_{\mathrm{dc-ac}}\right\}\Delta\lambda^{\mathrm{dc}} + [k^c_{\mathrm{dc}}]A_{\mathrm{dc-ac}}\Delta\lambda^{\mathrm{ac}} \quad \text{(B.18)}$$

Considering the expressions for $\Delta V$, $\Delta\lambda^{\mathrm{dc}}$ and $\lambda^{\mathrm{ac}}$, we have:

$$\begin{aligned}
\Delta\dot{\Omega}^{\mathrm{dc}} =& -\left\{[k^b_{\mathrm{dc}}]\left(D_{\mathrm{dc-dc}} - A_{\mathrm{dc-dc}}\right) + [k^c_{\mathrm{dc}}]D_{\mathrm{dc-ac}}\right\}[a^k_{\mathrm{dc}}]\Delta P^{\mathrm{G}}_{\mathrm{dc}} \\
& - [k^a_{\mathrm{dc}}]\left([M_{\mathrm{dc}}]\Delta P^{\mathrm{G}}_{\mathrm{dc}} + \Delta\Omega^{\mathrm{dc}}\right) + [k^c_{\mathrm{dc}}]A_{\mathrm{dc-ac}}[a^k_{\mathrm{ac}}]\Delta P^{\mathrm{G}}_{\mathrm{ac}} \\
\Delta\dot{\Omega}^{\mathrm{dc}} =& -\left\{[k^a_{\mathrm{dc}}][M_{\mathrm{dc}}] + [k^b_{\mathrm{dc}}]\left(D_{\mathrm{dc-dc}} - A_{\mathrm{dc-dc}}\right)[a^k_{\mathrm{dc}}] + [k^c_{\mathrm{dc}}]D_{\mathrm{dc-ac}}[a^k_{\mathrm{dc}}]\right\}\Delta P^{\mathrm{G}}_{\mathrm{dc}} \\
& - [k^a_{\mathrm{dc}}]\Delta\Omega^{\mathrm{dc}} - [k^c_{\mathrm{dc}}]A_{\mathrm{dc-ac}}[a^k_{\mathrm{ac}}]\Delta P^{\mathrm{G}}_{\mathrm{ac}} \\
\Delta\dot{\Omega}^{\mathrm{dc}} =& G^{\mathrm{dc}}_5\Delta P^{\mathrm{G}}_{\mathrm{dc}} + G^{\mathrm{dc}}_6\Delta\Omega^{\mathrm{dc}} + G^{\mathrm{dc}}_7\Delta P^{\mathrm{G}}_{\mathrm{ac}}
\end{aligned} \quad \text{(B.19)}$$

Equation (B.19) corresponds to the state equation for the state variables $\Delta\Omega^{\mathrm{dc}}$.

## B.3 Closed-loop model for the *IC*

In this Section, the closed-loop model for the *IC* is obtained, including the controllers' characteristics.

### B.3.1 Secondary control loop

Since the *IC* is operating within limits, the Lagrange multipliers associated to the power limit constraints are zero ($\alpha^+_{\mathrm{IC}} = \alpha^-_{\mathrm{IC}} = 0$). Thus, from (4.16a), the secondary controller for the *IC* is:

$$\dot{P}^*_{\mathrm{IC}-k} = -\tau_{\mathrm{IC}-k}\sum_{\mathrm{i}\in\mathbb{N}_{\mathrm{ac}}}\sum_{j\in\mathbb{N}_{\mathrm{dc}}} a_{\mathrm{i}k}a_{jk}\left(\lambda_{\mathrm{ac-i}} - \lambda_{\mathrm{dc}-j}\right) \quad \text{(B.20)}$$

Now, if the **modified in-degree** defined in (A.19) is considered, linearizing the controller from (B.20), in vector notation we obtain:

$$\begin{aligned}
\Delta\dot{P}^{\mathrm{ac}}_{\mathrm{IC}} &= -[\tau]D_{\mathrm{IC-dc}}A_{\mathrm{IC-ac}}\Delta\lambda^{\mathrm{ac}} + [\tau]D_{\mathrm{IC-ac}}A_{\mathrm{IC-dc}}\Delta\lambda^{\mathrm{dc}} \\
\Delta\dot{P}^{\mathrm{ac}}_{\mathrm{IC}} &= -[\tau]D_{\mathrm{IC-dc}}A_{\mathrm{IC-ac}}[a^k_{\mathrm{ac}}]\Delta P^{\mathrm{G}}_{\mathrm{ac}} + [\tau]D_{\mathrm{IC-ac}}A_{\mathrm{IC-dc}}[a^k_{\mathrm{dc}}]\Delta P^{\mathrm{G}}_{\mathrm{dc}} \\
\Delta\dot{P}^{\mathrm{ac}}_{\mathrm{IC}} &= G^{\mathrm{IC}}_1[a^k_{\mathrm{ac}}]\Delta P^{\mathrm{G}}_{\mathrm{ac}} + G^{\mathrm{IC}}_2\Delta P^{\mathrm{G}}_{\mathrm{dc}}
\end{aligned} \quad \text{(B.21)}$$

Equation (B.21) corresponds to the state equation for the state variable $\Delta P^{\mathrm{ac}}_{\mathrm{IC}}$.

## B.4 Summary

In the following, a summary of the state variables and state equations are presented.

### B.4.1 State variables

The closed-loop model for the studied hybrid *ac/dc*-microgrid with the proposed control strategy for operation cost minimization has 28 state variables, as follows:

- 3 angles from the *ac*-microgrid ($\theta_{\mathrm{i}}, \forall \mathrm{i} \in \mathbb{N}_{\mathrm{ac}}$).
- 3 active powers from the *ac*-microgrid ($P^{\mathrm{G}}_{\mathrm{ac}}, \forall \mathrm{i} \in \mathbb{N}_{\mathrm{ac}}$).
- 3 reactive powers from the *ac*-microgrid ($Q^{\mathrm{G}}_{\mathrm{ac}}, \forall \mathrm{i} \in \mathbb{N}_{\mathrm{ac}}$).
- 3 frequency secondary control variables from the *ac*-microgrid ($\Omega^{\mathrm{ac}}_{\mathrm{i}}, \forall \mathrm{i} \in \mathbb{N}_{\mathrm{ac}}$).
- 3 voltage secondary control variables from the *ac*-microgrid ($\chi_{\mathrm{i}}, \forall \mathrm{i} \in \mathbb{N}_{\mathrm{ac}}$).
- 6 active powers from the *dc*-microgrid ($P^{\mathrm{G}}_{\mathrm{dc}}, \forall j \in \mathbb{N}_{\mathrm{dc}}$).
- 6 voltage secondary control variables from the *dc*-microgrid ($\Omega^{\mathrm{dc}}_{j}, \forall j \in \mathbb{N}_{\mathrm{dc}}$).
- 1 *IC* power ($P^{\mathrm{ac}}_{\mathrm{IC}}$).

### B.4.2 State equations

The state equations for the closed-loop model of the studied hybrid *ac/dc*-microgrid with the proposed control strategy are repeated below:

$$
\begin{aligned}
\Delta\dot{\theta} &= G^{\mathrm{ac}}_{8}\Delta P^{\mathrm{G}}_{\mathrm{ac}} + \Delta\Omega^{\mathrm{ac}} && \text{(B.6)}\\
\Delta\dot{P}^{\mathrm{G}}_{\mathrm{ac}} &= G^{\mathrm{ac}}_{9}\Delta Q^{\mathrm{G}}_{\mathrm{ac}} + G^{\mathrm{ac}}_{10}\Delta\chi + G^{\mathrm{ac}}_{11}\Delta\theta + G^{\mathrm{ac}}_{12}\Delta P^{\mathrm{ac}}_{\mathrm{IC}} + G^{\mathrm{ac}}_{13}\Delta P^{\mathrm{G}}_{\mathrm{ac}} && \text{(B.5)}\\
\Delta\dot{Q}^{\mathrm{G}}_{\mathrm{ac}} &= G^{\mathrm{ac}}_{5}\Delta Q^{\mathrm{G}}_{\mathrm{ac}} + G^{\mathrm{ac}}_{6}\Delta\chi + G^{\mathrm{ac}}_{7}\Delta\theta && \text{(B.3)}\\
\Delta\dot{\Omega}^{\mathrm{ac}} &= G^{\mathrm{ac}}_{14}\Delta P^{\mathrm{G}}_{\mathrm{ac}} + G^{\mathrm{ac}}_{15}\Delta\Omega^{\mathrm{ac}} + G^{\mathrm{ac}}_{16}\Delta P^{\mathrm{G}}_{\mathrm{dc}} && \text{(B.11)}\\
\Delta\dot{\chi} &= G^{\mathrm{ac}}_{17}\Delta Q^{\mathrm{G}}_{\mathrm{ac}} + G^{\mathrm{ac}}_{18}\Delta\chi && \text{(B.12)}\\
\Delta\dot{P}^{\mathrm{G}}_{\mathrm{dc}} &= G^{\mathrm{dc}}_{2}\Delta P^{\mathrm{G}}_{\mathrm{dc}} + G^{\mathrm{dc}}_{3}\Delta\Omega^{\mathrm{dc}} + G^{\mathrm{dc}}_{4}\Delta P^{\mathrm{ac}}_{\mathrm{IC}} && \text{(B.15)}\\
\Delta\dot{\Omega}^{\mathrm{dc}} &= G^{\mathrm{dc}}_{5}\Delta P^{\mathrm{G}}_{\mathrm{dc}} + G^{\mathrm{dc}}_{6}\Delta\Omega^{\mathrm{dc}} + G^{\mathrm{dc}}_{7}\Delta P^{\mathrm{G}}_{\mathrm{ac}} && \text{(B.19)}\\
\Delta\dot{P}^{\mathrm{ac}}_{\mathrm{IC}} &= G^{\mathrm{IC}}_{1}\Delta P^{\mathrm{G}}_{\mathrm{ac}} + G^{\mathrm{IC}}_{2}\Delta P^{\mathrm{G}}_{\mathrm{dc}} && \text{(B.21)}
\end{aligned}
$$